

**Development of an acellular annuloplasty ring for
atrioventricular valve repair**

Mark Thomas Hepples

Submitted in accordance with the requirements for the degree of
Doctor of Philosophy

The University of Leeds

School of Mechanical Engineering

July 2015

The candidate confirms that the work submitted is his/her own and that appropriate credit has been given where reference has been made to the work of others.

This copy has been supplied on the understanding that it is copyright material and that no quotation from the thesis may be published without proper acknowledgement.

© 2015 The University of Leeds and Mark Thomas Hepples

The right of Mark Thomas Hepples to be identified as Author of this work has been asserted by him in accordance with the Copyright, Designs and Patents Act 1988.

Acknowledgements

First and foremost I would like to thank my supervisor Professor Eileen Ingham for constantly providing much help, support and guidance throughout my study. This thanks also extends to my co-supervisors; Dr Stacy-Paul Wilshaw, especially for assistance in gaining ethical approval, Professor John Fisher for guidance during the biomechanical testing that was undertaken and also to my industrial sponsors NHS Blood and Transplant, Tissue Services and supervisors Professor Paul Rooney and Professor John Kearney. Without their insight and support much of this project would not have been feasible. Thank you also to the donors and donor families for providing the much needed human tissue for this study and research projects like it.

Deepest gratitude to my lab tutor Dr Tayyabe Vafae who gave me the insight and training for the studies required for this thesis. The same goes to Dr Daniel Thomas and Dr Blessing Mukonweshuro for providing training and assistance during my studies.

Thanks also to Mr Irvin Homan and Dr Nagitha Wijayathunga for ordering all of the required animal tissue for the research, as well as Mr Phillip Wood , Mrs Amisha Desai and Dr Rodolfo Paniagua for support and assistance whilst undertaking the mechanical testing.

Thanks also goes to all the friends and colleagues I have met along the way during my time at Leeds, special thanks to: Jake, Jap, Carl, Keeley, Leyla, Ruth, Normalina, Ash and Helen, amongst many others.

Special mention to my family who have supported me throughout my time at Leeds; to my mum and dad for their moral and financial support as well as providing a roof over my head during the writing up of my thesis. Also to my two sisters Jacqueline and Michelle for all the guidance and moral support offered throughout.

Finally to my amazing girlfriend Debs, your patience, love and understanding during my PhD, even when faced with your own larger challenges ensured that I persevered during the hardest times and finally finished writing my thesis!

Abstract

Annuloplasty is a common technique used for repair of the mitral valve. It is hypothesised that an acellular biological ring may provide a superior solution by encouraging tissue integration and improved annular dynamics whilst offering similar structure and composition to the native annulus.

Human mitral valve annuli (n=3) were characterised using histological methods to reveal the histoarchitecture of the native tissue. The histological features of porcine mitral valve annuli (n=5) were compared to the human annuli, as an alternative source of tissue. Haematoxylin and eosin, alcian blue and Sirius red Miller's stained sections illustrated the morphology of both species revealing a highly fibrous region at the anterior of the annulus compared to the posterior region. The continuum of the fibrosa layer in the mitral leaflet into the fibrous region around the annulus was also visualised. Differences between species were observed at the trigones where cartilaginous tissue was present in the porcine annuli compared to fibrous tissue in the human tissue. The human mitral valve annuli were heavily calcified and showed signs of ossification, hence porcine annuli were used as the starting material for developing a biological acellular annuloplasty ring.

Porcine mitral valve annuli (n = 36) were decellularised using a series of eight iterative protocols. The annuli were successfully decellularised using a protocol comprising two freeze thaw cycles (one cycle in hypotonic buffer), followed by four alternate cycles of washing in hypotonic buffer plus proteinase inhibitors and 0.1% (w/v) sodium dodecyl sulfate in hypotonic buffer plus proteinase inhibitors followed by treatment with nuclease solution, washing in hypertonic buffer and final disinfection wash in 0.1% (v/v) peracetic acid. Histological analysis of the treated tissue revealed removal of nuclei apart from apparent "ghost nuclei" in the trigones. Immunohistochemical analyses revealed loss of collagen IV and laminin associated with the basement membrane but retention of collagens I, II and III responsible for structural integrity. Total DNA content of the processed tissue was less than 50 ng.mg⁻¹ wet weight and *in-vitro* biocompatibility assays showed decellularised porcine mitral valve annulus tissue was not cytotoxic to BHK and L929 cells. Biomechanical tensile tests using low strain rate to failure of the decellularised porcine mitral annuli showed increased tensile strain and transition strains and stresses compared to the native porcine annuli. A method for functional testing revealed that the acellular rings performed as well as synthetic annuloplasty rings in static tests of regurgitant porcine hearts.

Table of Contents

Acknowledgements	iii
Abstract	iv
Table of Contents	v
List of Tables	xiii
List of Figures	xiv
List of Abbreviations	xx
Chapter 1 Introduction	1
1.1 General Introduction.....	1
1.2 The Heart	2
1.2.1 Atrioventricular Valves.....	4
1.2.2 Mitral Valve Annulus.....	10
1.2.2.1 Structure.....	10
1.2.2.2 Function	12
1.3 Mitral valve disease.....	15
1.3.1 Epidemiology.....	15
1.3.2 Types of disease	15
1.3.2.1 Mitral regurgitation	15
1.3.3 Annulus remodeling due to disease	18
1.4 Mitral Valve Disease Treatment	21
1.4.1 Replacement.....	21
1.4.2 Types of Replacement Valve	21
1.4.2.1 Mechanical valves.....	21
1.4.2.2 Bioprosthetic valves	21
1.4.2.3 Pulmonary autograft.....	22
1.4.2.4 Synthetic valves	22
1.4.3 Repair.....	22
1.5 Annuloplasty.....	23
1.5.1 Annuloplasty rings.....	23
1.5.1.1 Synthetic rings.....	23
1.5.1.2 Biodegradable ring	32
1.5.1.3 Biological replacement ring	33
1.5.2 Annuloplasty in children	35

1.6 Tissue Engineering.....	38
1.6.1 Overview	38
1.6.2 Synthetic polymer matrices in cardiovascular tissue engineering	39
1.6.3 Natural polymer scaffolds in cardiovascular tissue engineering	40
1.6.4 Biological scaffolds in cardiovascular tissue engineering	42
1.6.4.1 Decellularised biological scaffolds.....	42
1.7 Decellularisation	44
1.8 Aims and objectives	48
Chapter 2 Materials and Methods	49
2.1 Materials.....	49
2.1.1 Equipment	49
2.1.2 Chemicals and reagents.....	53
2.1.3 General stock solutions	57
2.1.3.1 Phosphate buffered saline (PBS)	57
2.1.3.2 Tris buffered saline (TBS)	57
2.1.3.3 TBS containing 0.05% (w/v) Tween 20	57
2.1.4 Cells	58
2.1.5 Glassware	58
2.2 Methods	59
2.2.1 General methods.....	59
2.2.1.1 Measurement of pH.....	59
2.2.1.2 Microscopic analysis	59
2.2.1.3 Sterilisation.....	59
2.2.2 Tissue processing	60
2.2.2.1 Dissection equipment.....	60
2.2.2.2 Ethics and tissue tracking.....	60
2.2.2.3 Dissection.....	61
2.2.3 Histological techniques.....	63
2.2.3.1 Fixation.....	63
2.2.3.2 Paraffin wax embedding	66
2.2.3.3 Tissue sectioning	67
2.2.3.4 Dewaxing and rehydration.....	67
2.2.3.5 Dehydration and mounting	67

2.2.4 Histological staining methods.....	67
2.2.4.1 Haematoxylin and Eosin staining	67
2.2.4.2 Sirius red Miller's staining.....	68
2.2.4.3 Alcian Blue staining	69
2.2.4.4 DAPI staining of paraffin wax embedded tissue samples.....	69
2.2.4.5 Von Kossa staining	70
2.2.4.6 Immunohistochemistry	70
2.2.4.7 Labelling the alpha-gal epitope using biotinylated GSL-1 lectin	74
2.2.5 Cell Culture techniques	76
2.2.5.1 Resurrection and maintenance of primary cells and cell lines	77
2.2.5.2 Cell passaging.....	77
2.2.5.3 Cell viability assay	77
2.2.6 Biomechanical testing	78
2.2.6.1 Preparation of the tissue samples	78
2.2.6.2 Test procedure	81
2.2.7 Statistical analysis	83
2.2.7.1 Confidence limits	83
2.2.7.2 Statistical analysis	83
Chapter 3 Characterisation of human and porcine mitral valve annulus	84
3.1 Introduction	84
3.1.1 Aims and objectives	86
3.2 Material and methods.....	87
3.2.1 Histological evaluation of the human and porcine mitral valve annulus	87
3.2.2 Immunohistochemical analysis of the human and porcine mitral valve annulus.....	88
3.3 Results	89
Part (1) Characterisation of the native human mitral annulus.....	89
3.3.1 Histological and histochemical characterisation of the native human mitral annulus	89
3.3.2 Distribution of proteins in the extracellular matrix of the human mitral annulus.....	99
3.3.2.1 Collagen I	100
3.3.2.2 Collagen II	103

3.3.2.3 Collagen III	106
3.3.2.4 Collagen IV.....	107
3.3.2.5 Collagen VI.....	110
3.3.2.6 Fibronectin	112
3.3.2.7 Laminin.....	114
3.3.3 Deposition of calcium in the extracellular matrix of the human mitral annulus.....	115
Part 2 Characterisation of the native porcine mitral annulus	117
3.3.4 Histological and histochemical characterisation of the native porcine mitral valve annulus	117
3.3.5 Distribution of proteins in the extracellular matrix of the porcine mitral annulus	126
3.3.5.1 Collagen I	126
3.3.5.2 Collagen II	128
3.3.5.3 Collagen III	131
3.3.5.4 Collagen IV.....	132
3.3.5.5 Collagen VI.....	134
3.3.5.6 Fibronectin	137
3.3.5.7 Laminin.....	139
3.4 Discussion.....	141
3.5 Conclusion	148
Chapter 4 Development of a decellularised porcine mitral valve annulus	150
4.1 Introduction	150
4.1.1 Chemical methods used in tissue decellularisation	152
4.1.1.1 Biological agents	152
4.1.1.2 Detergents.....	152
4.1.1.3 Hypotonic/hypertonic buffers.....	154
4.1.2 Physical methods	154
4.2 Aims	156
4.3 Objectives	156
4.4 Methods	157
4.4.1 Decellularisation solutions.....	157
4.4.1.1 EDTA solution (10% w/v EDTA).....	157
4.4.1.2 SDS solution (10%; w/v SDS)	157
4.4.1.3 BSA solution (5 mg.ml ⁻¹ BSA)	157

4.4.1.4 Magnesium Chloride (1M)	157
4.4.1.5 Magnesium Chloride (10M)	157
4.4.1.6 Hypertonic solution (50 mM tris, 1.5 M sodium chloride)	157
4.4.1.7 Hypotonic buffer (10 mM tris, 2.7 mM EDTA, 10 KIU.ml ⁻¹ aprotinin)	158
4.4.1.8 SDS hypotonic buffer (0.1 %; w/v SDS, 2.7 mM EDTA, 10 KIU.ml ⁻¹ aprotinin)	158
4.4.1.9 Nuclease solution 1 (50 mM Tris, 10 mM MgCl ₂ , 50 U.ml ⁻¹ DNase, 1 U.ml ⁻¹ RNase)	158
4.4.1.10 Nuclease solution 2 (50 mM Tris, 10 mM MgCl ₂ , 1 U.ml ⁻¹ Benzonase)	158
4.4.1.11 Nuclease solution 3 (50 mM Tris, 1 mM MgCl ₂ , 10 U.ml ⁻¹ Benzonase)	158
4.4.1.12 PBS	159
4.4.1.13 PBS wash buffer with aprotinin (10 KIU.ml ⁻¹ aprotinin)	159
4.4.1.14 Peracetic acid (PAA) solution (0.1 %; v/v)	159
4.4.1.15 PBS wash buffer with EDTA, Aprotinin	159
4.4.2. Decellularisation of the porcine mitral annulus	159
4.4.2.1 Method 1 - 1 cycle SDS	159
4.4.2.2 Method 2 – 2 cycles SDS	160
4.4.2.3 Method 3 – 3 cycles SDS	160
4.4.2.4 Method 4 – RNase and DNase	160
4.4.2.5 Method 5 - 2 cycles of SDS with freeze thaws	161
4.4.2.6 Method 6- Increased Benzonase and reduced magnesium chloride concentration	161
4.4.2.7 Method 7 - 6 x freeze thaw	161
4.4.2.8 Method 8 - Multiple wash cycles	161
4.4.3 Determination of the effectiveness of the decellularisation methods (Methods 1-8)	161
4.4.3.1 Histological evaluation of the porcine mitral valve annuli following application of various decellularisation methods	162
4.4.3.2 DNA quantification of the porcine mitral valve annuli following application of various decellularisation methods	163
4.5 Results	164
4.5.1 Method 1: One cycle of SDS	164

4.5.2 Method 2: Two cycles of SDS	164
4.5.3 Method 3: Three cycles of SDS.....	165
4.5.4 Method 4: RNase and DNase	165
4.5.5 Method 5: Two freeze thaw cycles	165
4.5.6 Method 6: Increased Benzonase and reduced magnesium chloride concentration.....	166
4.5.7 Method 7: Multiple freeze thaw cycles.....	166
4.5.8 Method 8: Multiple wash cycles post PAA sterilisation	167
4.6 Discussion	172
Chapter 5 Characterisation of the decellularised porcine mitral valve annulus	175
5.1 Introduction	175
5.2 Aims	178
5.3 Objectives	178
5.4 Methods	179
5.4.1 Analysis of the final decellularisation method (Method 8).....	181
5.4.2 Histological evaluation of the human and porcine mitral valve annulus	182
5.4.3 Immunohistochemical analysis of the decellularised porcine valve annulus	182
5.4.4 Labelling the α -gal epitope using biotinylated GSL-1 lectin.....	182
5.4.5 Extract cytotoxicity assay of the decellularised porcine valve annulus	183
5.4.6 Contact cytotoxicity assay of the decellularised porcine valve annulus	184
5.4.7 Biomechanical testing of the native and decellularised porcine mitral valve annuli.....	185
5.5 Results	186
5.5.1 Histological and histochemical characterisation of decellularised porcine mitral valve annulus	186
5.5.2 Distribution of proteins in the extracellular matrix of decellularised porcine mitral annulus	191
5.5.2.1 Collagen I	191
5.5.2.2 Collagen II	193
5.5.2.3 Collagen III	195
5.5.2.4 Collagen IV.....	197
5.5.2.5 Collagen VI.....	199

5.5.2.6 Fibronectin	201
5.5.2.7 Laminin.....	204
5.5.2.8 Alpha-gal localisation using lectin	206
5.5.3 Extract cytotoxicity assays of decellularised porcine mitral valve annuli	209
5.5.4 Contact cytotoxicity assays of decellularised porcine mitral valve annuli	211
5.5.5 Biomechanical characterisation of native and decellularised porcine mitral valve annuli.....	213
5.6 Discussion.....	222
Chapter 6 In vitro evaluation of decellularised porcine mitral annulus for annuloplasty repair.....	228
6.1 Introduction	228
6.1.1 Aims and objectives	230
6.2 Material and methods.....	231
6.2.1 Working solutions.....	231
6.2.1.1 PBS wash buffer with EDTA (0.1 % w/v), Aprotinin (10 KIU.ml ⁻¹ aprotinin).....	231
6.2.1.2 Transport medium	231
6.2.1.3 Trypsin (11250 U.ml ⁻¹) solution	231
6.2.2 Static regurgitation testing of porcine mitral valves	231
6.2.2.1 Fresh porcine heart preparation	232
6.2.2.2 Static test rig preparation	233
6.2.2.3 Healthy heart model	235
6.2.2.4 Positive control heart model.....	236
6.2.2.5 Regurgitant porcine heart model.....	237
6.2.2.6 Repaired heart model.....	243
6.3 Results	247
6.3.1 Healthy porcine heart model	247
6.3.2 Positive control heart model	248
6.3.3 Regurgitant models	248
6.3.3.1 Stretched annulus	248
6.3.3.2 Trypsin injection around the mitral valve annulus..	249
6.3.3.3 Ruptured chordae	249
6.3.3.4 Papillary muscle dilation.....	250
6.3.3.5 Super glued leaflets and annulus	250
6.3.3.6 Trimmed left ventricular myocardium	250

6.3.3.7 Bisected mitral valve annulus at the left commissure.....	251
6.3.3.8 Cauterising the mitral valve leaflets.....	251
6.3.3.9 Zinc fixed mitral valve.....	252
6.3.4 Mitral valve repair.....	252
6.4 Discussion.....	254
Chapter 7 Discussion.....	258
7.1 General Discussion.....	258
7.2 Conclusion.....	270
References.....	271

List of Tables

Table 1.1 – Comparison of the annular geometry of normal valves (controls) to valves suffering from ischaemic mitral regurgitation at end-diastole.....	18
Table 1.2 – Comparison of the annular geometry of normal valves (controls) to valves suffering from ischaemic mitral regurgitation at end-systole.....	19
Table 1.3 – Summary of papers presenting patients who have undergone mitral valve annuloplasty with synthetic rings.....	28
Table 1.4 – Repair techniques used in children (more than one technique could be used per repair).....	37
Table 2.1 – Equipment used during the research.....	49
Table 2.2 – Consumables and plastic ware used during the research.	51
Table 2.3 – The chemicals and reagents used during this study.....	53
Table 2.4 – Cell lines used in this study.	58
Table 2.5 – Equipment used for dissection.	60
Table 2.6 – Tissue processor station solutions and durations.....	66
Table 6.1 – Regurgitation rates for mitral valves of healthy porcine hearts.....	247
Table 6.2 – Regurgitation rates for mitral valves of positive control hearts.....	248
Table 6.3 – Regurgitation rates for porcine mitral valves with ruptured chordae	249
Table 6.4 – Regurgitation rates for porcine mitral valves with bisected mitral valve annuli	251

List of Figures

Fig 1.1 – Anatomical view of the heart during diastole	5
Fig 1.2 – Microstructure of the mitral valve anterior leaflet layers in sheep	6
Fig 1.3 – Heart right lateral view of the left ventricle.....	8
Fig 1.4 – Top view of the mitral annulus and surrounding mitral complex.....	10
Fig 1.5 – Reconstruction of the human mitral annulus acquired by transesophageal echocardiography	12
Fig 1.6 – The changes of annular area index (annular area/body area) during the cardiac cycle.....	13
Fig 1.7 – Pericardial strip used for posterior annuloplasty.....	34
Fig 2.1a – Dissection of porcine and human mitral valve annulus. Images of the porcine dissection	62
Fig 2.1b – Dissection of porcine and human mitral valve annulus. Images of the porcine dissection.....	63
Fig 2.2 – Top view of mitral valve	65
Fig 2.3 – Mitral annulus and leaflets.....	79
Fig 2.4 – Tissue specimen dimensions	80
Fig 2.5 – Equipment used for tensile testing of native and decellularised porcine annuli	80
Fig 2.6 – Instron 3365 test rig with Instron Biobath set at 37 °C with tissue clamped in custom made grips undergoing the test procedure.....	81
Fig 2.7 – Typical stress-strain curve of mitral valve annuli tissue subjected to uniaxial tensile loading to failure.	82
Fig 3.1 – Mitral annulus split into segments	87
Fig 3.2a – Images of H&E stained sections from different segments of the native human mitral valve annulus	92
Fig 3.2b – Images of H&E stained sections from different segments of the native human mitral valve annulus	93
Fig 3.3 – Images of alcian blue stained sections from different segments of the native human mitral valve annulus.....	94
Fig 3.4a – Images of Sirius red Miller's stained sections from different segments of the native human mitral valve annulus viewed under (a) polarised light and (b) bright field microscopy	96

Fig 3.4b – Images of Sirius red Miller's stained sections from different segments of the native human mitral valve annulus viewed under (a) polarised light and (b) bright field microscopy	97
Fig 3.5 – Images of Von Kossa stained sections from different segments of the native human mitral valve annulus.....	98
Fig 3.6a – Sections of human mitral valve annulus stained with antibody to collagen I	101
Fig 3.6b – Sections of human mitral valve annulus stained with antibody to collagen I	102
Fig 3.7a – Sections of human mitral valve annulus stained with antibody to collagen II	104
Fig 3.7b – Sections of human mitral valve annulus stained with antibody to collagen II	105
Fig 3.8a – Sections of human mitral valve annulus stained with antibody to collagen III	106
Fig 3.8b – Sections of human mitral valve annulus stained with antibody to collagen III	107
Fig 3.9a – Sections of human mitral valve annulus stained with antibody to collagen IV	108
Fig 3.9b – Sections of human mitral valve annulus stained with antibody to collagen IV	109
Fig 3.10a – Sections of human mitral valve annulus stained with antibody to collagen VI	110
Fig 3.10b – Sections of human mitral valve annulus stained with antibody to collagen VI	111
Fig 3.11a – Sections of human mitral valve annulus stained with antibody to fibronectin	112
Fig 3.11b – Sections of human mitral valve annulus stained with antibody to fibronectin	113
Fig 3.12a – Sections of human mitral valve annulus stained with antibody to laminin	114
Fig 3.12b – Sections of human mitral valve annulus stained with antibody to laminin	115
Fig 3.13 – Sections of native human mitral valve annulus stained with H&E, Von Kossa and labelled with antibodies to collagen II	116
Fig 3.14a – Images of H&E stained sections from different segments of the porcine mitral valve annulus.....	118
Fig 3.14b – Images of H&E stained sections from different segments of the porcine mitral valve annulus.....	119
Fig 3.15 – Images of alcian blue stained sections from different segments of the native porcine mitral valve annulus.....	121

Fig 3.16a – Images of Sirius red Miller's stained sections from selected segments of the native porcine mitral valve annulus viewed under (a) polarised light and (b) bright field microscopy	123
Fig 3.16b – Images of Sirius red Miller's stained sections from selected segments of the native porcine mitral valve annulus viewed under (a) polarised light and (b) bright field microscopy	124
Fig 3.17 – Images of Sirius red Miller's stained sections from selected segments of the native porcine mitral valve annulus viewed under polarised light microscopy	125
Fig 3.18a – Sections of porcine mitral valve annulus stained with antibody to collagen I	127
Fig 3.18b – Sections of porcine mitral valve annulus stained with antibody to collagen I	128
Fig 3.19a – Sections of porcine mitral valve annulus stained with antibody to collagen II	129
Fig 3.19b – Sections of porcine mitral valve annulus stained with antibody to collagen II	130
Fig 3.20a – Sections of porcine mitral valve annulus stained with antibodies to collagen III.....	131
Fig 3.20b – Sections of porcine mitral valve annulus stained with antibodies to collagen III.....	132
Fig 3.21a – Sections of porcine mitral valve annulus stained with antibody to collagen IV.....	133
Fig 3.21b – Sections of porcine mitral valve annulus stained with antibody to collagen IV.....	134
Fig 3.22a – Sections of porcine mitral valve annulus stained with antibody to collagen VI.....	135
Fig 3.22b – Sections of porcine mitral valve annulus stained with antibody to collagen VI.....	136
Fig 3.23a – Sections of porcine mitral valve annulus stained with antibody to fibronectin	137
Fig 3.23b – Sections of porcine mitral valve annulus stained with antibody to fibronectin	138
Fig 3.24a – Sections of porcine mitral valve annulus stained with antibody to laminin	139
Fig 3.24b – Sections of porcine mitral valve annulus stained with antibody to laminin	140
Fig 4.1 – Mitral valve annulus, following application of various decellularisation methods split into segments	162
Fig 4.2a – Images of H&E stained sections from anterior and posterior segments of the porcine mitral valve annulus decellularised using different methods	168

Fig 4.2b – Images of H&E stained sections from anterior and posterior segments of the porcine mitral valve annulus decellularised using different methods	169
Fig 4.2c – Images of H&E stained sections from anterior and posterior segments of the porcine mitral valve annulus decellularised using different methods	170
Fig 4.3 – Images of DAPI stained sections from segments of the porcine mitral valve annulus decellularised using alternative methods	171
Fig 4.4 – DNA content of native and decellularised mitral valve annulus decellularised using Methods 5 to 8	172
Fig 5.1 – Porcine mitral valve annulus decellularisation protocol	180
Fig 5.2 – Decellularised mitral valve annulus split into segments.....	181
Fig 5.3a – Images of Sirius red Miller's stained sections from the anterior segments of the decellularised porcine mitral valve annulus viewed under polarised light microscopy and bright light microscopy	187
Fig 5.3b – Images of Sirius red Miller's stained sections from the posterior segments of the decellularised porcine mitral valve annulus viewed under polarised light microscopy and bright light microscopy	188
Fig 5.4 – Images of alcian blue stained sections from the anterior and posterior segments of the decellularised porcine mitral valve annulus.....	190
Fig 5.5a – Sections of decellularised porcine mitral valve annulus stained with antibodies to collagen I.....	192
Fig 5.5b – Sections of decellularised porcine mitral valve annulus stained with antibodies to collagen I.....	193
Fig 5.6a – Sections of decellularised porcine mitral valve annulus stained with antibodies to collagen II.....	194
Fig 5.6b – Sections of decellularised porcine mitral valve annulus stained with antibodies to collagen II.....	195
Fig 5.7a – Sections of decellularised porcine mitral valve annulus stained with antibodies to collagen III.....	196
Fig 5.7b – Sections of decellularised porcine mitral valve annulus stained with antibodies to collagen III.....	197
Fig 5.8a – Sections of decellularised porcine mitral valve annulus stained with antibodies to collagen IV	198
Fig 5.8b – Sections of decellularised porcine mitral valve annulus stained with antibodies to collagen IV	199
Fig 5.9a – Sections of decellularised porcine mitral valve annulus stained with antibodies to collagen VI	200

Fig 5.9b – Sections of decellularised porcine mitral valve annulus stained with antibodies to collagen VI	201
Fig 5.10a – Sections of decellularised porcine mitral valve annulus stained with antibodies to fibronectin	202
Fig 5.10b – Sections of decellularised porcine mitral valve annulus stained with antibodies to fibronectin	203
Fig 5.10c – Sections of decellularised porcine mitral valve annulus stained with antibodies to fibronectin	204
Fig 5.11a – Sections of decellularised porcine mitral valve annulus stained with antibodies to laminin.....	205
Fig 5.11b – Sections of decellularised porcine mitral valve annulus stained with antibodies to laminin.....	206
Fig 5.12a – Sections of decellularised porcine mitral valve annulus labelled with lectin	207
Fig 5.12b – Sections of decellularised porcine mitral valve annulus labelled with lectin	208
Fig 5.13 – ATP content of BHKs incubated with decellularised annulus extracts.....	209
Fig 5.14 – ATP content of L929s incubated with acellular annulus extracts.....	210
Fig 5.15 – Contact cytotoxicity of decellularised porcine mitral valve annulus tissues cultured with BHK cells	211
Fig 5.16 – Contact cytotoxicity of decellularised porcine mitral valve annuli cultured with L929 cells	212
Fig 5.17 – Stress/strain curves for native and decellularised porcine mitral valve annuli in region 1 (posterior region).....	213
Fig 5.18 – Stress/strain curves for native and decellularised porcine mitral valve annuli in region 2 (right commissural region).....	214
Fig 5.19 – Stress/strain curves for native and decellularised porcine mitral valve annuli in region 3 (anterior region)	214
Fig 5.20 – Stress/strain curves for native and decellularised porcine mitral valve annuli in region 4 (left commissural region).....	214
Fig 5.21 – The Young's Modulus in the elastic phase of each region of the native and decellularised porcine mitral valve annulus.....	216
Fig 5.22 – The Young's Modulus in the collagen phase of each region of the native and decellularised porcine mitral valve annulus.....	217
Fig 5.23 – The ultimate tensile stress in each region of the native and decellularised porcine mitral valve annulus	218
Fig 5.24 – The ultimate tensile strain in each region of the native and decellularised porcine mitral valve annulus	219
Fig 5.25 – The transition stress in each region of the native and decellularised porcine mitral valve annulus	220

Fig 5.26 – The transition strain in each region of the native and decellularised porcine mitral valve annulus	221
Fig 6.1 – Preparation of porcine tissue for static testing.....	233
Fig 6.2 – Side profile of static test rig	234
Fig 6.3 – Porcine heart attachment to the static test rig	235
Fig 6.4 – Positive control for the regurgitant porcine heart model.	237
Fig 6.5 – Different methods of inducing mitral valve regurgitation in the porcine heart	238
Fig 6.6 – Injection sites for trypsin	240
Fig 6.7 – Preparation of porcine heart tissue repaired with synthetic annuloplasty ring for static testing	244
Fig 6.8 Preparation of porcine heart tissue repaired with decellularised porcine mitral valve annuloplasty ring for tissue for static testing.....	246
Fig 6.9 – Regurgitation testing of porcine hearts using synthetic and decellularised annuloplasty rings	253
Fig 6.10 – Percentage decrease in regurgitation after repair with an annuloplasty ring (n=5).....	253

List of Abbreviations

A	Annulus
AT	Anterior Annulus
Ao	Aorta
AA	Ascending Aorta
AC	Anterior coronary artery
AM	Atrial myocardium
ATP	Adenosine triphosphate
AML	Anterior mitral valve leaflet
ANOVA	Analysis of variance
AV	Atrioventricular
AVL	Aortic valve leaflet
t	Average thickness
BHK	Baby hamster kidney cells
BSA	Bovine Serum Albumin
c	Cable Tie
cm	Centimetre
Δ/	Change in length
CHAPS	3-[(3-cholamidopropyl)dimethylammonio]-1-propanesulfonate
Coll-E	Collagen phase
CI	Confidence interval
A₁	Cross sectional area
DAPI	4',6-diamidino-2-phenylindole
DNase	Deoxyribonuclease I
DNA	Deoxyribonucleic acid
DMSO	Dimethyl sulfoxide
DMEM	Dulbecco's Modified Eagle Medium
EI-E	Elastin phase
EDTA	Ethylenediaminetetraacetic acid
ECM	Extracellular matrix
FBS	Foetal bovine serum
F	Force
FI	Flow
α-gal	Galα1,3-Galβ1-4GlcNAc-R
GAG	Glycosaminoglycan
GFs	Growth factors
GMEM	Glasgow's minimal essential media
H&E	Haematoxylin & eosin

H	Heart
h	Hour
HBSS	Hanks Balanced Salts Solution
HEPES	Hydroxyethyl-piperazineethane-sulfonic acid buffer
HRP	Horseradish peroxidase
IMR	Ischaemic Mitral Regurgitation
KIU	Kallidinogenase Inactivator Units
L929	Murine adipose fibroblast cells
L	Leaflet
LA	Left Atrium
AU	Left Auricle
LV	Left Ventricle
MA	Mitral to aortic continuum
MB	Mounting Block
MMPs	Matrix metalloproteinases
MS	Mean square
MSCs	Mesenchymal stem cells
ml	Millilitre
mm	Millimeter
MSD	Minimum significant difference
min	Minute
MPa	Megapascals
MV	Mitral valve
MVR	Mitral valve regurgitation
M	Molarity
NYHA	New York Heart Association
L_o	Original length
P	Posterior annulus
PAA	Peracetic acid
PBS	Phosphate buffered saline
P4HB	Poly-4-hydroxybutyrate
PCL	Poly(caprolactone)
PGA	Polyglycolic acid
PGS	Poly(glycerol sebacate)
PGA/PLLA	Polyglycolic acid/ poly L-lactic acid
PGA/PLA	Polyglycolic acid/ polylactic acid
PLA	Polylactic acid
PLGA	Polylactic acid/ polyglycolic acid
PERV	Porcine endogeneous retrovirus
ΔP	Pressure difference across valve
R	Resistance to flow
RNase	Ribonuclease I

RNA	Ribonucleic acid
RV	Right ventricle
SVR	Saddle height ratios
s	Second
S	Spigot
SMCs	Smooth muscle cells
SD	Standard Deviation
SDS	Sodium dodecyl sulphate
SE	Standard error
ϵ	Strain
δ	Stress
SRM	Sirius red Miller's
3D	Three dimensional
TE	Tissue engineering
ϵ_t	Transition strain
σ_t	Transition stress
TOE	Transoesophageal echocardiography
T	Trigones
TBS	Tris buffered saline
ϵ_s	Ultimate tensile strain
UTS	Ultimate tensile strength
σ_s	Ultimate tensile stress
VM	Ventricular muscle
v/v	Volume per volume
VICs	Valve interstitial cells
w	Width
w/v	Weight per volume

Chapter 1 Introduction

1.1 General Introduction

Annuloplasty is a common surgical procedure used to treat mitral valve dysfunction by reconstructing a part of the heart valve called the annulus. The technique is used to treat people who have a leaky valve, known as regurgitation. Annually there are over 300,000 people who undergo open heart surgery for mitral valve treatment (Bonow *et al.*, 2006). Mitral regurgitation is the second most common valve disease in European treatment centres (lung *et al.*, 2007) and the most common valve disease in the US (Nkomo *et al.*, 2006) which equates to a prevalence in the US population of 1.7% (Nkomo *et al.*, 2006). There has been a year on year increase in the number of mitral valve repair operations and the requirement for improved materials for repair is an important factor for providing better outcomes for patients who have valve disease.

Current annuloplasty strategies predominantly use synthetic annuloplasty rings to reconstruct the annulus. This benefits the patient by reducing the valve orifice area which allows the leaflets to coaptate during systole, thereby removing or reducing valve regurgitation. Many types of ring are available which each have their advantages and disadvantages but none have been found to be significantly better than another (Chee *et al.*, 2008; Bothe *et al.*, 2010a). The main drawbacks to using the synthetic rings include a change in normal annular dynamics, geometry and force distribution when compared to a healthy valve (Yamaura *et al.*, 1997; Glasson *et al.*, 1999; Jensen *et al.*, 2008). Moreover, they are not suitable for use in children as the rings do not grow with the child.

A biological acellular annuloplasty ring could reduce mitral valve regurgitation by ensuring effective leaflet coaptation whilst offering improved performance compared to annuloplasty rings currently in use. The main advantage of using a biological acellular ring would be that it could integrate with the mitral valve of the patient and remodel over time. It is anticipated that the remodelling process will permit the ring to closely match the dynamics of the valve for the duration of the cardiac cycle whilst eliminating mitral regurgitation.

This thesis is concerned with using novel techniques to remove all the cells from annulus tissues to produce a biological acellular annuloplasty ring, removing the risk of tissue rejection whilst retaining the biological and biomechanical properties of the tissue extracellular matrix.

1.2 The Heart

The heart pumps blood around the body via the arteries, capillaries and veins. The blood contains oxygen and nutrients required by the cells in the body to function normally. The heart is encased in the pericardium, a double walled membrane which encloses the pericardial cavity, containing serous fluid. The pericardium helps protect the heart and reduces friction during the cardiac cycle. There are four chambers of the heart, these are composed of myocardium which is lined with endocardium on the inside and epicardium on the outside, the endocardium surface is smooth to prevent clotting as the blood interacts with it. The top two chambers are called the left and right atria which have relatively thin walls compared to the bottom two chambers. The bottom two chambers are called the left and right ventricles which are thick walled in comparison.

The right atrium receives deoxygenated blood from the body via the superior vena cava and the inferior vena cava and delivers it to the right ventricle, between the right atrium and right ventricle is the tricuspid valve. This valve prevents backflow of blood into the right atrium during systole. During systole the ventricle contracts and pumps blood to the lungs via the pulmonary artery, from the lungs oxygenated blood flows into the left atrium via four pulmonary veins. During diastole blood flows from the left atrium into the left ventricle via the mitral valve, this valve prevents backflow of blood into the left atrium during systole. The wall of the left ventricle is the thickest of all the heart chambers, this is to enable blood within the ventricle to be pumped to the rest of the body. The blood leaves the left ventricle via the aorta; this is the largest artery in the body (Sanders & Scanlon, 1997). The heart undergoes a specific sequence of muscular contractions during the cardiac cycle. The atria simultaneously contract followed by the simultaneous contraction of the ventricles. The atria contract at a point when blood delivered into the atria from the veins reaches a pressure which forces the atrioventricular valves to open, the main volume of blood is delivered into the ventricles passively but the final milliliters of blood are delivered by the contraction of the atria. Once delivered the atria relax and the ventricles contract which forces the atrioventricular valves shut, this contraction forces

the blood into the arteries and the ventricles start to relax. The cardiac cycle continuously repeats this sequence (Sanders & Scanlon, 1997).

The blood within the atrium at pressure P_1 is forced through into the ventricle at pressure P_2 when there is a difference in blood pressure across the valve ($P_1 - P_2$), known as the pressure gradient (ΔP). The pressure gradient is the force driving the flow which can be calculated as the flow (FI) multiplied by the resistance to the flow (R):

$$\Delta P = FI \times R$$

The pressure gradient increases if either the flow rate or resistance increases. A valve that is functioning normally has a small resistance to flow which minimises the pressure gradient. If the valve experiences stenosis the resistance will increase due to the narrowing of the valve which increases the pressure gradient. Exercise further exacerbates the pressure gradient by increasing the flow rate (Klabunde, 2011). In a regurgitant valve there is normally a smaller change in the pressure gradient, this is due to the heart remodelling to increase its size in an attempt to pump more blood around the body.

The cardiac skeleton encircles the aortic, pulmonary, mitral and tricuspid valves which are positioned in a plane, often referred to as the base of the heart. It is composed of dense connective tissue which provides structure and support for the dynamic heart tissue, including the myocardium, leaflets and arteries. The skeleton helps anchor the valves and prevents them from distending under pressure during the cardiac cycle. It also provides an insertion point for the atrial and ventricular muscle whilst separating them (Hill, 1986), this insulates the atria and ventricles which helps regulate the cardiac cycle by preventing a singular contraction of the muscle (du Plessis *et al.*, 2014). The strongest region of the cardiac skeleton is the central fibrous body, this is formed from the membranous region of the ventricular septum and the right trigone. The right fibrous trigone is located between the anterior mitral valve and the aortic valve leaflets. The left fibrous trigone also makes up this area of fibrous tissue but is smaller in size and situated towards the left zone of the region (Bateman *et al.*, 2013). A membranous region is formed between the right and left trigone, known as the mitral to aortic continuum or the intertrigonal space, which lacks the fibrous skeletal structure that forms the cardiac skeleton (Kunzelman, 1997). From the fibrous trigones and an additional smaller fibrous body which is situated at the right coronary leaflet of the aortic valve, the cardiac skeleton extends around the cardiac valves of the heart (Zimmerman, 1966), thereby

providing the supporting function to the valves alongside the additional roles previously mentioned.

1.2.1 Atrioventricular Valves

Heart valves open and close approximately 40 million times per year, this equates to about three billion times over an average lifetime (Schoen, 2008). The atrioventricular valves (AV) are situated between the atria and ventricles on both sides of the heart. They act as fluid control components which permit only unidirectional blood flow during the cardiac cycle (Sacks *et al.*, 2009). The AV valves comprise the mitral valve (MV) and the tricuspid valve which vary only slightly in their anatomical structures (Fig 1.1). The interactions between the components of the valve are important to consider when the valve is being repaired (Fedak *et al.*, 2008). A valve that is functioning normally coordinates each component of the valve, this enables the leaflets to coaptate and provide low leaflet stresses during systole (Schoen, 2008). The AV apparatus consists of a set of leaflets, chordae, a set of papillary muscles and an annulus. The main focus of this study will be the mitral valve and so this will be described in further detail.

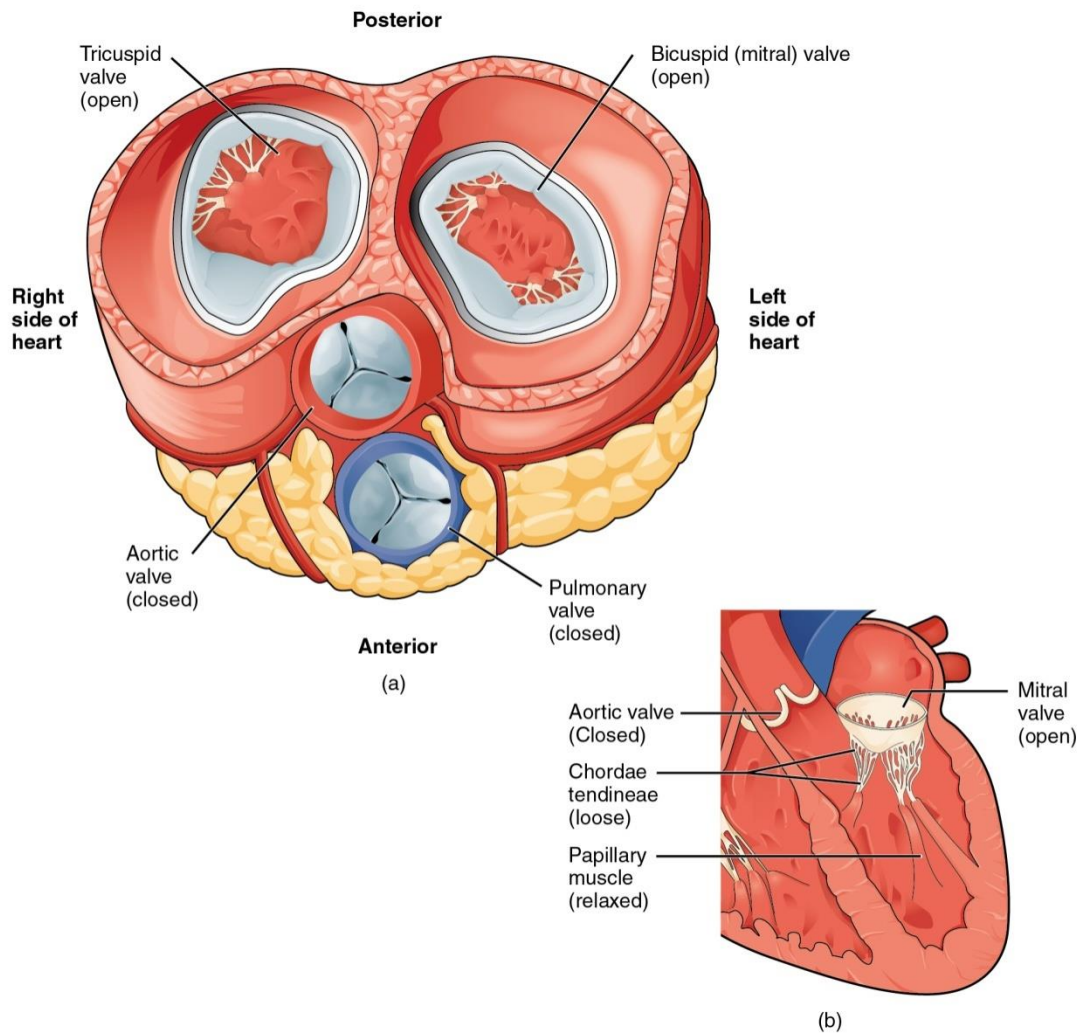


Fig 1.1 – Anatomical view of the heart during diastole¹

Normal healthy leaflets of the mitral valve are thin, flexible, soft and translucent (Ho, 2002). In the mitral valve the leaflets are split into the anterior and posterior leaflets which are separated by two depressions; these are the anterolateral and posteromedial commissures. At this point the commissural chordae insert into the ventricular surface of the leaflet. The leaflets are never completely separate from each other. The anterior leaflet is located in close proximity to the aortic root (Ho, 2002). The anterior leaflet can be split into a rough zone and clear zone which are separated by a ridge; this ridge forms the site of leaflet closure during systole. The rough zone is a region where the marginal chordae insert and is located close to

¹ Reprinted from OU Human Physiology: Heart Anatomy, Eric Bright & Heather Ketchum. OpenStax CNX. Jun 17, 2015
<http://cnx.org/contents/ba66e9d1-0a16-49a5-8724-233dcec203f5@1>
Licensed under Creative Commons BY 4.0.

the free edge of the leaflet on the ventricular surface. During systole the rough zone will coapt with the corresponding rough zone on the posterior leaflet (Ranganathan *et al.*, 1970). The clear zone is located between the rough zone and the annulus and is so called because it is void of any chordae insertions. The posterior leaflet is located close to the coronary sinus and is opposite the aortic root. The posterior leaflet surrounds a larger portion of the perimeter of the valve than the anterior leaflet (Ho, 2002). The posterior leaflet comprises of three zones; the rough zone, the clear zone and the basal zone. The rough and the clear zones have the same characteristics as the anterior leaflet zones. In addition, the basal zone, which is located between the clear zone and the annulus, is the insertion point for the basal chordae.

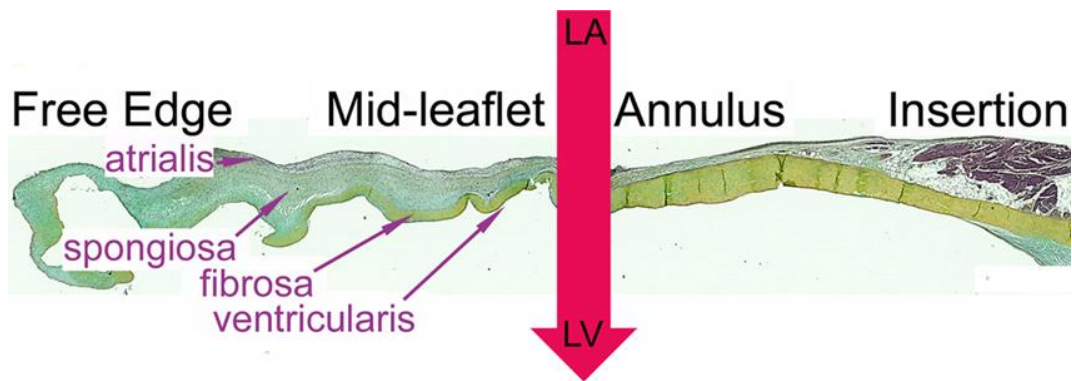


Fig 1.2 – Microstructure of the mitral valve anterior leaflet layers in sheep. Red arrow denotes direction of blood flow from left atrium (LA) to left ventricle (LV).²

The mitral valve leaflets are composed of four layers (Fig 1.2): these are the ventricularis, fibrosa, spongiosa and atrialis (Gross & Kugel, 1931; Kunzelman *et al.*, 1993; Flanagan & Pandit, 2003). Situated closest to the ventricular side of the leaflet is the ventricularis. This layer is the thinnest layer composed of collagen and profuse with elastin, functionally this permits the leaflets to undergo repeated cyclic deformation during the cardiac cycle (Kunzelman *et al.*, 1993; Culav *et al.*, 1999). The fibrosa is the central layer of the leaflet, the layer consists of thick collagen bundles orientated predominantly circumferentially. Collagen is crimped during diastole and

² Reprinted from Stephens *et al.*, (2008) The Effects of Mitral Regurgitation Alone Are Sufficient for Leaflet Remodeling, *Circulation*, 118, 14-1, S243-249 Copyright © 2008 by Wolters Kluwer Health, Inc. Reprinted by permission of Wolters Kluwer Health, Inc.

uncrimps during systole, this uncrimping of the collagen allows the leaflets to close. The thick collagen bundles of the fibrosa form the load bearing element of the mitral valve leaflets which help prevent prolapse of the valve leaflets when the valve is closed during systole (Kunzelman *et al.*, 1993). The spongiosa bounds the fibrosa on the atrial side of the leaflet, loose randomly orientated connective tissue and proteoglycans make up this layer, the glycosaminoglycan's (GAGs) in this layer absorb the compressive forces produced during the cardiac cycle. On the outer atrial side of the leaflet is the atrialis, composed predominantly of elastin fibres which are able to tolerate the cyclic loading which the leaflets experience throughout systole and diastole. The relative thicknesses of the four layers vary from the free edge to the attachment at the annulus (Kunzelman *et al.*, 1993). The fibrosa is abundant at the annular junction but absent from the free edge, replaced by the spongiosa, atrialis and ventricularis where the high GAG content in the spongiosa help buffer the leaflets as they oppose each other when the valve is closed (Kunzelman *et al.*, 1993).

The papillary muscles originate close to the apex and the middle third of the left ventricle wall (Lam *et al.*, 1970). They prevent the leaflets from prolapsing during systole by contracting and tethering the leaflets via the chordae attachments. There are two regions of papillary muscle, the anterolateral papillary muscle and the posterolateral papillary muscle (Fig 1.3). The anterolateral papillary muscle is supplied by the left anterior descending artery whilst the posteromedial papillary muscle is supplied by the right coronary artery. The chordae arise from the tips of the papillary muscles which then insert into the ventricular surfaces of the mitral valve leaflets (Ho, 2002). The chordae tether the leaflets to the papillary muscles; during systole chordae prevent the movement of the mitral valve into the atrium ensuring regurgitation does not occur (Sacks *et al.*, 2009).

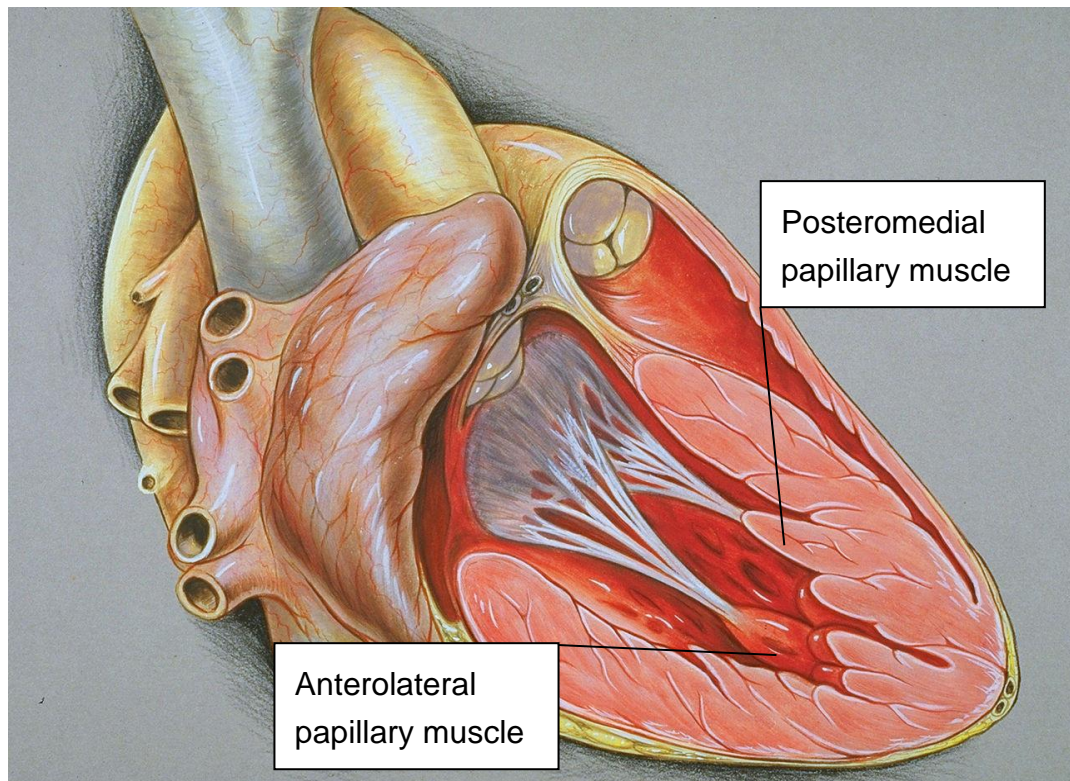


Fig 1.3 – Heart right lateral view of the left ventricle.³

Chordae must be elastic, strong and resistant to fatigue in order to transmit forces through them during the cardiac cycle (Millington-Sanders *et al.*, 1998). Chordae tendineae have two structural levels; a dense collagen core and an elastin sheath. During the cardiac cycle the valves experience three types of loading; tension when preventing back flow, shear when blood is passing and flexure when the valve is opening and closing (Sacks *et al.*, 2009). The anterior leaflet comprises of two types of chordae, the marginal chordae and strut chordae. The posterior leaflet comprises of three types of chordae; marginal, basal and the commissural chordae (Liao & Vesely, 2003). Collagen in the chordae consists of crimped fibrils, these orientate in the direction of maximum stress (Shi & Vesely, 2004) whilst interwoven elastin fibres are found spread around the inner core, as well as in a distinct layer near the outer surface surrounding by a layer of endothelial cells.

³ "Heart right lateral view" by Patrick J. Lynch, medical illustrator - Patrick J. Lynch, medical illustrator. Licensed under CC BY 2.5 via Wikimedia Commons -

https://commons.wikimedia.org/wiki/File:Heart_right_lateral_view.jpg#/media/File:Heart_right_lateral_view.jpg

The ventricular myocardium is a highly organised structure which is mainly composed of fibroblasts and cardiac myocytes; it is the cardiac myocyte that provides the primary contractile function to the myocardium (Walker & Spinale, 1999). The wall contains three layers; the endocardium, the myocardium and the epicardium. The endocardium is composed of simple squamous epithelium and thin subendothelial tissue. The myocardium is composed of the cardiac muscle fibres and the epicardium is composed of simple squamous mesothelium and subepicardial tissue (Ho, 2002). The ventricular myocardium is responsible for the change in circumference of the posterior part of the mitral valve during the cardiac cycle (Walmsley, 1978).

The myocardium has been studied by Ho (2009) who observed that the myocardium of the left ventricle comprised of three layers; the superficial (subepicardial), middle and deep (subendocardial) layers. The fibre orientation in each layer changed, but the layers interconnected with each other and were not isolated. The superficial layer contained fibres which were orientated approximately 10-20° to the long axis, originating at the mitral valve and occupying approximately 25% of the myocardial wall thickness. The middle layer contained fibres which were circumferentially orientated, these aligned almost parallel to the orifice of the mitral valve but did not insert into it. The middle layer occupied approximately 53-59% of the wall thickness. The deep layer of the myocardium was found to contain muscle fibres which were longitudinally orientated and inserted into the mitral valve.

The primary contractile cell of the ventricle is the myocyte, this is surrounded by collagenous connective tissue known as the basement membrane, endomysium and the perimysium. The basement membrane is present between the myocyte and the network of endomysium (Fratzl, 2008). The membrane functions to provide the myocyte with an interface for adhesion and to act as a barrier for exchange of macromolecules between the myocyte and extracellular space (Walker & Spinale, 1999). The endomysium surrounds the myocyte and provides a supporting structure and coordinates force transmission. The perimysium surrounds groups of myocytes and absorbs shear forces (Fratzl, 2008).

The collagen content of the mitral valve leaflets and chordae has been analysed. In normal valves 83 % of the content has been shown to be water and 67 % of the dry weight was collagen. The types of collagen found in normal valves were collagens I, III and V (Hammer *et al.*, 1979; Cole *et al.*, 1984). Type I accounted for 49 % of the dry weight, type III accounted for

16.1 % and type V accounted for 1.4 % of the dry weight (Cole *et al.*, 1984). The cardiac myocardium contains collagen IV. This is primarily found in the basement membrane of the myocardium, found between the extracellular space and intracellular space of the myocyte (Walker & Spinale, 1999). The basement membrane also contains glycoproteins, laminin, fibronectin, glycosaminoglycans and proteoglycans.

1.2.2 Mitral Valve Annulus

1.2.2.1 Structure

The mitral valve annulus is a junction where the atrial and ventricular muscles are separated and the leaflets intersect the valve. The annulus has been described as a thin fibrofatty membrane (Silbiger & Bazaz, 2009) that is divided into posterior and anterior regions which are separated by the left and right trigones (Ormiston *et al.*, 1981) (Fig 1.4).

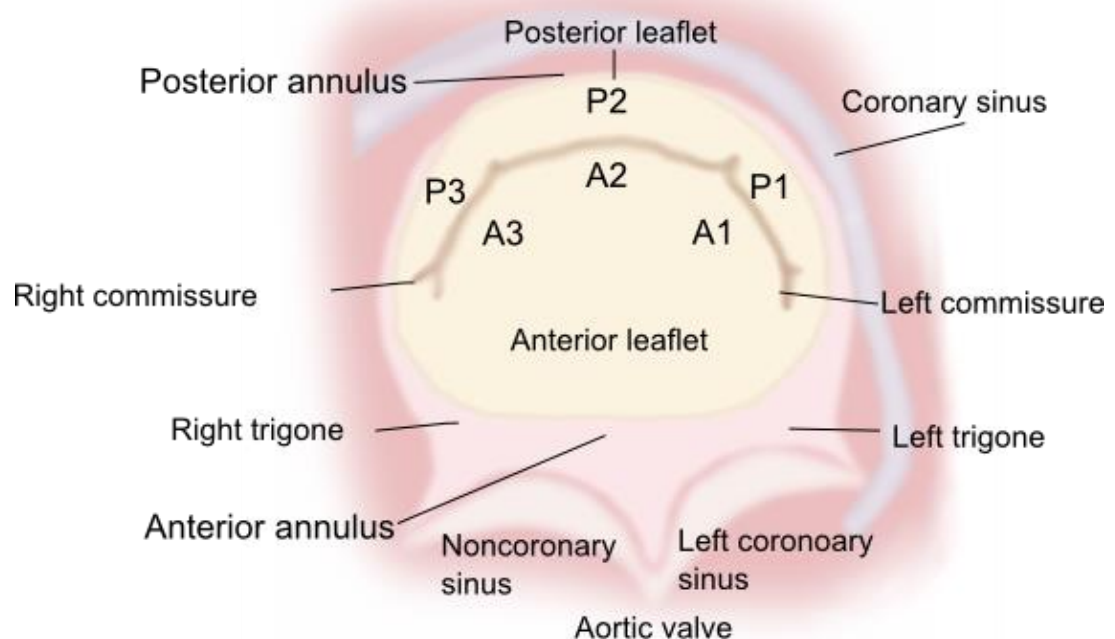


Fig 1.4 – Top view of the mitral annulus and surrounding mitral complex. P1, P2, P3 are the posterior leaflet clefts; A1, A2, A3 are the anterior leaflet clefts.

In the region of the left and right trigones there is a thick and organized fibrous structure (Angelini *et al.*, 1988), at this point the annulus acts as a hinge for the anterior leaflet into which the atrial myocardium inserts. The right fibrous trigone accommodates the atrioventricular conduction bundle

(Ho, 2002) and is situated in the midline of the heart. This forms a link between the aortic, mitral and tricuspid valves (Ormiston *et al.*, 1981). The left trigone forms an attachment for part of the fibrous skeleton of the heart and links the left margin of the aortic and mitral valves (Ormiston *et al.*, 1981). The annulus forms a hinge point with the atrial myocardium, the mitral valve leaflet and the ventricular myocardium. The posterior part of the annulus has muscular and flexible properties, whilst the anterior region is fibrous and stiff (Levine *et al.*, 1989; Jimenez *et al.*, 2003). The posterior region is more prone to dilation and is more likely to be affected by calcification (McCarthy *et al.*, 2010) due to the lack of fibrous tissue (Ho, 2002). The anterior region makes up a third of the annulus; it is in continuity with the aortic valve and the fibrous trigones, this results in the anterior annulus being fibrous and relatively stiff. Angelini *et al.* (1988) performed a histological study to visualize the histioarchitecture of the mitral annulus in human hearts. The fibrous tissue of the annulus was found to be organized in segments as a thin curtain like structure or a cord like structure. Adipose tissue was often found in the gaps where the atrial myocardium did not meet the hinge of the leaflet and only one of the hearts analysed (n=11) had a fibrous cord like structure running around the whole of the heart. The human annulus has been studied by using ventricular illumination and histological analysis (Berdajs *et al.*, 2007). A translucent band like membrane structure was found between the left ventricular myocardium and the atrial myocardium when using ventricular illumination. The band separated the atrial myocardium and the ventricular myocardium and provided attachment to the leaflets centrally to it. The band surrounded the mitral orifice and continued to the fibrous trigones, extending to the membranous septum. At a histological level the translucent membrane was found to be a fibrous band connecting the posterior leaflet, the left atrium and left ventricle. The hinge point of the valve was the attachment point of the left atrium close to the leaflet. The ventricular side of the mitral leaflet was found to continue into the fibrous membrane whilst the atrial side of the leaflet continued into the left atrium. The atrial muscle on the posterior portion of the valve extended into the proximal half of the posterior leaflet. This was thought to provide a sphincter like contraction. The aortic to mitral continuum at the anterior region of the valve was anchored across the valve orifice by the fibrous tissue between the trigones. Histological analysis of the anterior leaflet showed no apparent membrane or fibrous condensations in the anterior region.

1.2.2.2 Function

The function of the annulus is to assist the leaflets to coapt during systole and provide stress reduction around the mitral valve through its fibrous structure and saddle like geometry (Fig 1.5). The annulus undergoes complex 3-dimensional changes throughout the cardiac cycle, including; changes to the saddle height, anterior-posterior diameter, commissure – commissure diameter and to the annular area (Glasson *et al.*, 1996; Watanabe *et al.*, 2005).

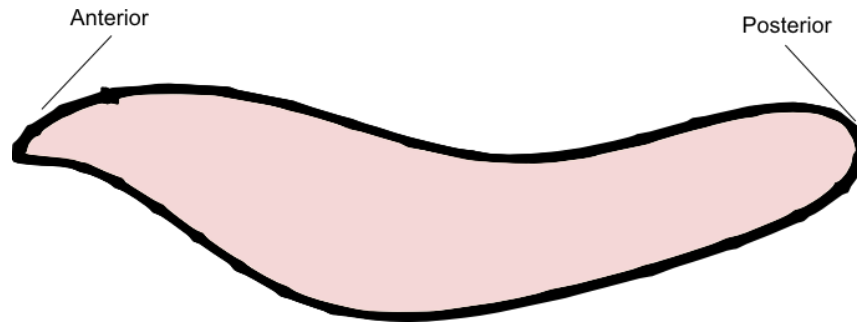


Fig 1.5 – Reconstruction of the human mitral annulus acquired by transesophageal echocardiography. The low points of the saddle are the commissures (Based on Salgo, 2002).

The healthy annulus deforms into a saddle shape during systole and reverts into a flat profile at diastole; the maximum ratio of the height of the annulus to the width of the annulus at the commissures is approximately 15% (Levine *et al.*, 1989; Salgo, 2002; Timek *et al.*, 2005; Jensen *et al.*, 2008).

There have been multiple studies using 2D and 3D echocardiography to examine the shape and motion of the mitral annulus. The dimensions of the annulus have been studied by Ormiston *et al.* (1981). Using 2D echocardiography the mitral valve annulus dimensions were calculated by taking recordings of the annular diameter at 30° intervals around the circumference and reconstructed 12 times during the cardiac cycle. Eleven healthy human volunteers were selected for the study which took place over a period of eight months. The average maximum area was $7.1 \pm 1.3 \text{ cm}^2$ (mean \pm SD) which occurred at late diastole, this reduced by $26 \pm 3 \%$ to a minimum of 5.2 cm^2 at mid-systole (Fig 1.6). The average maximum circumference was $9.3 \pm 0.9 \text{ cm}$ which reduced by $13 \pm 3 \%$ to 8.0 cm during systole. During systole the annulus was found to move down towards the apex of the heart. The main limitation of this study was that data was processed from 2D echocardiography, the 3D motion and geometry could not be measured and it was assumed that the annulus was flat in profile.

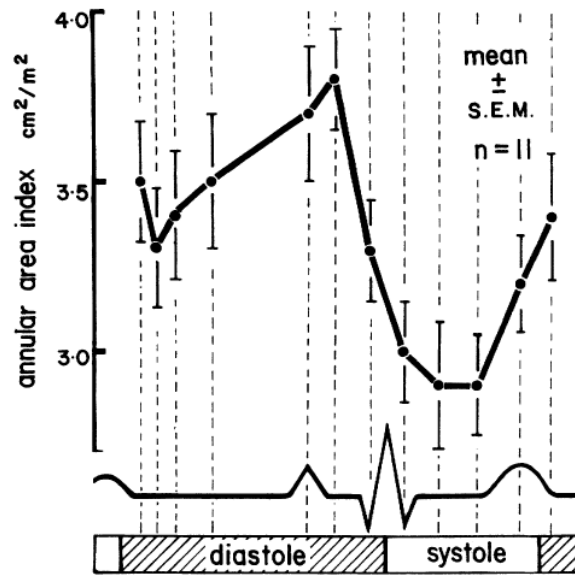


Fig 1.6 – The changes of annular area index (annular area/body area) during the cardiac cycle. Reprinted by permission of Wolters Kluwer Health, Inc.⁴

Flachskampf *et al.* (2000) conducted a study of the annulus in ten healthy adults using 3D transoesophageal echocardiography (TOE). The results showed that during systole the annular area contracted by approximately 23.8 %; this reached a minimum at end-systole and a maximum at end-diastole. The average area was $11.8 \pm 2.5 \text{ cm}^2$ which agreed with a similar study by Kaplan *et al.* (2000). Ormiston *et al.* (1982) also conducted a study to investigate annular area but the area was found to be smaller. The reasons for these differences may have been in the way that the perimeter of the annulus was calculated either using 2D or 3D methods.

Salgo *et al.* (2002) conducted a study on three healthy adults using 3D TOE and undertook computational analysis of the results to recreate the annular perimeter. The aim of the study was to further understand what effect the dynamic annular shape had on the function of the valve during the cardiac cycle. Using computational methods, the saddle height to inter-valley distance ratio (SVR) was altered in order to understand how the changes

⁴ Reprinted from Ormiston *et al.*, (1981) Size and motion of the mitral valve annulus in man. I. A two-dimensional echocardiographic method and findings in normal subjects, *Circulation*, 61, 4, 113-120 Copyright © 1981 by Wolters Kluwer Health, Inc. Reprinted by permission of Wolters Kluwer Health, Inc.

affected stresses in the annular perimeter. It was found that the lowest stresses were found when the parabola had a SVR of between 15-25 % and highest when the parabolic surface was flat.

The saddle shape of the annulus is thought to reduce systolic strain on the central region of the mitral valve anterior leaflet (Jimenez *et al.* 2007), reduce leaflet stress (Salgo, 2002) and optimize the distribution of chordal forces (Jimenez *et al.*, 2003; Padala *et al.*, 2009). The highpoints of the saddle shaped annulus are found close to the mid-anterior and mid-posterior regions, the low points are found at the antero-lateral and postero-medial commissures (Rausch *et al.*, 2011). The saddle shape is associated with the normal function of the mitral valve; any deviation away from the normal geometry can cause MV insufficiency (Rausch *et al.*, 2011).

In an *in vitro* study by Jimenez *et al.* (2003), eight porcine mitral valves were tested under normal physiological haemodynamic conditions in a left heart simulator. The aim of the study was to identify the stress and strains experienced by the leaflets from an increasing annular saddle curvature. The authors found that as the saddle curvature increased there was a significant reduction in the area for the anterior region of the anterior leaflet. The largest reduction in strain was in the radial direction of the annulus, with a smaller reduction in the circumferential strain. These findings illustrated that a change in the annulus saddle curvature causes anisotropic behaviour in the mitral leaflets.

Two main types of motion have been identified during the cardiac cycle (Silbiger & Bazaz, 2009); sphincteric contraction and translation in the vertical plane. The movement of the annulus is the product of the contraction in the muscles of the atrium and ventricles (Pai *et al.*, 2003). During systole the annulus translates along the left ventricular major axis resulting from torsion at the base of the left ventricle (Burns *et al.*, 2008). This translation generates an increase in left atrial filling (Keren *et al.*, 1988). Through the period of diastole the annulus experiences an increase in area and translates from the apex of the left ventricle towards the atrium; this motion assists in the transfer of blood from the atrium into the ventricle (Toumanidis *et al.*, 1992).

1.3 Mitral valve disease

1.3.1 Epidemiology

Every year over 300,000 people undergo treatment for mitral valve dysfunction worldwide. In Europe mitral regurgitation (MR) was found to be the second most common form of valve disease in a survey of treatment centres, with just under half of the patients with MR undergoing mitral valve repair (Iung *et al.*, 2003). Approximately 44,000 people undergo treatment for mitral valve dysfunction per year in the US (Bonow *et al.*, 2006). The prevalence of heart valve disease in the US population is approximately 2.5% and this approximates to 4.2-5.6 million US adults (Nkomo *et al.*, 2006), a number which is expected to double by 2030 due to longer life expectancy and population growth. Mitral regurgitation was found to be prevalent in 1.7% of this population, making it the most common form of valve disease in the US (Nkomo *et al.*, 2006). The type of therapeutic procedure that is undertaken depends on the experience of the surgeon, the mechanisms involved and the cause of regurgitation as these factors determine if a valve is suitable for repair (Carpentier, 1983).

The main causes of mitral valve regurgitation in developed countries are mitral valve prolapse due to degenerative disease and ischemia due to coronary artery disease. In developing countries rheumatic disease is the main cause (Enriquez-Sarano *et al.*, 2009). Mitral regurgitation can often progress without any symptoms because the heart is initially able to balance the reduction in left ventricle output by remodeling the left atrium and left ventricle to a larger volume which can lead to poor long term outcomes for the patient (Enriquez-Sarano *et al.*, 2009).

1.3.2 Types of disease

There are two main forms of mitral valve dysfunction; mitral valve stenosis and mitral regurgitation. Mitral valve stenosis can be treated with a replacement valve or by balloon catheter valvuloplasty, regurgitation can be treated with repair or valve replacement. Annuloplasty is the repair of choice for valves that suffer from mitral regurgitation.

1.3.2.1 Mitral regurgitation

There are two types of mitral regurgitation (MR); primary and secondary. Primary MR, also known as organic MR, is caused by a valve apparatus which has been structurally disrupted or compromised (Schmitto *et al.*, 2010). Secondary MR, also known as functional MR, results from the failure

of coaptation between the leaflets when the valve is structurally normal and regurgitation is caused by disease extrinsic to the valve (Schmitto *et al.*, 2010). In this type of regurgitation the papillary muscles, chordae, leaflets and annulus all appear normal.

1.3.2.1.1 Primary mitral regurgitation

Primary MR is often caused by degenerative or congenital MV disease. Degenerative MV disease can result from a range of conditions in which changes in the tissue cause rupture or elongation of the MV chordae, this can result in leaflet prolapse and annular dilation (Anyanwu & Adams, 2007). The main types of degenerative diseases are; primary myxomatous, primary flail leaflet and annular calcification. A valve with myxomatous disease is associated with mitral valve prolapse (Etchells *et al.*, 1997; Anyanwu & Adams, 2007). Prolapse can be described as a valve leaflet which moves into the left atrium during systole (Levine *et al.*, 1987). Myxomatous degeneration has been found to alter the leaflets in the mitral valve; an increase in glycosaminoglycans (GAGs) and change in matrix composition alters the spongiosa layer, valve water content and increases leaflet thickness (Grande-Allen *et al.*, 2003). In a study by Gupta *et al.* (2009) the primary proteoglycans involved were found to be decorin, biglycan and versican which were more abundant in valves with myxomatous disease than in normal controls.

In developing nations, rheumatic fever is the most prevalent form of MV disease, in its chronic stage rheumatic disease causes chordal shortening and leaflet retraction along with annular dilation (Acar *et al.*, 2004). In developed nations the incidence of patients with rheumatic fever has reduced when compared to the start of the twentieth century but there has been an increase in recent years (Ryan *et al.*, 2000).

When the endothelial lining of the heart is damaged due to intravascular trauma, the change to the endothelium combined with increased coagulation leads to the deposition of platelets and fibrin on the injured site of the tissue. The correct environment is established for bacterial attachment and proliferation which most commonly occurs in the mitral valve (Karchmer, 2001), resulting in infective endocarditis. The frequent sites of attachment in the valves are downstream from regurgitant flow; in the case of the mitral valve this would be the atrial surface. The effects of endocardial infection can be severe, ranging from; valve regurgitation due to the destruction of tissue, embolic infarction from the debris of the vegetative infection, the

spread of the infection to other organs and tissue damage because of immune complex deposition (Karchmer, 2001). Antibiotics are the first line of treatment used to manage endocarditis with the choice of antibiotic depending upon the etiological organism, the type of valve (native or prosthetic) and the immune status of the patient (Bonow *et al.*, 1998).

1.3.2.2.2 Secondary Mitral Regurgitation

Secondary MR commonly results from left ventricular systolic dysfunction. The dysfunction of the left ventricle coexists with neuro-hormonal activation, myocyte loss and local hemodynamics which produce dilation of the left ventricle and left ventricle remodeling (Andrus & Baldwin, 2006). The lack of leaflet coaptation due to secondary MR results from annular dilation, a reduction in annular contraction during systole and displacement of the papillary muscles due to left ventricle dysfunction and dilation (Schmitto *et al.*, 2010). Other reasons for secondary MR include ischaemic papillary muscle dysfunction which occurs when the muscle or muscle wall attachment is ischaemic. This causes abnormal muscle contraction (Andrus & Baldwin, 2006) leading to lack of leaflet coaptation. Severe hypertension and extrinsic volume overload can also be the cause for secondary MR (Andrus & Baldwin, 2006). Treatment for secondary MR is not well defined and controversy still exists regarding the pathophysiology and best treatment. Current opinion generally agrees with the view that secondary MR derives from a ventricular etiology which has caused ventricular dilation. Treatment for this type of MR has remained controversial because of its association with poor long term survival (Schmitto *et al.*, 2010).

Ischaemic heart disease is commonly a chronic disease which causes secondary mitral regurgitation. The valve appears normal in ischaemic heart disease. Regurgitation occurs due to the displacement of the apex of the left ventricle and tethering of the chordae which results in lack of leaflet coaptation. The displacement of the apex caused by left ventricle remodelling in patients who have had myocardial infarction leads to movement of the papillary muscles away from the annulus (lung, 2003), which increases tension on the chordae and tethering of the leaflets (Messas *et al.*, 2001; Tanemoto, 2005; Yiu *et al.*, 2000). If ischaemic heart disease is caused by myocardial infarction then ventricular function will often be reduced, decreasing the leaflet closing force (He *et al.*, 1997). Dysfunction in the ventricle is further compounded by ventricular remodeling resulting from ischaemic mitral regurgitation. There is an increase in left ventricular end-diastolic volume and wall stress resulting from an increased pre-load

(Laskey *et al.*, 2007; Yiu *et al.*, 2000), this causes further dysfunction and an increase in tenting from papillary muscle displacement (Rumberger, 1994). The annulus can enlarge if the left ventricle dilates which will further increase ischaemic mitral regurgitation (Kron *et al.*, 2002). Grande-Allen *et al.* (2005) assessed if mitral valves that appeared normal in patients with heart failure exhibited signs of primary MR. Regurgitation in patients with congestive heart failure is normally thought of as secondary because the valve appears normal on echocardiographs or on gross pathological examination. Changes to the structure of the valve are thought to occur because the geometry of the ventricle and valves alter from their normal state, this leads to an increase in loading on the valves after long term changes to valvular loading patterns. In the study by Grande-Allen *et al.* (2005) they established that the extracellular matrix components in mitral valves were significantly different from those of normal control subjects matched for age. It was suggested that the loading conditions experienced by the valve contribute to the remodeling. When compared to the controls the patient's valves were found to have become fibrotic with significantly increased proportions of collagen, concentrations of GAG's and DNA with a decrease in water concentration.

1.3.3 Annulus remodeling due to disease

Mitral valve disease can change the annular geometry which can have a negative impact on the whole of the valve. The dimensions of the human annulus in normal and diseased valves were found to be significantly different by Ahmad *et al.* (2004). Using three dimensional echocardiography normal valves were compared to regurgitant valves. The results showed that there was a significant increase in the annular perimeter and annular area of regurgitant valves during the whole cardiac cycle compared to the normal controls (Table 1.1 and 1.2). At end-systole (Table 1.2) the inter-trigonal distance and posterior area of the regurgitant valves also showed a significant difference when compared to the controls.

Table 1.1 – Comparison of the annular geometry of normal valves (controls) to valves suffering from ischaemic mitral regurgitation at end-diastole

Variable	Controls	IMR	p Value
Annular perimeter (cm)	8.6 ± 0.2	10.7 ± 0.7	0.03
Anterior annular perimeter (cm)	4.1 ± 0.2	5.0 ± 0.4	0.08
Posterior annular perimeter (cm)	4.5 ± 0.2	5.6 ± 0.5	0.06

Intertrigonal distance (cm)	2.1 ± 0.1	2.8 ± 0.3	0.06
Annular area (cm ²)	5.7 ± 0.3	9.1 ± 1.2	0.03
Anterior annular area (cm ²)	2.5 ± 0.2	4.0 ± 0.7	0.08
Posterior annular area (cm ²)	3.2 ± 0.3	5.1 ± 0.9	0.08
Values are mean ± standard error of the mean			
IMR = ischaemic mitral regurgitation			

Adapted from Ahmad *et al.*, (2004)

Table 1.2 – Comparison of the annular geometry of normal valves (controls) to valves suffering from ischaemic mitral regurgitation at end-systole

Variable	Controls	IMR	p Value
Annular perimeter (cm)	9.5 ± 0.4	10.2 ± 0.6	0.03
Anterior annular perimeter (cm)	4.4 ± 0.4	4.6 ± 0.3	0.06
Posterior annular perimeter (cm)	5.2 ± 0.2	5.6 ± 0.4	0.04
Intertrigonal distance (cm)	2.3 ± 0.2	2.7 ± 0.2	0.01
Annular area (cm ²)	7.1 ± 0.5	8.3 ± 1.0	0.03
Anterior annular area (cm ²)	2.9 ± 0.5	3.4 ± 0.5	0.06
Posterior annular area (cm ²)	4.1 ± 0.2	4.9 ± 0.7	0.03
Values are mean ± standard error of the mean			
IMR = ischaemic mitral regurgitation			

Adapted from Ahmad *et al.*, (2004)

In pathological conditions the posterior part of the annulus was initially thought to increase in circumference whilst the anterior annulus did not, this was thought to be due to the vicinity of the fibrous trigones to the annulus. Research by Hueb *et al.* (2002) and Ahmad *et al.* (2004) however, established that the anterior annulus dilated in patients with pathological conditions which could trigger mitral regurgitation. Ahmad *et al.* (2004) used 3D echocardiography to characterise annular geometry and motion in patients with ischaemic MR. Patients were found to have annular dilation with an increase in inter-trigonal distance and anterior and posterior perimeters; this was coupled with restriction in annular motion. This was in agreement with a study by Nguyen *et al.* (2008) who established that

annular dilation occurred predominantly in the septal-lateral dimension in patients and was accompanied by a flattening of the annular 3D saddle shape. Jimenez *et al.* (2005) conducted a study to investigate the effects of annular motion, annular flexibility and papillary muscle displacement on the distribution of chordal forces in an *in-vitro* model on human mitral valves. The investigators used a left heart simulator with a flexible annulus model and established that papillary muscle displacement significantly increased force on the anterior strut, posterior intermediate and commissural chordae. They also found that annular motion increased tension on the basal chords. The displacement of the papillary muscles induced tenting of the leaflets because of increased tension on the intermediate chords which lead to regurgitation. The authors also hypothesized that the lengths of the basal chords may cause the annulus to be saddle shaped during systole. Mihalatos *et al.* (2007) investigated the effects that remodeling of the mitral annulus had on mitral regurgitation. A 3D echocardiography imaging study was completed which established that as the severity of MR increased there was an associated increase in the majority of 3D systolic annular dimensions as well as an increase in diastolic measurements. It was also established that the sphericity index decreased as MR increased which demonstrated that either the length of the left ventricle decreased or the left ventricle width increased. The sphericity index was measured by dividing the length of the left ventricle by the width of the left ventricle, the length was defined as the distance between the mitral annulus to the apex. With an increase in MR there was a significant increase in all the systolic and diastolic measurements for the left ventricle and left atrium ($P < 0.001$). Annular tension was studied by He & Bhattacharya (2008) during valve closure. The annulus experienced two different types of force whilst the valve was closed; it received centripetal forces from the leaflets and the left ventricle myocardium delivered centrifugal forces. In the study the tension increased with an increase of annulus area, trans-mitral pressure and in apical papillary muscle displacement. Nguyen *et al.* (2008) found that the mitral annular dimensions for valves suffering from pure mitral regurgitation underwent dilation only in the commissure to commissure dimension.

1.4 Mitral Valve Disease Treatment

1.4.1 Replacement

The surgical procedure most commonly used for advanced valvular heart disease is valve replacement (Schoen & Levy, 1999). Mechanical heart valves were the first replacement valves to be introduced clinically in 1960's (Bonow *et al.*, 1998). Mechanical, bioprosthetic, donor and synthetic valves have all been investigated for valve replacement. The majority of prostheses available have been designed for aortic valve replacement and are inverted for use in the mitral valve position. The flow characteristics through the mitral valve differ from the aortic valve; therefore, prosthetic valves are not always suited for mitral valve implantation (Daebritz *et al.*, 2003).

1.4.2 Types of Replacement Valve

1.4.2.1 Mechanical valves

Mechanical valves were the first type of replacement to be used. Mechanical valves have the inherent problems of thrombogenicity and perivalvular leak when the valve is in a closed position (Hammermeister *et al.*, 1993). Mechanical valves have excellent durability, which means they are often used in younger patients and those who have an active lifestyle. However lifelong use of anti-coagulants are required to reduce the risk of thrombosis (Jones, 1994).

1.4.2.2 Bioprosthetic valves

Bioprosthetic valves are constructed from glutaraldehyde treated xenogeneic tissue obtained from bovine or porcine sources (Mohammadi & Mequanint, 2011), which are either sewn into a synthetic stent or are stentless.

Bioprosthetic valves are often used when it is thought the valve will outlive the patients, this limits their use to older patients and those with chronic diseases (Jones, 1994). Compared to mechanical valves bioprosthetic valves allow a central flow providing good haemodynamics.

Bioprosthetic valves do not require the use of anticoagulants, but compared to mechanical valves they have a reduced lifespan of between 10-15 years because of the effect that cross-linking has on durability (Oliveira & Antunes, 2006).

1.4.2.3 Pulmonary autograft

Valve replacement with an inverted pulmonary autograft has been used in patients with mitral valve dysfunction (Kumar *et al.*, 2009). The technique is based around the Ross procedure. The pulmonary autograft is inserted onto a Dacron conduit 2.5 cm long. The mitral valve is prepared by excising the valve whilst preserving the papillary muscles. The Dacron conduit is sutured onto the mitral annulus, which fastens the valve into place. Subsequently, a cryopreserved pulmonary homograft is used to replace the pulmonary valve. By using an autograft, lifelong anticoagulation is avoided whilst retaining valve function and combined with a tissue that is living leads to a graft that offers good durability and good haemodynamics (Kumar *et al.*, 2009).

1.4.2.4 Synthetic valves

Early hopes with synthetic valves were based on the hypothesis that they could combine the advantages of bioprosthetic and mechanical valves by offering good durability, good haemocompatibility and reduced risk from thrombosis (Zdrahala & Zdrahala, 1999; Bernacca *et al.*, 2002). Although they offer good haemocompatibility and reduced thrombogenic risk, durability is a major problem which has been attributed to low biostability and calcification during *in-vivo* animal studies (Ghanbari *et al.*, 2009). This has limited their use and they are not yet clinically used.

1.4.3 Repair

Compared to mitral valve replacement and medical management, mitral valve repair has been found to offer improved long term survival, freedom from cardiac morbidity and quality of life in patients with mitral regurgitation (Gillinov *et al.*, 2001; Grossi *et al.*, 2001).

Five main techniques have been used for mitral valve repair; quadrangular resection, edge to edge repair, re-suspension of leaflet, bow-tie and annuloplasty. Of these techniques, annuloplasty has often been performed simultaneously with other techniques. The outcomes of mitral valve repair are assessed by freedom from residual or recurrent mitral regurgitation. Mitral regurgitation is commonly associated with annular deformation (Raffoul *et al.*, 1998) highlighting the requirement for annulus reconstruction as an important factor for this type of repair.

1.5 Annuloplasty

Annuloplasty is a repair procedure performed to optimise annular dimensions and shape (Rausch *et al.*, 2011) when the annulus has undergone dilation, or it can be used to provide support and reinforcement to the valve when used in association with other repair techniques. The aim of annuloplasty is to increase leaflet coaptation and preserve annular shape and motion. Ideally a repair to the annulus should reconstruct the native valve apparatus while preserving the dynamic nature of the annulus (Kheradvar & Gharib, 2007). Reconstruction of the annulus is conventionally performed using an annuloplasty ring or pericardial patch, of which four main types are available; rigid ring, flexible ring, semi-rigid ring and bioprosthetic ring. Rings are usually only available in adult sizes, these range from 26 mm to 40 mm in diameter measured commissure to commissure.

1.5.1 Annuloplasty rings

1.5.1.1 Synthetic rings

The rigid ring has been designed to provide reshaping of a substantially dilated annulus occurring with left ventricular dysfunction (De Bonis *et al.*, 2011). The flexible ring has been designed to retain the three dimensional geometry of the native annulus (Cosgrove *et al.*, 1995). The semi-rigid ring has been designed to provide leaflet coaptation and maintain valve integrity during systole and offer good hemodynamics during valve opening in diastole (Carpentier *et al.*, 1995).

1.5.1.1.1 Rigid ring

Carpentier created the rigid ring. These rings employed the philosophy of preserving the systolic shape of the mitral annulus. The Carpentier rigid ring is constructed from a titanium core and polyester fabric sheath. The core provides the strength and durability whilst the fabric allows integration of the mitral valve tissue into the ring.

1.5.1.1.2 Flexible Ring

Duran *et al.* (1978) proposed the idea of a flexible ring that would permit continuous changes of the geometry of the mitral annulus during the cardiac cycle. Functionally, it was thought that they would cause less restriction on annular dynamics, improve interaction between the valve and ventricle and preserve left ventricle function. Flexible rings were also introduced in an attempt to prevent geometric deformation and annular fixation during the annuloplasty procedure (Borghetti *et al.*, 2000).

1.5.1.1.3 Semi-rigid

The semi-rigid ring is flexible in the posterior segment becoming increasingly rigid in the anterior segment to accommodate the motion of the annulus. The rigidity in the ring was incorporated in order to reduce the stress on the sutures whilst supporting remodelling of the annulus (Bruno *et al.*, 2009). There are many different types of ring on the market. The Carpentier-Edwards Physio Annuloplasty Ring is a semi-rigid ring, it is constructed from layers of Elgiloy bands separated by polyester film strips and is surrounded by a silicon layer covered in polyester knit fabric. Elgiloy is a cobalt chromium alloy which has high strength, good ductility, long fatigue life, corrosion resistance and good biocompatibility (Shrivastava, 2003). The Sorin Memo 3D ring is a semi rigid complete ring. Its core consists of nitinol, which is a shape memory alloy; this alloy is used to re-establish the systolic diameter ratio during the cardiac cycle. On the outer core there is a sewing ring for attachment to the mitral valve. This is made from silicone and knitted polyester fabric and coated in turbostratic carbon (Carbofilm, Sorin Biomedica, Italy) to enhance haemocompatibility and biocompatibility (Bruno *et al.*, 2009). Saddle shaped annuloplasty rings were introduced to create a ring that was closer to the physiological shape of the native annulus. Saddle shaped rings do not lift the papillary muscles in the direction of the posterior annulus unlike planar rings, this allows greater leaflet mobility in the valve (Jensen *et al.*, 2011).

1.5.1.1.4 Pathology Specific rings

To improve outcomes annuloplasty rings addressing specific pathologies have also been produced. These include the Edwards Geform and IMR-ETlogix ring. The IMR-ETlogix ring was developed to deal with geometric asymmetric changes that can occur in the annulus and ventricle. Short term results have been positive, and have shown improvement in mitral annular diameter, tethering area and tenting height for ischaemic mitral regurgitation; although no long term results currently exist for this ring (Daimon *et al.*, 2006). Currently there is no treatment for ischaemic mitral regurgitation that provides improved outcomes. The most common procedure is an undersized annuloplasty using size 24 to 26 rings, alternative repair techniques using pericardial bands and patches have been found to deliver poor long term outcomes (McGee *et al.*, 2004). The results from a study involving 585 patients over a 17 year period showed that postoperatively 28% of patients had moderate MR or above (Tahta *et al.*, 2002).

1.5.1.1.5 Partial ring

Partial rings have also been used clinically, these were suggested by Odell *et al.*, (1995) because it was thought that the posterior annulus dilated and the anterior section was fixed with mitral valve disease. The ring is attached onto the posterior portion of the annulus to improve the posterior dynamics and restore the natural antero-posterior to transverse diameter ratio. There is now evidence that the dilation of the anterior mitral annulus increases in proportion with the posterior dilation of the annulus (Hueb *et al.*, 2002) and is not fixed as previously thought.

1.5.1.1.6 Ring comparisons

Of the techniques available for repair, annuloplasty is recommended because it offers improved outcomes when compared to all other type of repair but there are still limitations. There are limitations to synthetic annuloplasty use as current rings can change annular dynamics, geometry and force distribution of the MV (Yamaura *et al.*, 1997; Glasson *et al.*, 1999; Jensen *et al.*, 2008;). Studies in sheep (Quick *et al.*, 1997; Kunzelman *et al.*, 1998b) established that increased stress can increase collagen deposition, this may lead to thicker leaflets and affect leaflet closure. Computer models have been used to predict that if leaflet mobility is preserved then closing stresses are distributed more evenly (Kunzelman *et al.*, 1998a). Using standard sized flexible or semi-flexible rings may reduce the annulus area during diastole by 30% or more (Glasson *et al.*, 1999) which can affect the transfer of blood during filling. As well as reducing the annular area, it has been reported in ovine animal studies that the posterior leaflet was frozen in the closed position which resulted in a single leaflet opening process (Green *et al.*, 1999).

In a study by Kunzelman *et al.* (1998a) a finite element model was used to compare rigid to flexible rings. For rigid rings, simulated by loss of annular flexibility, there was increased stress in the leaflets and chordae and delayed leaflet coaptation. In an ideal flexible ring there was normal coaptation between leaflets and close to normal stresses (Kunzelman *et al.*, 1998a), although it was found that both sets of rings often behaved similarly when comparing annular dynamics (Dagum *et al.*, 2001; van Rijk-Zwikker *et al.*, 1990).

Another study investigated the annular dynamics of valves that were implanted into sheep with flexible partial (Tailor, St Jude Medical, Inc, St Paul, Minn) or complete rings (Duran, Medtronic, Inc, Minneapolis) (Dagum

et al., 2001). Radiopaque markers were sutured around the mitral annulus in the sheep. It was found that mitral annular folding, described as when the anterior section of the annulus flexes towards the atrium relative to the posterior part, was dampened in the complete ring group but was no different in the partial ring group when compared to the control. The partial ring in this instance preserved the mitral annular folding dynamics seen in normal valves. Importantly it was found that both of the ring types fixed the annular area throughout the cardiac cycle and no change in septal to lateral dimensions or commissural to commissural dimensions was observed showing that no annular contraction took place and leaflet coaptation was restricted. Tibayan *et al.* (2004) hypothesized that by preserving annular dynamics, coaptation between leaflets was likely to be assisted as the annulus contracts during systole.

The results from a completely randomised trial involving both rigid and flexible rings using 363 patients with mitral regurgitation showed that there was no significant difference in the rate of recurrence of significant mitral regurgitation over an eight year period (Chang *et al.* 2007). In the study a Carpentier Rigid Ring (n=186) or Duran Flexible Ring (n=170) was randomly assigned. Data was collected prospectively. The mean follow up was 46.6 ± 32.6 months (mean \pm SD). Left ventricle end diastolic diameter, left ventricle end systolic diameter and left atrial size significantly decreased for each group. Overall actuarial survival at ten years was $85.9\% \pm 4.9\%$ ($\pm 95\%$ CI) (Rigid Ring) and $75.7\% \pm 7.2\%$ (Flexible Ring). Eight year freedom from recurrence of significant MR (grade \geq 3) was $62.6\% \pm 19\%$ ($\pm 95\%$ CI) (Rigid Ring) and $55\% \pm 14.1\%$ (Flexible Ring) ($p=0.172$) using the Kaplan-Meier method. Rings implanted in those with a degenerative disease had the best durability with ten year freedom from operation of $87.6\% \pm 8.1\%$ ($\pm 95\%$ CI). Freedom from recurrence of significant MR (grade \geq 3) was $95.5\% \pm 2.2\%$ at 4 years and $53.8\% \pm 17\%$ at 8 years.

Chee *et al.* (2008) conducted a best evidence review for patients with mitral regurgitation and found that flexible rings improved left ventricle systolic function compared to rigid and semi-rigid rings but did not improve clinical outcomes. Other studies have reported varying degrees of mitral regurgitation over the medium to long term of grade three or above with a range from 18% (Flameng *et al.*, 2003) at seven years to close to 45% (Chang *et al.*, 2007) at eight years. The incidence of ischaemic MR is increasing which poses a challenge because ring annuloplasty is more likely to fail in this set of patients (Fedak *et al.*, 2008). Recurrence of severe MR in

this group is as high as 25% one year after surgery (McGee *et al.*, 2004; Tahta *et al.*, 2002).

A study of 169 patients with ischaemic mitral regurgitation by (Silberman *et al.*, 2009) comparing flexible rings (117 patients) to rigid rings (52 patients) found an increased frequency of regurgitation for those who had flexible rings. The postoperative follow up for the flexible ring group was 58 ± 30 months and 14 ± 7 months for the rigid ring group; 34% of the flexible group had residual mitral regurgitation of moderate grade or greater compared to 15% for the rigid group ($p=0.03$). Late mortality was observed in 32 of the patients within the flexible group. It was suggested that the rigid ring has improved results because it determines the annular shape by maintaining the anteroposterior to lateral diameter ratio more than the flexible ring. The large difference in the follow up period between the two groups and the retrospective nature of the study were shortfalls. Hu & Zhao (2011) performed a meta-analysis of flexible and rigid rings and established that flexible rings offer improvements in ejection fraction and in preserving the mitral orifice area. The flexible ring remained comparable to rigid rings for overall survival, mortality, reoperation, recurrence of regurgitation and left ventricle performance.

A study that compared the effectiveness of complete rings and partial rings for patients with chronic ischaemic mitral regurgitation found that complete rings achieved better results. Partial rings (semi-rigid ring Colvin-Galloway Future band) demonstrated $55.6 \pm 12.7\%$ freedom from recurrent mitral regurgitation and complete rings demonstrated $92.3 \pm 7.4\%$ (Semi rigid symmetric Carpentier-Edwards Physio ring) and $94.1 \pm 5.7\%$ (Semi rigid asymmetric Carpentier-McCarthy-Adams ring) freedom from recurrent MR (Onorati *et al.*, 2009).

A summary of the main papers describing the clinical outcomes of mitral valve annuloplasty repair are described in Table 1.3.

Table 1.3 – Summary of papers presenting patients who have undergone mitral valve annuloplasty with synthetic rings

Author ,date	Patient Group	Variable	Results
Chang et al., 2007	Flexible Ring n=170 Rigid Ring n=186	10 year survival 8 year freedom from significant regurgitation	Flexible ring: 75.7 ± 7.2 % (95 % CI) Rigid ring: 85 ± 4.9 % Flexible ring: 55 ± 14.1 % Rigid ring: 62.6 ± 18 %
Flameng et al., 2003	Rigid Ring n=218 Flexible Ring: n=24	7 year freedom from severe regurgitation	Rigid ring (90% of operations) and flexible ring (10% of operations): 71.1 ± 7.4 % (95 % CI) No comparison of outcomes between ring types
Hu & Zhao. 2011	Flexible Rigid Meta analysis		Rigid: Improvement in ejection fractions and in preserving the mitral orifice area Flexible: Comparable to rigid rings for overall survival, mortality, reoperation, recurrence of regurgitation and left

			ventricle performance
Silbiger & Bazaz. 2009	Ischaemic mitral regurgitation. Flexible: n=117 Rigid: n=52	Freedom from moderate mitral regurgitation	Flexible ring: 66 % (follow up 58 ± 30 months) Rigid ring: 85 % (follow up 14 ± 7 months)
Onorati. 2009	Ischaemic mitral regurgitation. Partial semi rigid: n=17 Complete semi rigid Physio ring: n=22 Complete semi rigid asymmetric: n=25	2 year freedom from chronic mitral regurgitation	Partial semi rigid: 55.6 ± 12.7% (SD) Complete semi rigid Physio ring: 92.3 ± 7.4 % Complete semi rigid asymmetric: 94.1 ± 5.7 %

Due to the multitude of different rings available it is difficult to determine which rings provide the best outcomes. Bothe *et al.* (2010) conducted two studies investigating the effects different types of rings have on mitral annular dimensions and dynamics using sheep. Five rings were used in both of the studies, these were; the Cosgrave Edwards rigid ring, St Jude rigid saddle shaped ring, Carpentier Edwards Physio flat ring, Edwards IMR ETLogix and the Edwards GEOForm cause specific rings. Of these, one ring was a partial ring (Cosgrave Edwards) and the rest were complete rigid rings of different geometries. The main findings showed that the maximum valve orifice size was reduced by all ring types, only the partial ring did not increase movement of the central region of the anterior leaflet and all except the ETLogix ring increased the closing and opening velocities of the anterior leaflet belly (Bothe *et al.*, 2010b). The four rigid rings reduced the anterior

mitral leaflet commissure to commissure distance during diastole but there was no effect on the septal to lateral dimensions. All of the rings decreased the septal to lateral and commissure to commissure distances when compared to the control. It was also found that the rings prevented changes in annular dimensions during systole and three of the rings, the Physio, IMR-ETlogix, and GeoForm produced a more planar annulus (Bothe *et al.*, 2010a).

Few studies had investigated the impact of device implantation on deformation, strain and curvature in the mitral valve; Rausch *et al.* (2012) conducted a study on 34 sheep to quantify how three frequently used annuloplasty rings affected native annular dynamics. Flexible incomplete, semi-rigid complete and rigid complete rings were implanted into the annuli of sheep and marked with tantalum markers around the circumference of the annulus. Biplane video-fluoroscopic images were sampled at a frequency of 60 Hz and mathematical splines were used to calculate changes to the mitral annulus. The splines were polynomial functions used to interpolate and approximate a given set of data points. The parameters that were analysed were septal to lateral and commissure to commissure dimensions taken from the best fit plane, using this data eccentricity and annular area were determined. From a line on the arc-length perimeter the three-dimensional perimeters were approximated. The saddle height was calculated as the distance of the commissure points to a plane passing through the mid anterior and posterior points. Using this data, strain, deformation and curvature were calculated. Without the devices implanted the changes in dimensions were $-14.4 \pm 5\%$ septal to lateral, $-5.7 \pm 2.1\%$ commissure to commissure, $+15.9 \pm 6.4\%$ in eccentricity, $-17.9 \pm 6.2\%$ in mitral annular area, $-6.4 \pm 2.1\%$ in annular perimeter and $+61 \pm 38.4\%$ saddle height. The strains in the normal annulus were 8% contraction in the posterior annulus and approximately 4% dilation in anterior annulus, relative to the strain at the minimum ventricular pressure. At all time-points for the flexible ring the strain did not go below zero in the posterior region, in contrast to this the normal annulus underwent contractile strains of -8%. Anterior strains remained unaffected when compared to the normally functioning annulus. At all time-points for the semi-rigid ring the posterior contractile strains were eliminated and tensile strains in the anterior region were smaller. For rigid rings the strain was significantly reduced in both the posterior and anterior annulus. All the rings exhibited reduced variation in curvature compared to the normal valves in which curvature increased from diastole to systole. The native dynamics of the valve were affected by all the rings, it has been

suggested that preventing normal mechanical dynamics may be unfavourable to mitral valve function and reduce repair outcomes (Carpentier *et al.*, 1995; Cosgrove *et al.*, 1995). In this study, only the flexible ring maintained the saddle height of the native valve. It has been suggested that the prevention of annular folding into the MV orifice, which occurred with the other rings, may negatively affect the motion of the left ventricle outflow tract during systole (Lansac *et al.*, 2002). The study established that for all devices there was significant reduction in annular dynamics, with loss of anterior dilation and posterior contraction, confirmed by strain and curvature analysis. The flexible incomplete ring retained the native annular dynamics the greatest when compared to the semi-rigid and rigid complete devices. Rausch *et al.* (2012) concluded that the heterogeneous nature of the strain and curvature of the annuli implies that a heterogeneous design solution should be sought.

Other limitations of current synthetic annuloplasty rings are that they can also cause secondary MV stenosis in children. Synthetic rings are also contraindicated to prosthesis use when there is presence of active bacterial endocarditis, there is risk of fibroblastic pannus growth and when there is a presence of a heavily calcified valve with reduced mobility.

The advantages and disadvantages of the conventional annuloplasty rings can be summarised as follows:

Partial:

- Used to retain physiological properties of anterior annulus whilst correcting the dilation of the posterior annulus.
- Does not correct dilation occurring with the anterior annulus

Complete:

- Restricts both anterior and posterior annulus
- Can be homogenous or heterogeneous

Rigid:

- Used to stabilise and restore mitral annulus geometry.
- Restricts annular dynamics and natural geometry of the annulus.
- Restricts contraction of left ventricle inflow tract and may obstruct left ventricle outflow tract.

Flexible:

- Provides flexibility for annular dilation and reduces annular size. Advantage of preserving left ventricular function.

- Only corrects dilation of the annulus and does not ensure normal configuration of the MV.

Semi-Flexible:

- Stiff anterior and flexible posterior.
- Thought to interfere less with the normal mitral annulus motion.
- Reduces stress on sutures while maintaining annulus remodeling

1.5.1.2 Biodegradable ring

Biodegradable rings were developed by Kalangos (2006). This type of ring consists of a curved 'C' shaped segment, manufactured from polydioxane polymer. A suture, manufactured from monofilament polypropylene, runs throughout the whole of the segment and extends out of either end. Attached at the distal ends of the suture are stainless steel needles. Two types of ring exist, a paediatric ring and an adult ring. The paediatric ring is available in sizes 26 and below. The paediatric ring differs from the adult ring because the suture does not run through the polymer, this is to ensure that the annulus can grow and remodel over time rather than be restricted in size by the suture.

During the biodegradation of the ring a fibrous tissue is formed at the annulus where the absorbed ring existed. This type of repair has the advantage of remodelling as the heart grows and therefore can be used in children without the need for re-operation. Biodegradable rings provide mechanical support only after the initial stages of implantation, subsequent growth of fibrous tissue provides mechanical support as the polydioxane ring is degraded by hydrolysis. A sub-endocardial fibrous reaction to the ring allows remodelling of the mitral annulus (Kalangos, 2006) but this has only been observed in animal models. The advantage of this method is that the ring is implanted within the annulus and therefore does not come into contact with the patient's blood, reducing the risk of thrombosis.

In preliminary tests in animals (model not described) inflammatory tissue found around the ring one month after implantation consisted of macrophages, polymorphonucleated cells, multinucleated giant cells, lymphocytes, fibrin and proliferating fibroblastic cells as well as there being evidence of collagen production. After three months there was still a foreign body reaction at the site of the ring but this had decreased compared to the one month reaction and it was suggested by the authors that the reaction could be surgery related rather than material related. Six months after the implantation the ring had started to degrade and had been replaced by a

thickened fibrous material, and the foreign body reaction to the ring had decreased over this period. At nine months there were limited signs of the original material and the reaction was composed predominantly of macrophages, multinucleated giant cells and lymphocytes. Fibrous scar tissue had formed at the implant site which was on average 1250 µm in diameter along the annulus. At 12 months there was a little biodegradable ring present and the inflammatory reaction had decreased with respect to the reaction at 9 months (Kalangos, 2006).

A four year trial in human patients (n=17) revealed that there was little or no regurgitation in 11 patients and mild regurgitation in 3 (Pektok *et al.*, 2010). There was also significant reduction in left ventricular dimensions after the repair. Three patients had died postoperatively within the first 35 days of the trial. Limited studies exist for this ring and no long-term results are available so the effects over longer periods are currently unknown.

1.5.1.3 Biological replacement ring

Autologous pericardium has been used clinically to treat patients who have valvular calcification or valvular destruction due to shrinkage of leaflets and chordae due to rheumatic carditis (Ng *et al.*, 2001) and endocarditis (Güden *et al.*, 2004). Pericardial patches have been used to reconstruct the calcified annulus in conjunction with mitral valve replacement, replace commissural tissue after tissue shrinkage, substitute part of a leaflet and re-implant ruptured papillary muscles and as replacement chordae (Ng *et al.*, 2001). Mitral valve replacements used for treating these problems are associated with complications such as atrioventricular rupture, paravalvular leakage and thrombosis (Güden *et al.*, 2004) and high rates of mortality and morbidity (Shinn *et al.*, 2009). Salati *et al.* (1991) performed an annuloplasty with an autologous pericardial ring, utilising a long strip of autologous pericardium. The tissue was marked with metal clips and rolled up into a tube ensuring that the smooth serosal surface was positioned on the outside of the tube. The ring was placed in close proximity to the posterior annulus and sutured into place just after the commissures (Salati *et al.*, 1991). A biological patch can also be used in annulus reconstruction; this involves full or segmented annular resection. A patch approximately 2cm wide is sutured into the left ventricle wall, positioned close to the posterior annulus and into the left atrial posterior wall, covering the annulus. Autologous pericardium (Fig 1.7) have been used in order to retain some of the dynamic motion of the annulus (Borghetti *et al.*, 2000). It is also readily available and cost effective, shows fast recovery and has resistance against infection (Güden *et al.*, 2004).

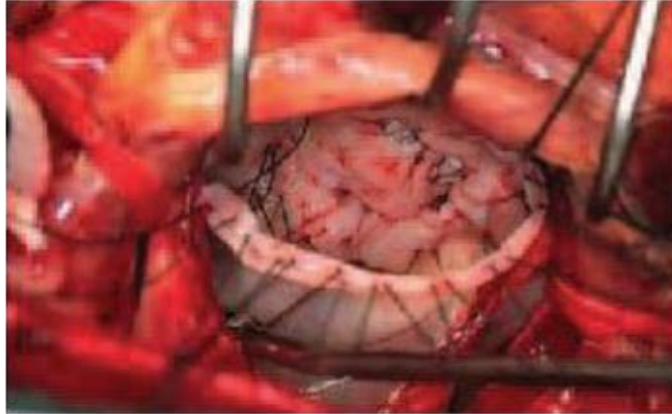


Fig 1.7 – Pericardial strip used for posterior annuloplasty⁵

Various problems have been associated with the use of autologous pericardium including; tissue contracture, progressive fibrosis, degeneration, loss of flexibility and endocarditis (Ng *et al.*, 2001). Glutaraldehyde treated patches have been considered to prevent early deterioration and prevent thickening, but cross-linked tissue has been associated with long-term degeneration (Vesely, 2003). In a study by Güden *et al.* (2004) autologous pericardial patches were sewn into eight patients who had calcification of the mitral annulus due to endocarditis. Pre-operatively, 50% of patients were in New York Heart Association (NYHA) class 2 and 50% in classes 3-4. One patient died postoperatively. During a short-term follow up of 6.5 ± 1.5 months, a NYHA class of 1-2 was observed for all patients with no reported perivalvular leakage, dehiscence, calcification or thrombosis. It was concluded that annular reconstruction using a pericardial patch could decrease mortality for patients with complicated mitral pathologies. Scrofani *et al.* (1996) used autologous pericardium in 113 patients and found that the majority of patients were in NYHA class I and had no or mild residual regurgitation over a follow up period of 32.41 ± 20.09 months. Borghetti *et al.* (2000) used glutaraldehyde treated pericardial strips for annuloplasty (group 1) and compared them against a group of patients who had undergone rigid ring annuloplasty with Carpentier-Edwards rings (group 2). At midterm follow up of 61.4 ± 12 months for group 1 and 46 ± 15 months for group 2, there was no or trivial mitral regurgitation observed in either group. There was a significant increase in left ventricle ejection fraction under stress conditions

⁵ Reprinted from Clinics, 60, Maria *et al.*, Mitral valve annuloplasty with a bovine pericardial strip - 18-year results, 305–310 (2005): taken from - http://www.scielo.br/scielo.php?pid=S1807-59322005000400008&script=sci_arttext#. Licensed under Creative Commons Attribution-NonCommercial 4.0 International.

for group 1 ($59.5 \pm 6\%$ to $65.8 \pm 6\%$ $p < 0.005$) whilst group 2 showed no significant increase ($61.4 \pm 5\%$ to $61.9 \pm 5\%$). This was reported as improved mitral dynamics and preserved left ventricular function in the pericardial group. These results were not compared against flexible or semi-flexible rings which would have given more relevant results. Other studies using autologous pericardium also concur with these results. In a study by Choi-Keung *et al.* (2001) 63 patients who had complex mitral valve pathologies underwent repair of their mitral valve using autologous glutaraldehyde treated pericardium. Repair included leaflets, chordae, annulus and reattachment of papillary muscle. Before the operation the mean regurgitation grade was 3.5 and patients were in NYHA class III or IV. At follow-up (mean 61.1 months) mitral regurgitation was absent in 92.1% of patients and freedom from re-operation was 95.2% at one and five years with no reported thromboembolic events.

1.5.2 Annuloplasty in children

Congenital heart disease is uncommon in children and often relates to other cardiac complications. The management of mitral valve disease in children is difficult because there are a range of pathologies with a high incidence of cardiac abnormalities present alongside the disease (Lee *et al.*, 2010). Mitral valve repair is desirable in children because left ventricle function is better preserved by retaining the subvalvular apparatus and geometry of the ventricle and the procedure is well established for congenital repair. Children who require valve replacement because either the repair has failed or the valve is comprehensively damaged have poor long term survival (Caldarone *et al.*, 2001; Ackermann *et al.*, 2007; Beierlein *et al.*, 2007; Selamet Tierney *et al.*, 2008; Alsoufi *et al.*, 2009). There are further problems because there are a limited number of replacement devices available in the correct size (Lee *et al.*, 2010) and they will require a secondary replacement later in life to ensure the valve is large enough for the adult heart. Due to the risk of stenosis in children, annuloplasty rings are normally only used when the child's annulus is large enough in diameter to accept the adult size annuloplasty rings; these rings are generally more than 26 mm in diameter. For children whose annulus is expected to grow further a commissuroplasty is used. A commissuroplasty involves stitching the commissures so that annular size is reduced and the anterior leaflet is moved so it is more in opposition with the posterior leaflet (Hillman *et al.*, 2004).

A retrospective study of repairs that took place between 1986 and 2003 focused on children that predominantly suffered from congenital MV

anomalies (Wood et al. 2005). The median age was 2.16 years with 40% of the children under 1 year of age. Just under 37% of cases had a pathology caused by annular dilation which lead to mitral regurgitation. The study found that the 15 year freedom from reoperation was 81.7% and had an event free rate of 73.5% over the same time period. Overall survival for the group was 86.5%. For this study the children were split into two groups; group 1 children were deemed as having a mitral anomaly with or without atrial septal defect or patent ductus arteriosus and group 2 were classified as complex which involved having a mitral anomaly with intracardiac disease or left ventricle outflow tract obstruction. Group 1 had a better 15 year survival of 93% compared to group 2 of 73% (Wood *et al.*, 2005). For the repairs the mitral orifice size was originally measured with a Hager dilator, this was compared to the normal MV diameter relative to the body surface area. For repair, complete synthetic rings were avoided in order to prevent the risk of stenosis due to valve growth and risks from endocarditis and thromboembolism. Partial posterior rings were only used if the child's mean body surface area was greater than 0.9 m². The most common technique used by Wood *et al.* (2005) was commissural plication annuloplasty in which sutures were used to reduce the size of the annulus at the commissures.

Lee *et al.* (2010) reviewed 139 cases of children who underwent MV repair between 1988 and 2007. The median age was 2.3 years (2 months – 17.6 years) and 90% of the group had mitral regurgitation. The aim of the study was to analyse the 20 year results of MV repair in children. In the retrospective study the freedom from reoperation was 77% and freedom from MV replacement was 90% with an overall survival of 97%. Various repair techniques were used which depended upon the functional and pathological findings of a saline injection test which evaluated the annulus, leaflets and subvalvular apparatus. Annular dilation was repaired using a variety of techniques (Table 1.4). The primary method used early on in the study used was Wooler-Kay annuloplasty but this was replaced in later years using artificial ring annuloplasty for older children and suture plication or posterior strip annuloplasty for younger children.

Table 1.4 – Repair techniques used in children (more than one technique could be used per repair)

Repair technique	Patients	% of patients undergoing procedure
Mitral regurgitation		
Wooler-Kay annuloplasty	57	45.6
Cleft repair	22	17.6
Strip annuloplasty	18	14.4
Ring annuloplasty	14	11.2
Artificial chordae	12	9.6
Chordae shortening	10	8.0
Posterior annulus placcation	9	7.2
Papillary muscle splitting	7	5.6
Secondary chordae resection	6	4.8
Edge-to-edge repair	5	4.0
Commissure obliteration	5	4.0
Chordae transfer	4	3.2
Mitral stenosis		
Papillary muscle splitting	11	78.6
Commissurotomy	4	28.6
Resection of supra- valvular ring	4	28.6
Secondary chordae resection	2	14.3
Leaflet slicing	1	7.1
Fenestration of chordae	1	7.1

Adapted from Lee et al. (2010)

1.6 Tissue Engineering

A more recent approach to repair and replacement of the mitral valve is through the emerging science of tissue engineering. This field has the potential to overcome the limitations associated with current strategies of mitral valve replacement such as the use of anticoagulation treatments, poor durability and unsuitability of current strategies for the paediatric population.

1.6.1 Overview

The field of tissue engineering has developed from unmet clinical needs for tissue reconstruction and repair. The aim of tissue engineering is to produce functional tissues in the laboratory that can be used to replace, repair, maintain, or improve diseased or damaged tissues or, potentially whole organs (Yang *et al.*, 2001). Approaches to tissue engineering include the development of (a) acellular scaffolds designed to regenerate with the patients endogenous cells following implantation (b) scaffolds seeded with living cells and conditioned in vitro prior to implantation and (c) use of cell therapies or biologics to induce endogenous repair. For the purposes of this review, only approaches (a) and (b) are relevant to the replacement or repair of the mitral valve.

Tissue engineering scaffolds need to offer comparable biological and biomechanical properties to the tissue that they designed to replace or repair in order that they might regenerate appropriately in the body. Two major types of tissue engineering scaffold have emerged, biological and synthetic substitutes. Scaffolds can be assembled from biodegradable synthetic polymers or natural polymers or produced via the decellularisation of natural allogeneic donor or xenogeneic tissues and used with or without cell seeding (Neuenschwander & Hoerstrup, 2004).

The scaffold for any type of application needs to provide the correct environment for cell attachment and proliferation (Sheridan *et al.*, 2000; Teebken *et al.*, 2001) whilst being non-inflammatory, non-immunogenic and provide suitable mechanical properties and durability (Khalil & Sun, 2007; Bloori Zadeh *et al.*, 2013). The scaffolds also need to have the correct mechanical characteristics to provide the appropriate environment for new tissue formation and correct function when implanted. The structure should provide porosity and permeability for cell integration and nutrient exchange along with the correct surface topography for cell attachment (Yang *et al.*, 2001), which is thought to contribute to the tissue engineered construct developing the required biological functions (Cima *et al.*, 1991).

Acellular scaffold approaches rely on the patient's own cells to grow into the scaffold and remodel the scaffold to provide a functional outcome post-implantation. The main drawback to this approach is the lack of cellular functionality of the tissue replacement/ repair immediately upon implantation. For acellular scaffolds with a primarily mechanical function, such as would be the case with an annuloplasty ring, which undergoes cyclic loading during the cardiac cycle, the initial lack of living cells to repair and remodel the scaffold may lead to scaffold degradation and alter the biomechanical characteristics.

In the approach of using scaffolds seeded with living cells, which to prevent immunological rejection would need to be autologous, the aim is to condition the cells with the purpose of producing a living construct that has the same function as the tissue it is replacing prior to implantation. Cell seeded scaffolds that have been conditioned in vitro prior to implantation have the potential for improved survival and integration compared to the acellular scaffold approach. However, a potential limitation to this approach is that, once implanted, the cells within living tissue engineered constructs may die by necrosis as a result of hypoxia, leading to degradation of the implanted construct. Moreover, the costs of the cell-seeded scaffold approach would be substantially higher compared to the acellular scaffold approach.

1.6.2 Synthetic polymer matrices in cardiovascular tissue engineering

There are a number of synthetic biodegradable polymers that are biocompatible and biodegradable and have been used in cardiovascular tissue engineering. These include; polygalactin (Shinoka *et al.*, 1995), PGA (polyglycolic acid) (Shinoka *et al.*, 1996), PLA (polylactic acid), and PLGA (copolymer of PGA and PLA) (Zund, 1997). PGA coated with P4HB (poly-4-hydroxybutyrate) has been used to manufacture complex three dimensional structures for example trileaflet heart valves (Hoerstrup *et al.*, 2000, 2002). Synthetic polymers can be tailored so that the biomechanical properties and biodegradation rate are designed for the function required of the scaffold. It is also possible to incorporate growth factors into the scaffold so that specific cell types can be targeted to promote tissue remodelling (Hubbell *et al.*, 1991; Zisch *et al.*, 2003). Shinoka *et al.* (1995) seeded a synthetic polyglycolic acid fiber matrix with fibroblasts and endothelial cells and implanted the cell- seeded scaffold into the right posterior leaflet of the pulmonary valve in sheep. Results showed no evidence of stenosis and minimal regurgitation and analysis of the explanted tissue revealed the

development of an extracellular matrix and appropriate cellular distribution. In a similar study Hoerstrup *et al.* (2000) fabricated heart valves using bioabsorbable polymers and seeded them with autologous ovine myofibroblasts and endothelial cells. The cell-seeded constructs were conditioned in a bioreactor for 14 days before implantation into the pulmonary position in the hearts of lambs. Their results showed degradation of the polymers at 8 weeks and a fully functioning valve during the study. The explanted constructs showed comparable characteristics to a normal heart valve in terms of the microstructure and mechanical properties. Biodegradable polymers have also been seeded with CD133(+) cells derived from umbilical cord blood with the aim of developing new strategies for the treatment of congenital defects (Sodian *et al.*, 2010). The constructs were placed in a bioreactor to encourage cell growth; analysis of the tissue showed signs of endothelialisation and connective tissue formation.

There are disadvantages associated with the use of synthetic polymers as scaffold materials. These relate to the isotropic nature of the manufactured scaffolds which may not lead to appropriate cell-signalling and 3D tissue remodelling. Native valves have an anisotropic structure coupled with non-uniform mechanical properties (Merryman *et al.*, 2006). To obtain anisotropic properties that characterise the structure of native heart valves Masoumi *et al.*, (2014) fabricated tri-layered scaffolds of micro-fabricated poly(glycerol sebacate) (PGS) and fibrous PGS/poly(caprolactone) (PCL) electrospun sheets. Mesenchymal stem cells and valve interstitial cells (VICs) grew within the scaffolds and deposited extracellular matrix on the scaffolds when conditioned in a bioreactor. An *ex-vivo* porcine heart model demonstrated that the constructs opened and closed similarly to native valve leaflets.

To the author's knowledge, there have been no studies that have used synthetic polymer scaffolds, either seeded with cells or without cells for mitral valve repair or replacement strategies.

1.6.3 Natural polymer scaffolds in cardiovascular tissue engineering

Natural polymers can be categorised as proteins, polysaccharides or polynucleotides. Proteins include actin, collagen, elastin, fibrinogen, gelatin, keratin and myosin; polysaccharides include amylose, cellulose and glycosaminoglycans whilst polynucleotides include DNA and RNA (Alexander & Brunski, 1996). A number of these polymers have been used in the fabrication of cardiovascular tissue engineered scaffolds. Shi and Vesely (2003) produced chordae constructs utilising a collagen gel

suspension. The construct was placed into a rig which exerted tensile forces through the material, aligning crimped collagen fibrils longitudinally and producing a sheath of elastin around the core, replicating the native chordae structure. Mechanical properties of early constructs were far weaker than native chordae, but were improved with the use of a bio-reactor and enhanced material and clamp design.

Hyaluronan, a glycosaminoglycan, is a natural polymer being investigated as a replacement for the native aortic valve leaflets which are characterised by GAG and elastin layers (Ramamurthi & Vesely, 2005). Directed collagen gel shrinkage has been used alongside a hyaluronan and divinyl sulfone GAG matrix to fabricate aortic valve leaflets (Shi *et al.*, 2002). Fibrin has also been investigated as a possible scaffold for valvular tissue engineering (Flanagan *et al.*, 2007; Jockenhoevel, 2001). Fibrin based tissue engineered heart valves were fabricated using moulds which were seeded with ovine carotid artery derived cells and conditioned in a bioreactor system for 12 days. Results showed increased cell attachment and cell alignment alongside deposition of extracellular matrix (ECM) proteins including collagens type I and III, fibronectin and laminin compared to controls (Flanagan *et al.*, 2007). An alternative fabrication approach is layer by layer 3D bioprinting. Using this method Duan *et al.* (2013) printed alginate and gelatin hydrogel valves incorporating sinus smooth muscle cells (SMCs) and aortic VICs. Cells were regionally constrained, the SMCs to the valve root and the VICs in valve leaflets which showed increased expression of α -smooth muscle actin and vimentin after 7 days of cell culture. Scaffolds have also been seeded with aortic valve interstitial, endothelial cells, endothelial progenitor cells (Simionescu *et al.*, 2012) and mesenchymal stem cells (Tedder *et al.*, 2011).

Cells that are entrapped in gel scaffolds undergo contraction, these processes have been compared to the processes involved with wound healing when collagen gels are utilised (Tamariz & Grinnell, 2002) and promote uniform cell distribution when used with fibrin gels (Jockenhoevel, 2001). Collagen gel shrinkage can be advantageous in enhancing properties of the construct (Tranquillo *et al.*, 1992) but can cause excessive shrinkage of the scaffold (Jockenhoevel, 2001). Cells entrapped in collagen can also promptly enter apoptosis, causing the synthesis of matrix metalloproteinases which degrade scaffold proteins (Grinnell, 2003).

1.6.4 Biological scaffolds in cardiovascular tissue engineering

The native ECM comprises of structural and functional proteins, glycoproteins and proteoglycans. Utilising the native ECM of the tissue that needs to be replaced or repaired offers many advantages such as retaining the components of the ECM. The ECM of each tissue is organised in a specific three-dimensional ultrastructure depending upon the function of the tissue in question. The ECM of each tissue provides attachment sites for cell surface receptors and growth factors which in turn influence processes such as cell migration, cell function and angiogenesis. The ECM also possesses the correct mechanical and structural properties for the function it plays in the body. This makes the natural ECM of a tissue a suitable material for tissue repair and replacement (Badylak, 2002).

The complexity of the mitral valve poses enormous challenges for tissue engineering to produce scaffolds that recapitulate the complex structure and function. The leaflets are of different sizes, chordae are numerous and have different mechanical characteristics (Ritchie *et al.* 2005). In addition, in a successful tissue engineering approach, the ECM composition and different phenotypes of the valvular cells would need to be reproduced. As a result of these difficulties, research has mainly focused on engineering individual mitral valve components. The major limitation of the current valve repair and replacement strategies is the inability for growth, repair and remodelling of the valve (Sacks *et al.*, 2009). Current strategies for tissue engineered solutions for the mitral valve have centred on the tissue engineering of chordae and mitral valve leaflets but more recently the whole mitral valve complex (Iablonskii *et al.*, 2015).

1.6.4.1 Decellularised biological scaffolds

Morticelli *et al.*, (2013) developed a decellularised porcine pericardium for repair of the mitral valve leaflets and found that the decellularised porcine pericardium could be a suitable option for the regeneration of the mitral leaflets. A recent approach has been the decellularisation of the whole mitral valve complex in sheep including the leaflet, chordae and papillary muscles (Iablonskii *et al.*, 2015). Acellular valves were reseeded with ovine endothelial progenitor cells *in-vitro*, preliminary studies showed that the leaflets were repopulated by endothelial cells and retained comparable mechanical properties to native tissue.

Whilst the development of tissue engineered mitral valves has been isolated mainly to preliminary studies of chordae, pericardium and the whole mitral

valve, acellular allogeneic and xenogeneic aortic and pulmonary valves have been implanted in humans. Acellular pulmonary valve allografts have been used to reconstruct the right ventricular outflow tract during the Ross procedure, with favourable results with the SynerGraft valve developed by CryoLife Inc (Goldstein *et al.*, 2000) in the short to medium term (Hawkins *et al.*, 2003; Bechtel *et al.*, 2005; Tavakkol *et al.*, 2005; Konuma *et al.*, 2009; Brown *et al.*, 2010b; Burch *et al.*, 2010; Ruzmetov *et al.*, 2012) and with valves decellularised using a process developed at the University of Leeds (Booth *et al.*, 2002; Korossis *et al.*, 2002) with excellent short to medium term performance (da Costa *et al.*, 2009). Decellularised CryoLife SynerGraft aortic valve allografts have also been implanted in humans which have shown good short term results (Zehr *et al.*, 2005). Acellular aortic valve allografts decellularised using the process developed at Leeds have shown good early and midterm results with valves maintaining structural integrity, a low rate of calcification, and acceptable haemodynamics (da Costa *et al.*, 2010).

Tissue engineered valve xenografts have also been implanted into humans but have shown variable regenerative capabilities. Studies using the SynerGraft decellularisation process (Goldstein *et al.*, 2000) on unseeded porcine pulmonary valves that were implanted into children failed catastrophically due to severe inflammatory reaction. Analysis of the explanted valves revealed whole cells, DNA and the α -gal epitope present in the walls of the explanted valves caused by the incomplete decellularisation of the valves before implantation (Simon *et al.*, 2003). Matrix P acellular porcine pulmonary valves developed by AutoTissue (GmbH, Berlin, Germany) have shown good short term performance (Erdbrügger *et al.*, 2006; Konertz *et al.*, 2005) and comparable results between CryoLife allografts in medium term studies (Erdbrügger *et al.*, 2006). Matrix P acellular pulmonary valves seeded with autologous endothelial cells have also demonstrated good performance long term (Dohmen *et al.*, 2011). There have however, also been reports of destruction of the pulmonary xenograft (Hiemann *et al.*, 2010) and poor results with the Matrix P Plus, a composite pulmonary valve of a glutaraldehyde fixed equine pericardial patch and the Matrix P porcine pulmonary valve (Cicha *et al.*, 2011). In this analysis Matrix P control valves showed signs of incomplete decellularisation and a foreign body reaction to implanted valves at the luminal surface of the acellular porcine tissue. There have been no studies of acellular aortic valves xenografts in humans. Using the methods developed for the pulmonary valves at the University of Leeds it was found that acellular

porcine aortic valves implanted into sheep showed signs of cellular repopulation (Paniagua Gutierrez *et al.*, 2015). Histological analysis of the explants displayed evidence that macrophages play an important role in the regeneration response. Calcification was present in some of the explanted valves which suggested incomplete DNA removal during the decellularisation process before implantation of the valves.

1.7 Decellularisation

Decellularisation is a technique in which host cells, cell fragments and antigens of a tissue are removed via chemical or mechanical processes. The presence of these components is largely responsible for the immunogenic response when donor human (allogeneic) or xenogeneic tissue used as a graft. The matrix of the tissue is preserved during decellularisation but damage to the structure may occur, changes to the biomechanics, GAG and collagen composition have all been reported (Booth *et al.*, 2002; Cartmell & Dunn, 2000; Korossis *et al.*, 2005; Schenke-Layland *et al.*, 2003; Woods & Gratzer, 2005; Gilbert *et al.*, 2006). It is important to retain the ECM during the decellularisation procedure as it has been shown to effect cell mitogenesis and chemotaxis (Bornstein & Sage, 2002; Vorotnikova *et al.*, 2010), influence cell differentiation (Allen *et al.*, 2010; Barkan *et al.*, 2010; Cortiella *et al.*, 2010) and the tissue remodeling process (Parekh *et al.*, 2009; Valentin *et al.*, 2010; Xu *et al.*, 2010). Studies that have looked at how the GAG content of tissue has been altered by the cell removal procedure have found that the majority of detergents remove at least some of the GAGs from the extracellular matrix which can impact the viscoelasticity of the scaffold (Lovekamp *et al.*, 2006; Mendoza-Novelo *et al.*, 2011).

Implanting a decellularised scaffold permits the body's own cells to integrate into the scaffold and remodel it in response to the environment it has been placed in. The decellularisation process has to be designed so that the underlying biomechanical and biochemical architecture of the tissue is not damaged so that it changes the nature of the tissue it has been derived from (Crapo *et al.*, 2011). Methods have been developed to decellularise a diverse spectrum of tissues. These include using hypotonic or hypertonic buffers (Wilson *et al.*, 1995; Bader *et al.*, 2000; Steinhoff *et al.*, 2000), detergents to extract the cells (Bader *et al.*, 1998; Booth *et al.*, 2002; Wilson *et al.*, 1995), enzymes for digestion (Gilbert *et al.*, 2006), photo-oxidation (von Rechenberg *et al.*, 2003) and freeze drying to puncture cell membranes and create cavities for repopulation of native cells (Curtill *et al.*, 1997).

Studies have established that some growth factors retain bioactivity in biological scaffolds after terminal sterilization and long term storage (McDevitt *et al.*, 2003). Decellularisation retains most of the components of the native extracellular matrix which should match or be similar to the tissue it is replacing. This offers considerable advantages over other methods of tissue engineering scaffold fabrication, such as those that use only individual components of the ECM (Brown *et al.*, 2010a).

Rationale for the project

An acellular biological annuloplasty ring could offer improved outcomes compared to current annuloplasty rings. The acellular ring could integrate with the patient's valve and remodel with it over time. This remodelling process would ensure that the ring would closely match the dynamics of the valve during the cardiac cycle whilst reducing the size of the annular area. The reduction in annular area would increase leaflet coaptation and decrease mitral regurgitation as with current strategies but the integration has the potential to offer improved annular dynamics and offer improved repair options in children.

Human mitral valve annuli will be investigated as a starting material for decellularisation because they retain the properties of the native annulus, including geometry and extracellular matrix components. Porcine tissue will also be investigated because of its comparable macroscale characteristics to native human annulus and increased availability compared to the human tissue.

Methods developed at the University of Leeds will be applied and adapted for the annuloplasty ring. The tissue will be decellularised by modifying existing protocols and assessing the acellular scaffold for suitability to be used as an annuloplasty ring. The decellularisation methods developed at the University of Leeds have delivered excellent results in aortic and pulmonary valves and will provide a suitable starting point for developing an acellular biological annuloplasty ring.

Specification for a proof of concept decellularised annuloplasty ring

- Diameter for the ring within the same range as a traditional annuloplasty ring (24 mm to 40 mm)
- Mechanical characteristics should closely match those of the native region of the mitral valve annulus to preserve the dynamics of the valve
- Biological characteristics should closely match the native region of the mitral valve annulus to enhance cell adhesion and integration
- Tissue needs to be readily available
- Tissue should be easy to handle for repair purposes
- Tissue should be void of cells to prevent an immune response and permit cell adhesion and integration
- Tissue should perform as well as synthetic annuloplasty rings during functional testing

1.8 Aims and objectives

It is hypothesised that an acellular biological annuloplasty ring will improve valve function, annular dynamics and grow with the mitral valve when compared to current annuloplasty rings on the market. The aim of this project is to develop a process for the decellularisation of a natural mitral valve annulus, characterise the tissue and undertake preliminary studies of functional performance in an *in-vitro* model. The objectives of the study are to:

- Determine the biological characteristics of the native human annulus using histological and immunohistological analysis.
- Determine the biological properties of the porcine mitral valve annulus and compare them to the human annulus using histological and immunohistological analysis.
- Determine the biomechanical properties of the porcine mitral valve annulus.
- Develop decellularisation protocols for the tissue most suitable for mitral valve repair based on existing protocols.
- Evaluate the effects of decellularisation on the tissue through assessment of the histoarchitecture, total DNA content, the retention of selected ECM proteins and the mechanical properties of the tissue by comparison with native tissue.
- Determine the *in-vitro* biocompatibility of the decellularised tissue.
- Investigate appropriate *in-vitro* mitral valve regurgitation models for annuloplasty repair using static regurgitation testing.
- Functionally test the decellularised tissue using static regurgitation testing and by comparison to synthetic annuloplasty rings.

Chapter 2 Materials and Methods

This chapter describes the general methods used in the histological, immunohistochemical and biomechanical analysis of the native and decellularised porcine mitral valve annulus and the native human mitral valve annulus. The cell culture techniques used for biocompatibility assays are also described.

2.1 Materials

2.1.1 Equipment

Equipment used in this research is listed in Table 2.1 along with the suppliers and product code where applicable.

Table 2.1 – Equipment used during the research

Equipment	Supplier	Product code
150 ml sterile containers	Scientific Laboratory Supplies (SLS)	CON7580
250 ml sterile containers	SLS	CON7570
500 N static load cell	Instron	2580-105
Autoclave	KUHN Rikon	5 L pressure cooker
Automatic pipettes	Gilson	Various
Balance	Jencons PLC	AND GR-200
Biopsy punch (5mm)	World Precision Instruments, inc.	504532
Cell [^] B	Olympus UK	Cell [^] B
Class II safety cabinet	Kendro	Heraeus H518
Custom made tissue cutter	Bioengineering labs, mechanical engineering, University of Leeds	
Stone personal	Stone	Eco saver 80+,

computer		Windows 7
Digital Camera	Olympus	XC50
Digital callipers	Mitutoyo digital callipers	
Dissection Kit	Thackray Instruments	N/A
Four figure balance	AND	GR-200-EC
Fridge	Jencons PLC	Lab cold 23
Histology moulds	Raymond A Lamb	E10.8/4161
Histology Water Bath	Barnstead Electrothermal	MH8515
Hot wax dispenser	Raymond A Lamb	E66
Hotplate	Raymond A Lamb	E18/1
Incubator	Heraeus	Jencons PLC
Instron 3130-100 BioPuls Bath	Instron	3130-100
Instron 3365 materials testing machine	Instron	3365
Magnetic Stirrer	Stuart Scientific	CB161
Microtome	Leica	RM2125 RTF
Microtome blade	Fisher Scientific	SD3050835
Orbital shaker	IKA	KS 130
pH meter	Jenway	3510
Pipette boy	Integra Bioscience	Integra acu
Plastic histology cassettes	Thermo Fisher Scientific	CMB-160-030R
Retractors	Mercian	SP4003-14
Single use filter unit	Sartorius Stedim	16532
Slide holder	Raymond A Lamb	E102
Static Test Rig	Bioengineering, Mechanical Engineering, University of Leeds	N/A
Table shaker	IKA	KS130

Tissue processor	Leica	TP1020
Upright microscope	Olympus UK Ltd.	BX40
Wax Oven	Raymond A Lamb	E18/31
Zen software	Zeiss	Zen Blue edition 2011

The consumables and plastic ware used in the study are described in Table 2.2 together with the supplier and product code/model.

Table 2.2 – Consumables and plastic ware used during the research.

Item	Supplier	Product code/ Model
3-0 Sutures Mersilk Suture Taper Point	Ethicon	W583
Bijous	SLS select	SLS7522
Biopsy punch WPI 5.0 mm W/Plunge	World Precision Instruments	504532
Cable tie (190 x 4.8 mm)	RS	178-484
Carpentier-Edwards Classic. Annuloplasty ring with Duraflo Treatment - Mitral	Baxter	4425M30
Cell culture flasks	Thermo Scientific 75cm Thermo Scientific 175cm	156699 159910
Eppendorf	Starlab	E1420-2000
Filter paper	Whatman International Ltd	Whatman Grades 1-5
G-clamp	Olympic	100 mm
Glass cover slips	SLS	MIC3228
Heart holder	Genzyme	80 77/78
Histology cassettes	Simport	Histosette, with lid

		M490-2
ImmEdge Hydrophobic Barrier Pen	Vector Laboratories	H-000
Medium temperature cauterisers	FIAB	F7288 thick tip
Measuring cylinders	Fisher Scientific	
Microtome blades	Fisher Scientific	SD3050835
Optiplate 96	PerkinElmer	6005290
'O' ring 40mm	RS	128-978
PEN-Membrane 1mm glass	PALM Membrane slides	1440-1000
Parafilm M	Sigma-Aldrich Ltd	
Pipette tips	Starlab	
Plastic container	Otto	Burkle D7850
Plastic syringe 1ml	Terumo	GS572
Pots	Bibby Sterillin	
Retractors	Mercian	SP400 3- 14
Spigot (15mm diameter x 55 mm length)	Bioengineering laboratory, University of Leeds	
Static test rig (120 mmHg max column pressure)	Bioengineering laboratory, University of Leeds	
Superfrost glass slides	SLS	MIC3040
Superfrost plus glass slides	SLS	MIC3022
Surgical Marker Pen	Universal Hospital Supplies	MAR001T
Stop watch (calibrated)	RS	278-682
Syringe needles 19G	Terumo	NN-19382
Test rig clamp	Bioengineering laboratory, University of Leeds	

Test tubes	Bibby Sterillin	
Universals	SLS	SLS7500
Well plates	Thermo Scientific	
6 well plate		140675
96 well plate		167008

2.1.2 Chemicals and reagents

The chemicals and reagents used in the study are described in Table 2.3 alongside the supplier and product code.

Table 2.3 – The chemicals and reagents used during this study.

Chemical/Reagent	Supplier	Product code
Alpha -galactosidase	Sigma-Aldrich	G8507
Aprotonin (10000 KIU.ml ⁻¹)	Mayfair house	AP012
Acetone	European Bios	LS8/1970/ G
Alcian blue	Atom scientific	RRSP4-E
Ammonium formate	Sigma-Aldrich	15-626-4
Antigen unmasking solution, Citrate based	Vector Laboratories	H-3300
Biotinylated GSL I – isolectin B ₄	Vector Laboratories	B-1205
Bovine serum albumin	Sigma-Aldrich	85041C
Benzonase (nuclease)	Millipore	70746
Calcium acetate	Thermo Fisher Scientific Ltd	C/0920/50
CarboFree Blocking Solution 10x concentrate	Vector Laboratories	SP-5040
Cyanoacrylate	Henkel	1575596
Disodium ethylenediaminetetraacetic acid (EDTA)	Thermo Fisher Scientific Ltd.	E/P140/53

DNase	Sigma-Aldrich	DN25-1
DPBS	Lonza	BE17-513F
DPX mountant	Thermo Fisher Scientific	M81330/C
Dulbecco's PBS tablets	Oxoid	BR0014
Envision+ Dual Link System-HRP (DAB+)	Dako	K4065
Eosin	VWR International	1.09844.10 00
Ethanol	Thermo Fisher Scientific Ltd	E/0555DF/ 25
Foetal bovine serum (FBS)	Lonza	DE14-870F
Galactose (360 mg)	Vector Laboratories	S-9003
Gentamycin	Sigma-Aldrich	G1397
Gills number 3 haematoxylin	Sigma	GH5316
Haematoxylin	Thermo Fisher Scientific	PS50/C
Hanks Balanced Salts Solution (HBSS)	Sigma	H9269
Histo-clear III	National diagnostics	HS-204
HEPES 1M	Sigma-Aldrich	H4034
HEPES buffer 1M in 0.85% (w/v) NaCl	Lonza	BE 17- 737E
Hydrochloric acid (6M)	VWR International	2611.5
Hydrochloric acid (specific gravity 1.18)	Thermo Fisher Scientific Ltd.	H1200/PB1 7
Hydrogen peroxide (30 %; v/v)	Sigma-Aldrich	H1009
ImmEdge Hydrophobic Barrier Pen	Vector Laboratories	H-4000
ImmPACT DAB Peroxidase (HRP) Substrate kit	Vector Laboratories	SK-4105
Low melting point Agarose	15517-014	Invitrogen

Magnesium chloride hexahydrate	MP	195304-1000G
Mayer's Haematoxylin (Mayer's Haemalum)	RRSP60	Atom Scientific
Methanol	428	Vickers Laboratories
Methylated spirits	Biostain Ready Reagents	GPS1000-K
Miller's Stain	Raymond A Lamb	LAMB/080-D
Oxalic acid	VWR International	1E+06
Paraffin wax	Thermo Fisher Scientific Ltd	PS138/E
Penicillin/streptomycin solution 5000 U.ml ⁻¹	Lonza	DE17-603E
Peracetic acid (32 wt. % solution)	Sigma-Aldrich	26933-6
Periodic Acid-Shiff (PAS kit): Aqueous periodic acid solution 0.1% Shiff's reagent Hematoxylin solution	Sigma	395B-1KT
Picric acid	Sigma-Aldrich	36011
Potassium permanganate	Thermo Fisher Scientific Ltd	P/6520/53
Proteinase K	Dako	S302080
RNase	Sigma-Aldrich	123879
Saline (0.9%)	Fresenius Kabi	31-58-736
Scott's tap water	Thermo Fisher Scientific Ltd	PS138/E
Silver nitrate	AnalaR	1023335
Sirius red	VWR International	F3B

Sodium azide 1 % (w/v) solution	G Biosciences	786-299
Sodium chloride	Thermo Fisher Scientific Ltd	42429-5000
Sodium dodecyl sulphate (SDS)	Sigma-Aldrich	71725-100G
Sodium hydroxide	Thermo Fisher Scientific Ltd	S/4920/53
Sodium thiosulphate	AnalaR	10268
Streptavidin/Biotin blocking kit	Vector Laboratories	SP-200
Streptavidin, Horseradish Peroxidase, R.T.U	Vector Laboratories	SA-5704
pH standards (4,7,10) pH 4 pH 7 pH 10	SLS	pH4- PHB1310 pH7- PHB1312 pH10- PHB1314
Trizma base	Sigma-Aldrich	T-1503
Trypsin	Sigma-Aldrich	T-7409
Trypsin inhibitor	Sigma-Aldrich	T-9128
Tween 20	Sigma-Aldrich	P1379
Ultra Vision One Large Volume Detection System, DAB plus substrate System: DAB Plus substrate DAB Plus Chromagen	Thermo Scientific	TA-125-HDX TA-125-HSX TA-004-HCX
Ultra Vision One detection system: HRP polymer DAB Plus substrate	Thermo Scientific	TL-125-HLJ TA-125-

		HDX
Weigerts haematoxylin	Atom Scientific	
Solution A		RRSP72-D
Solution B		RRSP73-D
Zinc acetate	Sigma-Aldrich	383317
Zinc chloride	Fluka	96470

2.1.3 General stock solutions

2.1.3.1 Phosphate buffered saline (PBS)

Ten Oxoid Dulbecco PBS tablets were dissolved in 1 L of distilled water and the pH adjusted to 7.2 – 7.4. Solutions were placed in an autoclave for 20 minutes at 121 °C at a pressure of 103 kPa. Items were stored for up to one month at room temperature.

2.1.3.2 Tris buffered saline (TBS)

Tris solution (25 ml; 2 M) was added to 50 ml 3 M sodium chloride solution, 925 ml of distilled water was added to the solution and the pH adjusted to 7.6. Solutions were placed in an autoclave for 20 minutes at 121 °C at a pressure of 103 kPa. Items were stored for up to one month at room temperature.

2.1.3.3 TBS containing 0.05% (w/v) Tween 20

Tween 20 (500 µl) was mixed with 1000 ml of autoclaved TBS and adjusted to a pH of 7.6. Solutions were used on the day.

2.1.4 Cells

The cell lines used in this study and suppliers are listed in Table 2.4

Table 2.4 – Cell lines used in this study.

Cells	Type	Species	Supplier
BHK	Fibroblast	Hamster	Health Protection Agency
L929	Fibroblast	Murine	European Collection of Animal Cell Culture

2.1.5 Glassware

Glassware was cleaned with 1 % (v/v) solution of phosphate-free detergent (Neutracon, Decon Laboratories Ltd) for 1 hour. Glassware was then rinsed with tap water followed by three rinses with distilled water. Items were then left to dry and sterilised at 180 °C for 4 hours by dry heat.

2.2 Methods

2.2.1 General methods

2.2.1.1 Measurement of pH

A Jenway 3020 pH meter was used for carrying out pH measurement. The meter was calibrated by using solutions with a pH of 4, 7 and 10. Temperature compensation was included in the measurement of solutions. 1 M or 6 M hydrochloric acid or sodium hydroxide were added drop-wise with stirring to solutions that required their pH adjusted.

2.2.1.2 Microscopic analysis

The histology slides were viewed using bright field microscopy using an Olympus BX51 microscope. The images were captured using an Evolution MP Colour digital camera attached to the microscope and then viewed and manipulated with the Olympus Cell[^]B or Zeiss Zen software. Polarised light microscopy involved the use of a polariser and analyser, incorporated in the same system. Fluorescence microscopy included the use of the fluorescent vertical illuminator (BX51-RFA) and selection of the correct filters. An inverted microscope (Olympus IX71) was used for viewing cells by using phase contrast microscopy and images were captured using Cell[^]B software via the attached camera.

2.2.1.3 Sterilisation

Three procedures were used depending upon suitability.

- Dry heat sterilisation - Suitable items were placed in a hot air oven for 4 hours at 180 °C.
- Moist heat sterilisation - Items not suited for dry heat sterilisation were placed in an autoclave for 20 minutes at 121 °C at a pressure of 103 kPa.
- Filter sterilisation - Solutions not suited for previous methods were filtered using 0.2 µm pore sized filters and a disposable syringe inside a class II safety cabinet.

2.2.2 Tissue processing

2.2.2.1 Dissection equipment

Equipment used for dissection are listed in Table 2.5.

Table 2.5 – Equipment used for dissection.

Equipment	Supplier	Model
Forceps, straight fine point	-	-
Scalpel handle	Swann-Morton	8112 Size 4
Scissors, straight with fine point	-	-
Scissors, curved with a fine point	-	-
Tissue clamps	Thackray Medical GU London	50-2650 GU-3800

2.2.2.2 Ethics and tissue tracking

The human mitral annulus tissue was used for research under research ethics approval. The REC reference for the research was 13/NW/0147 and the committee used for obtaining approval was Lancaster. The planned start date of the study using the tissue was 01/01/2013 and the end date of the study was 31/12/2016, the approval of using human hearts for research of the mitral valve annulus in this study was granted on 14/02/2013. All human tissue used for this study was provided by NHS Blood and Transplant, Tissue Services based in Liverpool. Human tissue used in the study was tracked using the Achiever system which logged all of the locations of the tissue used throughout the study. Tissue was disposed of using the

University of Leeds guidelines for human tissue disposal and recorded via Achiever.

2.2.2.3 Dissection

Porcine and human mitral annuli were removed using similar methods. The native porcine mitral valves were dissected from porcine hearts of Large White pigs, supplied by local abattoirs and taken from animals approximately 24-26 weeks old and slaughtered within 24 hours. The native human mitral valves were dissected from hearts of cadavers aged between 57 and 84 which had been stored at -20 °C and warmed to room temperature using a water bath set at 37 °C. The pulmonary trunk, superior vena cava and the aortic arch were removed, if required, being careful not to damage the aortic valve. Any other excess tissue such as the pericardium was removed. An incision was made approximately half of the way up from the bottom of the apex of the heart (Fig 2.1a; a). The heart was cut at this point around the circumference to remove the apex (Fig 2.1a; b). The left and right ventricles of the heart were identified from the anterior inter-ventricular artery which runs down the septum of the heart. Once identified, an incision was made near to the base of the heart which followed the anterior inter-ventricular artery towards the pulmonary trunk, being careful to cut towards the side of the right ventricle to avoid the mitral valve, situated between the left ventricle and left atrium (Fig 2.1a; c). The posterior descending inter-ventricular artery was identified on the posterior side of the heart and an incision was made close to the base up towards the right atrium where the right hand side of the heart was removed, being careful not to remove the aortic valve (Fig 2.1a; d). The left auricle of the mitral valve was removed (Fig 2.1a; e) to reveal the top of the mitral valve (Fig 2.1a; f). Viewing the mitral valve from the base, an incision was made at the point just above where the papillary muscles and chordae combine (Fig 2.1a; g), the incision was carried out around the circumference of the heart (Fig 2.1a; h). The aorta was removed up to the aortic-mitral valve continuum and a cut made through the septum separating the left and right ventricles (Fig 2.1b; i). Incremental steps of muscle removal were then made on the ventricular side of the mitral valve (Fig 2.1b; j) and the atrial side of the mitral valve (Fig 2.1b; k). The mitral leaflets were trimmed until they were just large enough to be identified for histology purposes (Fig 2.1b; l). Approximately 5 mm of muscle was retained at the junction between the mitral valve leaflets and the heart muscle (Fig 2.1b; j). Small incremental incisions were made to remove parts of the atrium until 5

mm of tissue was left between the atrium and junction of the mitral leaflets (Fig 2.1b; m). The remaining tissue was stored in PBS at room temperature and processed as described in the various methods.

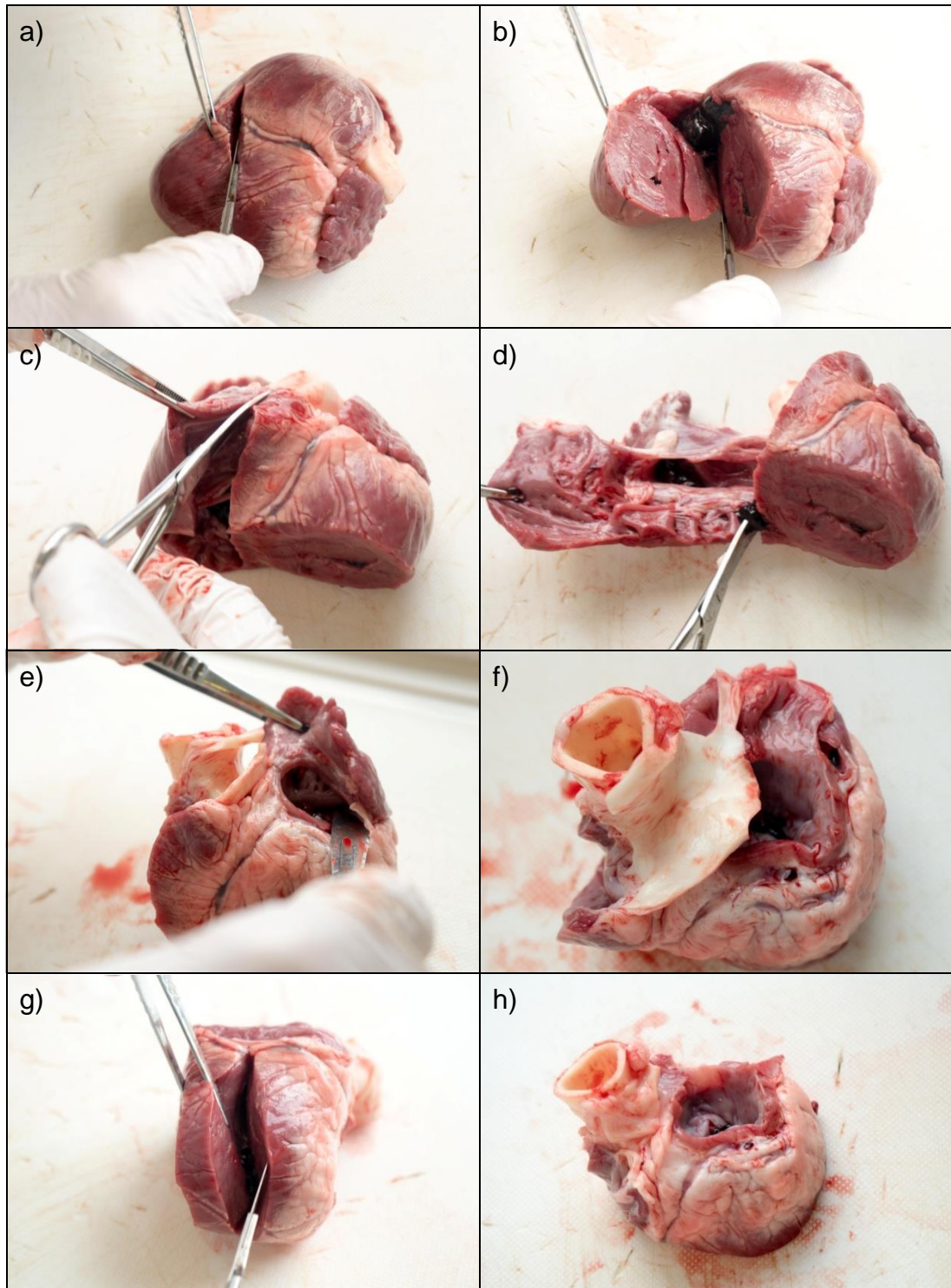


Fig 2.1a – Dissection of porcine and human mitral valve annulus.
Images of the porcine dissection. Cutting the apex (a, b), removal of the right side of the heart (c, d), removal of left auricle (e, f), cutting chordae and papillary muscles (g, h).

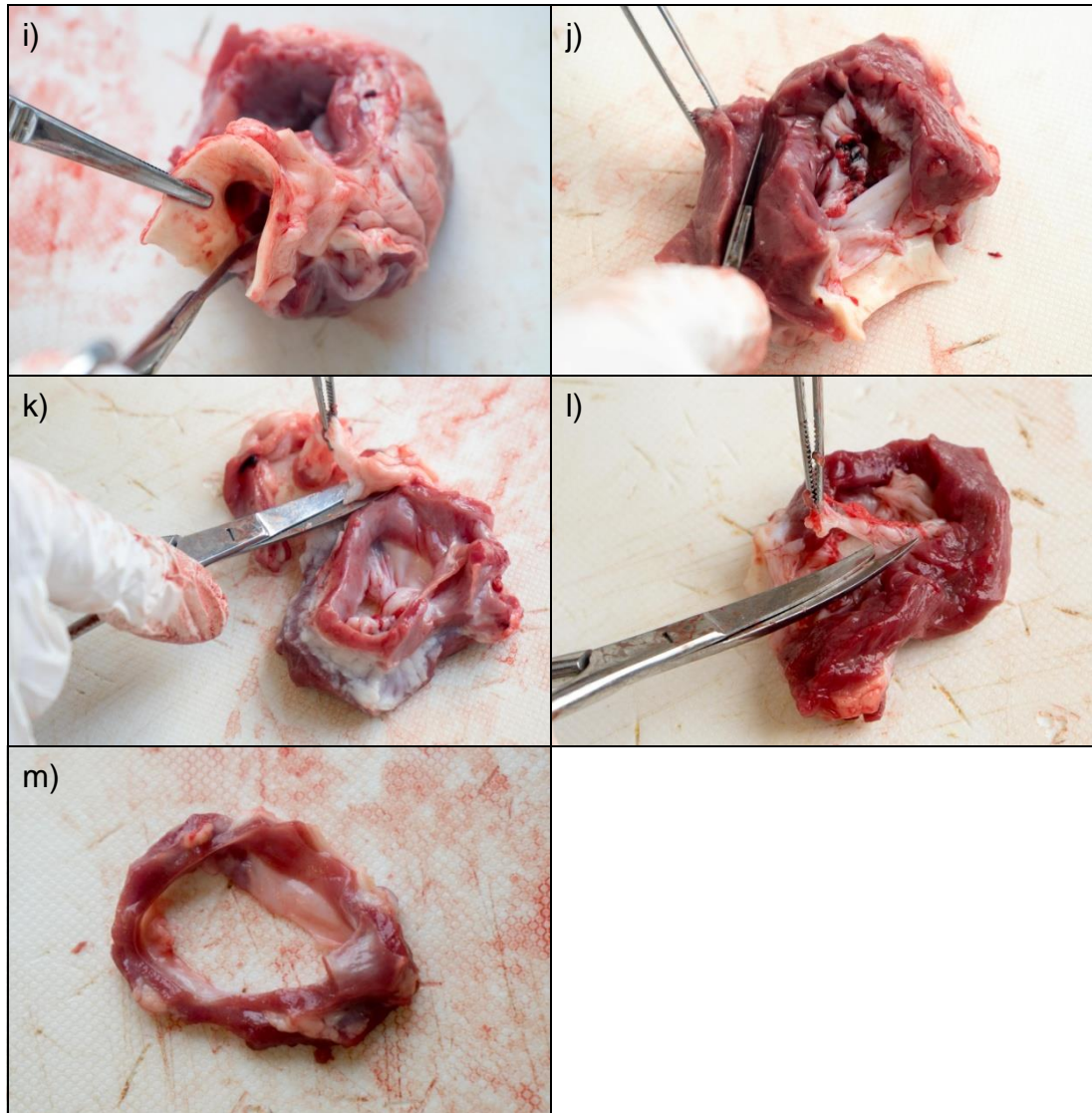


Fig 2.1b – Dissection of porcine and human mitral valve annulus. Images of the porcine dissection. Splitting the aorta (i), removal of the myocardium from the left ventricle (j), steps of incremental muscle removal (k), cutting the anterior and posterior leaflets up to the annulus (l), atrial side of the annulus (m).

2.2.3 Histological techniques

2.2.3.1 Fixation

Zinc fixation was utilised as a replacement to neutral buffered formalin (NBF). NBF can mask antigens on the surface of tissue which may affect the immunohistochemical characterisation of the mitral valve annuli. Zinc fixative offers improved antigen survival whilst maintaining the underlying morphological structure that is associated with the use of formalin (Beckstead, 1994). Zinc has also been used with formaldehyde based fixatives to improve morphology (Jensen *et al.*, 2010). Additional advantages are that it is non-hazardous, cheap and quick to prepare. Little has been

reported about the exact mode of operation for zinc, it is thought that the acetate may destabilise protein structures (Jensen *et al.*, 2010) whilst the zinc ions help stabilise the tertiary structures of proteins when exposed to chaotropic agents, such as acetate (Selevsek *et al.*, 2009). It has been suggested these work in tandem to cause mild denaturation of proteins which may harden them into a more rigid configuration so that they can be used as a fixative (Jensen *et al.*, 2010).

Reagents:

- Zinc fixative solution

Calcium acetate (0.5 g) was dissolved in 1000 ml of 0.1 M tris solution and adjusted to a pH of 7.0 – 7.4. Zinc acetate (5.0 g) was dissolved into the solution using a magnetic stirrer followed by 5.0 g of zinc chloride and stirred using a magnetic stirrer until dissolved.

Method

Each sample of the mitral valve annulus was cut vertically along its long axis and split into regions in order to facilitate placement in histocassettes. The annulus was split into suitable regions by using visible anatomical markers visible. The main markers were the left coronary sinus and non-coronary sinus for the anterior section, the commissures separating the anterior and posterior leaflets and the medial, middle and lateral scallops for the posterior section.

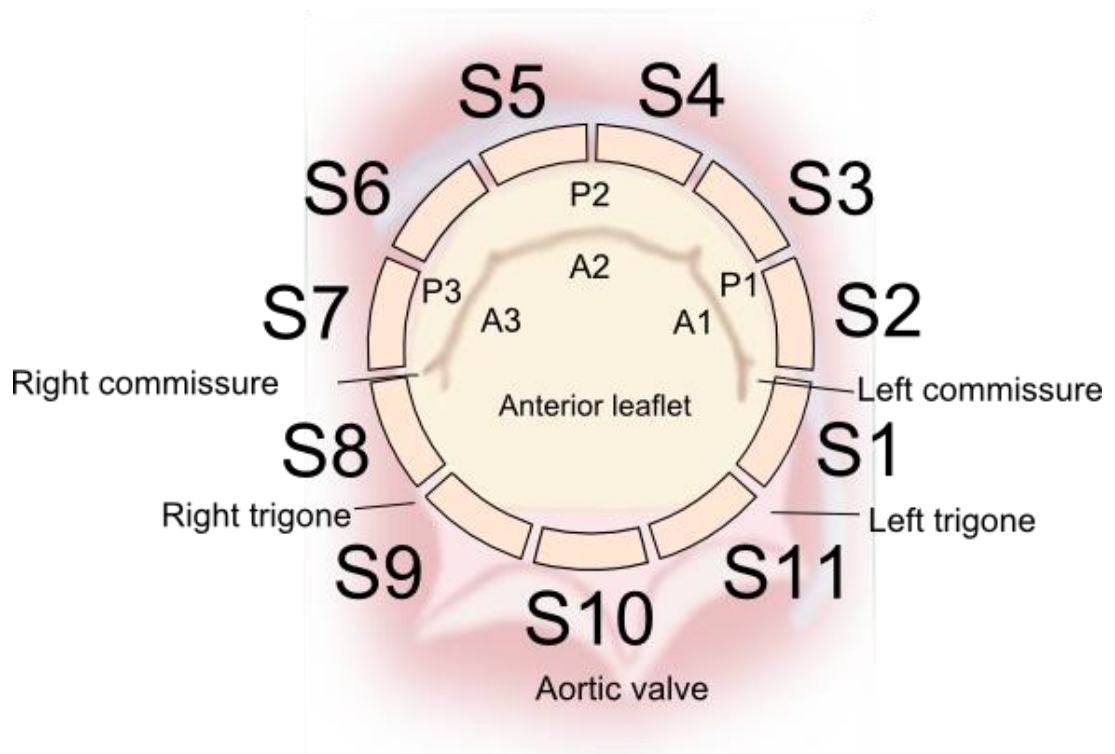


Fig 2.2 – Top view of mitral valve. All sections were cut along the long axis. S1 was cut vertically between the left trigone and the left commissure. S2 was between the left commissure and part of P1 scallop. S3 was half of the P1 scallop and part of the P2 scallop. S4 was half of the P2 scallop. S5 was half of the S5 scallop. S6 was part of the P2 and P3 scallop. S7 was part of the P3 scallop to the right commissure. S8, S9, S10 and S11 were part of the anterior mitral valve; S8 was from the right commissure to the right trigone, S9 was cut from the right trigone to half of the posterior leaflet of the aortic valve, S10 was cut from the second half of the posterior leaflet to half of the left leaflet of the aortic valve. S11 was the region of half of the left leaflet up to the left trigone. A1, A2, A3 are the anterior leaflet cleft. P1, P2 and P3 are the posterior leaflets clefts.

The plane of sectioning throughout was through the long axis. Samples were cut vertically and separated into 11 regions using anatomical markers as shown in Fig 2.2. Region S1 was the section between the left trigone and the left commissure. Region S2 encompassed the left commissure and part of the posterior leaflet (P1) scallop. Region S3 comprised of half of the P1 scallop and part of the P2 scallop. Region S4 comprised of half of the P2 scallop. Region S5 comprised of the second half of the S5 scallop, section S6 traversed part of the P2 and part of the P3 scallop. Region S7 comprised of part of the P3 scallop up to the right commissure. Regions S8, S9, S10 and S11 encompassed the aortic valve and were split into five regions; S8

comprised of the region from the right commissure to the right trigone, S9 encompassed the right trigone up to the first half of the posterior leaflet of the aortic valve, S10 comprised of the second half of the posterior leaflet and first half of the left leaflet of the aortic valve and finally, S11 was the region of the second half of the left leaflet up to the left trigone. Once cut into sections the samples were placed into histocassettes ready for processing. The vertical sections were placed into the cassettes and orientated so the cross sections would face the microtome blade. The cassettes containing the tissue samples were left for 24 hours in the zinc fixative which fixed the tissue for embedding.

2.2.3.2 Paraffin wax embedding

Following fixation the tissue samples were placed into a Leica Microsystems tissue processor. The processor was set to program three which processed the tissue as shown in Table 2.6.

Table 2.6 – Tissue processor station solutions and durations.

Station number	Solution	Time
1	70 % (v/v) ethanol	1 h
2	90 % (v/v) ethanol	1 h
3	100 % (v/v) ethanol	1 h
4	100 % (v/v) ethanol	1 h
5	100 % (v/v) ethanol	1 h
6	Xylene	1 h
7	Xylene	1 h
8	Xylene	1 h
9	Paraffin Wax	1 h
10	Paraffin Wax	1 h
11	Paraffin Wax	1 h

Samples were taken from the tissue processor, removed from the cassettes and placed into wax block moulds and covered with molten wax. The tops of the cassettes were placed on top of the wax moulds and then left to cool until set. When set, the blocks were removed from the moulds and any excess wax trimmed off.

2.2.3.3 Tissue sectioning

The tissue was sectioned using a Leica microtome. Sections were cut at a thickness of 6 μm at a microtome blade angle of 5°. The sections were placed onto a water bath set at 45°C and collected onto glass superfrost or superfrost plus slides. The slides were left to dry on a hot plate at a temperature of 45°C for four hours.

2.2.3.4 Dewaxing and rehydration

The slides were placed into a slide holder and immersed into histoclear for ten minutes and then a second pot of histoclear for a further ten minutes. The slides were then placed into three consecutive pots of ethanol (100% v/v) for dehydration for three minutes, two minutes and a further two minutes. The slides were transferred to another pot of ethanol (70% v/v) for a further two minutes and then rinsed under running tap water for three minutes for rehydration of the sections.

2.2.3.5 Dehydration and mounting

Sections were dehydrated by placing the slides into ethanol (70% v/v) for five seconds, moving the slides into three consecutive pots of ethanol (100% v/v) for one minute, two minutes and finally three minutes. The slides were removed from the ethanol and placed into histoclear for ten minutes and a second pot of histoclear for a further ten minutes. A disposable pipette was used to drop DPX on each of the tissue sections which were then covered with cover slips, removing any air bubbles with stainless steel forceps. The slides were left to dry for 4 hours in a fume hood.

2.2.4 Histological staining methods

2.2.4.1 Haematoxylin and Eosin staining

Haematoxylin was used to stain nuclei and eosin was used to stain for the tissue architecture. After the dewaxing process (Section 2.2.3.4) the slides were placed into haematoxylin for one minute and then rinsed with running tap water until the water ran clear. The sections were then immersed into an eosin counter stain for three minutes. This was followed by dehydration and mounting (Section 2.2.3.5). Sections were viewed under the microscope using Koehler illumination. Distances were measured using ImageJ software (National Institute of Health, USA).

2.2.4.2 Sirius red Miller's staining

Sirius red Miller's staining was used to visualise collagen and elastin.

Reagents:

- 5 % (w/v) potassium permanganate.

Potassium permanganate (15 g) was added to 300 ml of distilled water and stirred using a magnetic stirrer until dissolved

- 1 % (w/v) oxalic acid

Oxalic acid (1 g) was added to 100 ml of distilled water and stirred with a magnetic stirrer until dissolved.

- 0.1 % (w/v) Sirius red

Sirius red (0.1 g) was dissolved into 100 ml of aqueous saturated picric acid solution and magnetically stirred.

Sirius red stains collagen fibres and the Miller's stains elastin fibres blue. Following dewaxing and rehydration (Section 2.2.3.4) the slides were rinsed under running tap water for three minutes and immersed in potassium permanganate (5 % (w/v)) for five minutes and rinsed using distilled water. The slides were then placed into oxalic acid (1 % (w/v)) for two minutes and rinsed twice using distilled water for one minute and then a further four minutes. Each slide was placed into ethanol (70 % (v/v)) for one minute and then into ethanol (95 % (v/v)) for a further minute. The slides were placed into Miller's stain and left for one hour and then rinsed using 70 % (v/v) ethanol until the ethanol ran clear. The slides were placed into ethanol (95 % (v/v)) for a further one minute and then rinsed using tap water for two minutes. The slides were then immersed in Weigerts haematoxylin for ten minutes and rinsed using tap water for one minute and then a further 30 seconds using distilled water. The final stain of picro sirius red was applied for one hour and the slides were then rinsed using distilled water and blotted dry before being dehydrated and mounted (Section 2.2.3.5). Sections were viewed using polarised light microscopy.

2.2.4.3 Alcian Blue staining

This staining procedure was used to visualise glycosaminoglycan localisation. Periodic acid and Schiff's reagent were used as a counter stain to visualise other structures, Gills number 3 haematoxylin was used to stain the nuclei. After the dewaxing process (Section 2.2.3.4) the slides were placed into Alcian blue (1% v/v) for 15 minutes, immersed in running tap water for one minute and then rinsed with distilled water. The slides were then placed into periodic acid for five minutes and rinsed with distilled water three times. The next step involved placing the slides into Schiff's reagent for 15 minutes and then rinsing the slides with running tap water for five minutes. The slides were placed into haematoxylin for 90 seconds before being dehydrated and mounted (Section 2.2.3.5). Sections were viewed under the microscope using Koehler illumination.

2.2.4.4 DAPI staining of paraffin wax embedded tissue samples

DAPI staining enables visualisation of double stranded DNA and cell nuclei if present within paraffin embedded tissue sections on glass slides.

Reagents

- Dye buffer (10 mM Tris, 1 mM Na_2EDTA , 1 mM NaCl)

Trizma base (1.211g) was dissolved into 1L of distilled water along with 0.3724 g disodium ethylenediaminetetraacetic acid and 0.058 g sodium chloride and autoclaved at 121 °C, 15 psi for 20 minutes.

- DAPI dye solution (1 mg.ml^{-1})

Nuclease free water (10 ml) was added to 10 mg of DAPI and stored at -25°C until required.

- Working dye solution ($0.1 \text{ }\mu\text{g.ml}^{-1}$)

DAPI dye solution (20 μl) was added to 200 ml of dye buffer in a dark bottle and mixed by inverting with the pH adjusted to 7.4 and used immediately.

The slides containing sections for staining were placed into a slide holder and dewaxed and rehydrated (Section 2.2.3.4). The slide holder was placed into 200 ml of DAPI working solution in the dark and incubated at room temperature for ten minutes. The slides were washed using PBS in the dark

for ten minutes and this was repeated twice. Glass cover slips were mounted onto each slide using Dako fluorescence mounting medium and dried in the dark until set. Sections were stored in the dark at 4°C until visualised. Sections were viewed using an upright fluorescent microscope and a DAPI filter.

2.2.4.5 Von Kossa staining

Von Kossa staining was used to help visualize regions of calcium deposits. The silver ions react with phosphate or carbonate anions that are bound to the calcium deposits in the tissue.

Reagents:

- Silver nitrate (1 % w/v solution)

Silver nitrate (2g) was added to 200 ml dH₂O to give a 1 % (w/v) solution.

- Sodium thiosulphate (2.5 % w/v solution)

Sodium thiosulphate (5 g) was added to 200 ml dH₂O to give a 2.5 % (w/v) solution.

The slides containing sections for staining were placed into a slide holder and dewaxed and rehydrated (Section 2.2.3.4). The slide holder was placed into 200 ml of silver nitrate solution (1 %) at room temperature for 18 hours under a bright light (1 x 60 watt bulb). Slides were washed in sodium thiosulphate (2.5 %) for five minutes and rinsed in distilled water for one minute. Slides were counterstained with eosin for one minute before being dehydrated and mounted (Section 2.2.3.5). Sections were viewed under the microscope using Koehler illumination.

2.2.4.6 Immunohistochemistry

Immunohistochemistry was used to visualise specific antigens in the tissue sections.

Reagents:

- Hydrogen Peroxide solution (3 % (v/v))

Hydrogen peroxide (20 ml; 30 % (v/v)) was added to 180 ml PBS

- Antibody diluent (TBS; 0.1 % (w/v) bovine serum albumin; 0.1 % (w/v) sodium azide)

Sodium azide (6 ml; 10 % (w/v)), 300 µl of 5 % (w/v) bovine serum albumin (BSA) and 59.1 ml Tris buffered saline were mixed together and the pH adjusted to 7.6.

- Proteinase K (pH 7.5)

Ready-to-use, diluted in 0.05 mol/L Tris-HCl, 0.015 mol.l⁻¹ sodium azide

- Tris buffer (2 M, pH 7.6)

Trizma base (42.26 g) was added to 758 ml of distilled water

- Sodium chloride solution (3 M)

Sodium chloride (175.32 g) was added to 1 L of distilled water

- Tris buffered saline (TBS)

Tris solution (25 ml; 2 M) was added to 50 ml 3 M sodium chloride solution, 925 ml of distilled water was added to the solution and the pH adjusted to 7.6. Solutions were placed in an autoclave for 20 minutes at 121 °C at a pressure of 103 kPa. Items were stored for up to one month at room temperature.

- TBS containing 0.05% (w/v) Tween 20

Tween 20 (500 µl) was mixed with 1000 ml of autoclaved TBS and adjusted to a pH of 7.6. Solutions were used on the day.

The antibodies and isotype controls used for immunohistochemical analysis are listed in Table 2.7

Table 2.7 – Antibodies and isotype control antibodies with their corresponding working concentrations

Antibody	Supplier	Isotype	Working dilution	Working concentration	Isotype dilution	Positive control tissue	Detection system
Collagen I	Millipore (MAB3391)	Mouse IgG1 (Dako X0931)	1:100	10 mg.L ⁻¹	1:10	Porcine common carotid artery	Ultra vision: human Envision: Porcine tissue
Collagen II	Millipore (MAB8887)	Mouse IgG1 (Dako X0931)	1:200	1 mg.L ⁻¹	1:100	Porcine articular cartilage	Envision: all
Collagen III	Abcam (AB7778)	Rabbit IgG (GeneTex GTX35035)	1:1000	1 mg.L ⁻¹	1:1000	Porcine common carotid artery	Ultra Vision: all
Collagen IV	Dako (M0785)	Mouse IgG1 (Dako X0931)	1:50	1.57 mg.L ⁻¹	1:63	Porcine common carotid artery	Ultra Vision: all
Collagen VI	Millipore (MAB3303)	Mouse IgG1 (Dako X0931)	1:800	2.5 mg.L ⁻¹	1:400	Porcine articular cartilage	Ultra Vision: all
Fibronectin	Dako (A0245)	Rabbit immuno	1:1000	4.9 mg.L ⁻¹	1:3000	Porcine common	Envision: all

		globu-lin fraction IgG (Dako X0936)				carotid artery	
Laminin	Sigma (L8271)	Mouse IgG1 (Dako X0931)	1:4558	1.57 mg.L ⁻¹	1:63	Porcine common carotid artery	Ultra Vision: all

Method:

For assessment of the expression of each antigen of interest in the mitral valve annulus tissue, three sections of the tissue and one section of the relevant control tissue were used. The first section of the mitral valve tissue served as a negative control (antibody diluent). The second section of the mitral valve tissue served as the isotype control (isotype control antibody in antibody diluent). The third section of the mitral valve tissue was the test section which was incubated with the primary test antibody in antibody diluent. The appropriate section of control tissue (known to express the antigen of interest) was also incubated with the primary test antibody in antibody diluent. The antibody staining protocol used the Ultra Vision One detection system unless there was background staining when Envision Detection system was used.

The Ultravision protocol was as follows:

Sections were dewaxed as described in Section 2.2.3.4. After the final ethanol step, sections were placed under running tap water for three minutes. An antigen retrieval step was carried out using proteinase K, this was placed dropwise onto all sections and incubated at room temperature for 20 minutes. The sections were then circled with a hydrophobic marker and then placed in 3 % (v/v) hydrogen peroxide solution for ten minutes and washed under running tap water for three minutes. Each of the slides was then washed in TBS for ten minutes and the excess solution blotted. Dual endogenous enzyme block (25 µl) was added to each section and incubated for ten minutes and washed twice using TBS for ten minutes each time. The diluted antibody was applied to the section of interest and the positive controls. The isotype control antibody was added to designated sections and

the negative control sections received only antibody diluent. The slides were then incubated in a moist atmosphere with TBS soaked tissue paper for 60 minutes. Following this the slides were washed twice in TBS-T for ten minutes each time and then washed twice in TBS for ten minutes each time. Labelled polymer-HRP (50 μ l) was applied to the sections and incubated for 30 minutes in the dark. This was washed with TBS-T twice for ten minutes each time followed by two washes in TBS for ten minutes with any excess tapped off. Substrate chromagen (50 μ l) was added to each section and incubated for ten minutes. Slides were then washed four times in distilled water. Following this step the slides were placed into haematoxylin for ten seconds before being dehydrated and mounted (Section 2.2.3.5).

The Envision+ protocol was as follows:

Sections were dewaxed as described in Section 2.2.3.4. After the final ethanol step, sections were placed under running tap water for three minutes. Sections were washed with TBS on a shaker and then circled with a hydrophobic marker. An antigen retrieval step was carried out using proteinase K, this was placed dropwise onto all sections and incubated at room temperature for 20 minutes. Following this step sections were rinsed with TBS. Dual endogenous enzyme block was added to each section and incubated for ten minutes. Sections were then washed for five minutes in TBS on a shaker and repeated three times. Primary antibody (50 μ l) was added to the section of interest and the positive controls. The isotype control antibody was added to designated sections and the negative control sections received only antibody diluent. The slides were then incubated for 30 minutes. Sections were then washed for five minutes in TBS on a shaker and repeated three times. Substrate chromagen (50 μ l) was added to each section and incubated for ten minutes. Slides were then washed four times in distilled water. Following this step the slides were placed into haematoxylin for ten seconds before being dehydrated and mounted (Section 2.2.3.5).

2.2.4.7 Labelling the alpha-gal epitope using biotinylated GSL-1 lectin

GSL-1 lectin binds specifically to galactosyl residues and can be used for labelling of α -gal epitopes in tissue sections. In the assessment of α -gal epitopes in tissue sections, two controls were utilized: α galactosidase treated tissue sections (negative control) and galactose-blocked lectin

controls (negative control) to determine the specificity of the lectin binding to the α -gal epitope.

Reagents:

- Ammonium formate buffer (50 mM)

Ammonium formate (315 mg) was dissolved in 50 ml distilled water using a magnetic stirrer and adjusted to pH 6.0

- Alpha galactosidase digestion solution

Ten units of α -galactosidase were dissolved in 2 ml of 50 mM ammonium formate solution, mixing by inversion and used immediately.

- Antigen unmasking solution

Antigen unmasking solution (2 ml) was mixed in 214 ml distilled water.

- Galactose blocking solution (200 mM galactose, 0.1 % sodium azide)

Galactose powder (360 mg) was reconstituted in 9 ml TBS and mixed with 1 ml 1 % (w/v) sodium azide.

- CarboFree blocking solution (1 %)

Stock CarboFree blocking solution (500 μ l; 10x) was added to 4.5 ml dH₂O and used immediately.

The staining procedure utilized the ImmPACT DAB Peroxidase (HRP) Substrate kit and the Streptavidin/Biotin blocking kit.

Sections were dewaxed as described in Section 2.3.3.4. After the ethanol step, sections were placed under running tap water for five minutes.

Samples were blotted and circled with an ImmEdge pen.

Digestion solution (20 μ l) was added to the control (α -galactosidase treated) sections and 20 μ l 50 mM ammonium formate buffer added to the test and

other negative control sections. Sections were incubated at 37 °C overnight in a moist environment. Each of the slides were then washed twice in TBS-T for ten minutes and then TBS twice. All sections were immersed in preheated antigen unmasking solution at 95 °C for 25 minutes followed by immersion in PBS for three minutes at room temperature. Sections were then immersed in 3 % (v/v) hydrogen peroxide in PBS for ten minutes and washed for three minutes with running tap water. Each section was blotted and covered with Streptavidin blocking solution dropwise, for 15 minutes.

The sections were rinsed with TBS and then covered with Biotin blocking solution dropwise for 15 minutes, followed by a further rinse with TBS. CarboFree blocking solution was applied for 30 minutes to prevent non-specific binding. Lectin was diluted in TBS to 5 µg. ml⁻¹ and added dropwise to the test and galactosidase treated sections. Lectin was also diluted in galactose blocking solution to 5 µg. ml⁻¹ and incubated for 30-60 minutes prior to use. Lectin blocked with galactose was added to the galactose-blocked lectin control sections.

Sections were washed twice with TBS-T for 10 minutes each followed by washes in TBS twice for 10 minutes each. Streptavidin, Horseradish Peroxidase, R.T.U was added to each section and incubated for 30 minutes. Sections were washed twice with TBS-T for 10 minutes each followed by washes in TBS twice for 10 minutes each. ImmPACT DAB working solution was prepared by adding 30 µl of Chromagen to 1 ml of diluent and mixed. Each section was blotted and 50 µl ImmPACT DAB working solution was added to cover each section which were incubated for five minutes until the tissue was stained. Slides were then washed four times in distilled water. Following this step the slides were placed into heamatoxylin for 30 seconds before being dehydrated and mounted (Section 2.2.3.5).

2.2.5 Cell Culture techniques

Reagents:

- BHK cell culture medium

Glasgow's minimal essential media (GMEM) was used with 5 % (v/v) foetal bovine serum (FBS), 10 % (v/v) tryptone phosphate broth, 2 mM L-glutamine and 100 U.ml⁻¹ penicillin and 100 U.ml⁻¹ streptomycin.

- L929 cell culture medium

Dulbecco's modified Eagle's medium (DMEM) was used with 10 % (v/v) FBS, 2 mM L-glutamine, 100 U.ml⁻¹ penicillin and 100 U.ml⁻¹ streptomycin.

Cells were cultured in the appropriate cell culture medium, aseptically in a class II safety cabinet. The cultures were incubated in 5 % CO₂ (v/v) in air at 37 °C and split when 70-80% confluent. Before use all culture media and solutions were equilibrated to 37 °C.

2.2.5.1 Resurrection and maintenance of primary cells and cell lines

Cells were removed from liquid nitrogen storage and thawed in a water bath at 37 °C and transferred to a plastic universal, 10 ml of the appropriate cell culture medium was added to the universal drop-wise. The cell suspension was centrifuged at 150 g for 10 minutes and the supernatant removed, the cell pellet was resuspended in 1 ml of fresh culture medium and added to 10 ml of culture medium in a T 75 cell culture flask. Flasks were incubated in 5 % CO₂ (v/v) in air at 37 °C. Cell culture medium was changed every two to three days and cells passaged when they were approximately 70 - 80 % confluent.

2.2.5.2 Cell passaging

Cell culture medium was aspirated from the flask and washed with 10 ml PBS without calcium or magnesium and removed. Trypsin/EDTA solution (3 ml) was added to the flask and incubated at 37 °C in 5 % CO₂ (v/v) for between two and five minutes. Flasks were tapped gently to dislodge the cells and checked for detachment under an inverted microscope. Fresh culture medium (10 ml) was added to the flask and then removed to a universal container. The medium was centrifuged at 150 g for ten minutes and the supernatant removed, the cell pellet was resuspended in 1 ml of fresh culture medium and added to 10 ml of culture medium in a T 75 cell culture flask.

2.2.5.3 Cell viability assay

The trypan blue dye exclusion method works on the notion that the cell membranes of dead cells are permeable to the dye and will appear blue. The membrane of viable cells are intact and therefore do not permit the dye to enter the cells which will leave them unstained.

A 50 μl volume of cell suspension was thoroughly mixed with 50 μl of the dye in a 2 ml Eppendorf. The combined cell suspension was transferred into a Neubauer counting chamber which had a volume of 0.1 μl per square and a cell count performed under an upright microscope observing the number of viable cells in a 5 x 5 matrix. The number of cells counted could be converted into the number of cells per ml by using the following equation:

$$\text{Number of cells. ml}^{-1} = \text{Mean cell count} \times 10^4 \times \text{Dilution factor (2)} \quad (2.1)$$

Where the dilution factor of two was used due to the dilution of the cell suspension in trypan blue dye.

2.2.6 Biomechanical testing

The biomechanical properties of porcine mitral annuli were investigated using low strain-rate to failure uniaxial tensile testing in an Instron 3365 test rig. Native and decellularised annulus samples (n=12) were compared in the study.

2.2.6.1 Preparation of the tissue samples

The mitral valve was removed from the porcine heart and the annulus was isolated following the procedure in Section 2.2.2.3. The annulus (Fig 2.3) was cut into four regions along its long axis, these regions were identified as the posterior R1 (between P2 segment of mitral leaflet), anterior R3 (left commissure to right commissure), right commissure R2 (P3 segment of mitral leaflet to right commissure) and left commissure R4 (P1 segment of mitral leaflet to left commissure) regions. Twelve samples were tested for each region. Each region was cut into 20 mm long sections in a circumferential orientation.

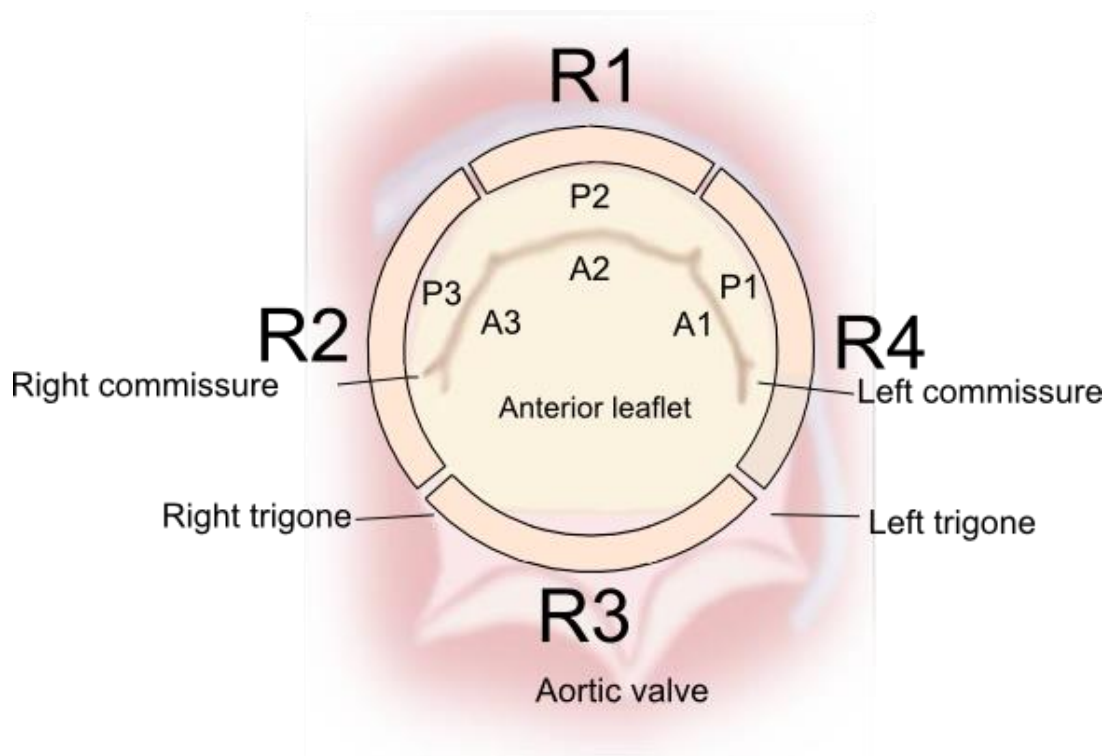


Fig 2.3 – Mitral annulus and leaflets. The annulus was split into four 20 mm circumferential regions. These were; R1: posterior (between P2 segment of mitral leaflet), R3: anterior (left commissure to right commissure), R2: right commissure (P3 segment of mitral leaflet to right commissure) and R4: left commissure (P1 segment of mitral leaflet to left commissure) regions.

Each region, 20 mm in length, was cut using a custom made cutter to a width of 5 mm. The cutter comprised of two parallel Stanley knife blades set at a width of 5 mm apart. The thickness of the tissue was measured by using Mitutoyo digital callipers at six points along the tissue strip and the average taken. The test specimens (Fig 2.4) were maintained moist throughout the procedure by irrigating with PBS solution. Custom made grips were used to secure the tissue into place to prevent slippage. A 10 mm gauge length was used for the tissue, this was set using a 10 mm spacer in the grips.

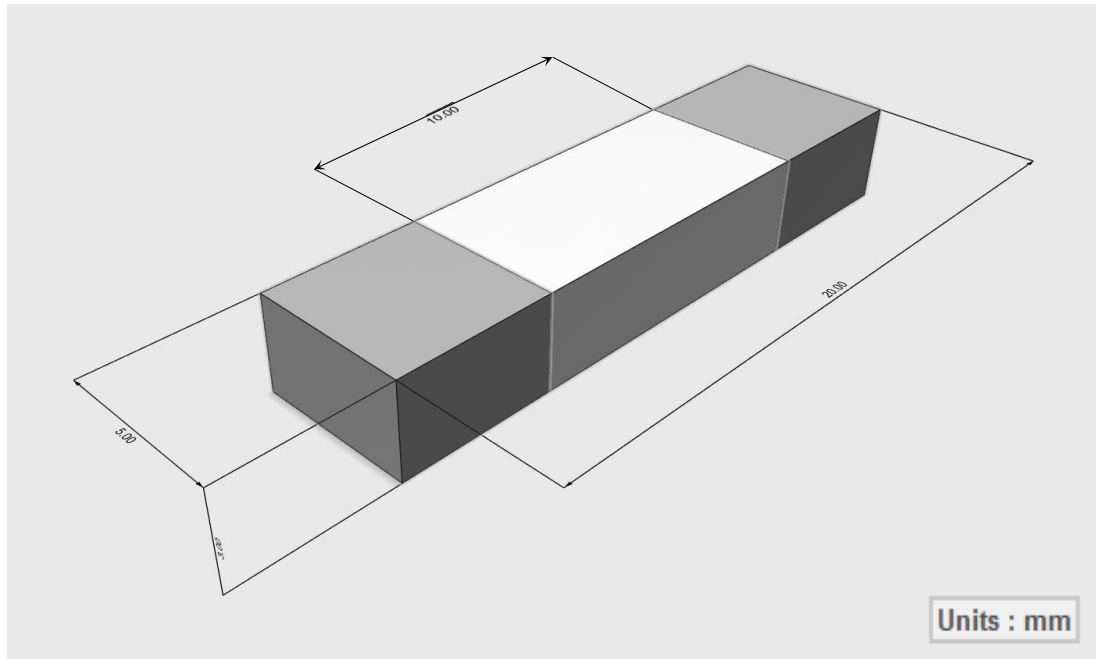


Fig 2.4 – Tissue specimen dimensions. Tissue length: 20mm, gauge length: 10mm, width: 5mm, thickness approximately: 3mm.

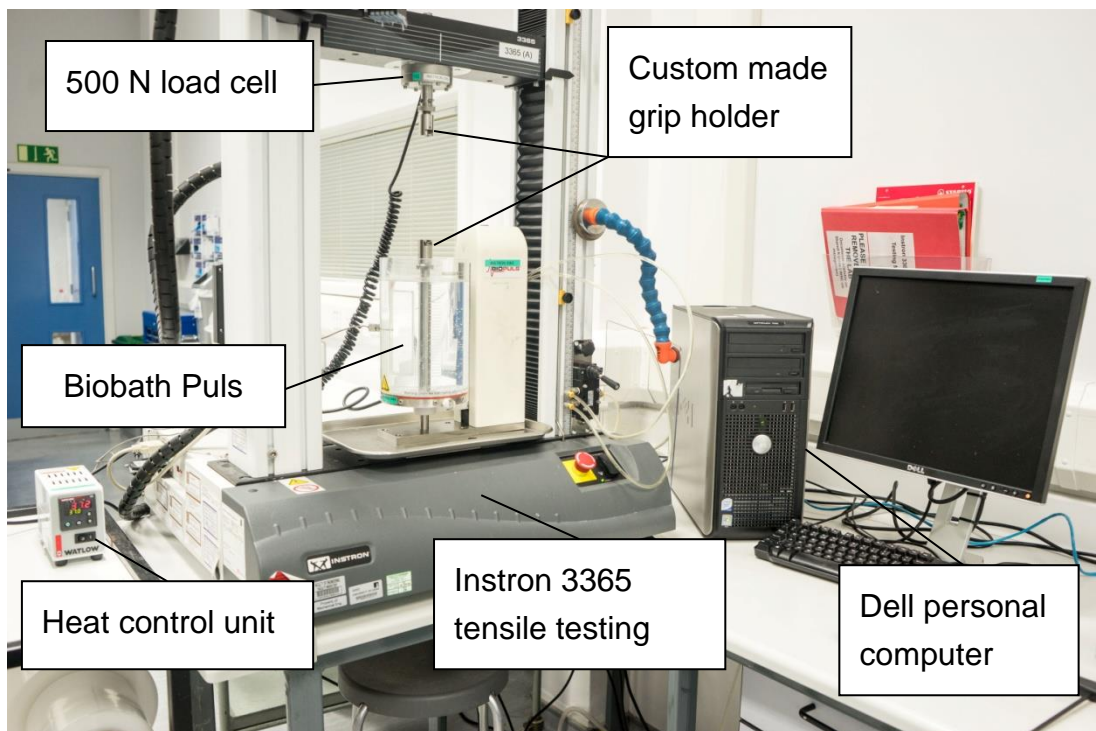


Fig 2.5 – Equipment used for tensile testing of native and decellularised porcine annuli. Instron 3365 test rig with Instron Biobath set at 37 °C.

The tissue specimens were tested using the Instron 3365 materials testing machine with 500 N load cell and an Instron 3130-100 Biopuls bath set at 37 °C (Fig 2.5).



Fig 2.6 – Instron 3365 test rig with Instron Biobath set at 37 °C with tissue clamped in custom made grips undergoing the test procedure.

The grips were mounted into the tensile testing rig and the spacer assembly was removed, the bio-bath was moved into position surrounding the tissue, ensuring that it was at the correct temperature (Fig 2.6).

2.2.6.2 Test procedure

The cross sectional area of the annulus was assumed to be rectangular for data calculation. Data regarding the width, depth, length and annulus specimen number were entered into the Instron program. Once the data had been entered and program setup had been completed the strain and load measurement were reset to zero. Initial length was classified as 10 mm gauge length. Testing data was recorded as the change in length of the tissue and the force detected on the load cell, data was stored in Excel and .dat formats. Slow strain rate loading to failure testing was completed on the tissue, a strain rate of $10 \text{ mm} \cdot \text{min}^{-1}$ was used for the test, with no preloading.

The data was converted to engineering stress and strains, from this the elastin phase slope, collagen phase slope, ultimate tensile stress, ultimate tensile strain, transition strain and stress values were obtained. The engineering stress was calculated using the formula:

$$\delta = \frac{F}{A_1} \quad (2.2)$$

Where: F = force (N), A_1 = cross sectional area (m^2), δ = stress (Pa). The cross sectional area was calculated as $w \times t$, where w was the width of the sample and t was the average thickness.

The engineering strain was calculating using the formula:

$$\varepsilon = \frac{\Delta l}{L_0} \quad (2.3)$$

Where: ε = strain, Δl =change in length (m) and L_0 = original length (m).

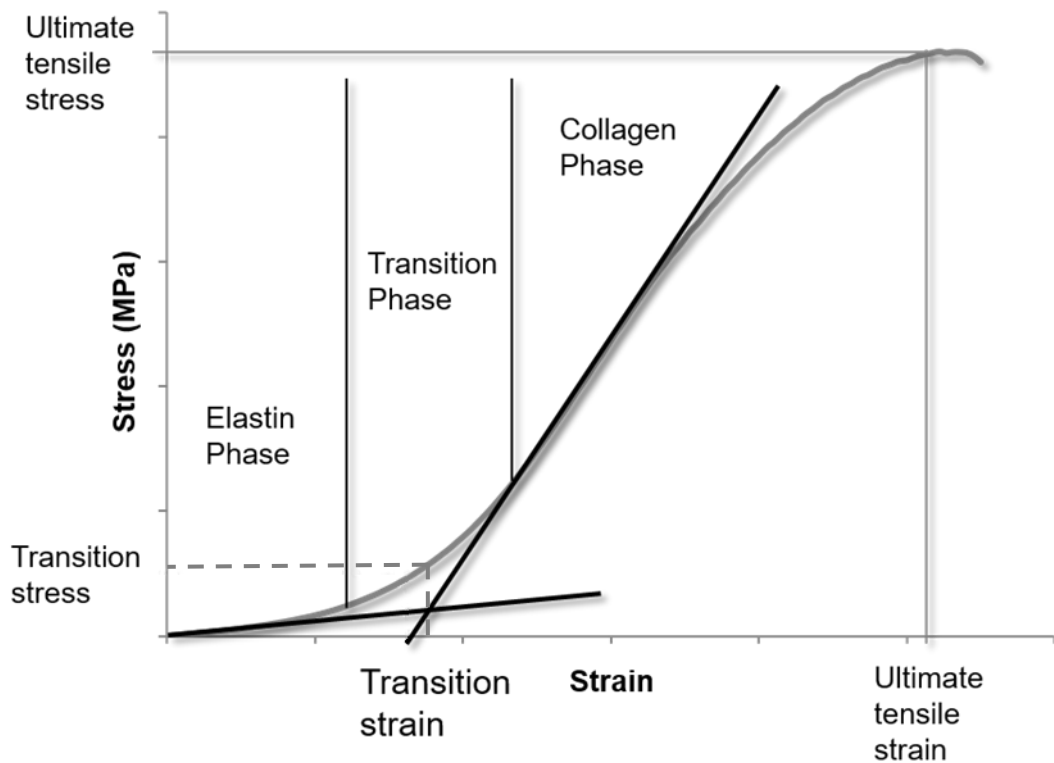


Fig 2.7 – Typical stress-strain curve of mitral valve annuli tissue subjected to uniaxial tensile loading to failure.

The stress-strain data was plotted using Microsoft Excel 2007 to attain the elastin phase (EI-E) and collagen phase (Coll-E) slopes along with the transition stress (σ_t), transition strain (ϵ_t), ultimate tensile stress (σ_s) and ultimate tensile strain (ϵ_s). A typical stress-strain curve of mitral valve annuli tissue is illustrated in Fig 2.7, demonstrating how the parameters from the uniaxial tensile testing were derived. The data was processed for each region with 12 replicates from 12 different pigs. Each parameter was averaged for the number of specimens in each region and data were presented as the mean and 95 % confidence intervals.

2.2.7 Statistical analysis

2.2.7.1 Confidence limits

Analysis was carried out in Microsoft Excel 2007 and numerical data presented as means \pm 95 % confidence intervals. The 95 % confidence intervals were calculated using Microsoft Excel data analysis package.

2.2.7.2 Statistical analysis

Groups of two means were compared using the student's t-test whilst groups of more than two means were compared using one-way analysis of variance (ANOVA). Post-hoc analysis was used to compare individual differences between groups by calculating the minimum significant difference (MSD) at $p = 0.05$ using the T-method, or T'-method for unequal group sample sizes. The Q value was obtained from a table of significant values.

$$MSD = Q \times SE$$
$$SE = \sqrt{\frac{MS}{n}}$$

Where SE is the standard error, MS is the mean square within groups and n is the number of replicates.

For data that is presented as a proportion Arcsin transformation was applied so that data met the assumption of standard distribution for ANOVA and allowed accurate calculation of the 95 % CI and statistical analysis. After statistical analysis had been undertaken values were back transformed so data could be reported as a proportion.

Chapter 3

Characterisation of human and porcine mitral valve annulus

3.1 Introduction

To understand the requirements for atrioventricular repair using a biological annuloplasty ring it was necessary to characterise the human mitral valve annulus. The reasons behind this were two-fold; to identify the structure and composition of the native human annulus and to establish if the human mitral valve annulus would be suitable for use as the starting material for the development of an acellular annuloplasty ring. The structure and composition of the human mitral valve annulus was compared to that of the porcine mitral valve annulus, in order to determine the utility of utilising the porcine tissue as an alternative, a more readily available source material.

The function of the annulus is to provide a foundation for the mitral valve leaflets, ensure complete leaflet competence during the systolic phase of the cardiac cycle whilst optimising stress reduction in the leaflets (Salgo, 2002).

The anatomical structure of both the human and porcine mitral valve annulus has been previously described (Kunzelman *et al.*, 1994). The total annular length was similar between species, albeit in both groups the excised annulus was significantly longer in the anterior region compared to the annulus in situ within the heart. The increase in length was attributed to redundancy existing in the posterior leaflet. The need for this redundancy arises from the adjustment of the valve to varying loading conditions during the cardiac cycle to ensure that the posterior and anterior leaflets remain opposed to each other when the valve closed.

The anterior and posterior regions of the human mitral valve annulus have contrasting architecture. Using histology it has been established that the anterior region comprises of the left and right fibrous trigones, with the anterior mitral leaflet forming a continuum into the aortic root between the trigones. In the posterior region the fibrosa layer of the posterior leaflet forms into a thin collagenous layer of the posterior annulus, separating the atrial and ventricular muscle (Walmsley, 1978; Angelini *et al.*, 1988; Berdajs *et al.*, 2007). No histological characterisation has been undertaken on the porcine mitral valve annulus previously.

The distribution of collagen types of the human mitral valve annulus has not been investigated. Collagen has an important structural role in tissue and understanding the distribution of collagen types in the annulus will provide an insight into the properties of the mitral valve annulus. The orientation of collagens within the mitral valve complex has been reported for the anterior and posterior mitral valve leaflets (Kunzelman *et al.*, 1993; Morticelli *et al.*, 2013) and the chordae (Cochran *et al.*, 1991; Kunzelman & Cochran, 1992) but has so far been unreported for the mitral valve annulus. Similarly the spatial distribution of glycosaminoglycans (GAGs) in the annulus has yet to be reported, GAGs are distributed in the spongiosa of the mitral valve leaflets which may extend into the mitral valve annulus. GAGs hold water within tissue which helps to resist compression during biomechanical loading (Grande-Allen *et al.*, 2004). Identifying the GAG distribution will provide an insight into the regions of the annulus which may aid in resisting compression during the cardiac cycle.

The porcine mitral valve annulus may be a suitable animal tissue for use in decellularisation due to its anatomical similarities to the human mitral valve annulus. It is important that the biomaterial should resemble the properties of the native tissue so that it can provide similar biomechanical and biological functions. Whilst the anatomical features have been studied between species and basic histological features identified in the human mitral valve annulus, an in depth analysis of the microstructure has not and this requires further investigation.

It is hypothesised that the use of the annulus as an acellular biomaterial will provide sufficient support for the repair of the regurgitant mitral valve, whilst retaining the dynamic properties of the native annulus. Prior to developing an acellular material the biological characteristics of the human and porcine mitral valve annulus were characterised in order to (a) determine whether the porcine mitral valve annulus and human mitral valve annulus exhibited similar biological characteristics and (b) determine any effects of decellularisation treatments on the properties of the porcine mitral valve annulus

3.1.1 Aims and objectives

The aims of the research presented in this chapter were to characterise, compare and contrast the human and porcine mitral valve annuli using histological and immunohistochemical techniques in order to (a) assess the suitability of using donor human tissue as the starting material for the development of an acellular mitral valve repair device and (b) determine whether the porcine mitral valve annulus offered an alternative, readily available alternative source material.

The objectives were divided into two Parts

Part (1) Characterisation of the human mitral valve annulus

- To characterise the human mitral valve annulus using histological techniques (staining of sections using; haematoxylin and eosin, alcian blue to detect GAGs, Sirius red Miller's to assess the orientation and localisation of collagen fibres)
- To assess the presence and distribution of collagen I, III, IV, VI in sections of the human mitral valve annulus using immunohistochemistry
- To assess the presence of calcification and ossification in sections of human mitral valve annulus tissue using Von Kossa staining and presence of collagen II.

Part (2) Characterisation of the porcine mitral valve annulus tissue using histological and immunohistochemical techniques:

- To characterise the porcine mitral valve annulus using histological techniques (haematoxylin and eosin, alcian blue, Sirius red Miller's staining of tissue sections)
- To assess the presence and distribution of collagen I, II, III, IV, VI in sections of the porcine mitral valve annulus using immunohistochemistry

3.2 Material and methods

3.2.1 Histological evaluation of the human and porcine mitral valve annulus

In order to characterise the human and porcine mitral valve annulus, in terms of histioarchitecture and to establish how closely the porcine mitral valve annulus resembled the native human annulus, the human and porcine tissue was evaluated using a range of histochemical methods. Three human mitral valve annuli, obtained from donors aged 84, 57 and 67 years old and labelled annulus 1, 2 and 3 respectively, were split into eleven regions. Mitral valve annuli (n=5), obtained from pigs aged 24-26 weeks old and labelled one to five, were each split into eleven regions.

The tissue specimens were fixed in zinc for 24 hours and processed for standard histology as described in Section 2.2. Sections from each of the eleven regions were stained with H&E (Fig 2.2; Chapter 2) in order to obtain a detailed analysis of the whole annulus.

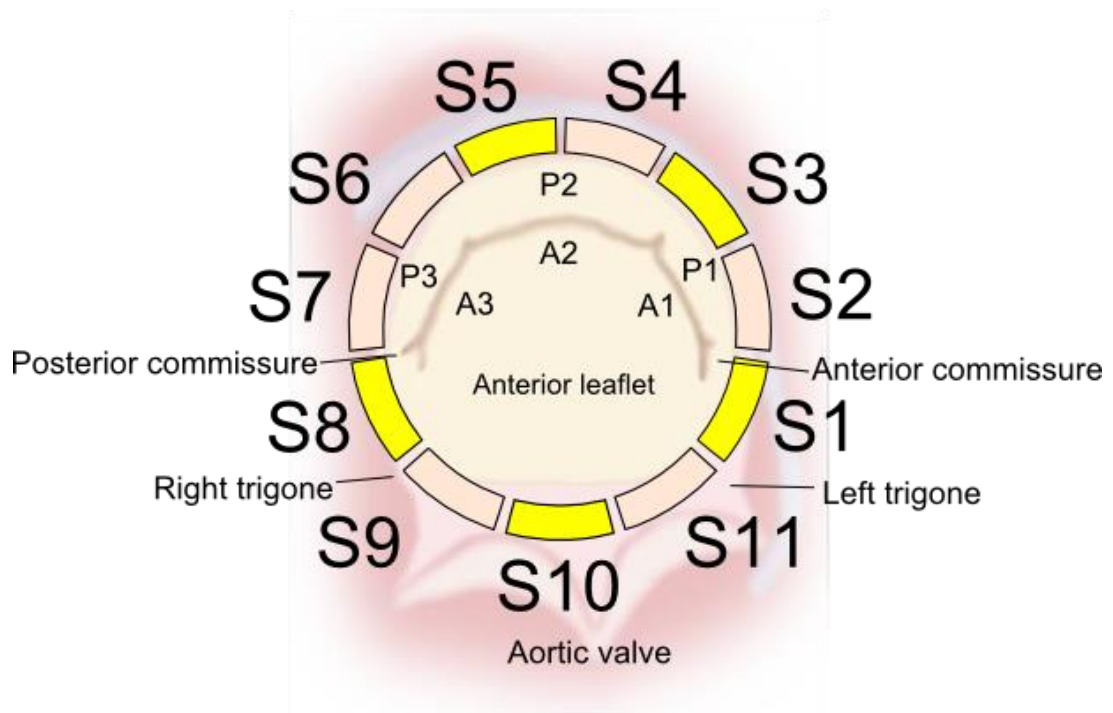


Fig 3.1 – Mitral annulus split into segments Regions S1-S11 were analysed using H&E stained tissue sections. Highlighted regions S1, S3, S5, S8 and S10 were selected for histochemical investigation of tissue sections using Sirius red Miller's, alcian blue, Von Kossa and immunohistochemistry. Anterior left trigone (S1), Posterior left (S3), Posterior right (S5), Anterior right trigone (S8), Anterior (S10).

Histochemical analysis of five regions of the native human and porcine mitral valve tissue (Fig 3.1) was undertaken using Sirius red Miller's (Section 2.2.4.2) and alcian blue (Section 2.2.4.3) stains. In addition, Von Kossa stain was used for the human tissue (Section 2.2.4.4).

3.2.2 Immunohistochemical analysis of the human and porcine mitral valve annulus

To assess the extracellular matrix of the tissue, immunohistochemical analysis was undertaken using tissue sections and antibodies to collagens I, II, III, IV and VI along with fibronectin and laminin. The positive control sample for collagens I, III, IV, fibronectin and laminin was porcine common carotid artery whilst for collagens II and VI it was porcine articular cartilage. Samples were split into regions S1, S3, S5, S8 and S10 as shown in Fig 3.1. The methods used for this part of the study have been described in Section 2.2.4.

3.3 Results

Part (1) Characterisation of the native human mitral annulus

3.3.1 Histological and histochemical characterisation of the native human mitral annulus

Sections of tissue from the eleven regions of the human mitral valve annulus were stained with H&E to determine the overall tissue structure. Images representative of the different regions are presented in Fig 3.2a and Fig 3.2b. Sections of the human mitral valve annulus stained with H&E exhibited a heterogeneous structure with varying characteristics in the anterior trigones, the mitral to aortic continuum and posterior region. Due to the age and health of the human tissue signs of calcification were present in the mitral valve of all three hearts. Calcification, indicated by violet staining in H&E sections was present in both the anterior region (Fig 3.2a; S1, Fig 3.2b; S8, S9, S10) and the posterior region (Fig 3.2a; S2, S4, Fig 3.2b; S7).

The anterior region comprised of the mitral to aortic continuum (Fig 3.2b; S10) and the left (Fig 3.2a; S1, Fig 3.2b; S11) and right trigonal regions (Fig 3.2b; S8, S9). The posterior annulus (Fig 3.2a; S2-S6, Fig 3.2b; S7) was more uniform in nature and comprised of thin collagenous region where the posterior mitral valve leaflet inserted. The thickness of the annulus at the junction where the leaflet inserted into the annulus was between 500 μm and 3000 μm in all samples. In the whole of the posterior region the atrial myocardium was isolated to the endocardial side of the mitral valve where adipose tissue comprised the majority of the atrial side of the valve from the atrial muscle to the epicardium. The atrial myocardium was approximately 500 - 1500 μm in width in both the posterior and anterior regions. The ventricular myocardial fibres close to the annulus were circumferential in orientation, whilst the atrial fibres were predominantly circumferential with some longitudinal fibres close the endocardium. The atrial myocardium also appeared to integrate into the atrial side of the anterior leaflet in some regions, on the atrial side of the annulus (Fig 3.2a; S1, Fig 3.2b; S8, S11).

Section 1 (Fig 3.2a; S1) formed part of the left trigone. It showed a heavily calcified fibrosa, but the calcification did not continue into the annulus. From the fibrosa, the annulus formed into a thickened zone of the trigone, this zone was defined by a dense collagenous-connective tissue at the junction of the anterior leaflet. Longitudinal fibrous extensions formed from the

trigones into the ventricular myocardium. Calcification was present in the region where the annulus joined the endocardium. Section 2 (Fig 3.2a S2) was part of the posterior annulus close to the left commissure, the annulus consisted of less collagenous-connective tissue and was heavily calcified, this calcification did not develop into the adjoining endocardium of the left ventricle. The annulus extended into the ventricular myocardium with longitudinal collagenous fibres which were separated by areas of ventricular myocardium. The ventricular myocardium extended from the annulus and ranged from the endocardium to the epicardium with a thickness of 3500 to 4000 μm at the annulus. In section 3 (Fig 3.2a; S3) the annulus was free from calcification, it had a cross section which was 900 μm to 1200 μm in diameter. The annulus integrated into the ventricular myocardium with longitudinal fibrous extensions. The ventricular myocardium was approximately 3000 μm thick close to the annulus and encompassed the region between the endocardium and epicardium. The annulus in section 4 (Fig 3.2a; S4) comprised of collagenous connective tissue approximately 1000 μm thick and double the width of the leaflet inserting into it. There were signs of calcification at the leaflet fibrosa close to the junction of the leaflet and annulus. The annulus formed into both the ventricular and atrial side of the valve. In section 5 (Fig 3.2a; S5) the mitral annulus had a cross section, 500 μm to 1000 μm in diameter with the appearance of circumferentially orientated collagen. The annulus formed into the ventricular myocardium with longitudinal collagen extensions which were separated by regions of ventricular myocardium. The ventricular myocardium encompassed the whole region between the endocardium and epicardium. The atrial muscle was separated from the annulus in this region. In section 6 (Fig 3.2a; S6) the annulus appeared free from calcification. The annulus was 1500 μm thick at the junction and elongated from the leaflet into the ventricular myocardium with collagen extensions, it had the appearance of collagen orientated circumferentially. The ventricular myocardium encompassed the whole region between the endocardium and epicardium.

Heavy calcification was present in the annulus and leaflet of section 7 (Fig 3.2b; S7a), the ventricularis and atrialis surfaces were the only regions free from calcification. Calcification was also present in the annulus close to the atrial muscle but there was no calcification bordering the ventricular muscle. Cells close to the areas of calcification (Fig 3.2b; S7b) had the appearance of osteochondral-like cells within lacunae, suggesting that ossification may have been present in this region. The annulus formed into the ventricular myocardium with longitudinal collagen extensions which were separated by

regions of ventricular myocardium. The atrial muscle was approximately 1500 μm in thickness and replaced by adipose tissue towards the epicardium whilst the ventricular myocardium traversed the whole region between the endocardium and epicardium. The right trigone (Fig 3.2b; S8) was part of the fibrous skeleton of the heart, calcification was present in the fibrosa and continued into the annulus. The atrial myocardium inserted into the atrial side of the trigone and was a similar thickness to the atrial myocardium in the posterior region with a width of approximately 1000 μm . The muscle was interspersed with loose connective tissue, adipose cells and blood vessels. Section 9 (Fig 3.2b; S9) formed part of the right trigone. The leaflet at the insertion into the annulus was approximately 1500 μm thick with the annulus forming into the left ventricle on the endocardial side of the valve. Calcification was present in the valve leaflet with some further calcification observed in the mitral annulus. Section 10 (Fig 3.2b; S10) formed part of the mitral to aortic continuum, composed of mitral valve leaflet, aortic wall and aortic valve leaflet. No ventricular myocardium was present. The maximum thickness was at the junction of the aortic valve leaflet of 500 μm , the minimum thickness was approximately 250 μm . Calcification was present in the aortic valve leaflet with some further calcification observed in the mitral leaflet and aortic wall. Section 11 (Fig 3.2b; S11) formed the left trigone, atrial myocardium was isolated to the atrial side of the anterior leaflet with a diameter of approximately 1000 μm which appeared to occupy part of the atrial side of the leaflet. Longitudinal collagen fibres extended from the annulus into the ventricular myocardium.

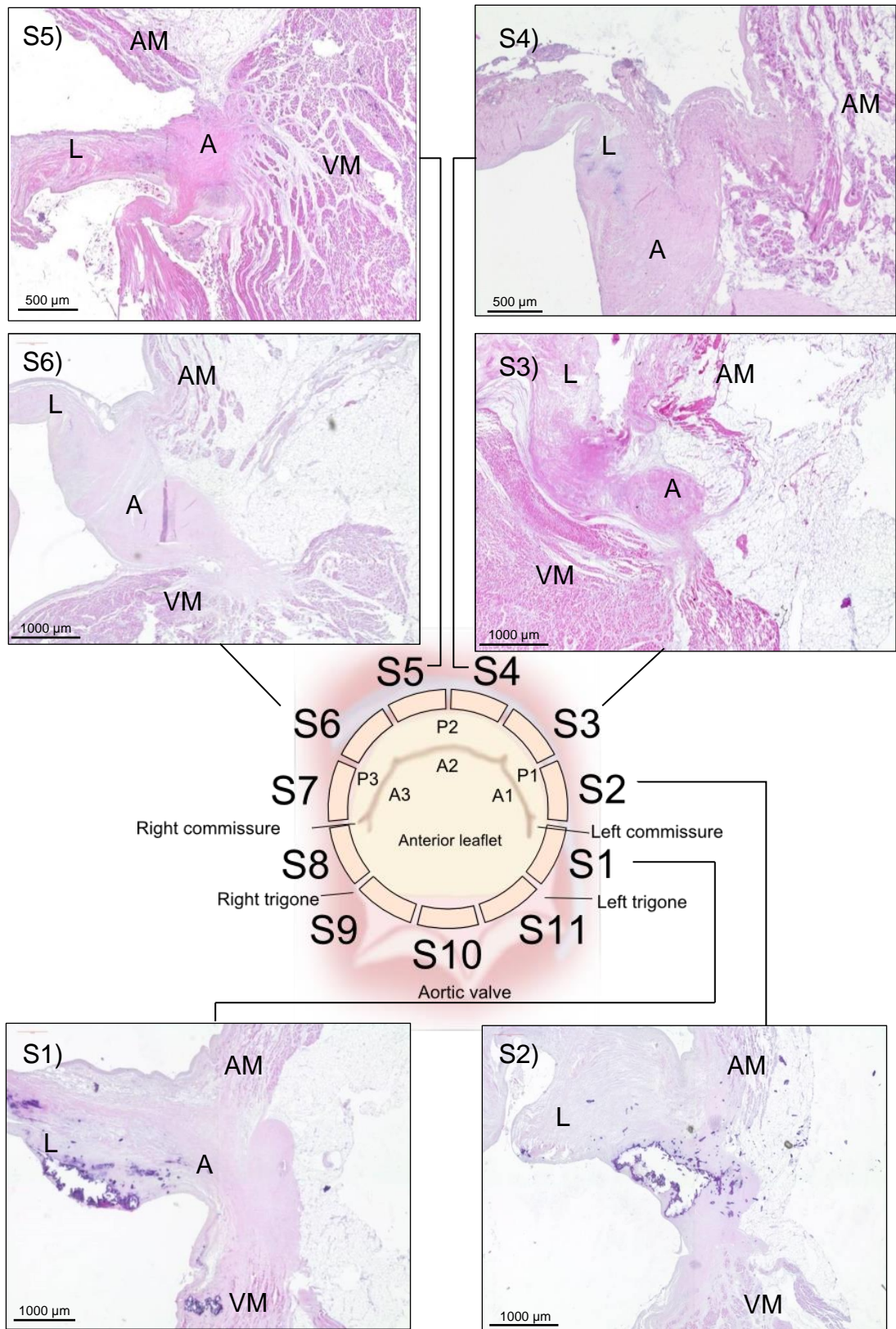


Fig 3.2a – Images of H&E stained sections from different segments of the native human mitral valve annulus. Representative images from three human annuli are shown. Section 1. Annulus 3 (S1), Section 2. Annulus 3 (S2), Section 3. Annulus 3 (S3), Section 4. Annulus 3 (S4), Section 5. Annulus 2 (S5), Section 6. Annulus 3 (S6). A: Annulus; T: Trigone; AM: Atrial Muscle; AV: Aortic Valve; AVL: Aortic Valve Leaflet; VM: Ventricular Muscle; L: Leaflet, MA: Mitral - Aortic continuum. Magnification x 20.

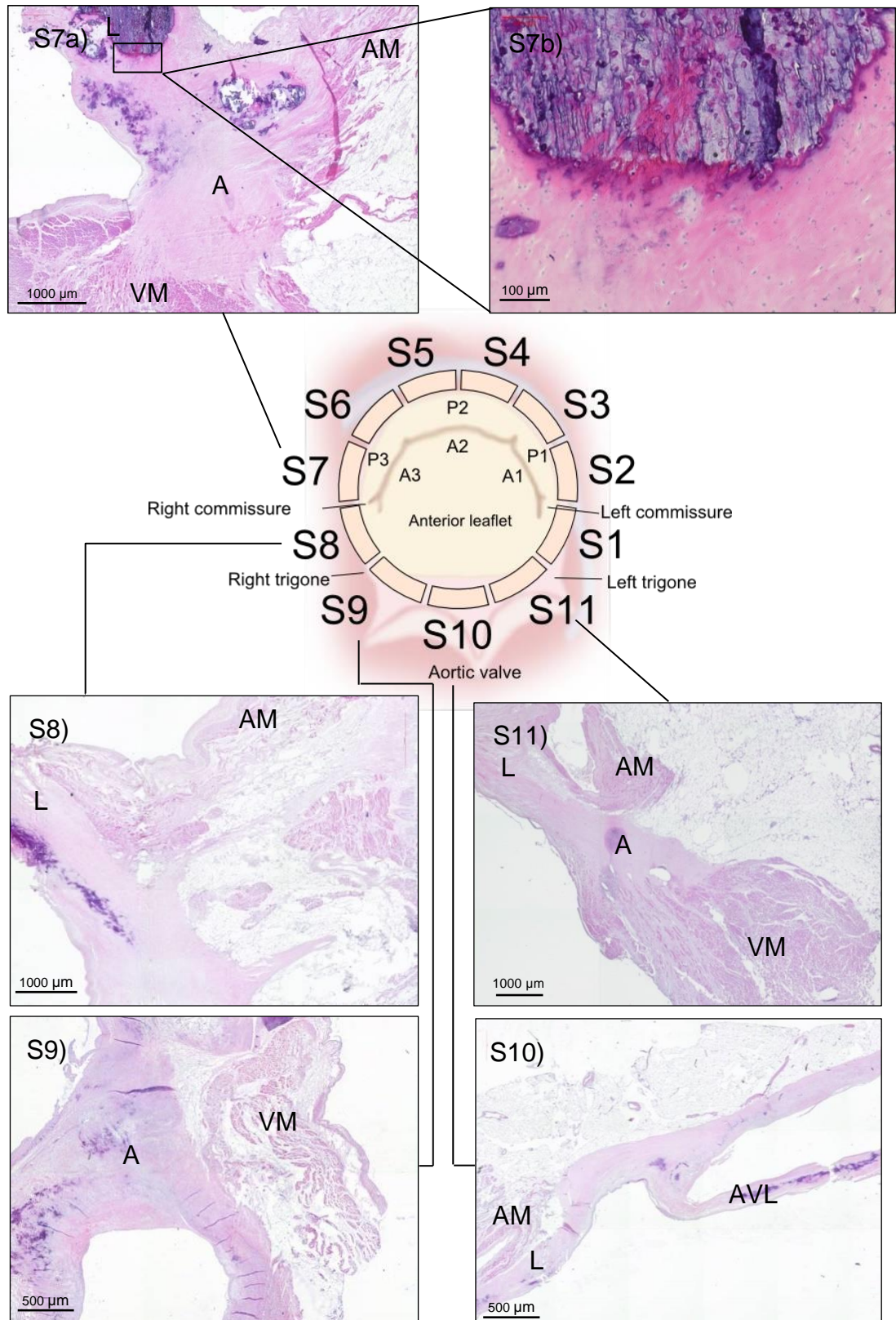


Fig 3.2b – Images of H&E stained sections from different segments of the native human mitral valve annulus. Section 7. Annulus 3 (S7a), Section 7. Annulus 3 x 100 magnification (S7b) Section 8. Annulus 3 (S8), Section 9. Annulus 1 (S9), Section 10. Annulus 3 (S10), Section 11. Annulus 2 (S11). A: Annulus; T: Trigone; AM: Atrial Muscle; AV: Aortic Valve; AVL: Aortic Valve Leaflet; VM: Ventricular Muscle; L: Leaflet, MA: Mitral - Aortic continuum. Magnification x 20 unless stated otherwise.

In selected segments (S1, S3, S5, S8 and S10) of the human mitral valve annulus, sections were stained with alcian blue to determine the presence and abundance of GAGs. GAGs were stained blue and were observed at the hinge point of both the anterior (Fig 3.3; S1) and posterior (Fig 3.3; S3 & S5) annulus where the leaflets inserted. In the atrial to mitral continuum GAGs were present in the spongiosa of the leaflet (Fig 3.3; S10).

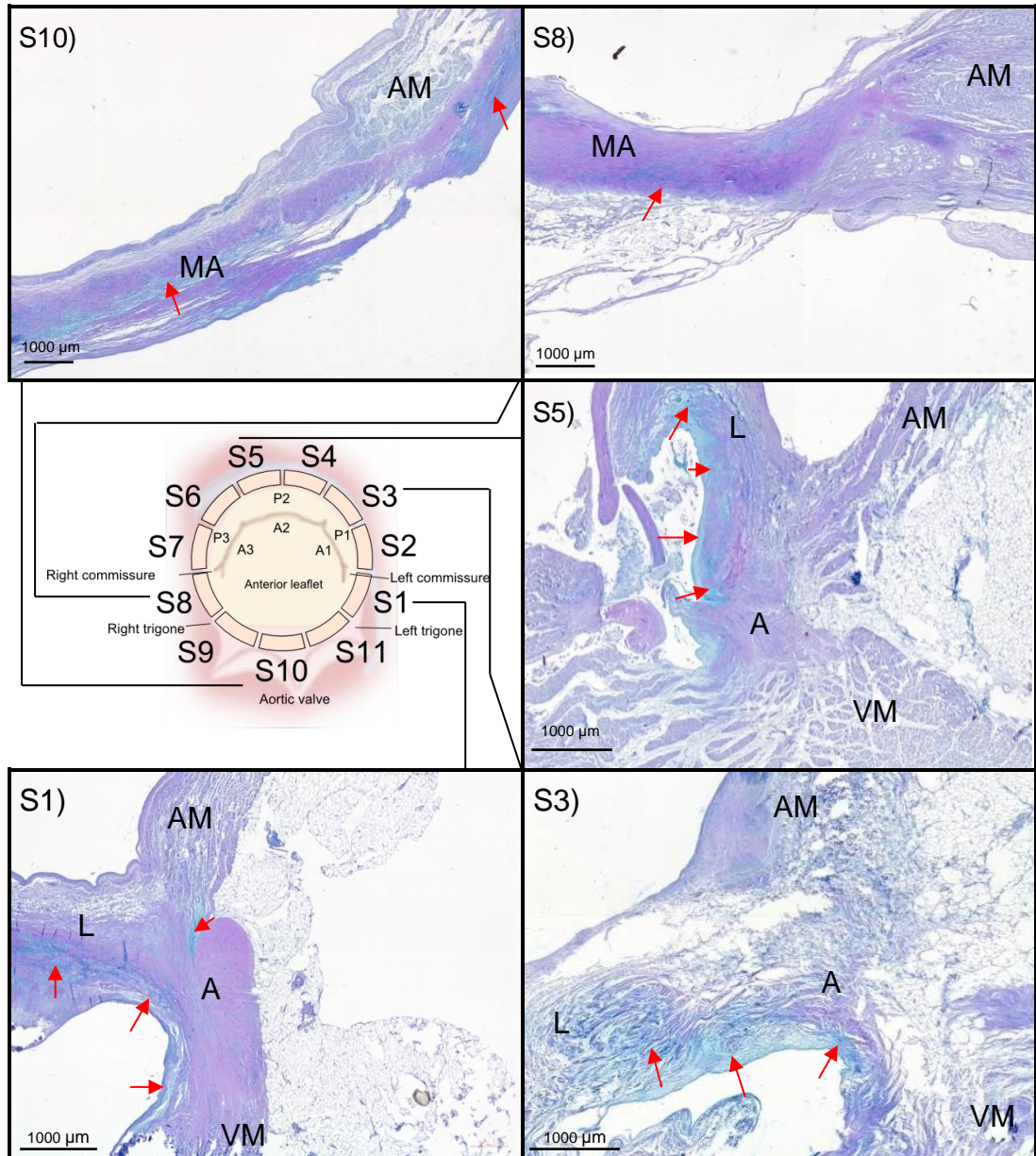


Fig 3.3 – Images of alcian blue stained sections from different segments of the native human mitral valve annulus. Representative images from three human annuli are shown. Blue regions highlight GAG content, red arrows indicate regions of GAGs. Section 1. Annulus 3 (S1), Section 3. Annulus 1 (S3), Section 5. Annulus 2 (S5), Section 8. Annulus 1 (S8), Section 10. Annulus 1 (S10). A: Annulus; T: Trigone; AM: Atrial Muscle; AV: Aortic Valve; AVL: Aortic Valve Leaflet; VM: Ventricular Muscle; L: Leaflet, MA: Mitral - Aortic continuum. Magnification x 20.

Sirius red Miller's stain was used to highlight the collagen within sections of the human mitral valve annulus. When viewed under polarised light the Sirius red gave an indication of the collagen orientation. When viewed under bright field microscopy the elastin fibres stained blue and collagen fibres stained red. The anterior and posterior leaflets forming into the annulus comprised of four layers; the atrialis, spongiosa, fibrosa and ventricularis. The atrialis of both the anterior and posterior leaflets was composed of densely packed elastin fibres (Fig 3.4a, 3.4b). The spongiosa was composed of a fine network of elastin fibres and collagen fibres, the spongiosa formed into the upper region of the annular junction and continued up towards the atrial myocardium. Densely packed collagen fibres were observed in the fibrosa which formed into the lower region of the annulus. The ventricularis was composed of a thin network of collagen and elastin which formed into the ventricular endocardium.

Under polarised light the fibrosa appeared densest in, or close to, the right and left trigones, with a thickness of approximately 1000 μm (Fig 3.4a; S1 b, Fig 3.4b; S8 b). Some of the central fibres appeared radially aligned under polarised light but most of the dense collagen observed in bright field microscopy (Fig 3.4a; S1 b, Fig 3.4b; S8 b) was weakly birefringent under polarised light, with no discernible collagen orientation (Fig 3.4a; S1 a, Fig 3.4b; S8 a). The mitral to aortic continuum (Fig 3.4b; S10) was defined by the layers of the mitral valve leaflet, the ventricularis which comprised a thin but dense elastin and collagen network, the fibrosa was comprised of prominent collagen approximately 500 μm thick, whilst a loose collagen and elastin network was present in the spongiosa and the atrialis comprised of dense elastin. There were some radially aligned collagen fibres running in parallel with the continuum but under polarised light, the collagen orientation appeared to be isotropic.

The posterior region (Fig 3.4a; S3, S5) was weakly birefringent in the fibrosa, suggestive of fewer radially aligned collagen bundles. This layer was thinner than in the anterior, with a fibrosa thickness of approximately 500 μm , and formed of loose bundles of collagen that formed into the lower region of the annulus. The lower region of the annulus continued down into the left ventricular myocardium. The spongiosa, characterised by loose elastin and collagen fibres formed into the upper half of the annulus and here it was thicker compared to the anterior annulus.

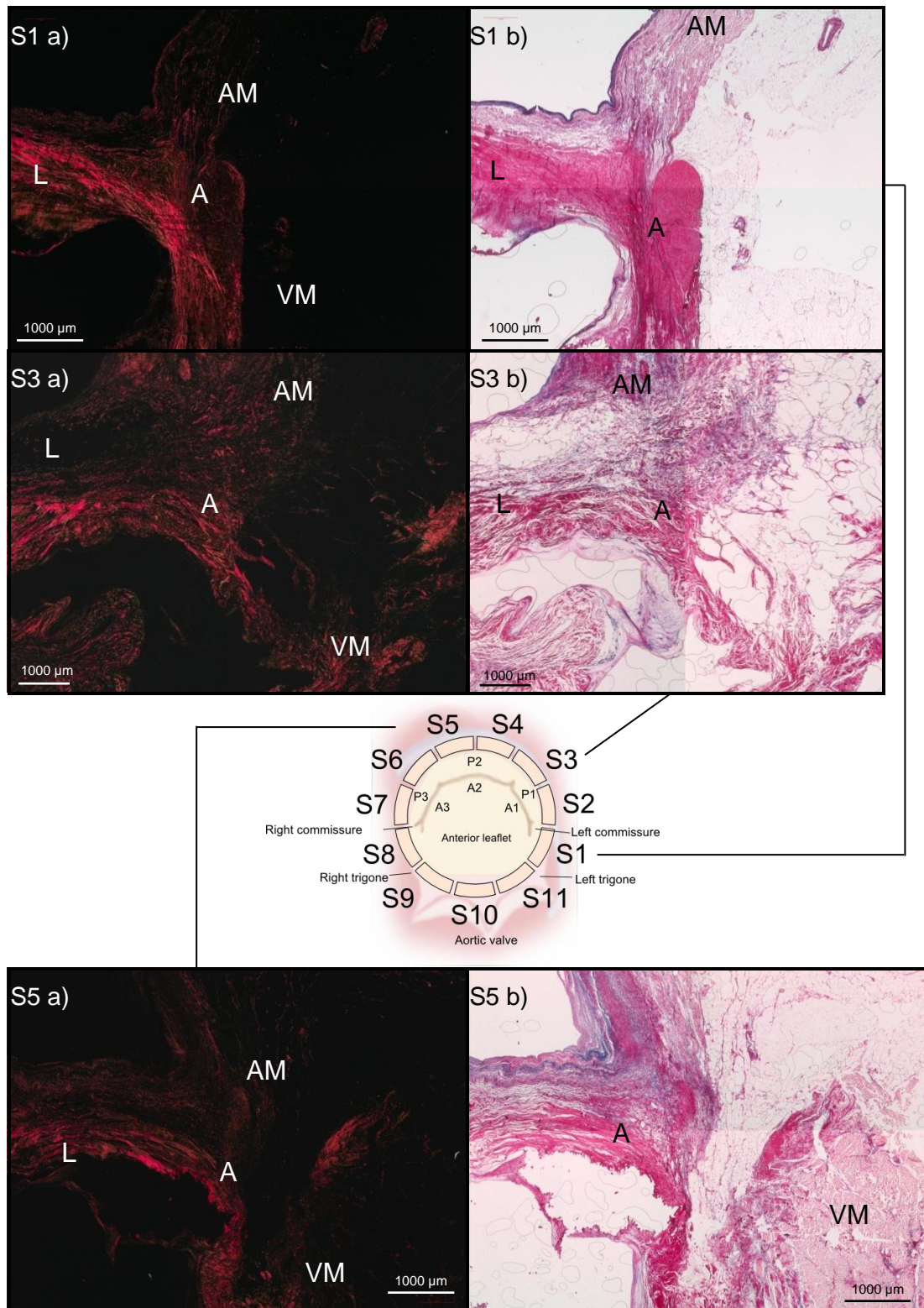


Fig 3.4a – Images of Sirius red Miller's stained sections from different segments of the native human mitral valve annulus viewed under (a) polarised light and (b) bright field microscopy. Representative images from three human annuli are shown. Section 1. Annulus 3 (S1 a), Section 1. Annulus 3 (S1 b), Section 3 Annulus 1 (S3 a), Section 3. Annulus 1 (S3 b), Section 5. Annulus 1 (S5 a), Section 5. Annulus 1 (S5 b).

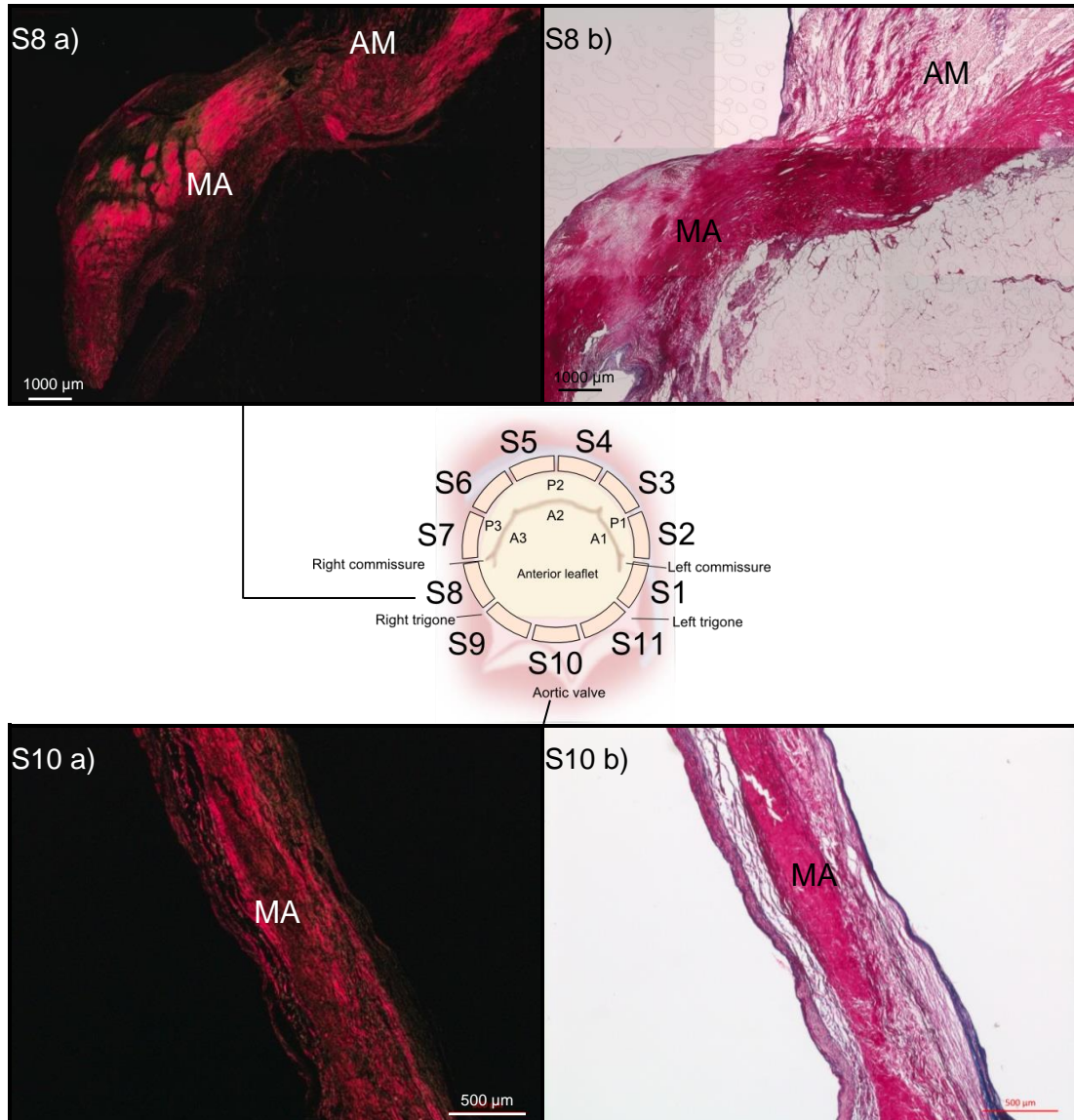


Fig 3.4b – Images of Sirius red Miller's stained sections from different segments of the native human mitral valve annulus viewed under (a) polarised light and (b) bright field microscopy. Collagen fibres are stained red, elastin fibres are stained blue. Section 8. Annulus 1 (S8 a), Section 8. Annulus 1 (S8 b), Section 10. Annulus 2 (S10 a), Section 10. Annulus 2 (S10 b). A: Annulus; T: Trigone; AM: Atrial Muscle; AV: Aortic Valve; AVL: Aortic Valve Leaflet; VM: Ventricular Muscle; L: Leaflet, MA: Mitral - Aortic continuum. Magnification x 20.

The Von Kossa stain was used to visualise calcium deposits within sections of the human mitral valve annulus and the surrounding tissue (Fig 3.5). Under bright field illumination calcium deposits appeared brown to black and the eosin counter stain stained basic components pink. Calcium deposits highlighted by brown staining were prominent along the endocardium and atrial and ventricular leaflet surface in every section of the tissue. The fibrosa of the leaflets in sections S1, S5 and S10 stained black and continued into the annulus, illustrating the deposition of calcium deeper within the annulus

region. Heavy calcification was identified in every layer of the posterior leaflet in section S8 with the calcification continuing into the annulus, as shown by the black staining.

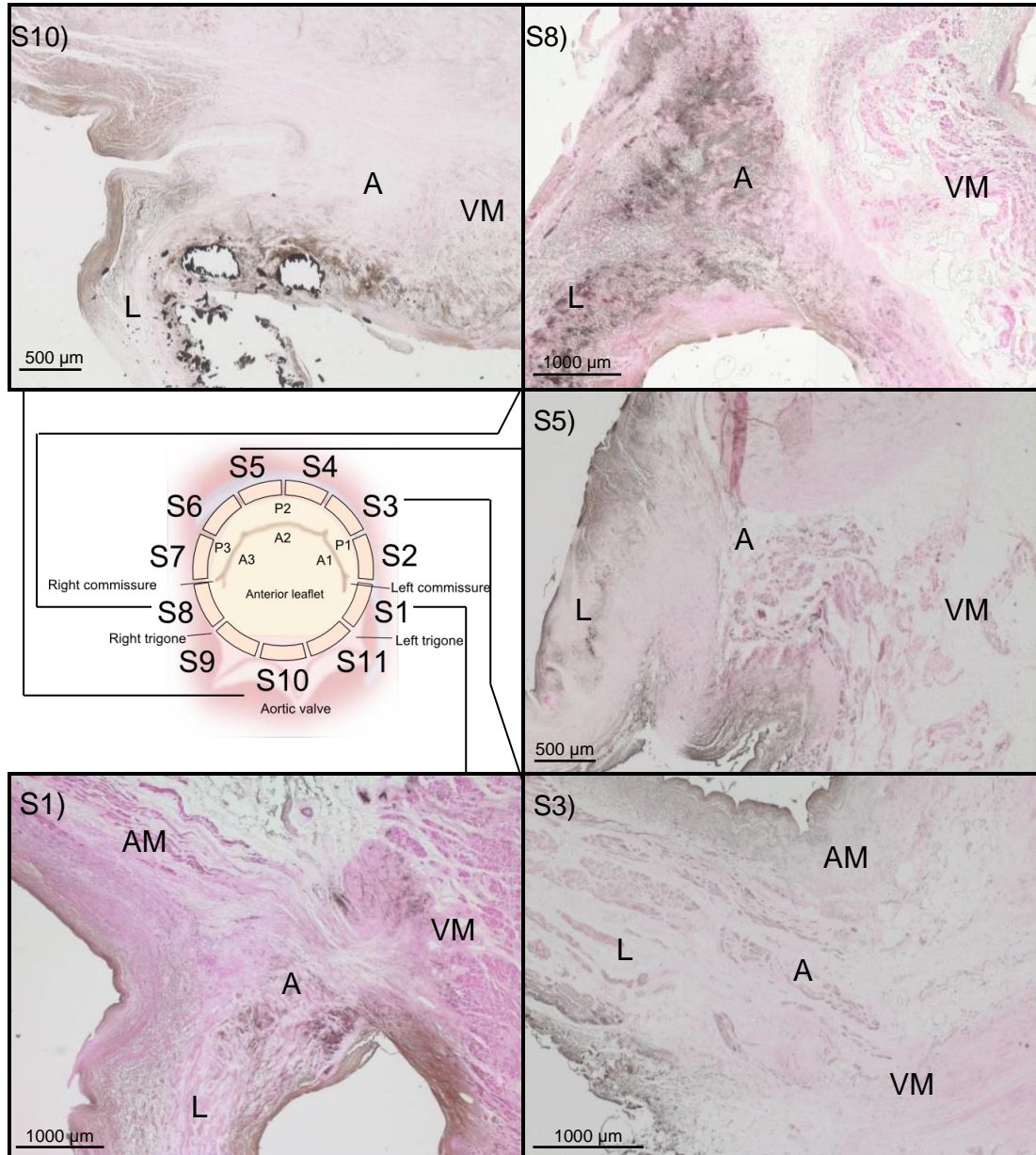


Fig 3.5 – Images of Von Kossa stained sections from different segments of the native human mitral valve annulus. Representative images from three human annuli are shown. Areas with apparent calcium deposits are stained brown to black. Section 1. Annulus 1 (S1), Section 3. Annulus 2 (S3), Section 5. Annulus 3 (S5), Section 8. Annulus 1 (S8), Section 10. Annulus 3 (S10). A: Annulus; T: Trigone; AM: Atrial Muscle; AV: Aortic Valve; AVL: Aortic Valve Leaflet; VM: Ventricular Muscle; L: Leaflet. Magnification x 20.

3.3.2 Distribution of proteins in the extracellular matrix of the human mitral annulus

The distribution of different structural proteins of the extracellular matrix of the human mitral valve annulus was investigated using immunohistochemistry.

3.3.2.1 Collagen I

Sections of the mitral valve annulus, described in Section 3.2.1, were labelled with antibodies to collagen I, indicated by brown staining in the images in Fig 3.6a. Positive staining was identified in the anterior regions of the trigones and mitral to aortic continuum as well as the posterior region (Fig 3.6a; S1-S10). Staining was more prominent in the fibrosa which integrated into the annulus, as well as the annulus, compared to the surrounding tissue such as the atrial and ventricular myocardium. Limited background staining was observed in the control sections labelled with the isotype control antibody (Fig 3.6b; a) and diluent alone (Fig 3.6b; b).

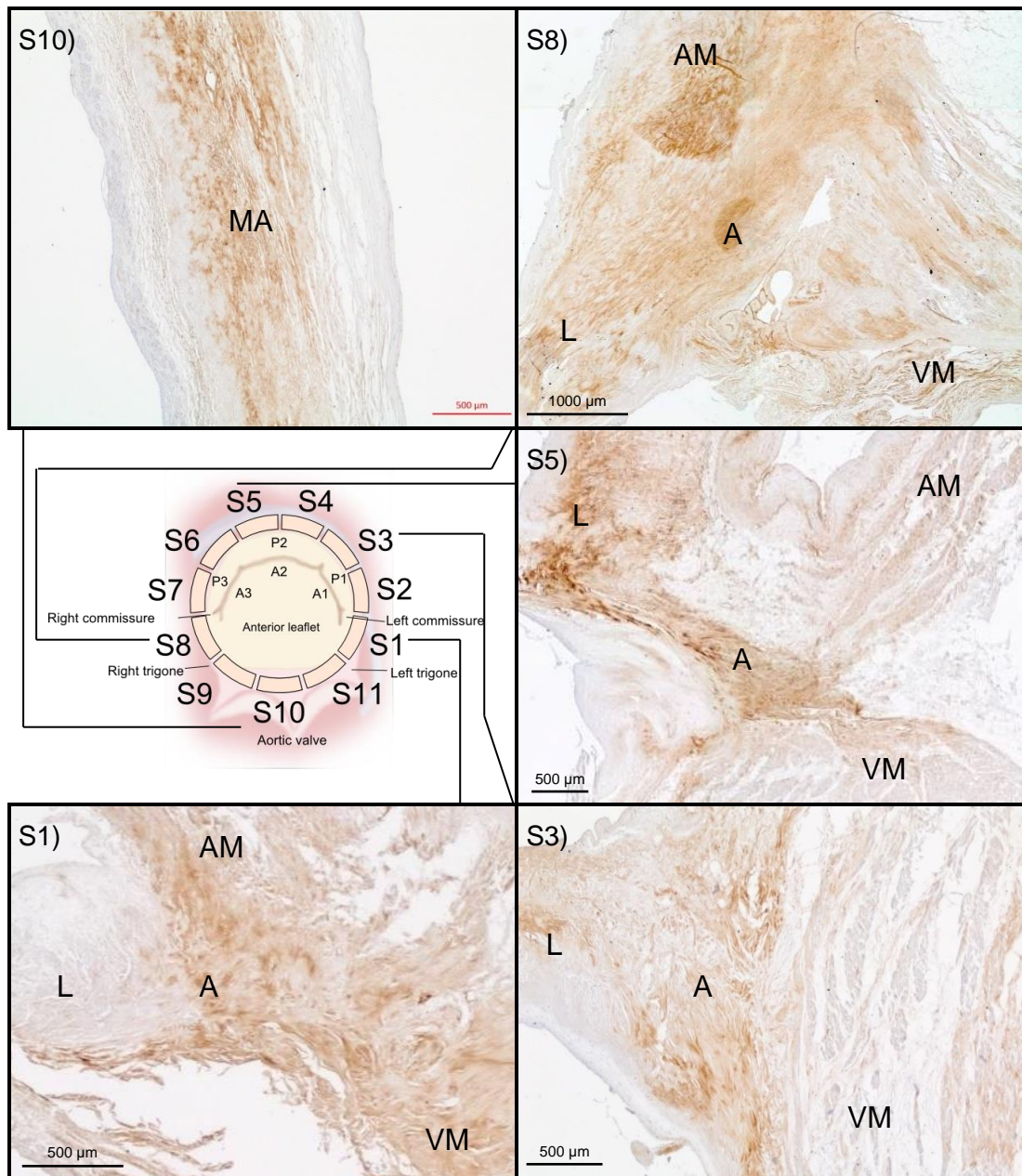


Fig 3.6a – Sections of human mitral valve annulus stained with antibody to collagen I. Representative images from three human annuli are shown. Sections labelled with antibodies to collagen I stained brown. Section 1. Annulus 2 (S1), Section 3. Annulus 2 (S3), Section 5. Annulus 2 (S5), Section 8. Annulus 3 (S8), Section 10. Annulus 1 (S10). A: Annulus; T: Trigone; AM: Atrial Muscle; AV: Aortic Valve; AVL: Aortic Valve Leaflet; VM: Ventricular Muscle; L: Leaflet, MA: Mitral-Aortic continuum. Magnification x 20

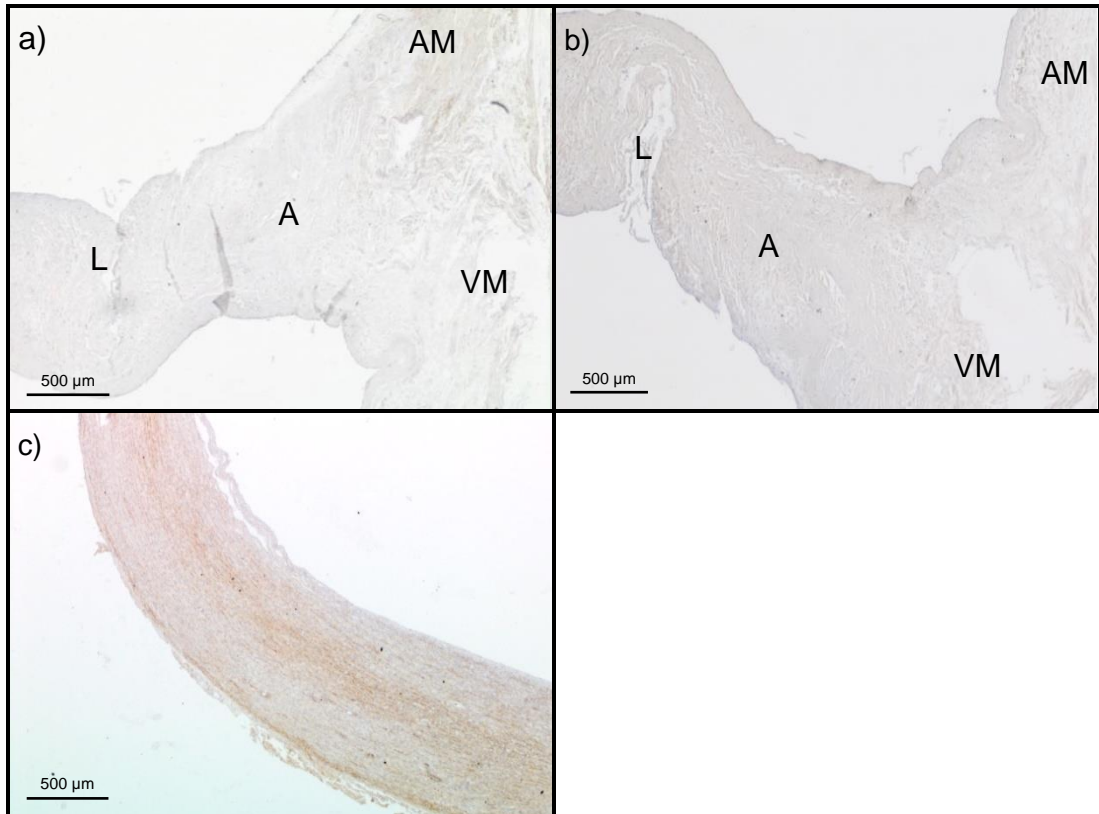


Fig 3.6b – Sections of human mitral valve annulus stained with antibody to collagen I. Representative images from three human annuli are shown. Sections labelled with antibodies to collagen I stained brown. Isotype control (a). Diluent control (b). Porcine common carotid artery positive control (c). A: Annulus; T: Trigone; AM: Atrial Muscle; AV: Aortic Valve; AVL: Aortic Valve Leaflet; VM: Ventricular Muscle; L: Leaflet, MA: Mitral-Aortic continuum. Magnification x 20.

3.3.2.2 Collagen II

Images of sections of the anterior and posterior regions (Fig. 3.7a) of the mitral valve annulus labelled with antibody to collagen II showed positive staining in the anterior region (Fig 3.7a; S8, S10), indicated by a dark brown colour. In the region that was positively stained for collagen II, lacunae type structures were visible (Fig 3.7a; S10b). Staining was not visible in the muscle surrounding the annulus. No staining was observed in the control sections stained with the isotype control antibody (Fig 3.7b; a) or diluent alone (Fig 3.7b; b).

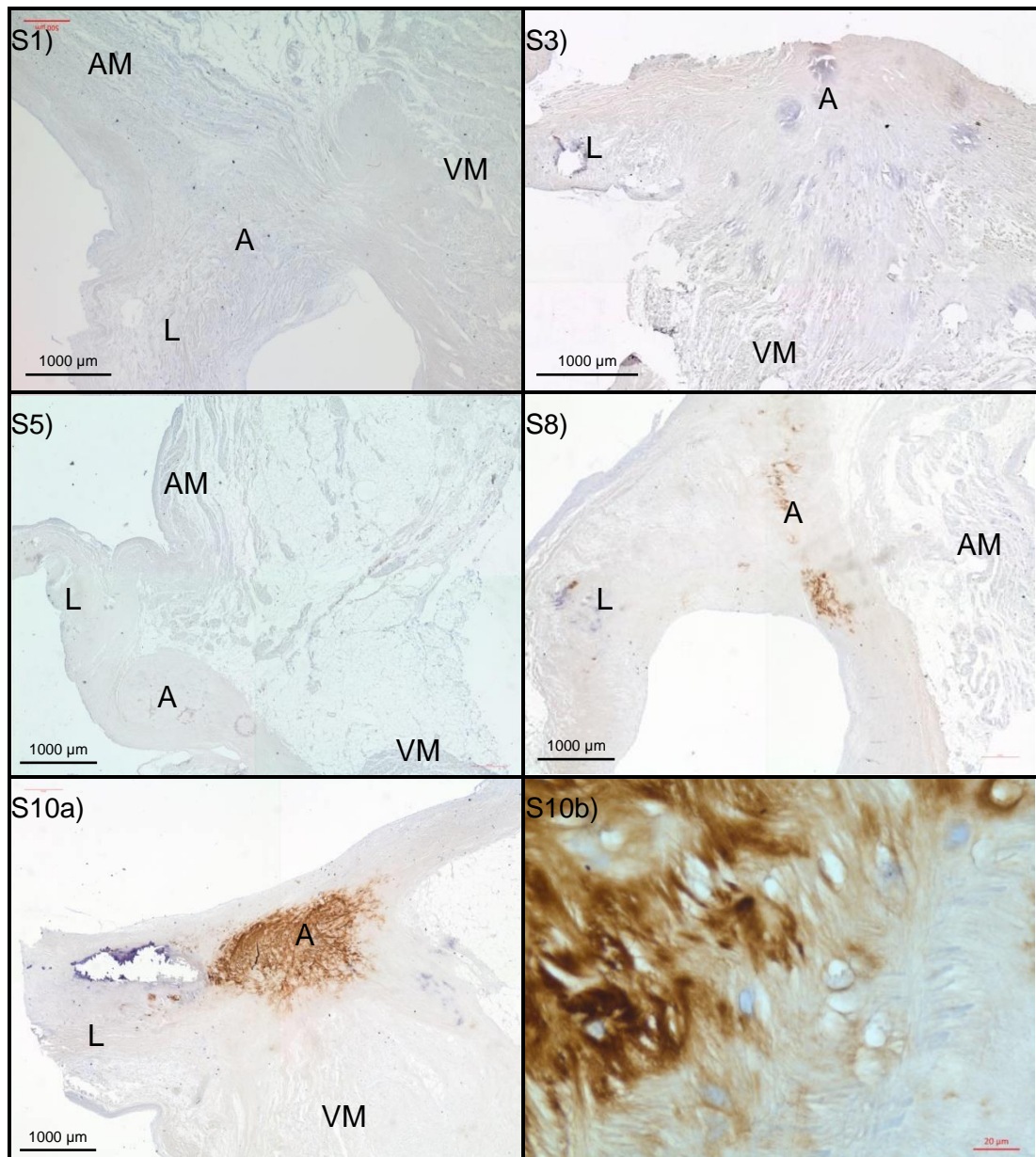


Fig 3.7a – Sections of human mitral valve annulus stained with antibody to collagen II. Representative images from three human annuli are shown. Sections labelled with antibodies to collagen II stained brown. Section 1. Annulus 1 (S1), Section 3. Annulus 2 (S3), Section 5. Annulus 3 (S5), Section 8. Annulus 1 (S8), Section 10. Annulus 1 (S10a). Section 10. Annulus 1 x 400 magnification (S10b). A: Annulus; T: Trigone; AM: Atrial Muscle; AV: Aortic Valve; AVL: Aortic Valve Leaflet; VM: Ventricular Muscle; L: Leaflet, MA: Mitral - Aortic continuum. Magnification x 20 unless stated otherwise.

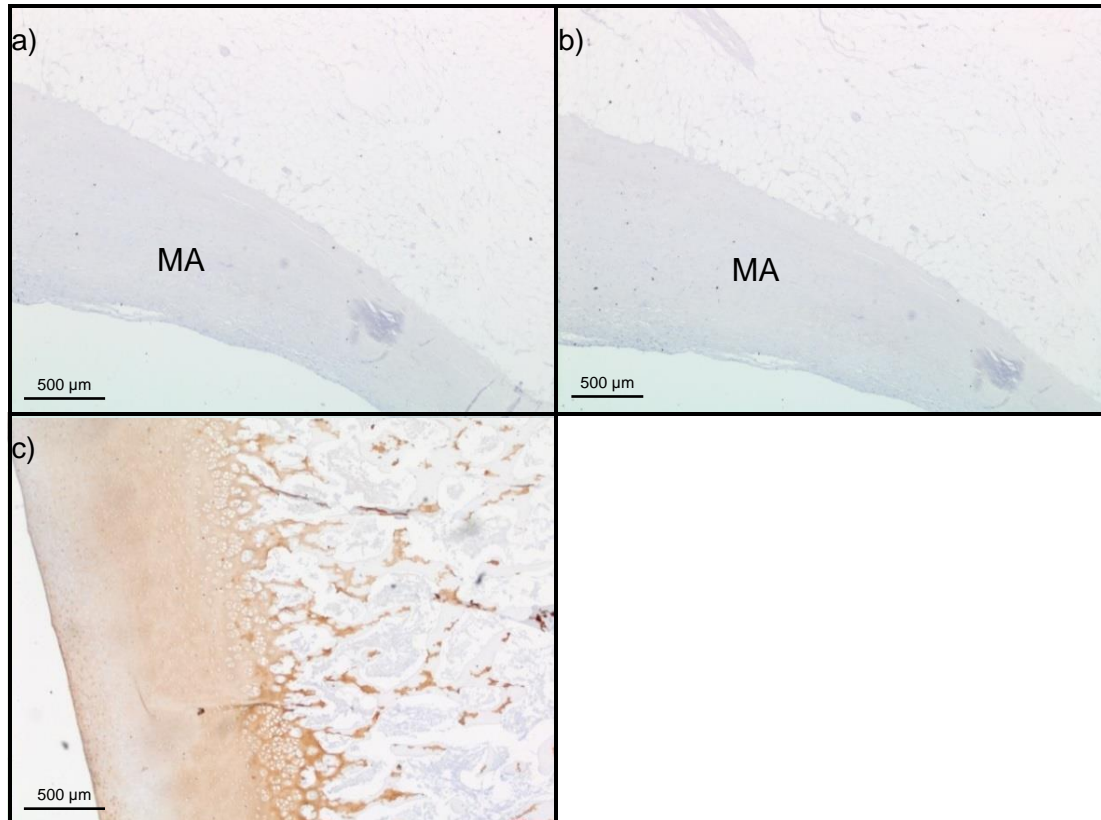


Fig 3.7b – Sections of human mitral valve annulus stained with antibody to collagen II. Sections labelled with antibodies to collagen II stained brown. Isotype control (a). Diluent control (b). Porcine articular cartilage control (c). A: Annulus; T: Trigone; AM: Atrial Muscle; AV: Aortic Valve; AVL: Aortic Valve Leaflet; VM: Ventricular Muscle; L: Leaflet, MA: Mitral - Aortic continuum. Magnification x 20 unless stated otherwise.

3.3.2.3 Collagen III

Images of sections of the anterior and posterior regions (Fig. 3.8a) of the human mitral annulus labelled with antibody to collagen III revealed that all regions stained positively. Collagen III staining was darker in the endocardium and at the surfaces of the leaflets. Positive staining was also observed in the annulus and atrial and ventricular myocardium in both the anterior and posterior regions. No staining was observed in sections stained with the antibody isotype control (Fig 3.8b; a) or diluent alone (Fig 3.8b; b).

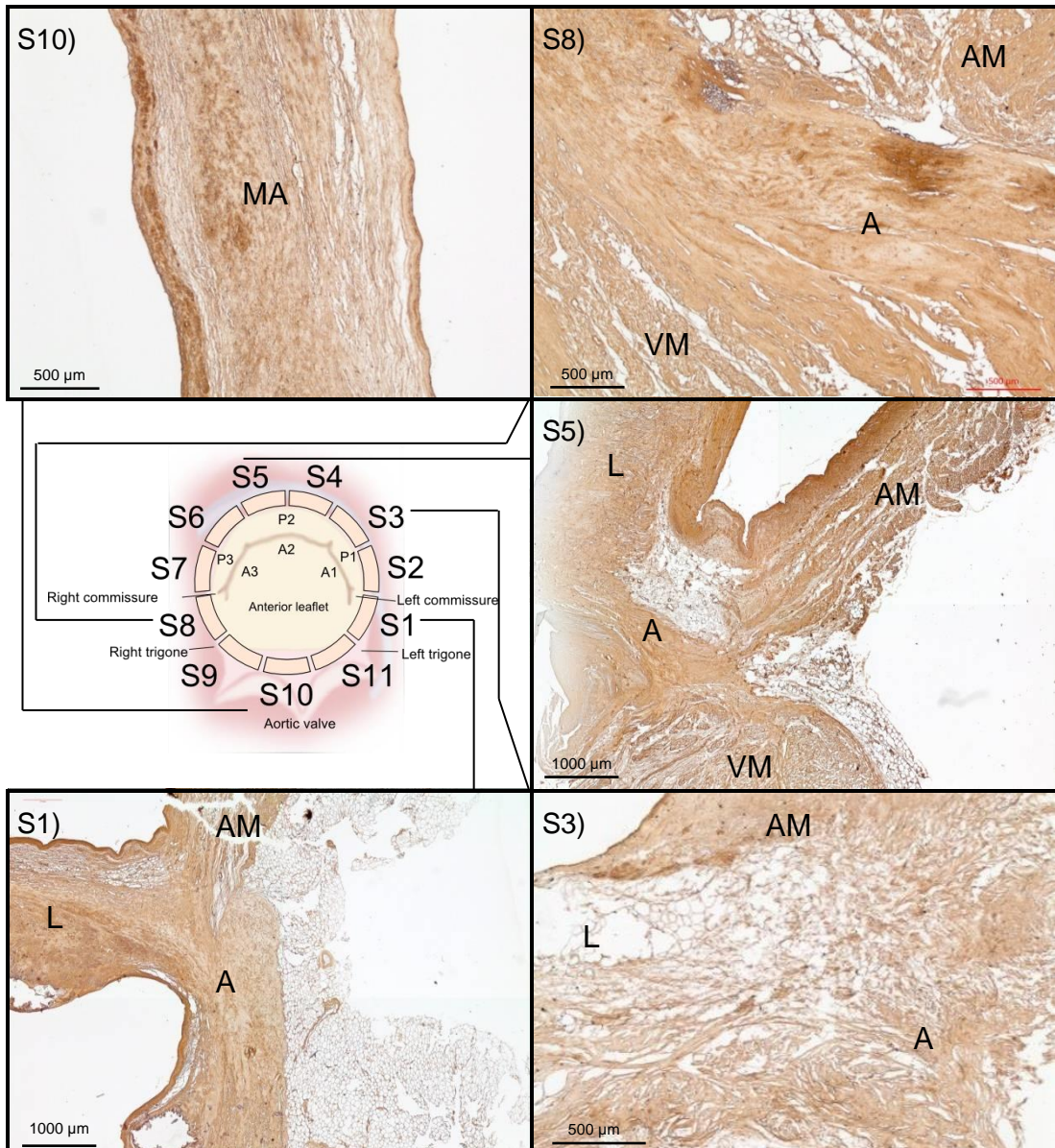


Fig 3.8a – Sections of human mitral valve annulus stained with antibody to collagen III. Representative images from three human annuli are shown. Sections labelled with antibodies to collagen III stained brown. Section 1. Annulus 3 (S1), Section 3. Annulus 1 (S3), Section 5. Annulus 2 (S5), Section 8. Annulus 1 (S8), Section 10. Annulus 1(S10). A: Annulus; T: Trigone; AM: Atrial Muscle; AV: Aortic Valve; AVL: Aortic Valve Leaflet; VM: Ventricular Muscle; L: Leaflet, MA: Mitral - Aortic continuum. Magnification x 20.

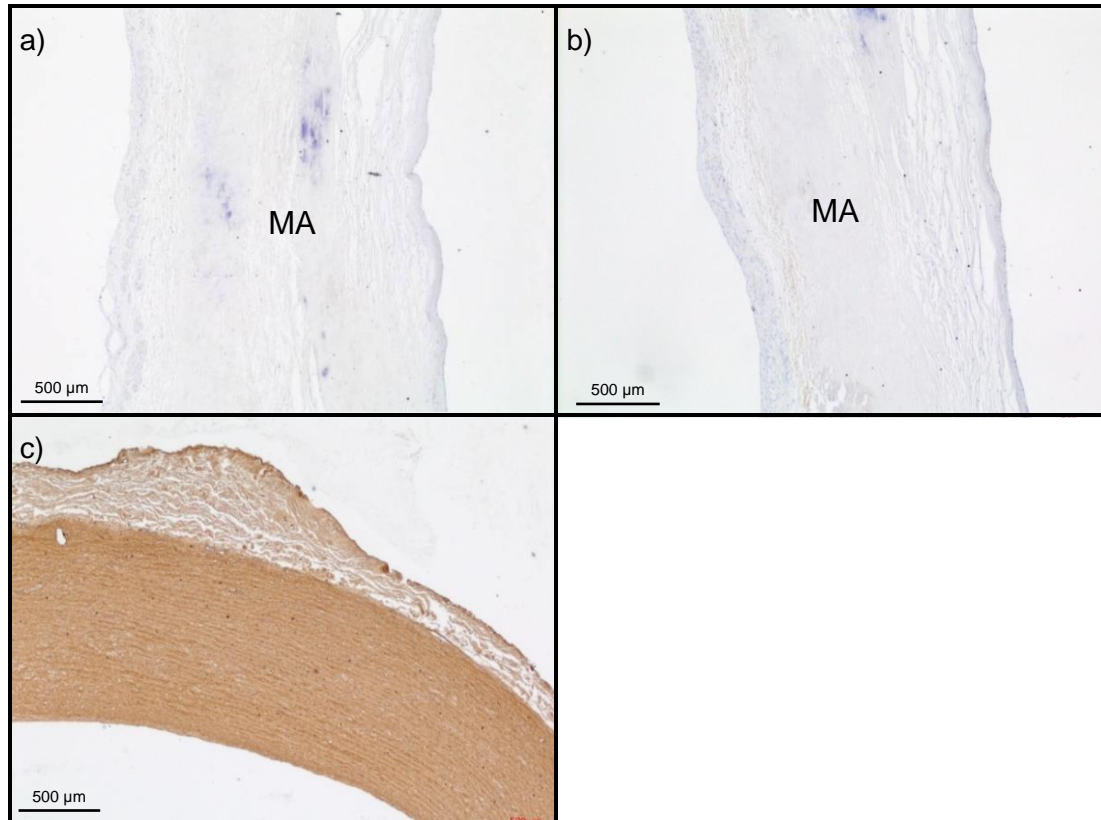


Fig 3.8b – Sections of human mitral valve annulus stained with antibody to collagen III. Sections labelled with antibodies to collagen III stained brown. Isotype control (a). Diluent control (b). Porcine common carotid artery positive control (c). A: Annulus; T: Trigone; AM: Atrial Muscle; AV: Aortic Valve; AVL: Aortic Valve Leaflet; VM: Ventricular Muscle; L: Leaflet, MA: Mitral - Aortic continuum. Magnification x 20.

3.3.2.4 Collagen IV

The anterior and posterior regions (Fig 3.9a) of the human mitral valve annulus were labelled with antibodies to collagen IV. Positive staining was observed in the annulus, atrial and ventricular myocardium in both the anterior and posterior regions. Staining was more prominent in the myocardium, endocardium and blood vessels compared to the annulus. In the annulus, staining was observed in the collagen fibres (Fig 3.9a; S8) and surrounding lacunae type regions in the mitral to aortic continuum (Fig 3.9a; S10 a, S10 b) which appeared to have ossified. No staining was observed in sections stained with the antibody isotype control (Fig 3.9b; a) or diluent alone (Fig 3.9b; b).

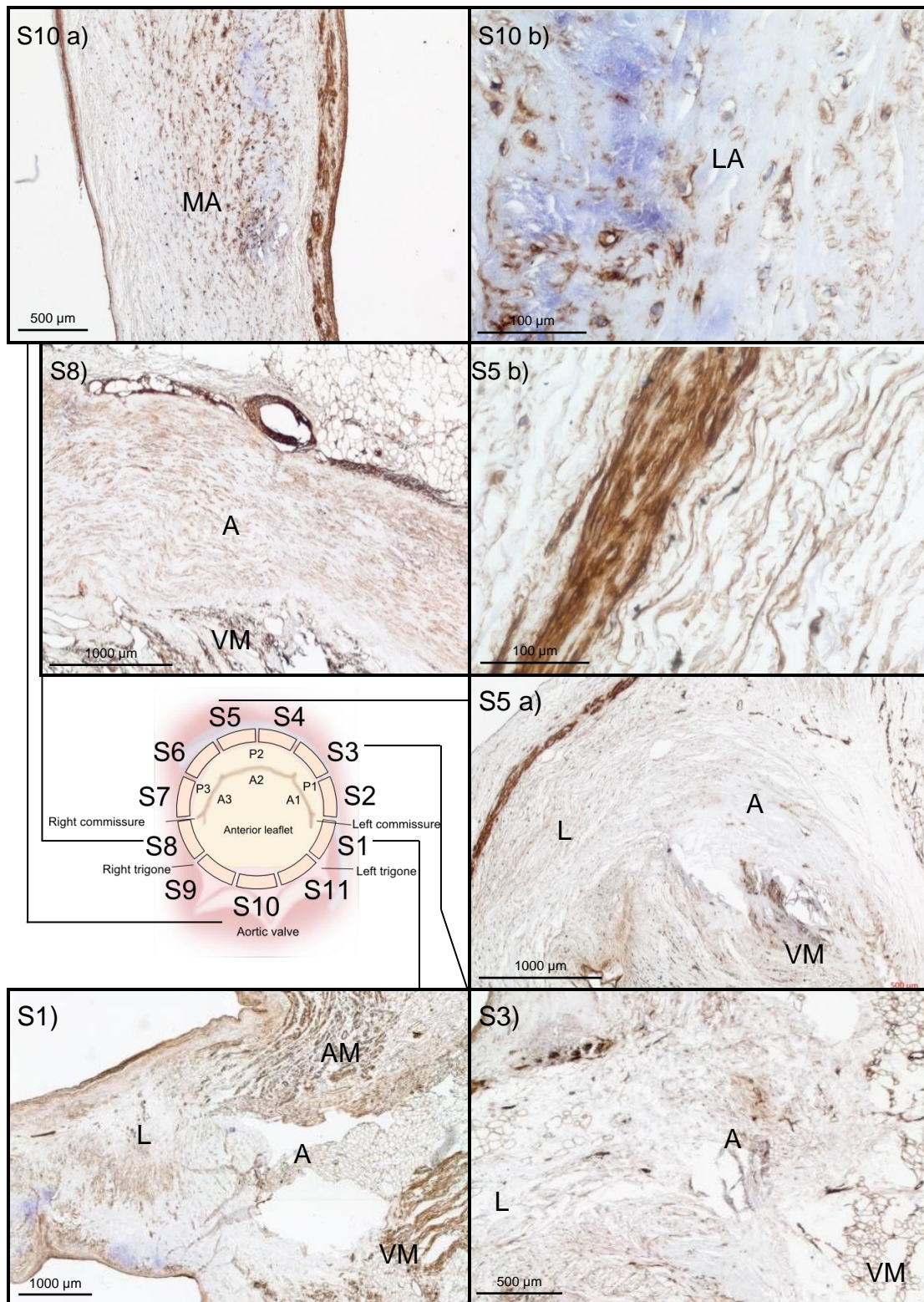


Fig 3.9a – Sections of human mitral valve annulus stained with antibody to collagen IV. Representative images from three human annuli are shown. Sections labelled with antibodies to collagen IV stained brown. Section 1. Annulus 3 (S1), Section 3. Annulus 1 (S3), Section 5. Annulus 1 (S5 a), Section 5 x 100 magnification (S5 b), Section 8. Annulus 1 (S8), Section 10. Annulus 2 (S10a), Section 10 x100 magnification (S10b). A: Annulus; T: Trigone; AM: Atrial Muscle; AV: Aortic Valve; AVL: Aortic Valve Leaflet; VM: Ventricular Muscle; L: Leaflet, LA: Lacunae, MA: Mitral - Aortic continuum. Magnification x 20 unless stated otherwise.

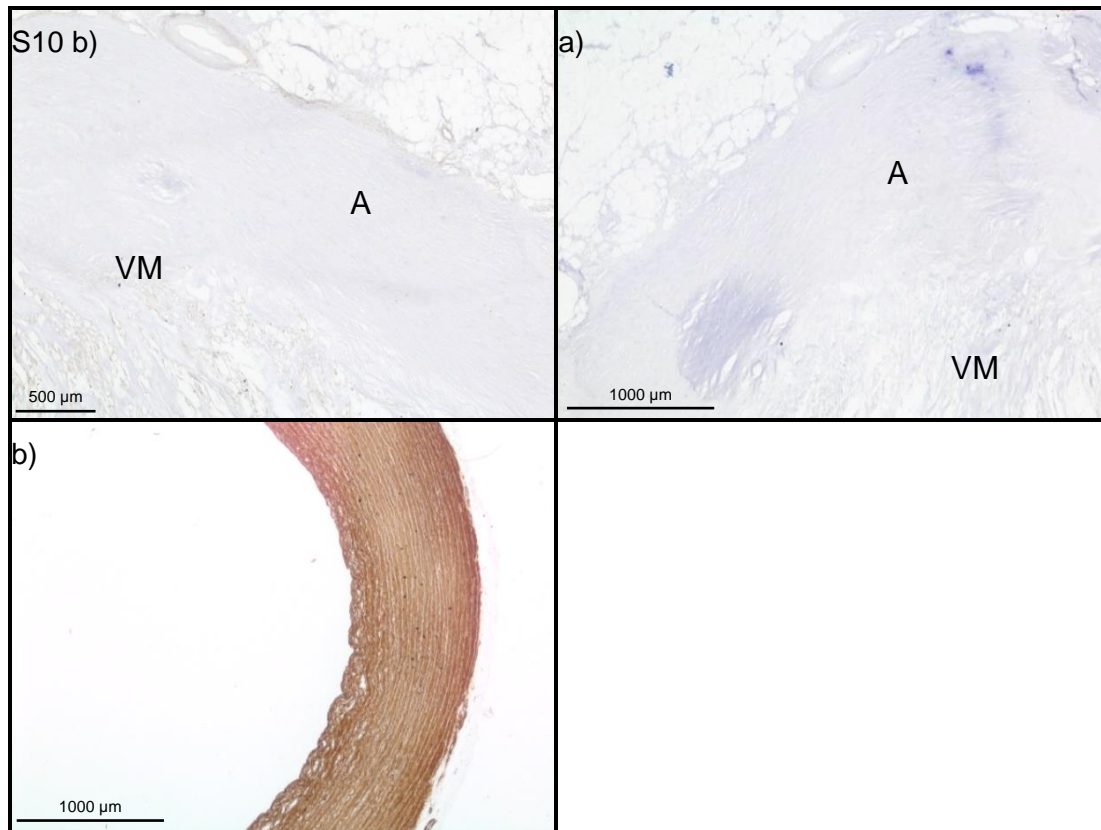


Fig 3.9b – Sections of human mitral valve annulus stained with antibody to collagen IV. Representative images from three human annuli are shown. Sections labelled with antibodies to collagen IV stained brown. Section 1. Annulus 3 (S1), Section 3. Annulus 1 (S3), Section 5. Annulus 1 (S5 a), Section 5 x 100 magnification (S5 b), Section 8. Annulus 1 (S8), Section 10. Annulus 2 (S10a), Section 10 x100 magnification (S10b). Isotype control (a). Diluent control (b). Porcine common carotid artery positive control (c). A: Annulus; T: Trigone; AM: Atrial Muscle; AV: Aortic Valve; AVL: Aortic Valve Leaflet; VM: Ventricular Muscle; L: Leaflet, LA: Lacunae, MA: Mitral - Aortic continuum. Magnification x 20 unless stated otherwise.

3.3.2.5 Collagen VI

Sections of human mitral valve annulus in both the anterior and posterior regions were stained with antibody to collagen VI (Fig 3.10a). Positive staining was observed in the annulus, atrial and ventricular myocardium in all regions. Staining was slightly more prominent in the endocardium. No staining was observed in the sections stained with the antibody isotype control (Fig 3.10b; a) or diluent alone (Fig 3.10b; b).

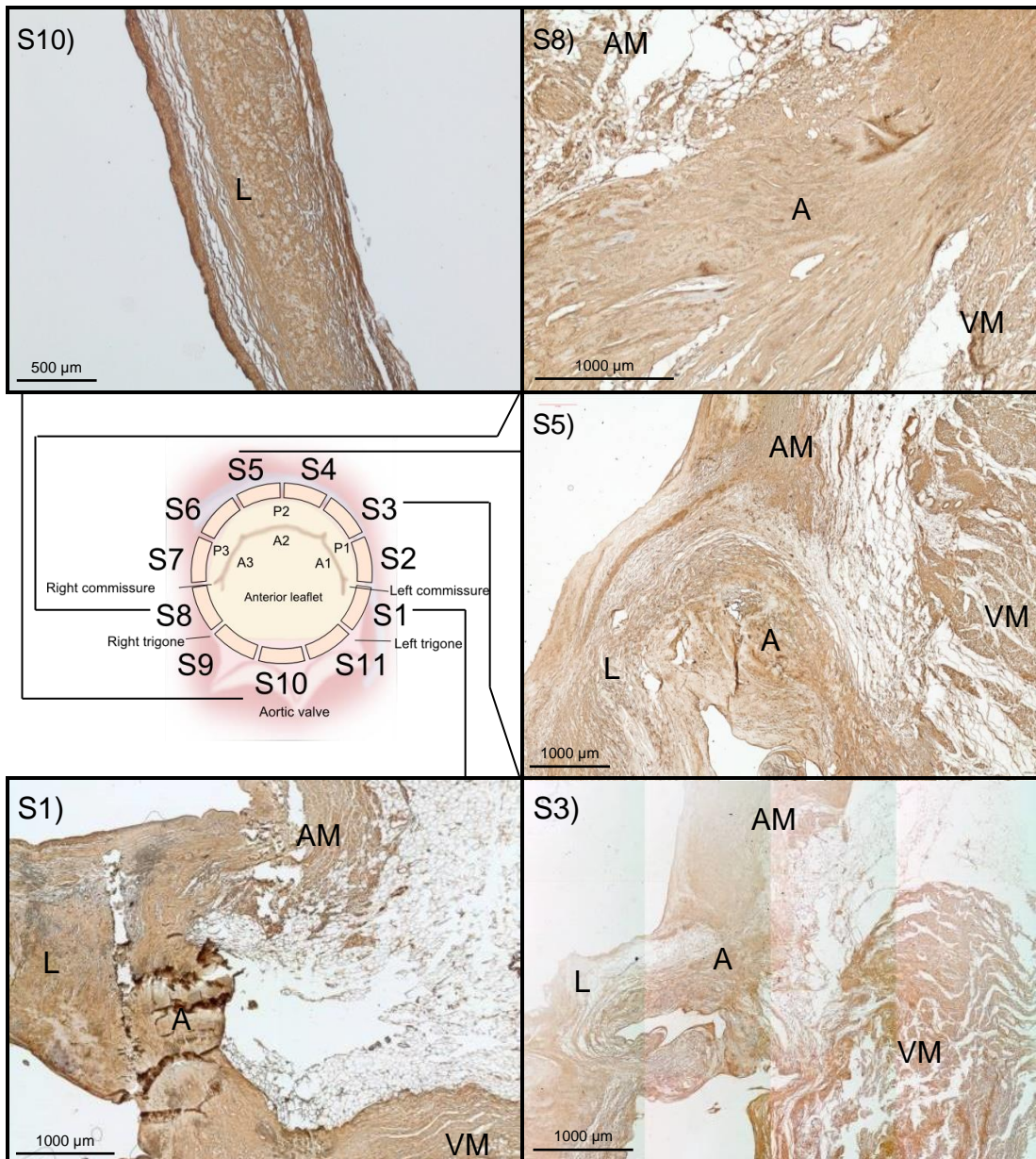


Fig 3.10a – Sections of human mitral valve annulus stained with antibody to collagen VI. Representative images from three human annuli (1-3) are shown. Sections labelled with antibodies to collagen VI stained brown. Section 1. Annulus 3 (S1), Section 3. Annulus 1 (S3), Section 5. Annulus 1 (S5), Section 8. Annulus 1 (S8), Section 10. Annulus 2 (S10). A: Annulus; T: Trigone; AM: Atrial Muscle; AV: Aortic Valve; AVL: Aortic Valve Leaflet; VM: Ventricular Muscle; L: Leaflet. Magnification x 20.

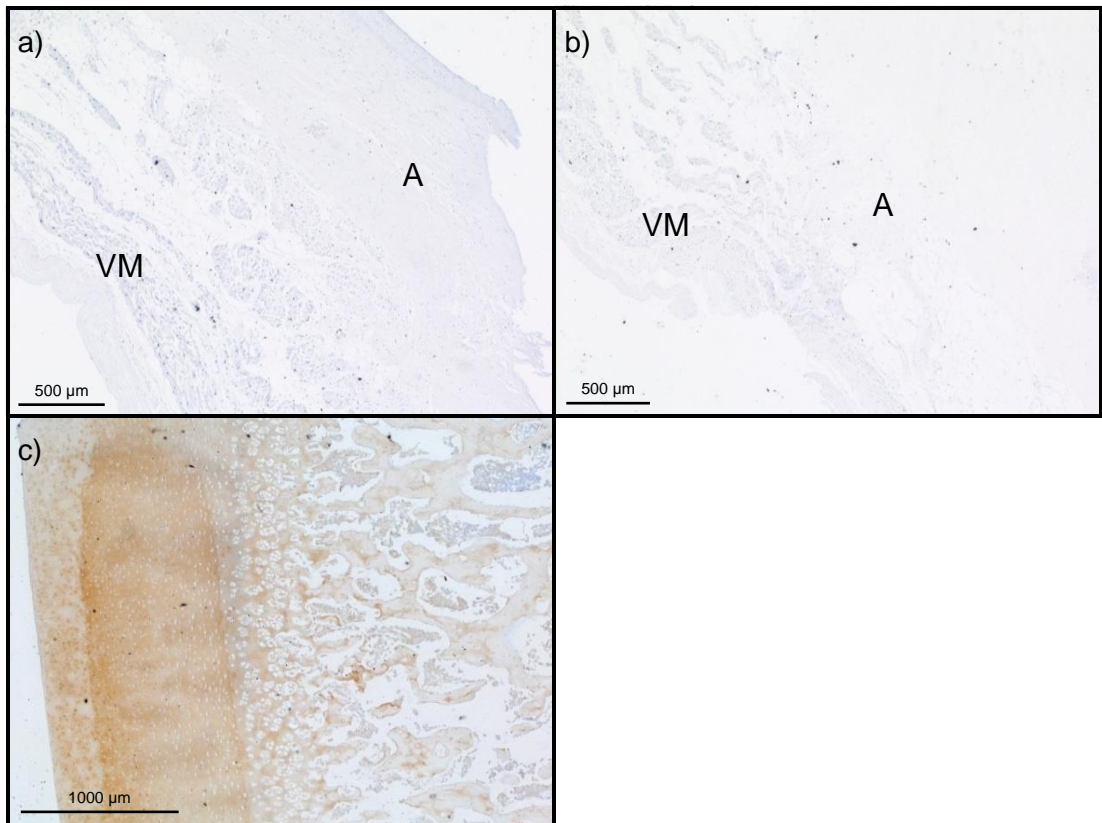


Fig 3.10b – Sections of human mitral valve annulus stained with antibody to collagen VI. Isotype control (a). Diluent control (b). Porcine articular cartilage positive control (c). A: Annulus; T: Trigone; AM: Atrial Muscle; AV: Aortic Valve; AVL: Aortic Valve Leaflet; VM: Ventricular Muscle; L: Leaflet. Magnification x 20.

3.3.2.6 Fibronectin

Sections of the human mitral annulus from the anterior and posterior regions (Fig 3.11a) were labelled with antibody to fibronectin. The results showed that both regions were stained positive. Staining was most prominent in the endocardium, leaflet surfaces and myocardium compared to the annulus but the annulus was also stained positive. No staining was observed in the sections stained with the antibody isotype control (Fig 3.11b; a) or diluent alone (Fig 3.11b; b)

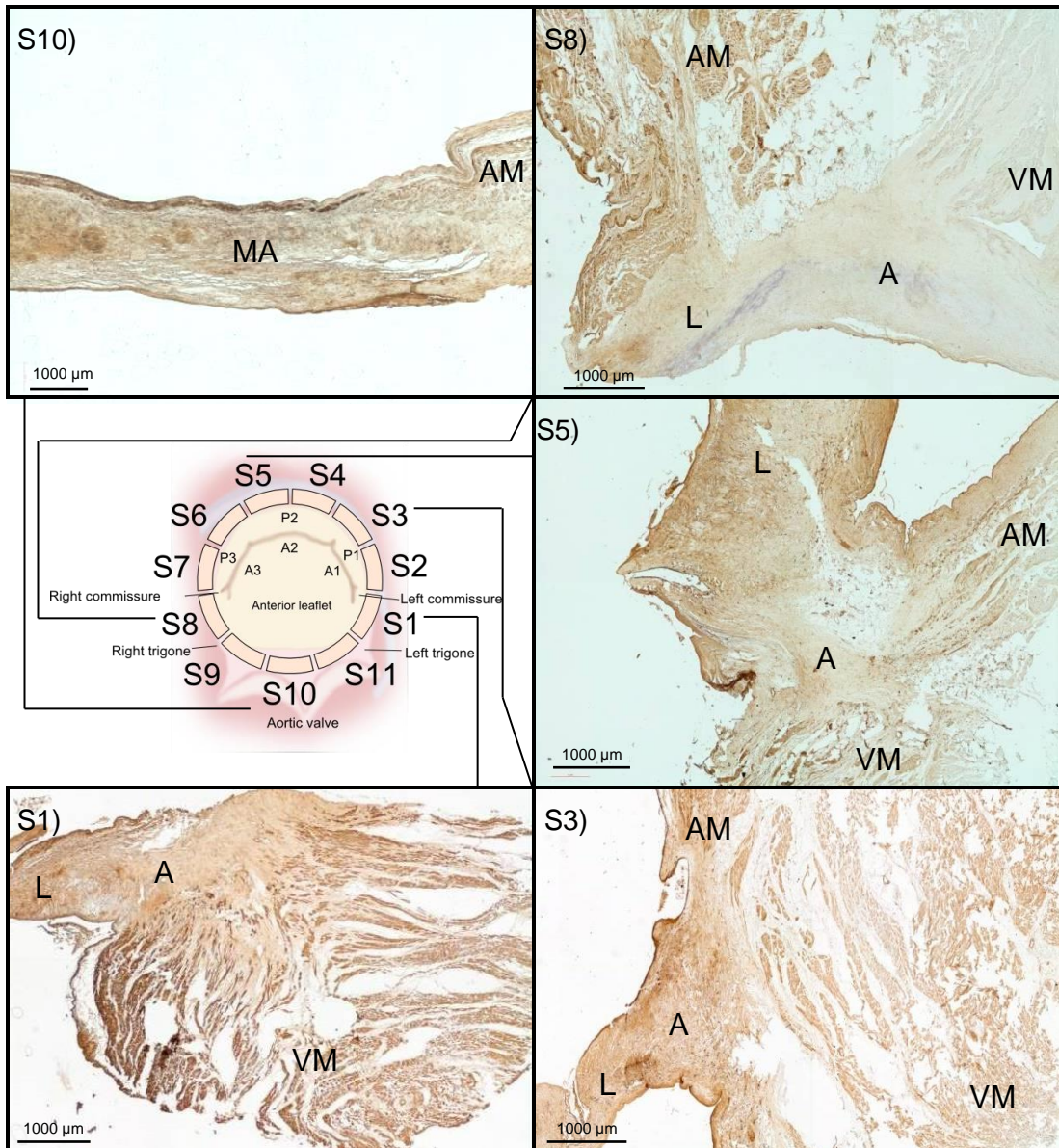


Fig 3.11a – Sections of human mitral valve annulus stained with antibody to fibronectin. Representative images from three human annuli are shown. Sections labelled with antibodies to fibronectin stained brown. Section 1. Annulus 2 (S1), Section 3. Annulus 2 (S3), Section 5. Annulus 2 (S5), Section 8. Annulus 3 (S8), Section 10. Annulus 1 (S10). A: Annulus; T: Trigone; AM: Atrial Muscle; AV: Aortic Valve; AVL: Aortic Valve Leaflet; VM: Ventricular Muscle; L: Leaflet, Mitral-Aortic continuum. Magnification x 20.

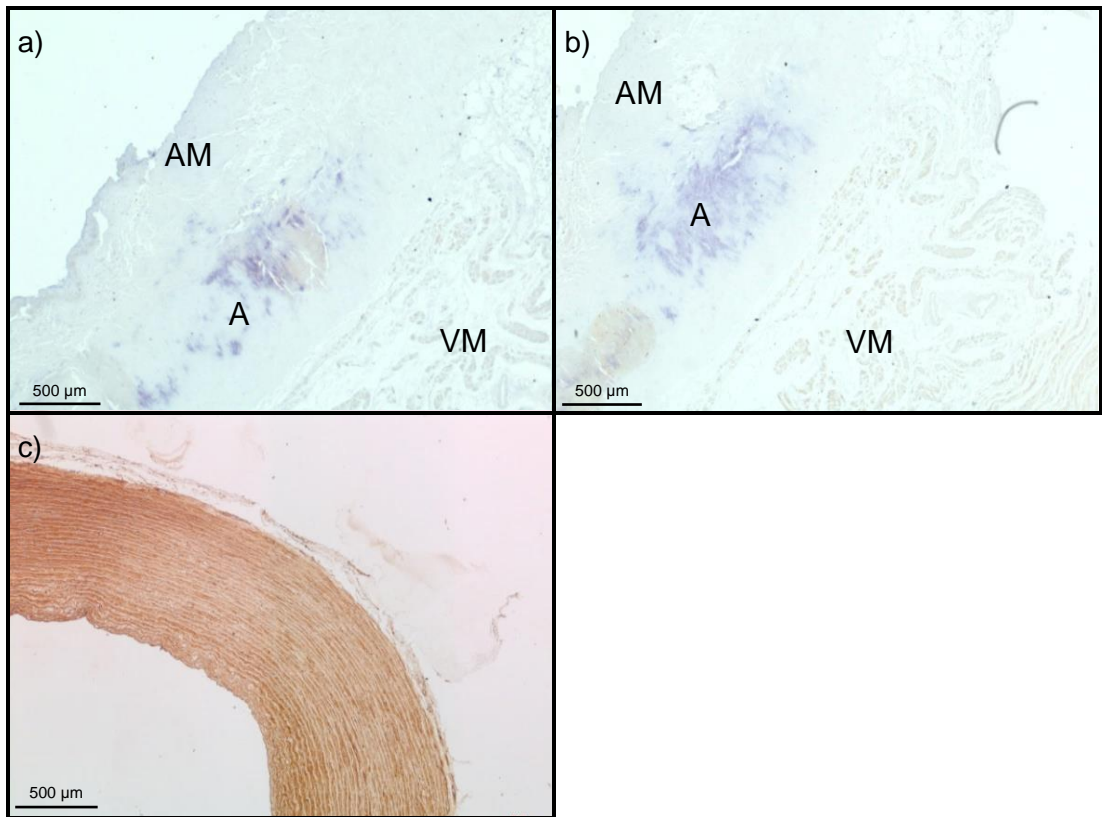


Fig 3.11b – Sections of human mitral valve annulus stained with antibody to fibronectin. Sections labelled with antibodies to fibronectin stained brown. Isotype control (a). Diluent control (b). Porcine common carotid artery positive control (c). A: Annulus; T: Trigone; AM: Atrial Muscle; AV: Aortic Valve; AVL: Aortic Valve Leaflet; VM: Ventricular Muscle; L: Leaflet, Mitral-Aortic continuum. Magnification x 20.

3.3.2.7 Laminin

The antibody to laminin was used to label sections of the anterior and posterior mitral valve annulus (Fig 3.12a). Positive staining was observed in the atrial and ventricular myocardium in all regions whilst the annulus stained weakly. Staining was more prominent in the muscle surrounding the annulus, endocardium and blood vessels. No staining was observed in sections stained with the isotype control antibody (Fig 3.12b; a) or diluent alone (Fig 3.12b; b).

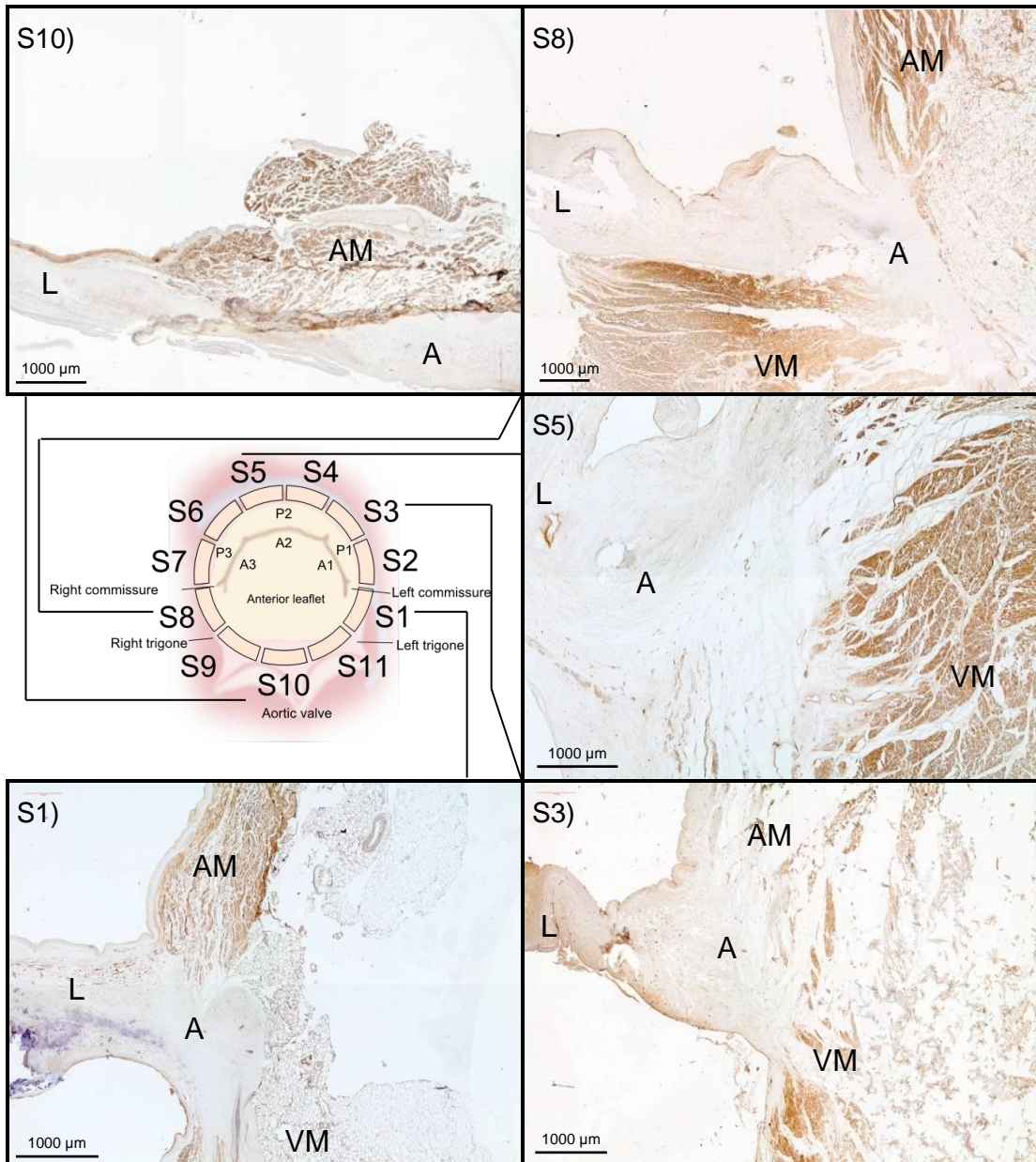


Fig 3.12a – Sections of human mitral valve annulus stained with antibody to laminin. Sections labelled with antibodies to laminin stained brown. Section 1. Annulus 3 (S1), Section 3. Annulus 2 (S3), Section 5. Annulus 1 (S5), Section 8. Annulus 2 (S8), Section 10. Annulus 2 (S10). A: Annulus; T: Trigone; AM: Atrial Muscle; AV: Aortic Valve; AVL: Aortic Valve Leaflet; VM: Ventricular Muscle; L: Leaflet. Magnification x 20.

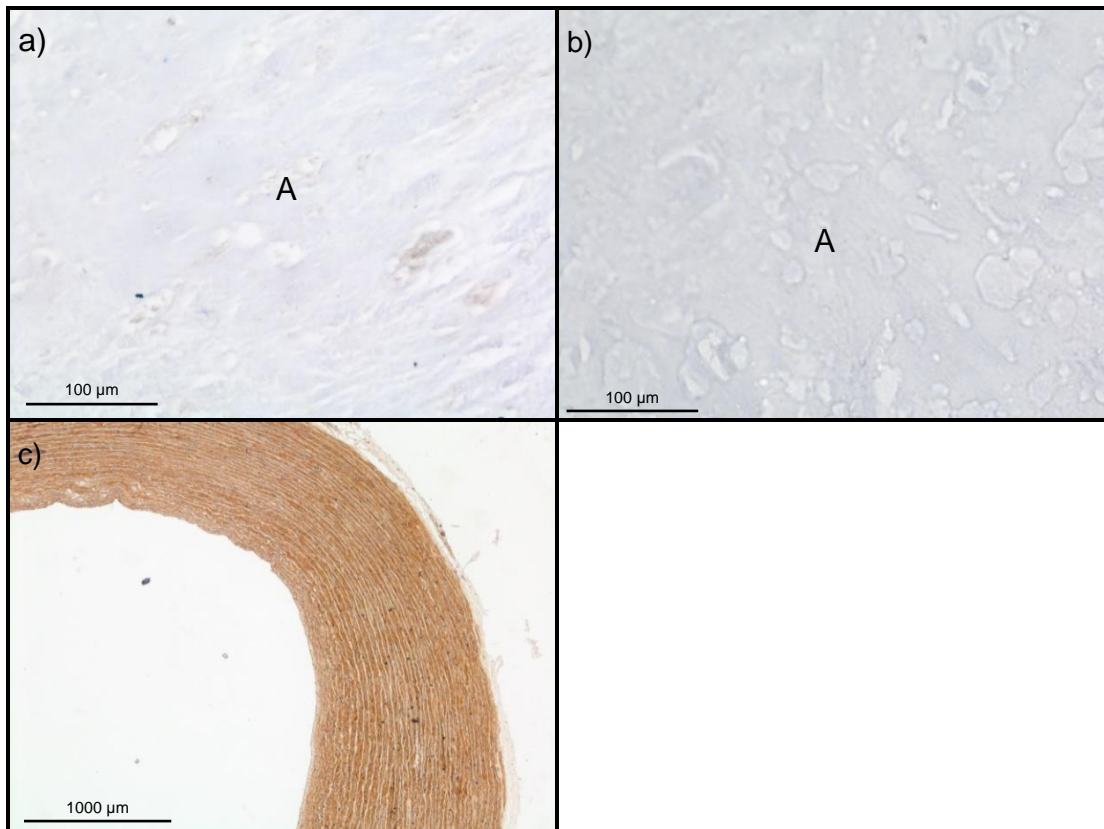


Fig 3.12b – Sections of human mitral valve annulus stained with antibody to laminin. Sections labelled with antibodies to laminin stained brown. Isotype control x 100 magnification (a). Diluent control x 100 magnification (b) Porcine common carotid artery positive control (c). A: Annulus; T: Trigone; AM: Atrial Muscle; AV: Aortic Valve; AVL: Aortic Valve Leaflet; VM: Ventricular Muscle; L: Leaflet. Magnification x 20.

3.3.3 Deposition of calcium in the extracellular matrix of the human mitral annulus

Upon excision of each of the human mitral valve annuli from donor hearts heavy calcification was apparent. In order to identify the presence and abundance of the calcification in the annulus, sections of the anterior and posterior regions of the human mitral annulus were stained with H&E (Fig 3.13; a, d), labelled with antibodies to collagen II (Fig 3.13; b, e) and stained with Von Kossa (Fig 3.13; c, f) to show regions where calcification was prominent and ossification might have been present. Regions of calcification stained deep purple in sections stained by H&E, regions with signs of cartilage development labelled with antibodies to collagen II and stained brown whilst regions of calcification stained dark brown to black when sections were stained by Von Kossa. Staining was most prominent in the

posterior annulus for both calcification (Fig 3.13; d, f) and signs of ossification (Fig 3.13; e) compared to the anterior annulus (Fig 3.13; a, b, c). The anterior annulus had signs of calcification (Fig 3.1; c) but ossification was not visible and did not stain positive for collagen II (Fig 3.13; b). The results indicate the overlap between the calcium deposition and collagen II present in the samples.

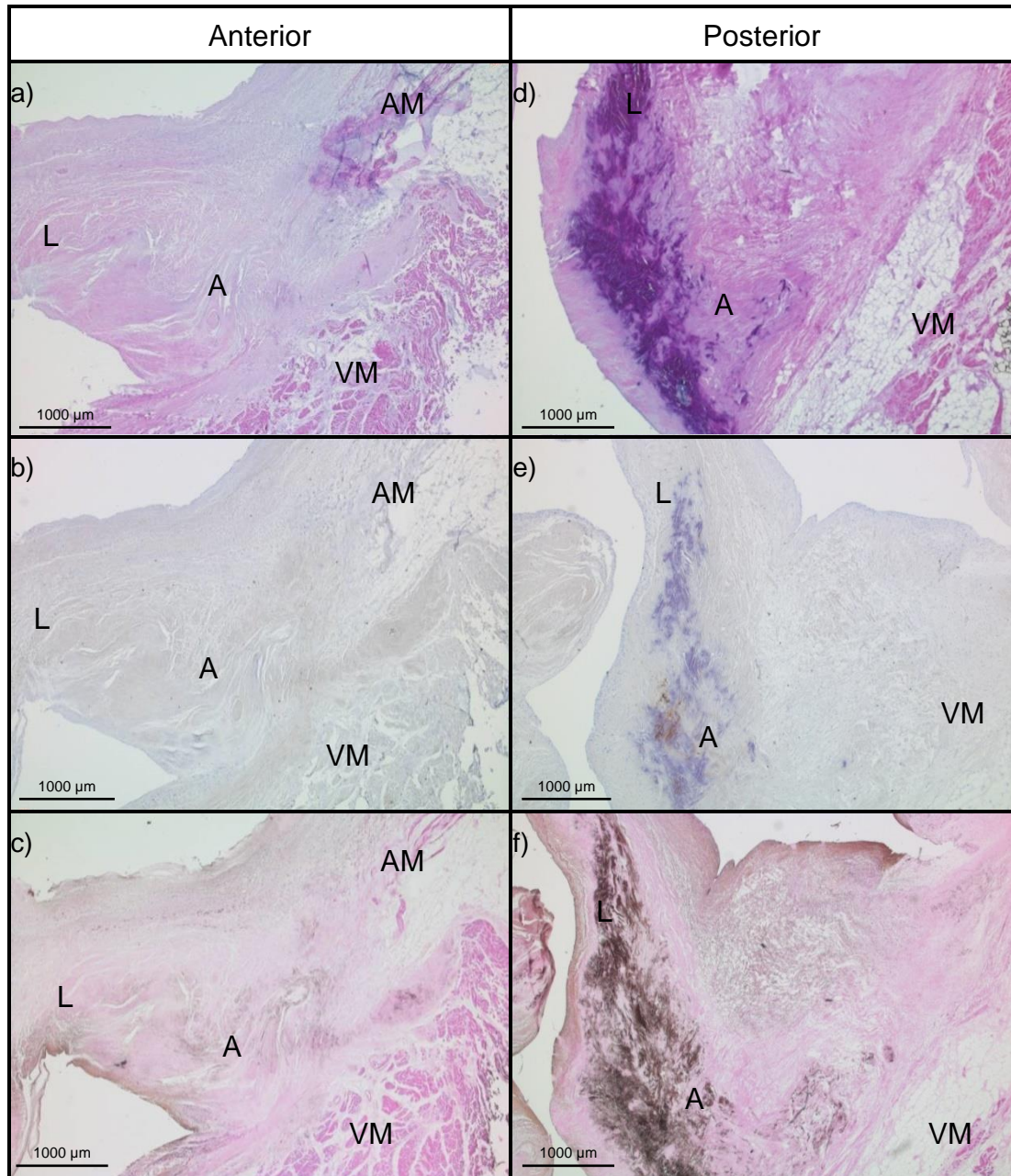


Fig 3.13 – Sections of native human mitral valve annulus stained with H&E, Von Kossa and labelled with antibodies to collagen II. Representative images from three human annuli (1-3) are shown. Anterior: H&E (a), collagen II (b), Von Kossa (c), Posterior: H&E (d), collagen II (e), Von Kossa (f). A: Annulus; T: Trigone; AM: Atrial Muscle; AV: Aortic Valve; AVL: Aortic Valve Leaflet; VM: Ventricular Muscle; L: Leaflet. Magnification x 20.

Part 2 Characterisation of the native porcine mitral annulus

3.3.4 Histological and histochemical characterisation of the native porcine mitral valve annulus

Sections of tissue from the eleven regions of the porcine mitral valve annulus (n=5; labelled annulus 1 to 5) were stained with H&E to determine the overall tissue structure. Images representative of the different regions are presented in Fig 3.14a and Fig 3.14b. The native porcine mitral annulus exhibited a diverse structure between the anterior and posterior annulus.

Connective tissue density appeared greatest in the anterior of the annulus (Fig 3.14a; S1, Fig 3.14b; S8-S11) or close to the anterior (Fig 3.14a; S2, Fig 3.14a; S7) where the annulus was thickest, ranging between 1000 μm close to the commissures and 5200 μm in thickness at the trigones, the connective tissue in this region also extended further towards the epicardial side of the heart compared to the posterior. The anterior comprised of the highly fibrous trigonal regions (Fig 3.14a; S1, Fig 3.14b; S8, S11) and the mitral to aortic continuum (Fig 3.14b; S9-S10). Cells within the trigones resembled chondrocytes located within lacunae (Fig 3.14b; S11b). The mitral to aortic continuum (Fig 3.14b; S10) appeared as a dense collagenous-connective membrane that formed the core of the tissue in this region and lacked the spongiosa that was visible in the posterior mitral leaflets.

The collagenous fibrosa of the mitral leaflets appeared to form into the mitral annulus in the posterior region and up to the trigones in the anterior (Fig 3.14a; S1-S6, Fig 3.14b; S7-S8), although the spongiosa appeared to form into the annulus in Section 4 (Fig 3.14a; S4). The fibrosa was defined by the densely packed collagenous connective tissue compared to the other layers of the mitral valve leaflets, the spongiosa, ventricularis and atrialis. The posterior mitral valve region (Fig 3.14a; S2-S6, Fig 3.14b; S7) consisted primarily of collagenous-connective tissue of the mitral valve annulus and of adipose cells, surrounded by myocardium. The posterior connective tissue ranged in thickness between 500 μm and 1100 μm . The atrial and ventricular myocardium were separated by the annulus or adipose tissue. Adipose tissue replaced the collagenous connective tissue towards the epicardium, separating the ventricular and atrial myocardium.

The muscle fibres close to the annulus were circumferential in orientation. The atrial myocardium also appeared to integrate into the atrial side of the posterior leaflet, above the annulus (Fig 3.14a; S3, S5, Fig 3.4b; S7).

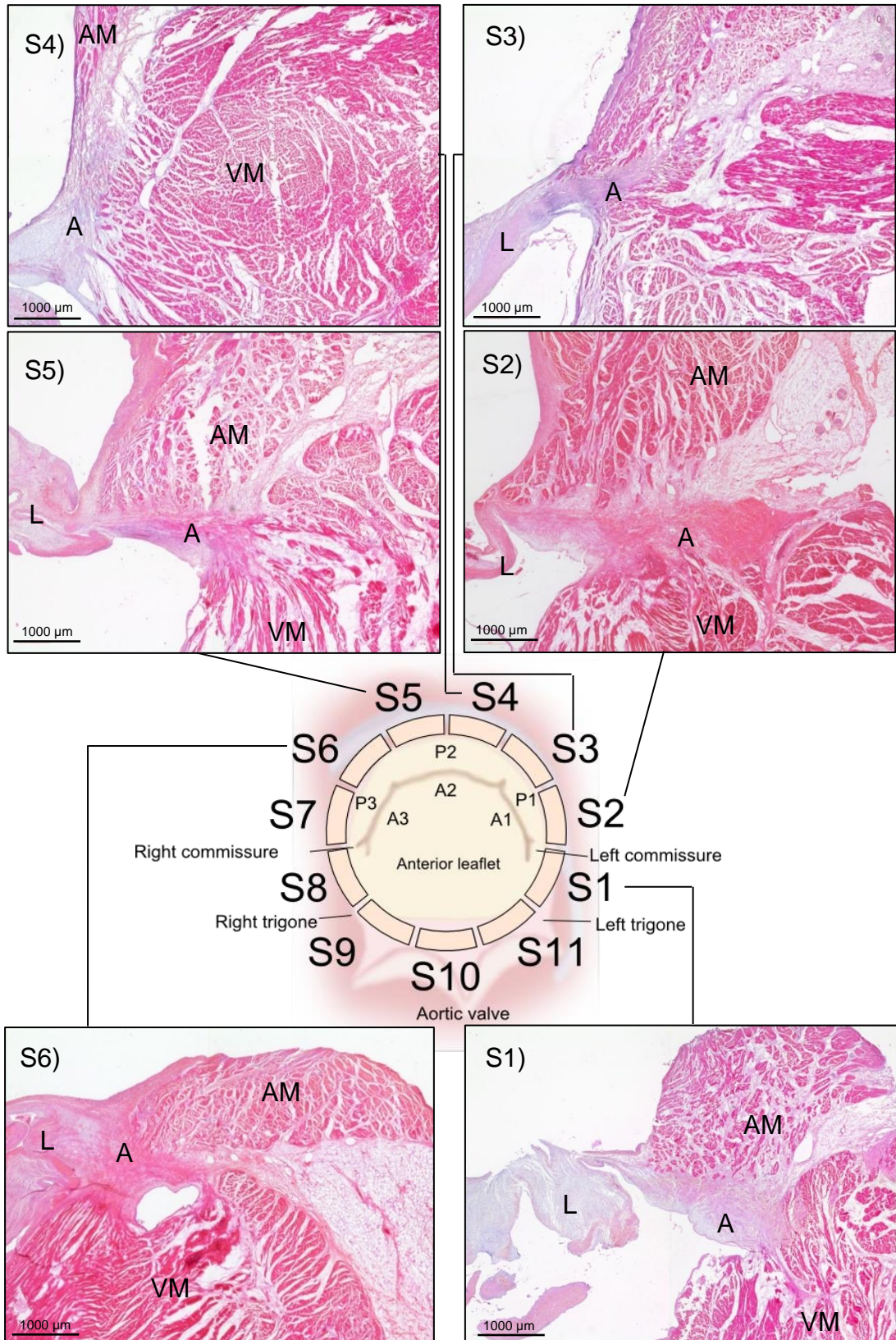


Fig 3.14a – Images of H&E stained sections from different segments of the porcine mitral valve annulus. Representative images from three porcine annuli are shown. Section 1. Annulus 3 (S1), Section 2. Annulus 2 (S2), Section 3. Annulus 3 (S3), Section 4. Annulus 3 (S4), Section 5. Annulus 1 (S5), Section 6. Annulus 1 (S6). A: Annulus; T: Trigone; AM: Atrial Muscle; AV: Aortic Valve; AVL: Aortic Valve Leaflet; VM: Ventricular Muscle; L: Leaflet. Magnification x 20.

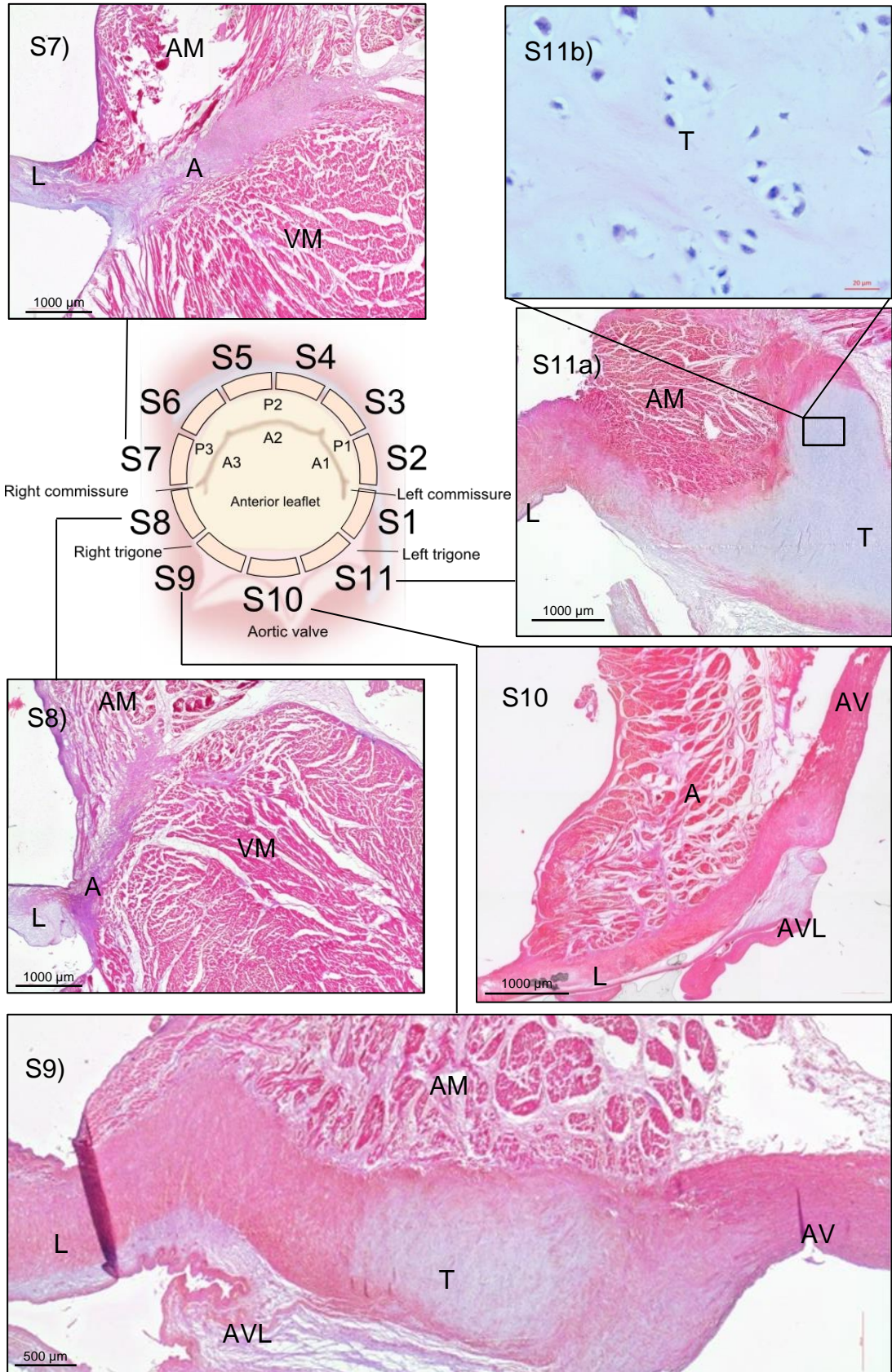


Fig 3.14b – Images of H&E stained sections from different segments of the porcine mitral valve annulus. Representative images from three porcine annuli are shown. Section 7. Annulus 3 (S7), Section 8. Annulus 3 (S8), Section 9. Annulus 1 (S9), Section 10. Annulus 3 (S10), Section 11. Annulus 1 (S11a), Section 11. Annulus 1x 400 magnification (S11b). Magnification x20 unless stated otherwise.

Selected segments of the porcine mitral valve annulus were sectioned and stained with alcian blue to determine the presence and abundance of GAGs. GAGs were observed at the hinge point of both the anterior (Fig 3.15; S1, S8 a, S8 b) and posterior (Fig 3.15 S3, S5) annulus, where the leaflets inserted. The trigonal region had a high concentration of GAGs (Fig 3.15; S8, S10) in the irregularly arranged tissue which had chondrocyte-like cells residing in lacunae (Fig 3.15; S8 b). GAGs were also present within the spongiosa of the mitral valve leaflet (Fig 3.15 S1, S3, S5, S10).

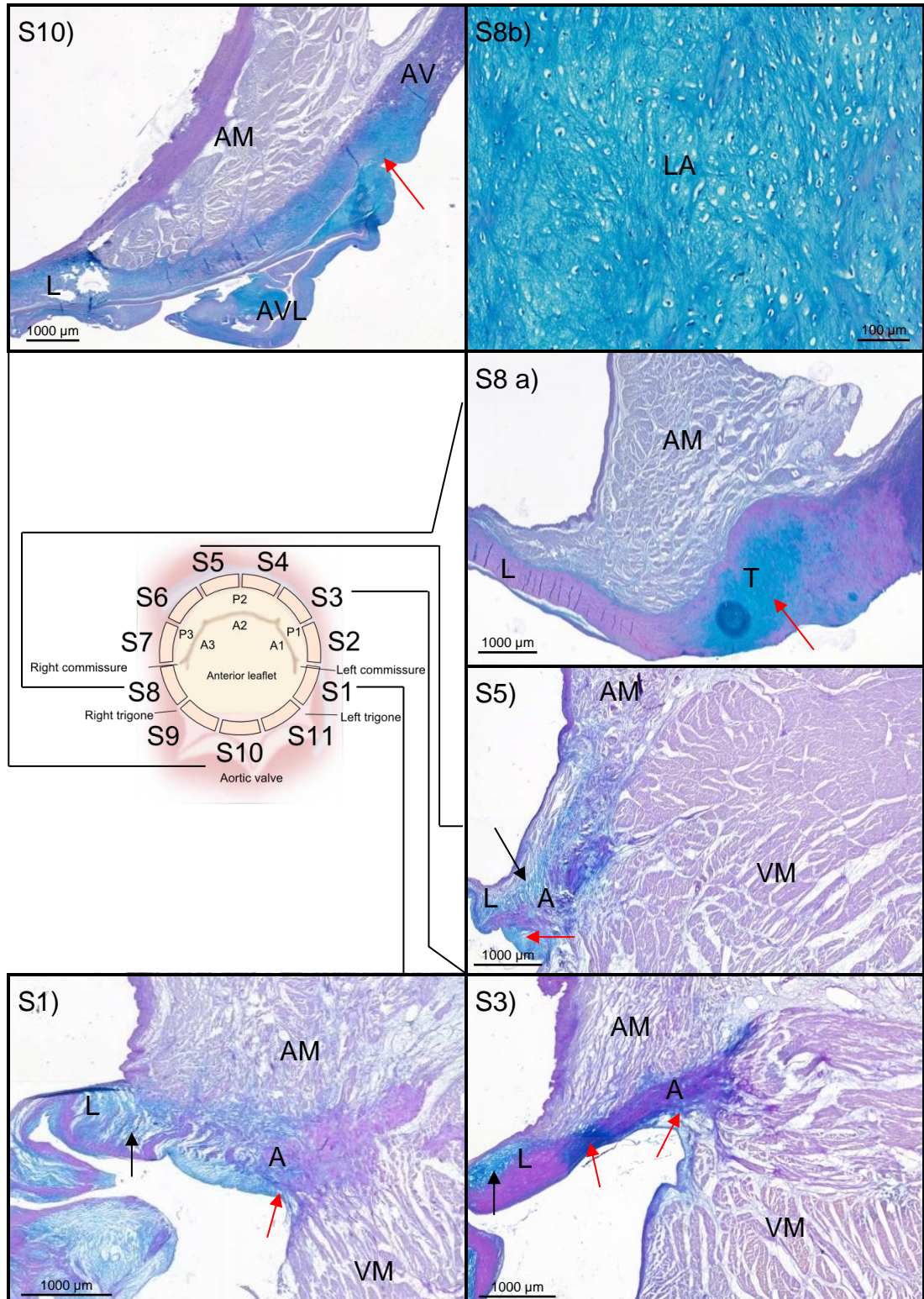


Fig 3.15 – Images of alcian blue stained sections from different segments of the native porcine mitral valve annulus. Representative images from three porcine annuli are shown. Black arrows represent GAGs within the spongiosa, red arrows represent GAGs present within the annular junction. Section 1. Annulus 3 (S1), Section 3. Annulus 3 (S3), Section 5. Annulus 3 (S5), Section 8. Annulus 5 (S8 a), Section 8 x100 magnification (S8 b), Section 10. Annulus 1 (S10). Chondron-like regions formed in an area high in GAGs (S8 b) magnification x 100. A: Annulus; T: Trigone; AM: Atrial Muscle; AV: Aortic Valve; AVL: Aortic Valve Leaflet; VM: Ventricular Muscle; L: Leaflet. LA: Lacunae. Magnification x 20 unless stated otherwise.

Sirius red Miller's staining of tissue sections from various regions of the porcine mitral valve annulus showed red/orange stained collagen fibres, when viewed under polarised light (Fig 3.16a; a, Fig 3.16b; a, Fig 3.17) and purple stained elastin fibres when viewed by bright field microscopy (Fig 3.16a; b, Fig 3.16b; b). Collagen concentration was highest in the trigones (Fig 3.16a; S1 a, Fig 3.16b; S8), the mitral to aortic continuum (Fig 3.16b; S10) and the fibrosa of the mitral leaflet (Fig 3.16a; S3, S5), which formed into the mitral annulus. The fibrosa of the anterior leaflet was thinnest in the posterior, between 250 and 370 μm thick and thickest in the anterior, between 500 and 620 μm . Elastin was concentrated around structures which closely resembled chondrons in the trigones and was suggestive of elastic cartilage (Fig 3.16a; S1 b, S1 c, Fig 3.16b; S8 b). Regions of lacunae appeared orange under polarised light and weakly birefringent, with denser collagenous regions appearing red surrounding them (Fig 3.16a; S1 a, Fig 3.16b; S8 a). Elastin was also present in the atrialis in both the posterior and anterior regions which integrated into the endocardium, high concentrations of elastin were present in the anterior regions in the wall of the aorta in the anterior (Fig 3.16a; S1 b, Fig 3.16b; S8 b) and the mitral to aortic continuum (Fig 3.16b; S10 b).

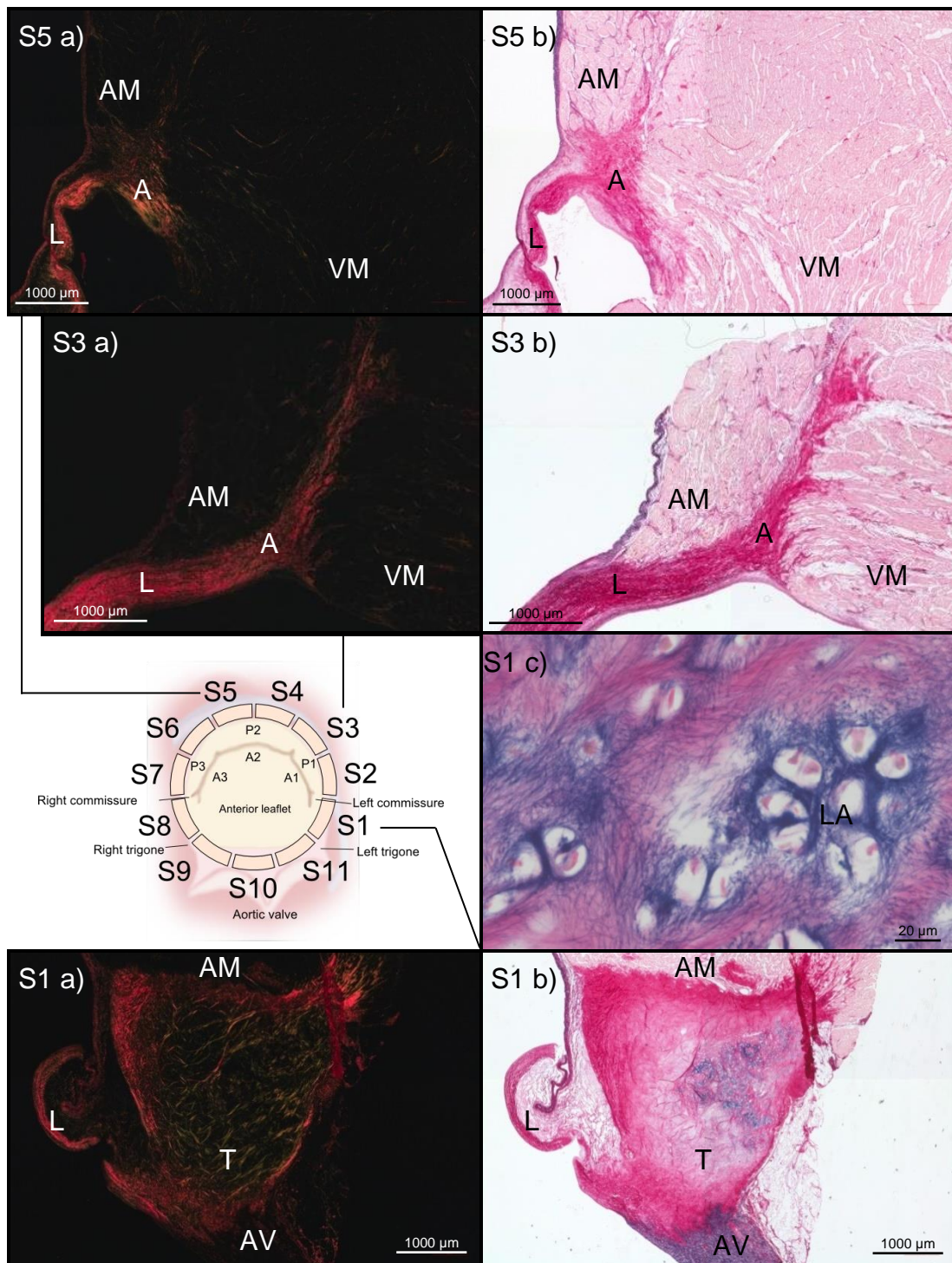


Fig 3.16a – Images of Sirius red Miller's stained sections from selected segments of the native porcine mitral valve annulus viewed under (a) polarised light and (b) bright field microscopy. Representative images from three porcine annuli are shown. Elastin fibres are stained dark blue, collagen fibres are stained red. Images are shown in pairs; polarised light images followed by bright field images. Section 1 (S1 a. Annulus 5, S1 b. Annulus 5), Section 1 x 400 magnification (S1 c. Annulus 5), Section 3 (S3 a. Annulus 5, S3 b. Annulus 5), Section 5 (S5 a. Annulus 3, S5 b. Annulus 3). A: Annulus; T: Trigone; AM: Atrial Muscle; AV: Aortic Valve; AVL: Aortic Valve Leaflet; VM: Ventricular Muscle; L: Leaflet. LA: Lacunae. Magnification x 20 unless stated otherwise.

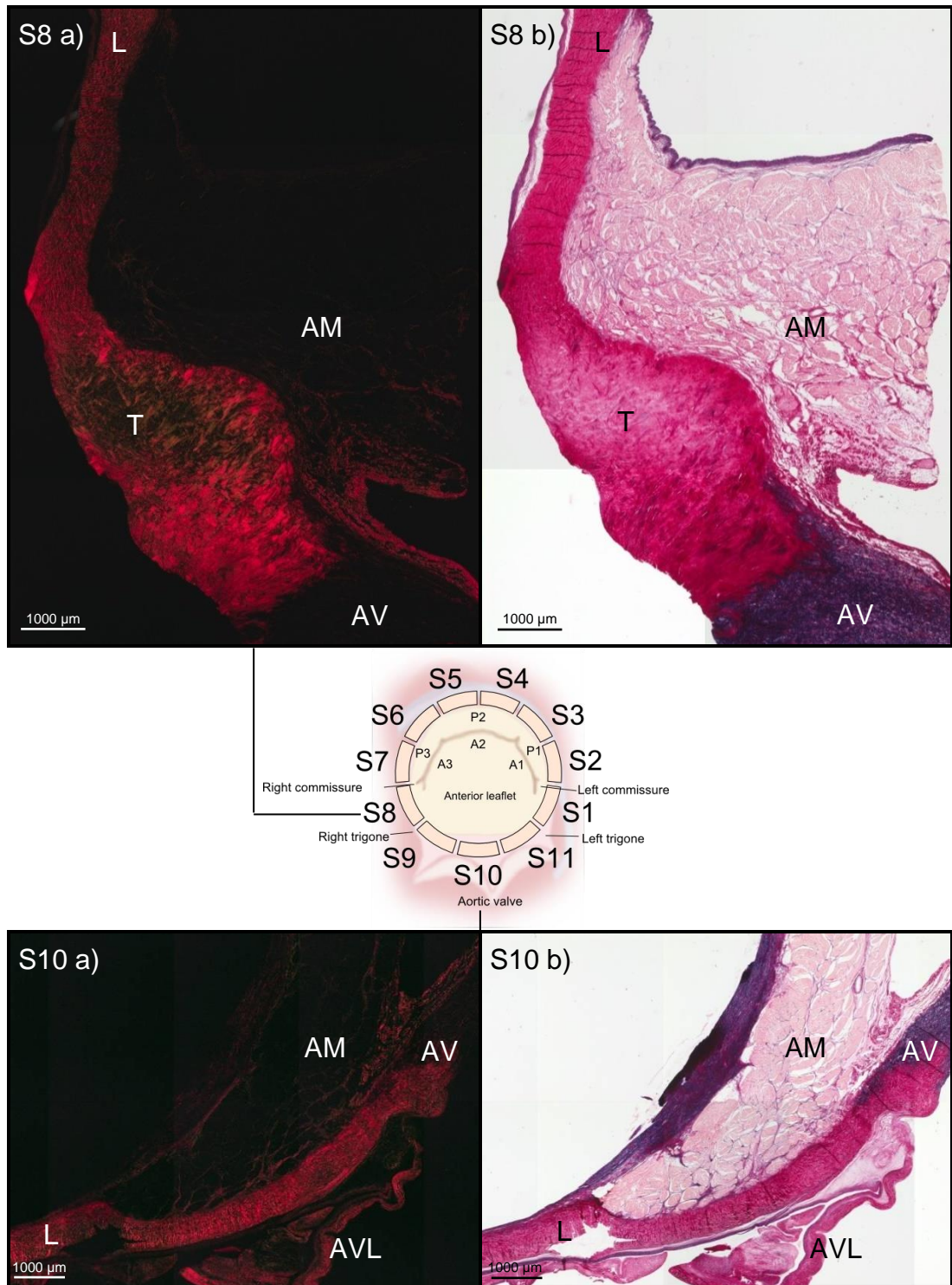


Fig 3.16b – Images of Sirius red Miller's stained sections from selected segments of the native porcine mitral valve annulus viewed under (a) polarised light and (b) bright field microscopy. Representative images from three porcine annuli are shown. Elastin fibres are stained dark blue, collagen fibres are stained red. Images are shown in pairs; polarised light images followed by bright field images. Section 8 (S8 a. Annulus 5, S8 b. Annulus 5), Section 10 (S10 a. Annulus 1, S10 b. Annulus 1). A: Annulus; T: Trigone; AM: Atrial Muscle; AV: Aortic Valve; AVL: Aortic Valve Leaflet; VM: Ventricular Muscle; L: Leaflet. LA: Lacunae. Magnification x 20 unless stated otherwise.

Magnified regions of Sirius red Miller's stained tissue sections shown in Fig 3.16 were viewed under polarised light at x100 or x200 magnification (Fig 3.17). Collagen fibres were aligned radially from the fibrosa in the posterior leaflet into the posterior annulus (Fig. 3.17; S3, S5), fibres were only weakly birefringent in Segment 5 suggesting that the majority of collagens were not orientated radially in this region. In the anterior region the collagen appeared isotropic in the trigones (Fig. 3.17; S1, S8) whilst in the mitral to aortic continuum fibres were aligned radially at the outer regions of the fibrosa and were isotropic towards the centre (Fig. 3.17 S10).

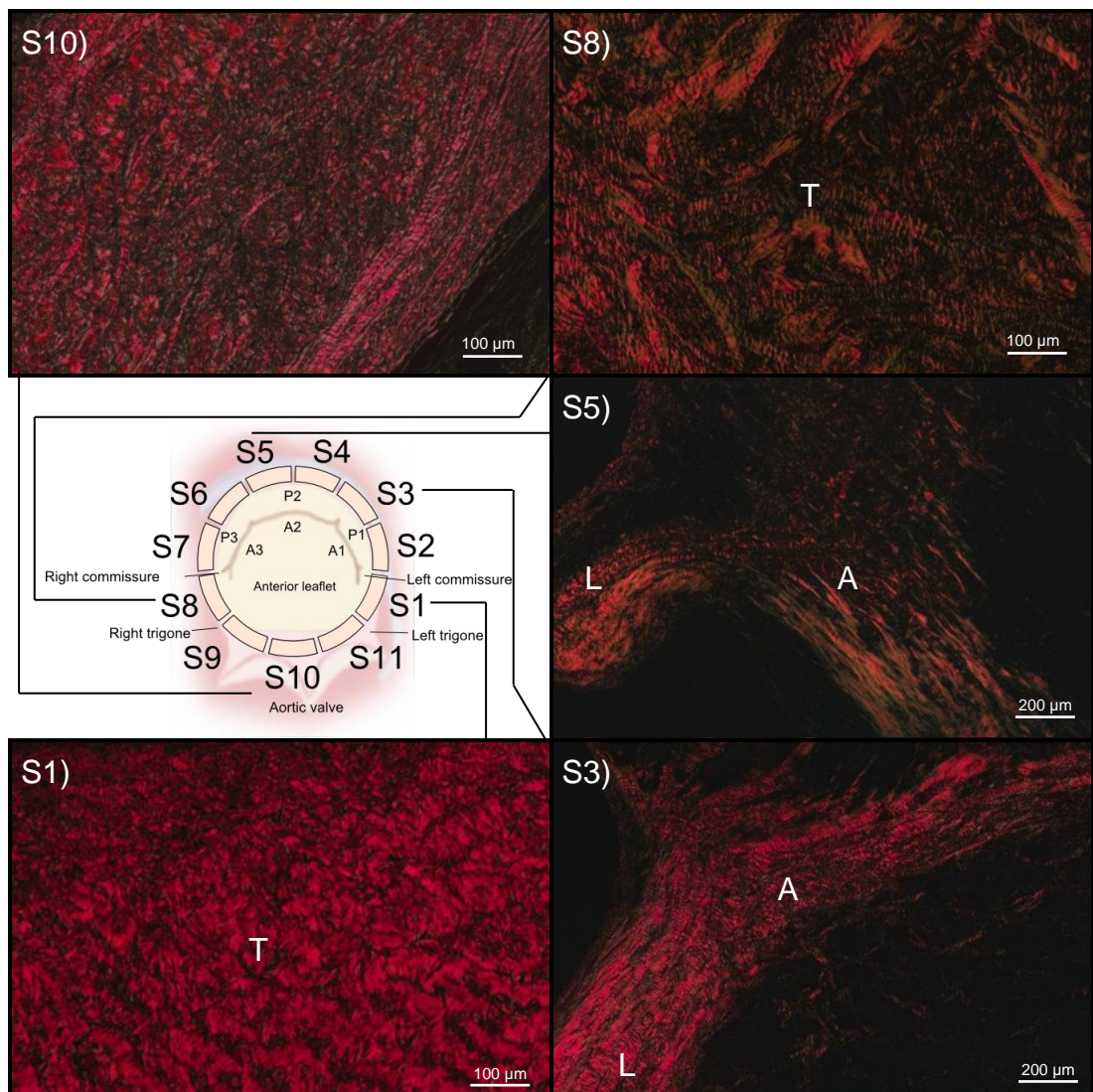


Fig 3.17 – Images of Sirius red Miller's stained sections from selected segments of the native porcine mitral valve annulus viewed under polarised light microscopy. Representative images from three porcine annuli are shown. Section 1 had isotropic fibres x 100 magnification (S1), Section 3 had radially aligned fibres x 50 magnification (S3), Section 5 had radially aligned fibres x 50 magnification (S5), Section 8 had isotropic fibres x 100 magnification (S8), Section 10 had isotropic fibres surrounded by radial fibres x 100 magnification (S10). A: Annulus; AM: Atrial Muscle; VM: Ventricular Muscle; L: Leaflet.

3.3.5 Distribution of proteins in the extracellular matrix of the porcine mitral annulus

The distribution of different structural proteins of the extracellular matrix of the porcine mitral valve annulus was investigated using immunohistochemistry

3.3.5.1 Collagen I

The anterior and posterior regions (Fig.3.18a) of the porcine mitral annulus were labelled with collagen I antibody. Images of annulus sections showed that both regions stained positive. Staining was observed in the fibrosa of the anterior and posterior mitral valve leaflets (Fig 3.18a; S5, S8, S10) and became more prominent in the annulus (Fig 3.18a; S1, S3, S5, S8, S10). In the trigonal region (Fig 3.18a; S1) collagen I intensity was greatest at the outer edges and diminished in regions where lacunae-like structures were apparent towards the centre. No staining was observed in the sections stained with the antibody isotype control (Fig 3.18b; a) or diluent alone (Fig. 3.18b; b).

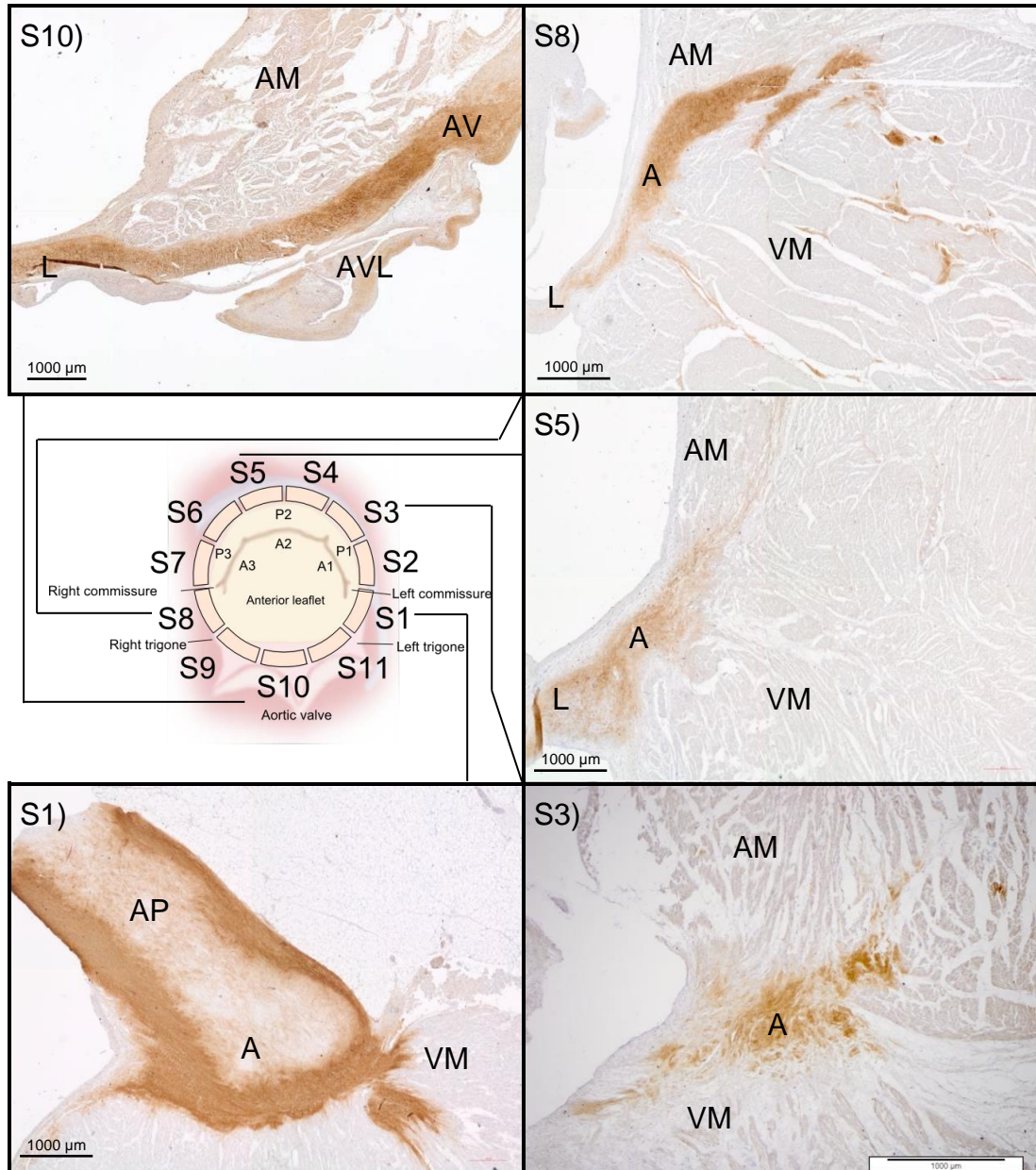


Fig 3.18a – Sections of porcine mitral valve annulus stained with antibody to collagen I. Representative images from three porcine annuli are shown. Anterior region with collagen I prominent in the outer layers of the thick trigones, (S1. Annulus 4, S3. Annulus 3, S8. Annulus 4, S10. Annulus 1). Posterior region (S3. Annulus 3, S5. Annulus 4). A: Annulus; T: Trigone; AM: Atrial Muscle; AV: Aortic Valve; AVL: Aortic Valve Leaflet; VM: Ventricular Muscle; L: Leaflet. Magnification x 20 unless stated otherwise.

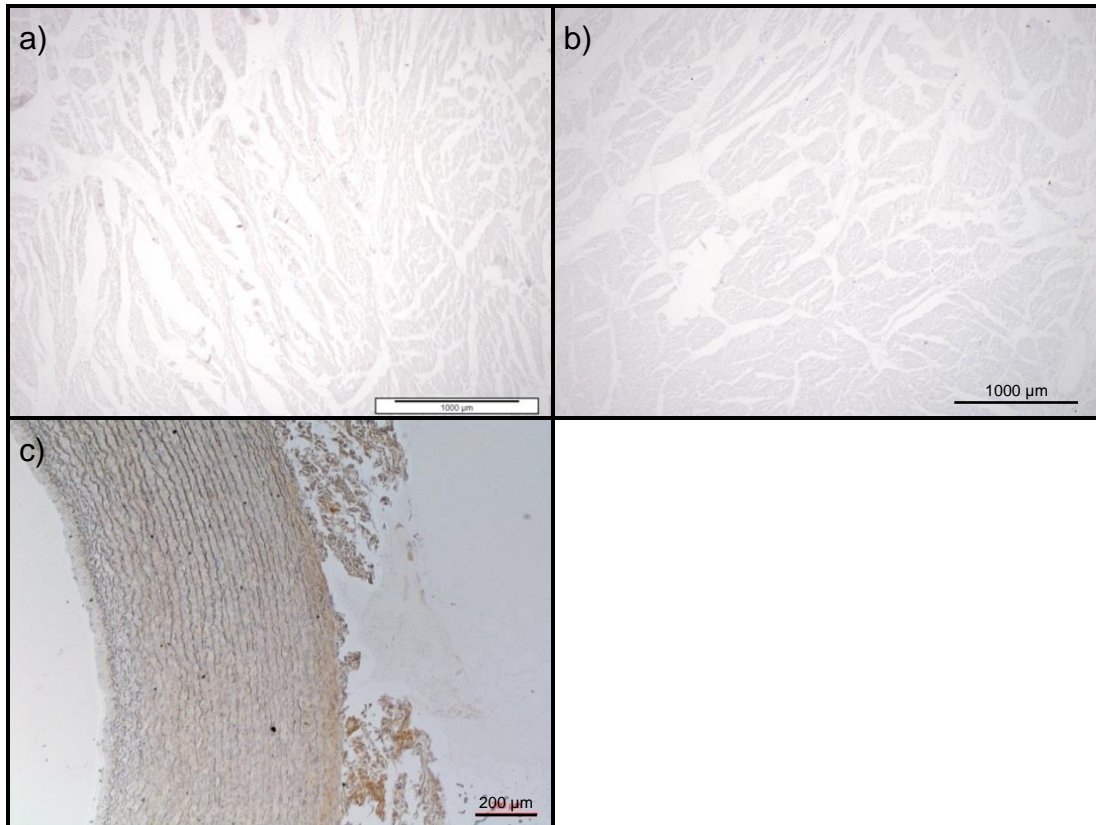


Fig 3.18b – Sections of porcine mitral valve annulus stained with antibody to collagen I. Representative images from three porcine annuli are shown. Isotype control (a). Diluent control (b). Porcine common carotid artery positive control x 50 magnification (c). A: Annulus; T: Trigone; AM: Atrial Muscle; AV: Aortic Valve; AVL: Aortic Valve Leaflet; VM: Ventricular Muscle; L: Leaflet. Magnification x 20 unless stated otherwise.

3.3.5.2 Collagen II

Images of sections of the anterior and posterior regions (Fig. 3.19a) of the porcine mitral annulus labelled with antibody to collagen II showed positive staining in the anterior region. Positive staining was observed in the anterior annulus in the dense cartilage-like regions (Fig 3.19a; S1, S8, S10). Staining was not seen in the muscle surrounding the annulus and it gradually decreased in the posterior region (Fig 3.19a; S3). There was no positive staining in the posterior annulus region (Fig 3.19a; S5). Structures resembling chondrons were apparent in the anterior region surrounded by collagen II stained tissue (Fig. 3.19a; S10 b). No staining was observed in the sections stained with the antibody isotype control (Fig 3.19b; a) or diluent alone (Fig. 3.19b; b).

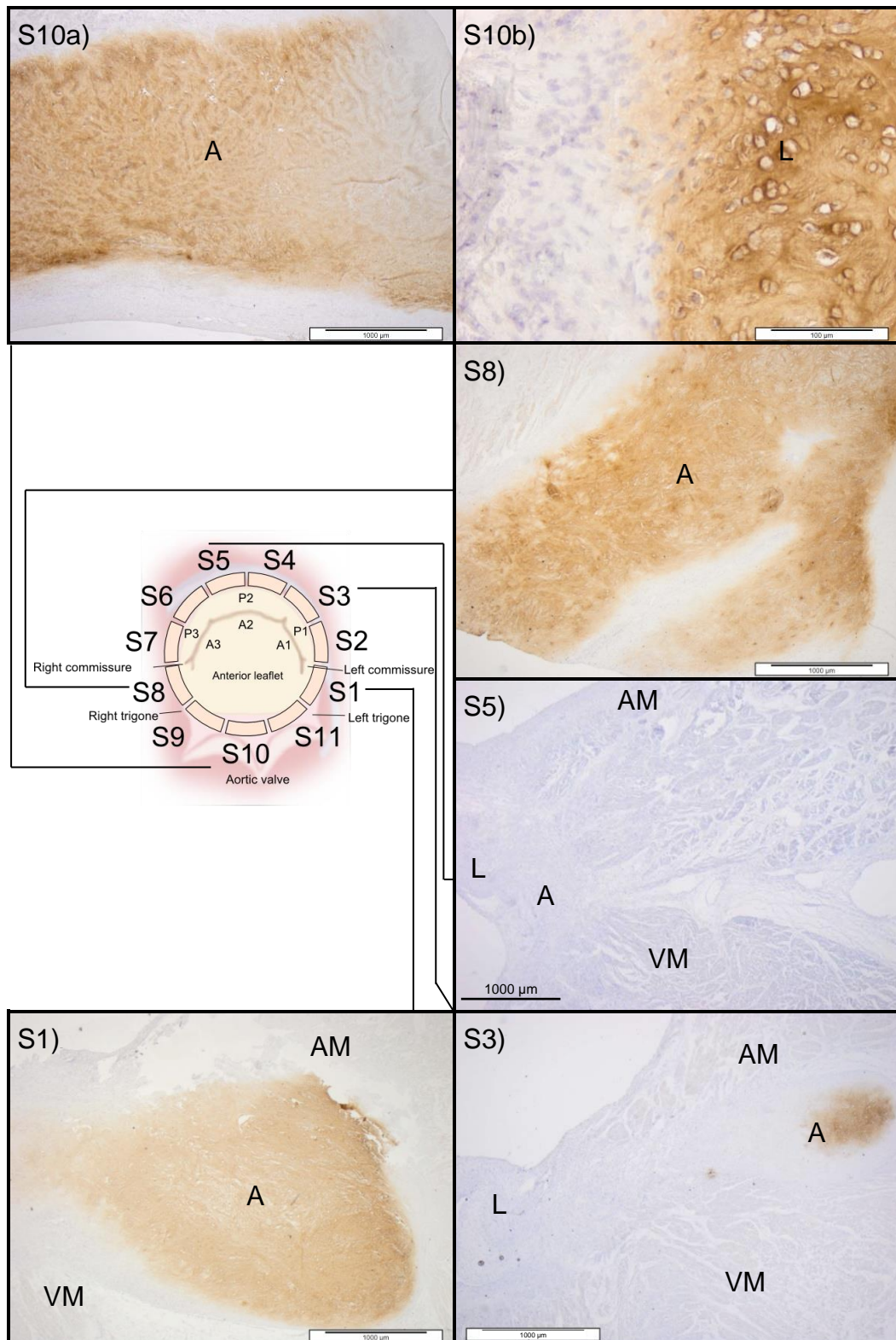


Fig 3.19a – Sections of porcine mitral valve annulus stained with antibody to collagen II. Representative images from three porcine annuli are shown. Anterior region with collagen II prominent in the inner regions of the trigones (in contrast to collagen I in the outer layers), (S1. Annulus 4, S8. Annulus 3, S10 a. Annulus 1). Posterior region showed little evidence of collagen II, magnification (S3. Annulus 4, S5. Annulus 1). Anterior region showing chondron-like regions enclosed by collagen II (S10 b. Annulus 1). A: Annulus; T: Trigone; AM: Atrial Muscle; AV: Aortic Valve; AVL: Aortic Valve Leaflet; VM: Ventricular Muscle; L: Leaflet. Magnification x 20 unless stated otherwise.

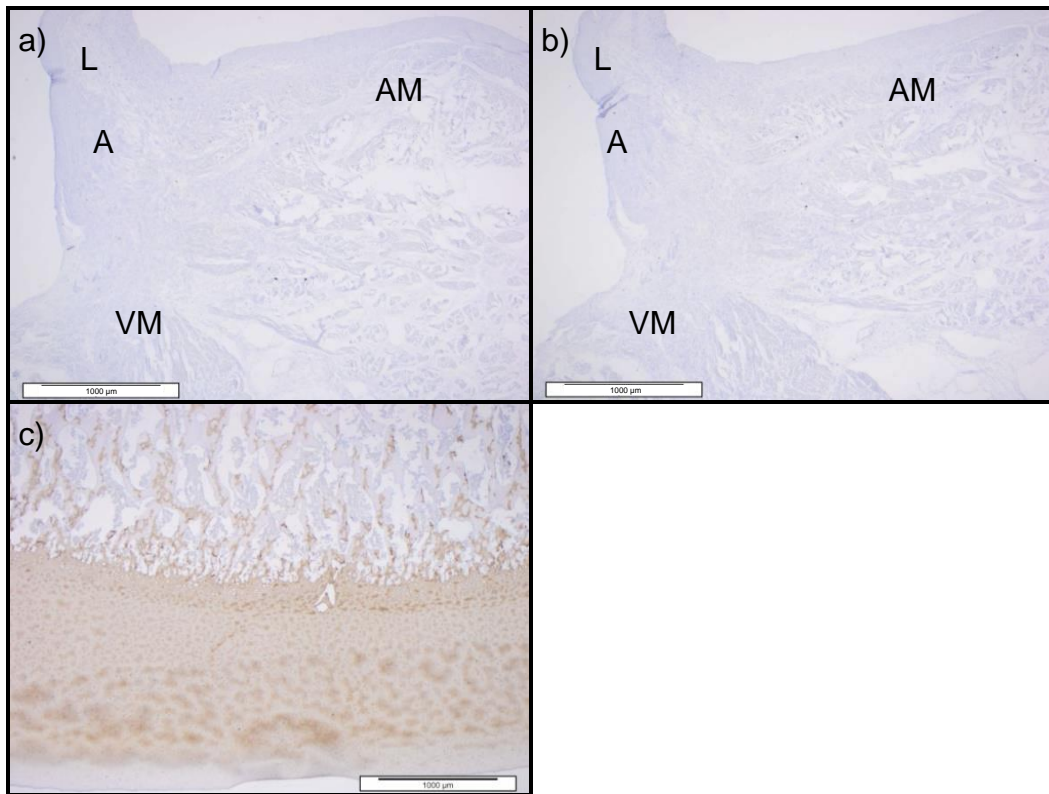


Fig 3.19b – Sections of porcine mitral valve annulus stained with antibody to collagen II. Representative images from three porcine annuli are shown. Isotype control (a). Diluent control (b). Porcine articular cartilage positive control (c). A: Annulus; T: Trigone; AM: Atrial Muscle; AV: Aortic Valve; AVL: Aortic Valve Leaflet; VM: Ventricular Muscle; L: Leaflet. Magnification x 20 unless stated otherwise.

3.3.5.3 Collagen III

Positive staining was observed in the anterior and posterior regions in images of sections of the porcine mitral valve annulus (Fig. 3.20a) labelled with antibody to collagen III. Staining was prominent in both the annulus and the surrounding muscle in all regions. Staining was more prominent in the endocardium and surfaces of the leaflets (Fig 3.20a; S1, S3, S8, S10). No staining was observed in the sections stained with the antibody isotype control (Fig 3.20b; a) or diluent alone (Fig. 3.20b; b).

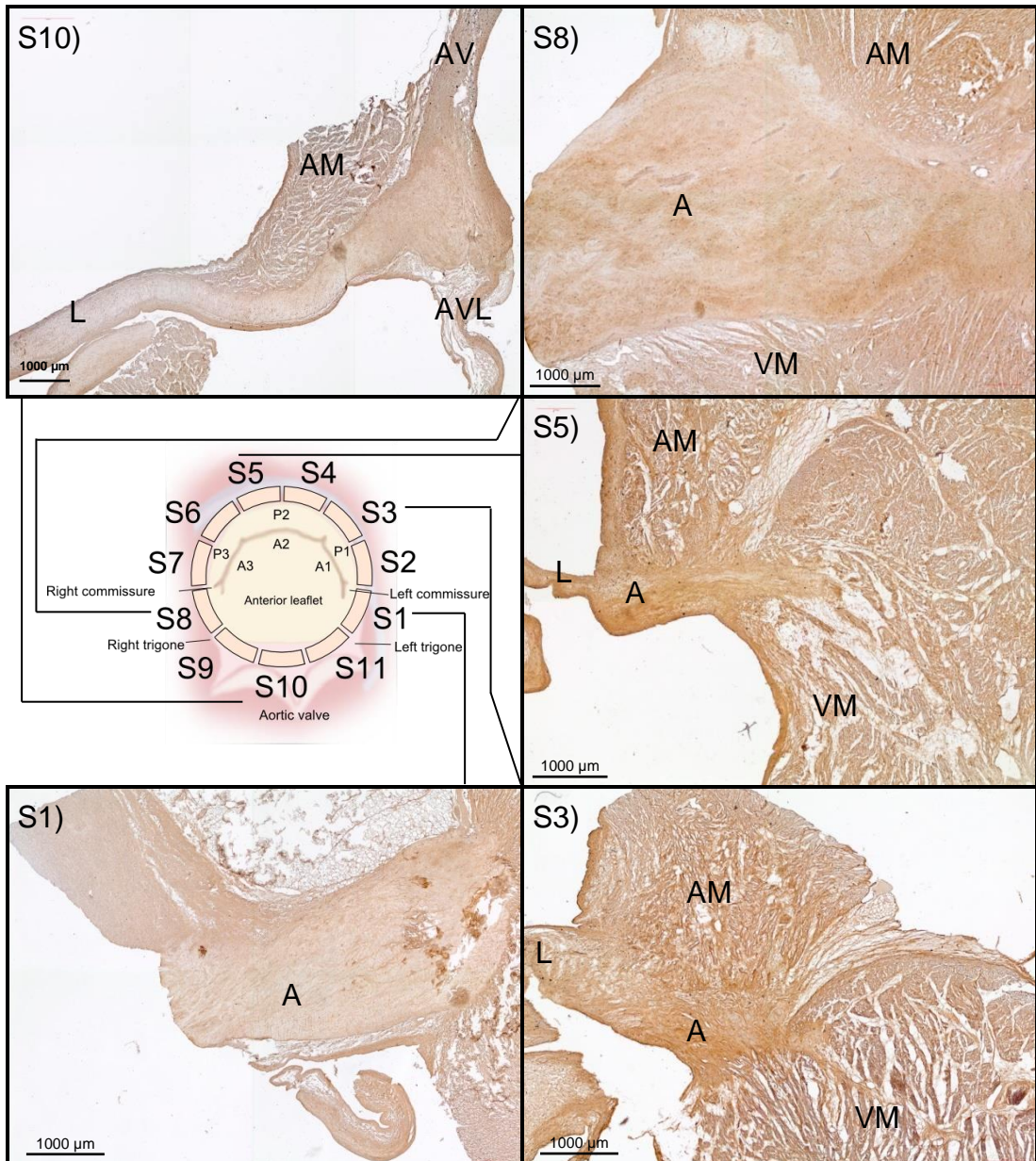


Fig 3.20a – Sections of porcine mitral valve annulus stained with antibodies to collagen III. Representative images from three porcine annuli are shown. Anterior region with collagen III, (S1. Annulus 4, S8. Annulus 4, S10. Annulus 4). Posterior region with collagen III, (S3. Annulus 3, S5. Annulus 1). A: Annulus; T: Trigone; AM: Atrial Muscle; AV: Aortic Valve; AVL: Aortic Valve Leaflet; VM: Ventricular Muscle; L: Leaflet. Magnification x 20 unless stated otherwise.

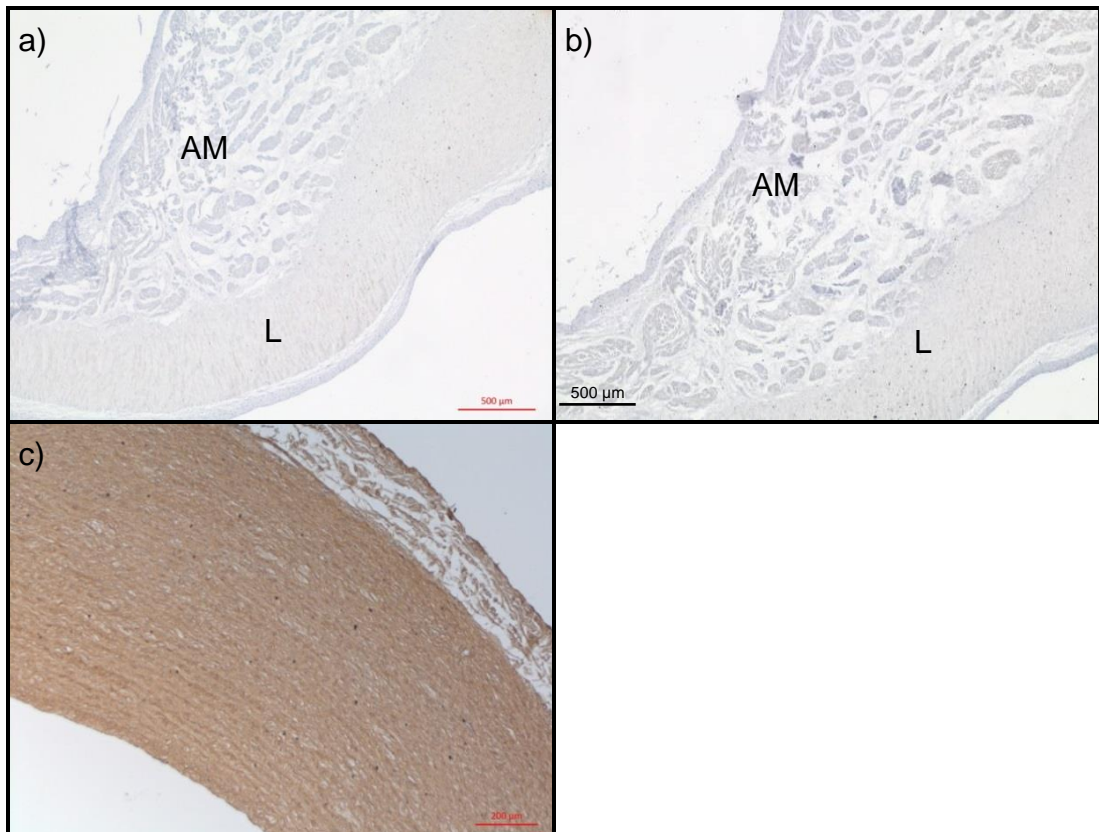


Fig 3.20b – Sections of porcine mitral valve annulus stained with antibodies to collagen III. Representative images from three porcine annuli are shown. Isotype control (a). Diluent control (b). Porcine common carotid artery positive control x 50 magnification (c). A: Annulus; T: Trigone; AM: Atrial Muscle; AV: Aortic Valve; AVL: Aortic Valve Leaflet; VM: Ventricular Muscle; L: Leaflet. Magnification x 20 unless stated otherwise.

3.3.5.4 Collagen IV

The images of the anterior and posterior regions (Fig 3.21a) of the porcine mitral annulus labelled with antibody to collagen IV revealed positive staining for both regions. Positive staining was observed primarily in the fibrosa of the leaflet and myocardium, staining was less prominent in the mitral annulus (Fig 3.21a; S1, S3, S5, S8). In the trigones collagen IV was identified in structures that resembled chondrons (Fig 3.21a; S1, S10 a, S10 b). No staining was observed in the sections stained with the antibody isotype control (Fig 3.20b; a) or diluent alone (Fig 3.20b; b).

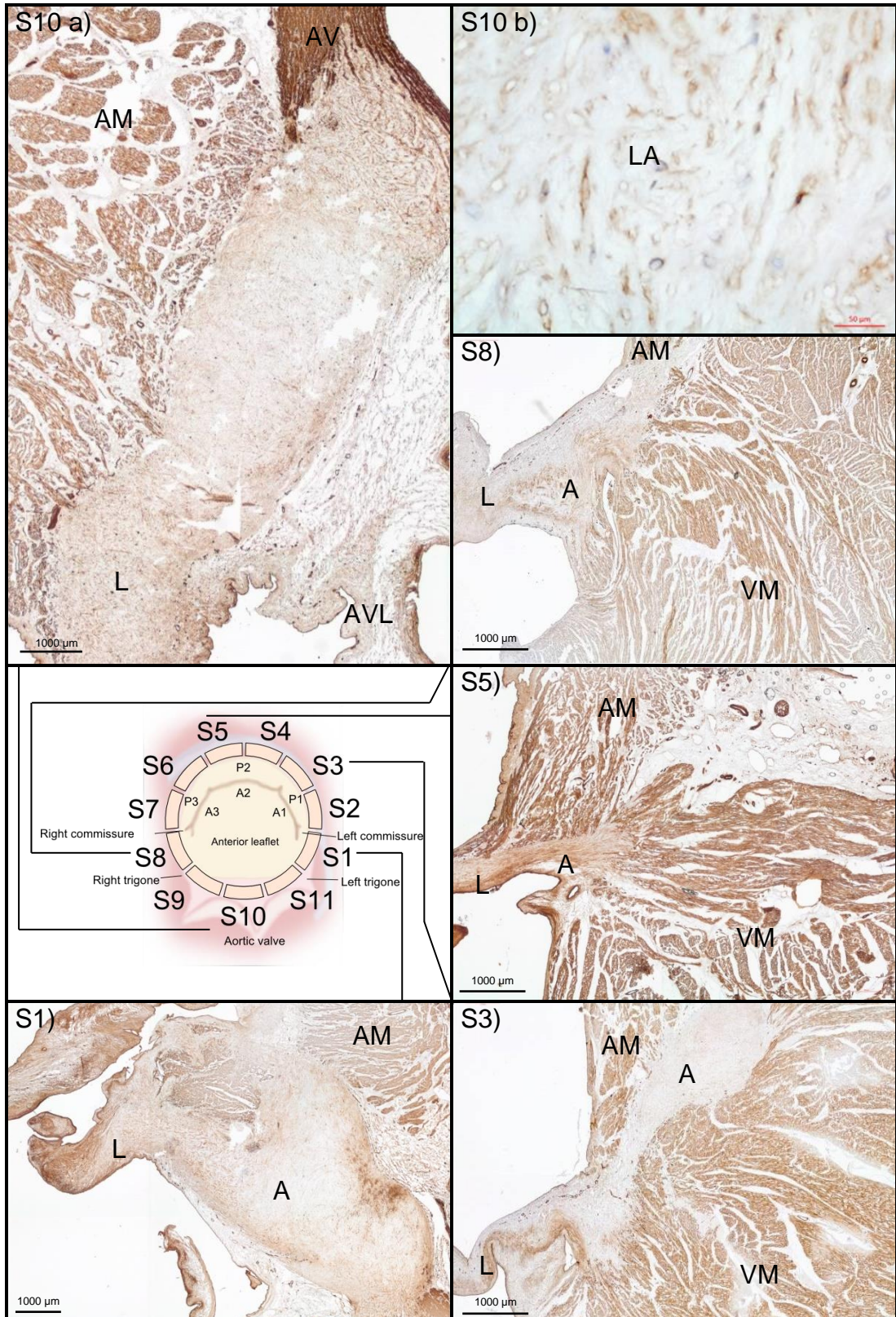


Fig 3.21a – Sections of porcine mitral valve annulus stained with antibody to collagen IV. Representative images from three porcine annuli are shown. Anterior region showing collagen IV (S1. Annulus 3, S8. Annulus 1, S10 a. Annulus 3). Brown staining observed around lacunae of anterior x 200 magnification (S10 b. Annulus 3). Posterior region showing collagen IV (S3. Annulus 4, S5. Annulus 3). A: Annulus; T: Trigone; AM: Atrial Muscle; AV: Aortic Valve; AVL: Aortic Valve Leaflet; VM: Ventricular Muscle; L: Leaflet; LA: Lacunae. Magnification x 20 unless stated otherwise.

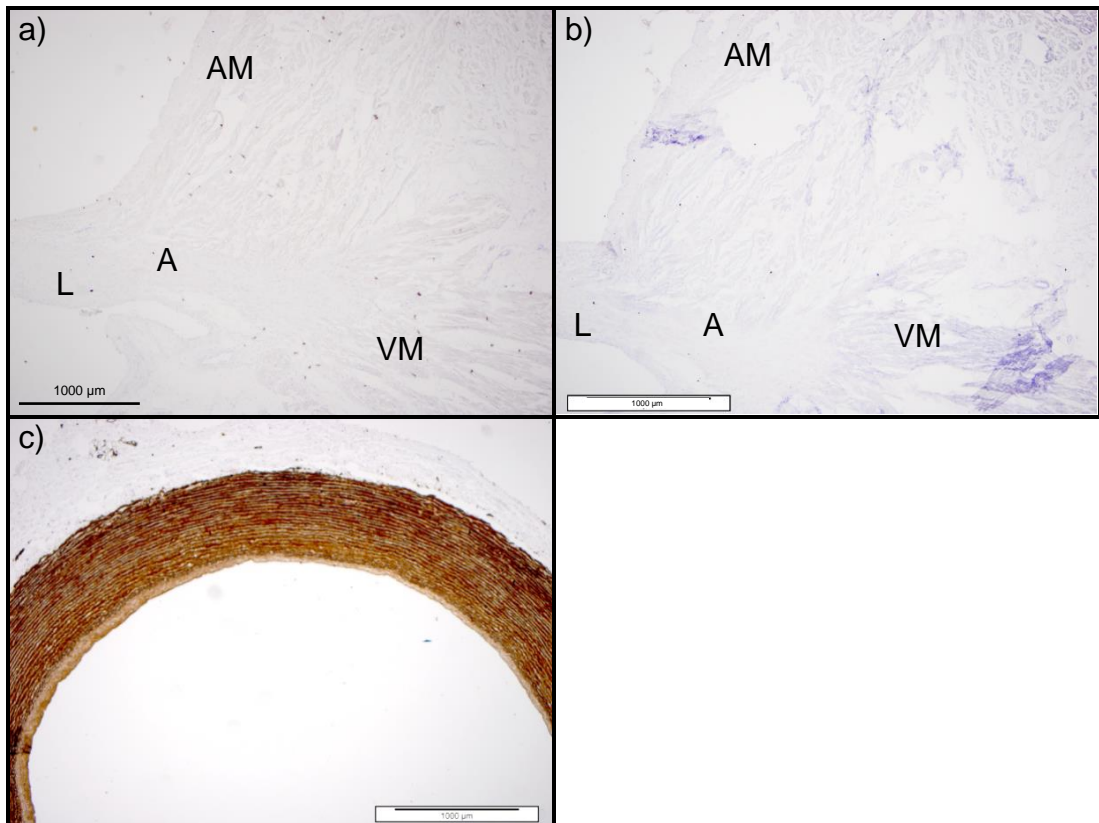


Fig 3.21b – Sections of porcine mitral valve annulus stained with antibody to collagen IV. Representative images from three porcine annuli are shown. Isotype control (a). Diluent control (b). Porcine common carotid artery positive control (c). A: Annulus; T: Trigone; AM: Atrial Muscle; AV: Aortic Valve; AVL: Aortic Valve Leaflet; VM: Ventricular Muscle; L: Leaflet; LA: Lacunae. Magnification x 20 unless stated otherwise.

3.3.5.5 Collagen VI

Images of sections of the anterior and posterior regions (Fig 3.22a) of the porcine mitral annulus labelled with antibody to collagen VI showed positive staining in both regions. Positive staining more prominent in the muscle surrounding the annulus in all regions (Fig 3.22a; S1-S10) and within the trigones of the annulus (Fig 3.22a; S1, S8) and the mitral to atrial continuum (Fig 3.22a; S10). No staining was observed in the sections stained with the antibody isotype control (Fig 3.22b; a) or diluent alone (Fig. 3.22b; b).

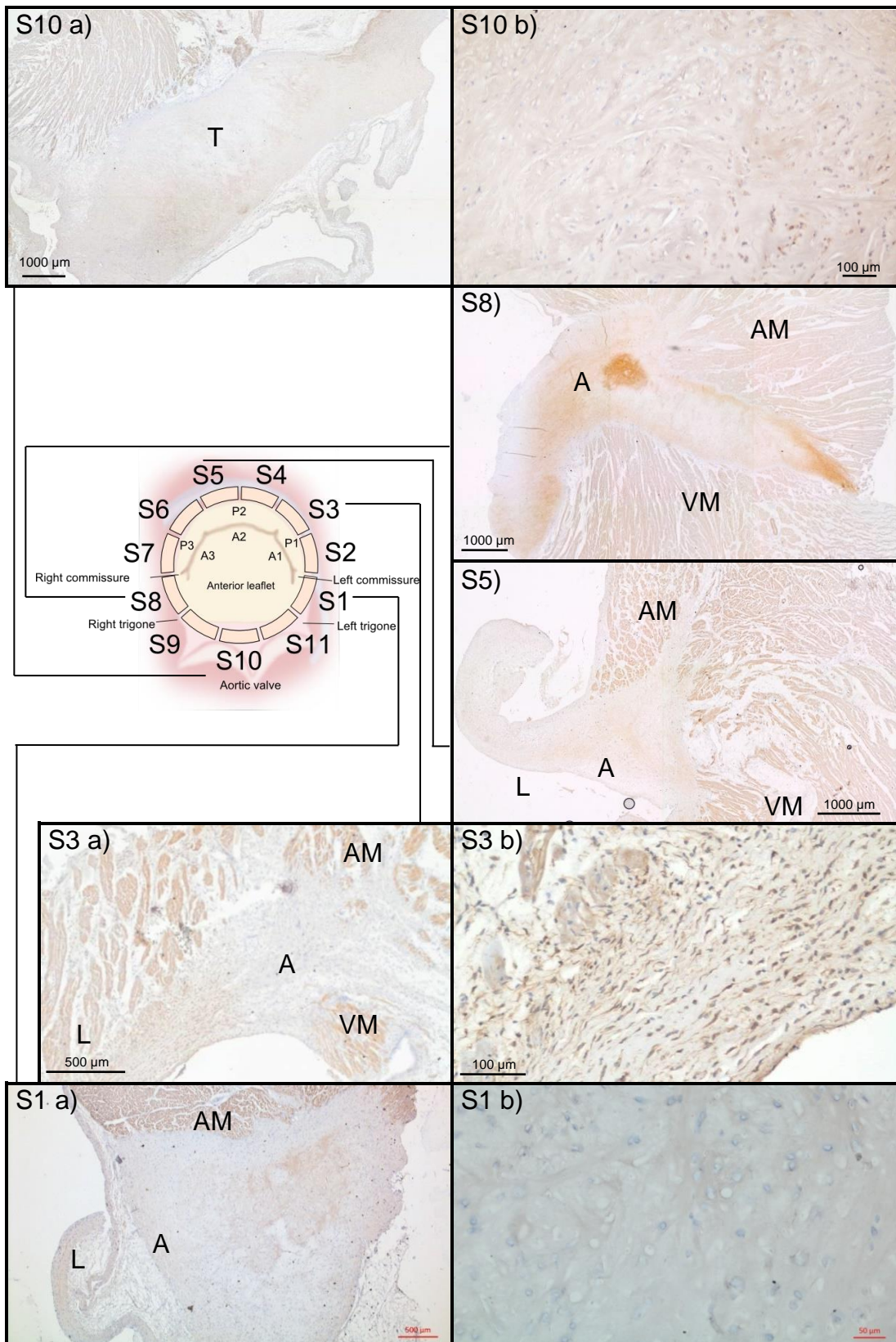


Fig 3.22a – Sections of porcine mitral valve annulus stained with antibody to collagen VI. Representative images from three porcine annuli are shown. Anterior region showing collagen VI (S1 a. Annulus 5, S1 b. Annulus 5 x 200 magnification, S8. Annulus 4, S10 a. Annulus 3, S10 b. Annulus 3 x100 magnification). Posterior region showing collagen VI, (S3 a. Annulus 5, S3 b. Annulus 5 x100 magnification, S5. Annulus 4). A: Annulus; T: Trigone; AM: Atrial Muscle; AV: Aortic Valve; VM: Ventricular Muscle; L: Leaflet.

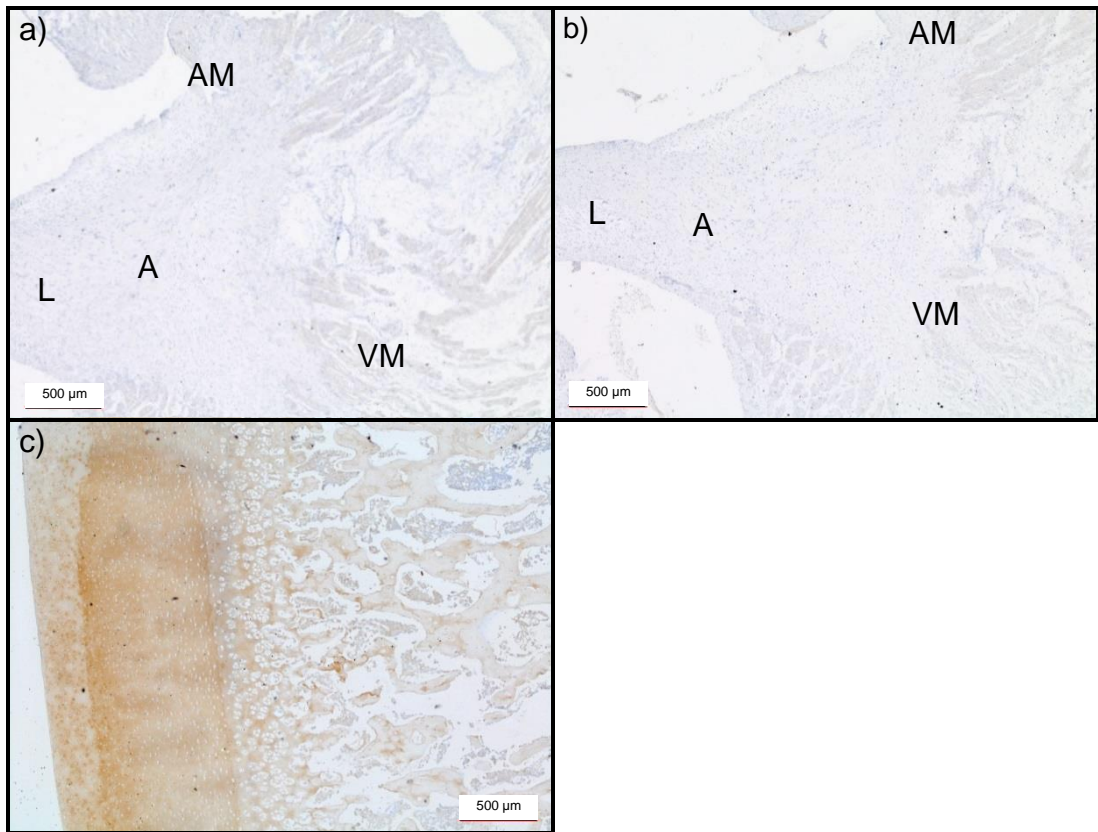


Fig 3.22b – Sections of porcine mitral valve annulus stained with antibody to collagen VI. Representative images from three porcine annuli are shown. Isotype control (a). Diluent control (b). Porcine articular cartilage positive control (c). A: Annulus; T: Trigone; AM: Atrial Muscle; AV: Aortic Valve; AVL: Aortic Valve Leaflet; VM: Ventricular Muscle; L: Leaflet. Magnification x 20 unless stated otherwise.

3.3.5.6 Fibronectin

Sections of the porcine mitral annulus labelled with fibronectin antibody stained positive in both the anterior and posterior regions (Fig 3.23a).

Positive staining was most intense in the fibrosa leading into the annulus in the posterior region and in the endocardium (Fig 3.23a; S3, S5, S8). Staining was also visible in the trigones (Fig 3.23a; S1, S10) and myocardium in all regions. No staining was observed in the sections stained with the antibody isotype control (Fig 3.23b; a) or diluent alone (Fig. 3.23 b).

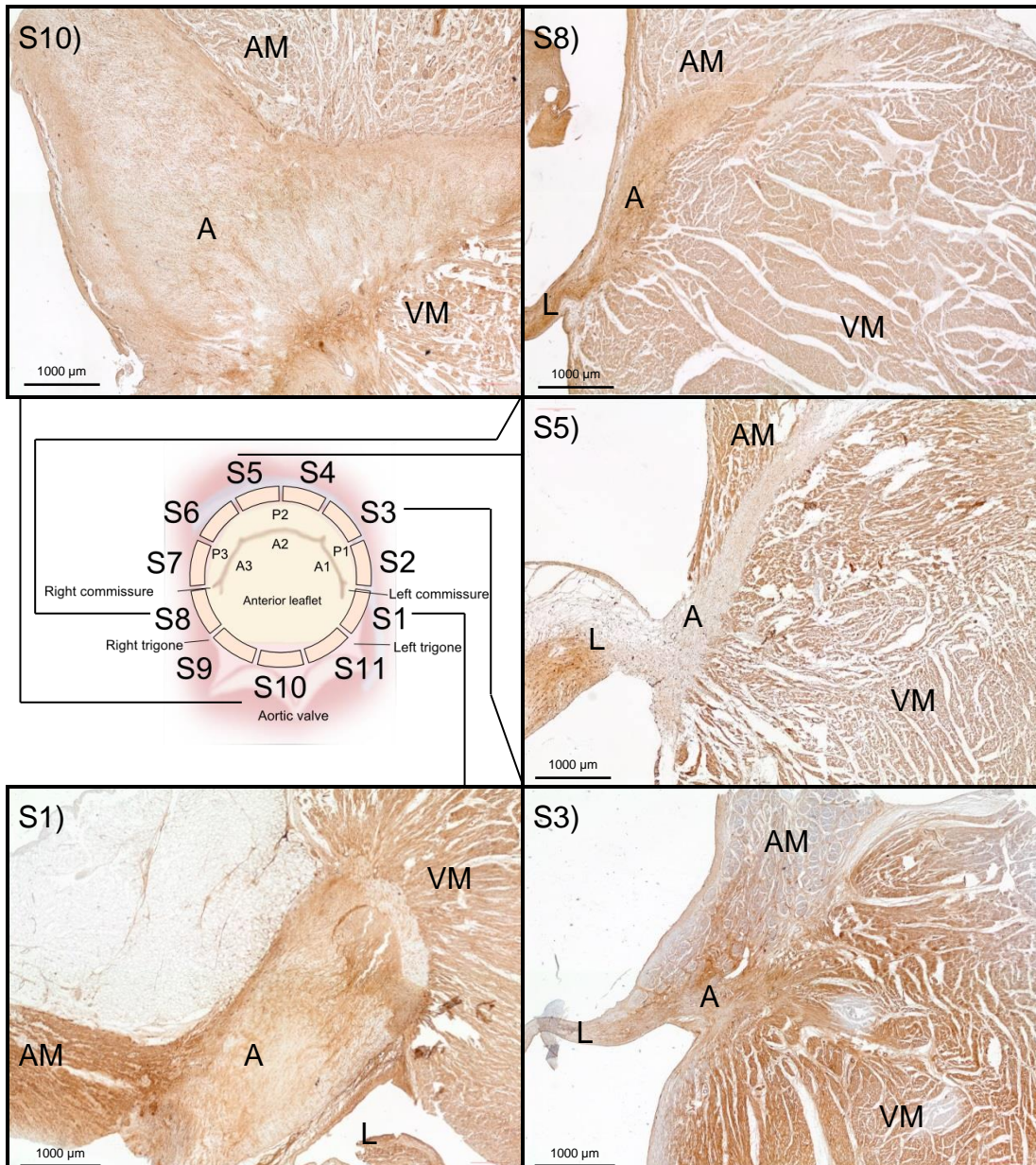


Fig 3.23a – Sections of porcine mitral valve annulus stained with antibody to fibronectin. Representative images from three porcine annuli are shown. Anterior region showing fibronectin, (S1. Annulus, S8. Annulus 3, S10. Annulus 2). Posterior region showing fibronectin, (S3. Annulus 4, S5. Annulus 3). Isotype control (a). A: Annulus; T: Trigone; AM: Atrial Muscle; AV: Aortic Valve; AVL: Aortic Valve Leaflet; VM: Ventricular Muscle; L: Leaflet. Magnification x 20 unless stated otherwise.

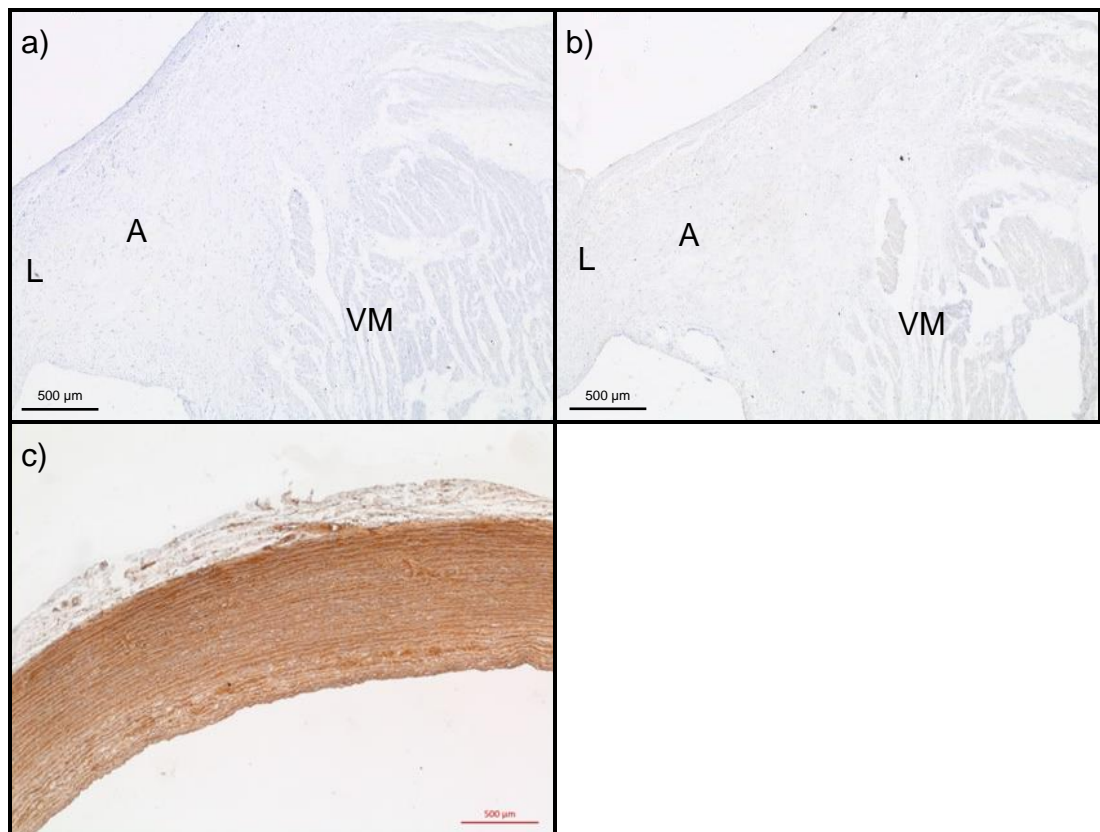


Fig 3.23b – Sections of porcine mitral valve annulus stained with antibody to fibronectin. Representative images from three porcine annuli are shown. Isotype control (a). Diluent control (b). Porcine common carotid artery positive control (c). A: Annulus; T: Trigone; AM: Atrial Muscle; AV: Aortic Valve; AVL: Aortic Valve Leaflet; VM: Ventricular Muscle; L: Leaflet. Magnification x 20 unless stated otherwise.

3.3.5.7 Laminin

Images of sections of the anterior and posterior regions (Fig 3.24a) of the porcine mitral annulus labelled with antibody to laminin revealed that both regions were stained positive. Positive staining was observed in the annulus and atrial and ventricular myocardium in all regions. Staining was more prominent in the muscle surrounding the annulus. No staining was observed in the sections stained with the antibody isotype control (Fig 3.24b; a) or diluent alone (Fig. 3.24b; b).

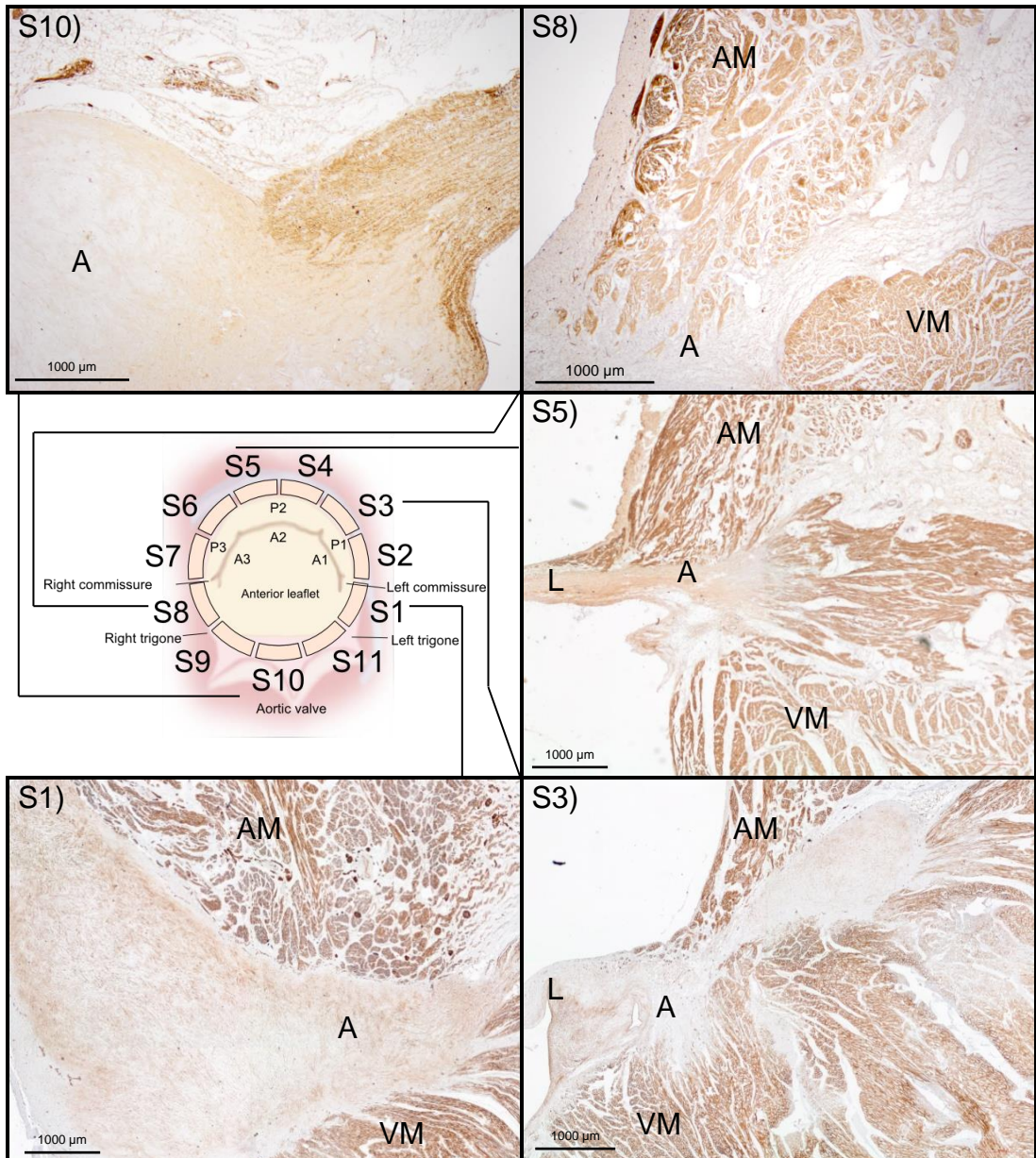


Fig 3.24a – Sections of porcine mitral valve annulus stained with antibody to laminin. Representative images from three porcine annuli are shown. Anterior region showing laminin, (S1. Annulus 4, S8. Annulus 1, S10. Annulus 3). Posterior region showing laminin, (S3. Annulus 4, S5. Annulus 3). A: Annulus; T: Trigone; AM: Atrial Muscle; AV: Aortic Valve; AVL: Aortic Valve Leaflet; VM: Ventricular Muscle; L: Leaflet. Magnification x 20 unless stated otherwise.

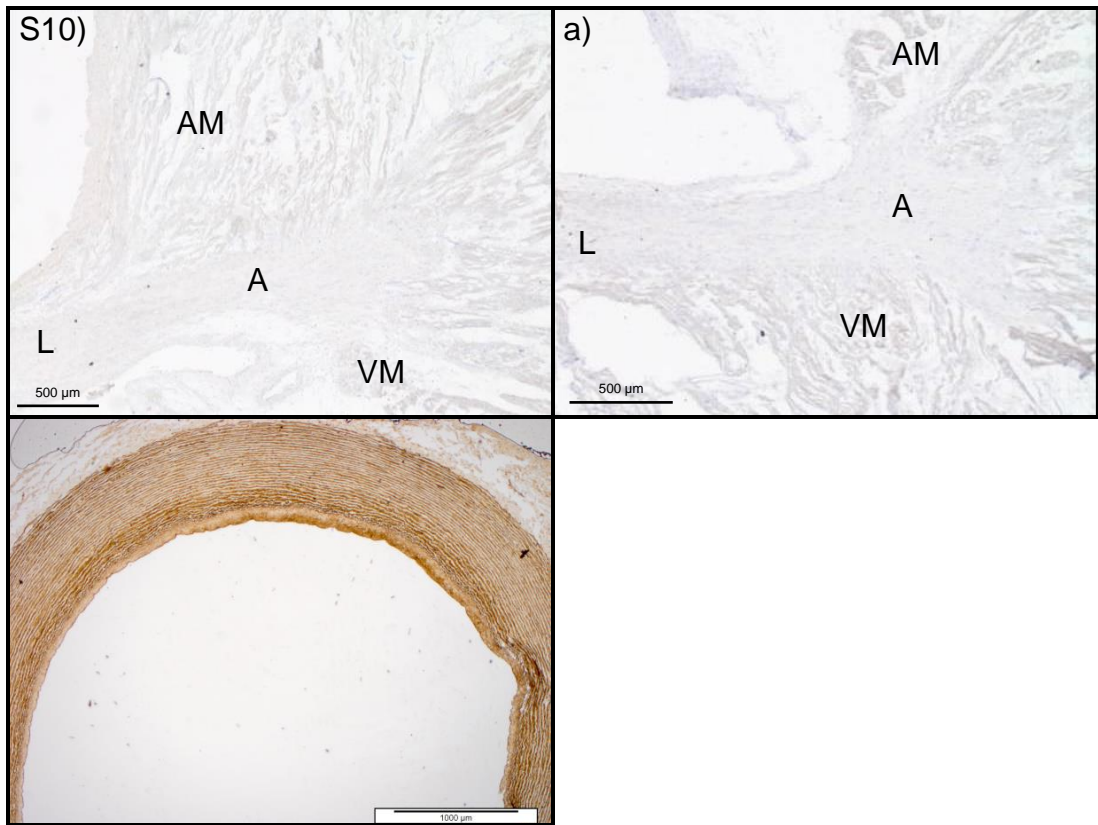


Fig 3.24b – Sections of porcine mitral valve annulus stained with antibody to laminin. Representative images from three porcine annuli are shown. Isotype control (a). Diluent control (b). Porcine common carotid artery positive control (c). A: Annulus; T: Trigone; AM: Atrial Muscle; AV: Aortic Valve; AVL: Aortic Valve Leaflet; VM: Ventricular Muscle; L: Leaflet. Magnification x 20 unless stated otherwise.

3.4 Discussion

The aim of the research presented in this chapter was to characterise, compare and contrast the human and porcine mitral valve annulus using histology and immunohistochemistry. H & E stained sections were used to visualise the general structure of the extracellular matrix. Alcian blue stained sections provided information on the spatial distribution of GAGs and Sirius red Miller's stained sections revealed the collagen orientation and elastin distribution in the tissue. Immunohistochemistry was used to assess the spatial distribution of proteins in and around the mitral valve annulus.

The annulus provides a foundation for the mitral valve leaflets and ensures complete leaflet competence during the systolic phase of the cardiac cycle. At the macroscopic level, the anterior region of the annulus comprises the left and right fibrous trigones, with the anterior mitral leaflet forming a non-thickened membranous septum into the aortic root between the trigones in human (Walmsley, 1978; Angelini *et al.*, 1988; Berdajs *et al.*, 2007) and porcine tissue (Rijk-Zwicker *et al.*, 1994). Observations of the histological sections of the annulus in the present study showed that the mitral-aortic continuum formed a membrane from the mitral valve anterior leaflet to the aortic valve. The continuum was identified in both the human and porcine mitral valve annulus. The major component of the continuum was the fibrosa which showed structural similarities between the two species. It formed a dense collagenous region which comprised of the central core of the human and porcine tissue in the mitral to aortic continuum and could be clearly identified in the Sirius red Miller's stained sections. The thickness of the fibrosa layer in the anterior leaflet has been reported to be significantly greater than in the posterior region for human tissue (Kunzelman *et al.*, 1993) and the results of this study concurred with this for both species, albeit the human tissue was thicker in both anterior and posterior leaflets compared to the porcine mitral valve fibrosa.

The trigones were present on either side of the mitral to aortic continuum in both the human and porcine annulus. Angelini *et al.* (1988) described the trigones in the human annulus as thickened well organised structures which were found to extend laterally around part of the annulus in some hearts. The results of the present work indicated a thickening of the annulus in the trigones of both the human and porcine annulus. In the human annulus, the trigonal collagenous-connective tissue extended further into the epicardial side of the mitral valve compared to the connective tissue in the posterior region, but lacked some of the features found in the porcine trigones. The

porcine trigones were visually more defined compared to the human trigones; they had the appearance of cartilage-like tissue with chondrocytes visible within lacunae.

Cartilage tissue is formed, organised and maintained by chondrocytes, these cells are surrounded by a matrix which together form a chondron. Chondrons appeared to be present in the cartilage-like region in the trigones of the porcine annulus. This suggested that a role of the trigones may be to resist compression in a manner similar to cartilage. In cartilage, the chondron also behaves as a compression resistant membrane acting to protect the chondrocyte (Broom & Myers, 1980). The presence of collagen II and GAGs in the trigonal tissue of the porcine annulus confirmed the cartilage-like properties of this region. Collagen II is a fibril forming collagen and the primary collagen present in articular cartilage (Gelse *et al.*, 2003). It has biomechanical properties which are similar to type I collagen (Bruckner & van der Rest, 1994). In the trigones of the porcine annulus, collagen II was the primary collagen with collagen I present only in the outer regions. The presence of abundant GAGs in this region was also indicative of cartilaginous tissue. In the extracellular matrix, GAGs are found associated with proteoglycans. Proteoglycans consist of a protein core with numerous attached GAG chains. GAGs contain negatively charged groups that are responsible for swelling of tissue; this is what provides compressive stiffness. The presence of collagen II in the trigones of the porcine annulus may indicate why there was an abundance of GAGs. Collagen II contains more hydroxylysine and glucosyl and galactosyl residues than collagen I; these permit interaction with proteoglycans, signifying the hydrating role that GAGs have in cartilage (Mayne, 1989).

Using computational modelling it has been found that the trigones undergo large peak stresses at peak pressure compared to other regions of the mitral valve annulus (Lim *et al.*, 2005). It has been hypothesised that the function of cartilage found in the aortic and pulmonary valves of hamsters, birds and terrapins (Sans-Coma *et al.*, 1994; López *et al.*, 2000, 2001, 2003) is to act as a pivot and resist the high mechanical loads. This could also explain the function of cartilage-like tissue in the trigones of the porcine annulus, and why this region consists of a large accumulation of GAGs compared to other regions in the mitral valve. The cartilage-like tissue in the trigones of the porcine annulus may act as a structural component helping to resist compressive forces whilst maintaining the structure of the mitral valve under load. This region extended laterally towards the commissures of each leaflet

and gradually reduced in size until it was not visible in the posterior most part of the annulus.

The lack of similar cartilage-like regions in the trigones of the human annulus may indicate either a difference between species or differences due to age of the tissue donors. Whilst collagen II was present in the human mitral valve annulus, the presence appeared to be due to disease rather than part of normal heart development. The collagen II in the human tissue was accompanied by calcification and signs of ossification, not just in the anterior region but also the posterior region. The porcine annulus was from animals aged 24-26 weeks old and the human tissue was from donors with a mean age of 69 years. It is possible that the trigones of the annulus of older pigs may also be absent of cartilage-like tissue. In human foetal hearts cartilage has been reported to be expressed during heart development in the endocardial cushions (Combs & Yutzey, 2009) but the presence of cartilage in fully developed human hearts has only been reported in diseased tissue in which calcification and ossification are apparent (Caira *et al.*, 2006).

Sirius red Miller's stained sections also revealed differences in the trigones between the species, there was a distribution of thick radially aligned fibres in the human trigones compared to the porcine trigones which appeared to show the presence of largely isotropic fibre distributions and high levels of elastin. The elastin in the porcine trigones surrounded the chondron-like regions which was suggestive of elastic cartilage. The high level of elastic fibres within the cartilage-like regions might endow the tissue with flexibility enabling it to withstand repeated bending whilst maintaining shape. These high levels of elastin were not found in the human annulus trigones but have been reported in cartilage foci in the aortic valve of Syrian hamsters, close to the attachment of the dorsal leaflet (Sans-Coma *et al.*, 1994). Sirius red Millers staining provided an insight into the isotropic orientation of the cartilage-like tissue in this region of the porcine annulus and supports the theory that the proteoglycans may influence the orientation of the collagens. The isotropic nature of the cartilage-like tissue in the porcine annulus trigones may be due to osmotic forces. Osmotic forces in cartilage cause the proteoglycans to expand, a hydrostatic pressure of 0.35 MNm^{-2} acts isotropically leading to a predominantly isotropic structure in the collagen network (Ottani *et al.*, 2001).

The thickened fibrosa in the anterior compared to the posterior region, along with the trigones in both species, indicated the important structural role this region has in the mitral valve. This region is often attributed to the cardiac

skeleton in human valves (Fedak *et al.*, 2008) where it acts to anchor the valve and surrounding heart tissue during the cardiac cycle. The posterior region of the porcine and human mitral valve annulus at the microscopic level consisted of a thin collagenous band of fibres which separated the atrial and ventricular muscle and provided insertion for the posterior leaflet.

Compared to the differing characteristics of the trigones in the anterior region between species, the posterior region shared a similar morphology. The fibrosa is the load bearing element of the mitral valve leaflets (McCarthy *et al.*, 2010) that provides effective valve closure without causing prolapse (Rabkin-Aikawa *et al.*, 2004). The fibrosa layer of the leaflet of both the human and porcine specimens showed some radially aligned fibres that formed into a thin collagenous layer of the posterior annulus, with most fibres weakly birefringent under polarised light. The load bearing properties of the fibrosa appeared to continue into the posterior annulus of both species for anchoring the leaflets and providing effective stress distribution in the mitral valve during the cardiac cycle. As for the anterior region, the fibrosa of the posterior region was thicker in the human tissue specimens compared to the porcine tissue. The presence of a thicker fibrosa in the human hearts may be the product of age; porcine hearts tend to resemble younger human hearts whilst canine hearts have been found to resemble older human heart tissue, which are more likely to show signs of heart disease (Hearse & Sutherland, 2000) and an increase in the thickness of the mitral valves along with other heart related changes (Kitzman & Edwards, 1990) .

In the posterior region of the annulus in both species an area high in GAGs was identified in the hinge point of the annulus where the posterior leaflet inserted. The presence of GAGs at the hinge of the mitral leaflet suggests that their role could be to resist compression in regions of tensile and compressive loading as the leaflets open and close, as found in the leaflets and chordae of the human mitral valve (Grande-Allen *et al.*, 2004). The spongiosa is clearly integrated into the annulus in the human tissue in the posterior annulus, the spongiosa consisted of loose collagen and elastin fibres interspersed with GAGs. In contrast, the spongiosa of the porcine leaflet was not integrated into the atrial side of the mitral valve, where only the fibrosa of the mitral valve leaflet formed into the annulus region.

The posterior part of the human valve comprised a high proportion of adipose tissue that was visible close to the epicardial side of the atrial and

ventricle myocardium. This adipose tissue appeared to support the coronary artery. In contrast to the human mitral valve the adipose tissue in the porcine valves was less prominent, separating the atrial and ventricular muscle only at the epicardial side of the valve. This adipose tissue has been suggested to provide a mechanical supportive structure for the vessels in the heart (Iozzo, 2011) and also act as an energy source for the heart and as a buffer against toxicity (Marchington *et al.*, 1989). Adipose tissue is an electrical insulator (Petrofsky, 2008), preventing electrical impulses travelling between the ventricular myocardium and atrial myocardium. The increase in adipose tissue in the human heart is likely a feature of age (Kitzman & Edwards, 1990).

The presence of atrial myocardium in the annulus and basal region of the mitral leaflets was a feature of both species. In both species atrial muscle appeared circumferential in orientation close to the annulus, with the presence of a thin band of longitudinal fibres in the human tissue in the posterior region, in a layer closest to the endocardium. The circumferential orientation in both species suggested that the function of this muscle was to contract to reduce the annular area during systole and assist in valve closure (Boucek *et al.*, 1978; Timek *et al.*, 2003), this is in agreement with another study by Berdajs *et al.* (2007) who found the same arrangement in human tissue. The wall of the left ventricle in human hearts has been analysed by Ho (2009) who observed that the myocardium of the left ventricle comprised of three layers; the superficial, middle and deep. Ho (2002) found that the middle layers of the human myocardium encircled the valve and were thickest close to the mitral valve, in the present study it was found that the middle layers of the myocardium of both the human and porcine valves contained fibres that ran circumferentially and were numerous and close to the annulus. The circumferential orientation of the muscle close to the annular region may explain how the human annulus undergoes a reduction in annular area of approximately 25% during systole (Ormiston *et al.*, 1981; Flachskampf *et al.*, 2000).

There was a similar distribution of proteins present in the ECM of the anterior and posterior regions of the mitral valve for both species. Immunohistochemistry staining was used to determine the spatial distribution of extracellular matrix proteins in the mitral annulus and surrounding regions. Positive staining for collagen I, III, IV, VI, fibronectin and laminin was observed in all regions of the annulus, for both the human

and porcine annulus and surrounding regions. Collagen I and III are closely linked primarily structural proteins, known to be fibril forming, and confer mechanical strength to the tissue with their highly orientated structure (Gelse *et al.*, 2003). Collagen I is the major collagen of bone, tendon and ligament along with other connective tissues and was distributed around the whole of the annulus. Collagen I has been shown to co-localise with collagen III. In the mitral valve annulus of both species there was evidence of the collagen I and collagen III network, although collagen I was more prominent in the fibrosa whilst collagen III was more prominent in the myocardium, adipose tissue and endocardium.

There was a high concentration of collagen IV in the myocardium, on the leaflet surfaces and the endocardium of the mitral valve annulus and surrounding tissue in both the species. Collagen IV forms collagen networks in the basement membrane, these interlink with the laminins and fibronectins, to form a structure important for cell adhesion, migration and differentiation (Charonis *et al.*, 1985; Khoshnoodi *et al.*, 2008) as well as providing mechanical stability (Aumailley & Timpl, 1986). Collagen IV is prominent in the basement membrane of the myocardium and acts as an anchoring site for the collagen fibrils (McLeod *et al.*, 2015). The annulus was largely devoid of collagen IV in both species. It was principally found surrounding the chondron-like regions in the trigones of the porcine tissue and in the mitral to aortic continuum of the porcine and human annulus.

Collagen VI was present in both the annulus and surrounding myocardium in the mitral valve annulus region of both species. Collagen VI is a beaded-filament-forming collagen that forms structural links with cells (Kadler *et al.*, 2007). It is found in the majority of interstitial tissues where it forms a network that attaches large interstitial structures such as blood vessels and collagen fibres to adjacent connective tissues (Keene *et al.*, 1988). In the porcine annulus, collagen VI also appeared close to the chondron-like regions in the trigones. In cartilage, collagen VI is present in the pericellular matrix; its role may be to help with anchoring of chondrocytes and cell signalling between the cells and the extracellular matrix of the cartilage (Poole *et al.*, 1992) as well as controlling the interactions within the chondron matrix. A similar role might occur in the porcine mitral valve annulus. Previous studies have shown that the collagen VI in myocardium is prevalent in the endomysium which distributes the loads and stresses from the muscle, these forces are then distributed to collagen III and then collagen I

(Bashey *et al.*, 1992). It is also thought to play a role in cardiac remodelling by enabling myofibroblast differentiation (Naugle *et al.*, 2006).

One major difference between species was the heavy calcification present in the human mitral valve. It was important to establish the extent of calcification in the annulus and determine whether this posed problems for decellularising the human mitral valve annulus. Calcification was visible in the human mitral valve during excision and the subsequent analysis showed that in some regions collagen II had formed. Calcium forms in the heart as people age (Carpentier *et al.*, 1996; Allison *et al.*, 2006), bone formation is also a feature in some diseased hearts, with heterotopic ossification occurring quite commonly in end stage valvular heart disease (Mohler *et al.*, 2001). This is thought to occur due to calcium formation in the process to repair damaged valves; as the calcium deposits fracture, ossification of the tissue is stimulated and bone formation can occur in the tissue. Mohler *et al.* (2001) found that of 347 aortic and mitral valves explanted from diseased human heart 83 % had calcium deposits and 13 % had evidence of bone formation. Calcification in the valves is a passive process which is part of the degeneration of connective tissues whilst ossification is more of an active process observed in abnormal tissue repair. Cartilage development has been reported in diseased mitral valve lesions, following a similar path to that of normal skeletal bone growth that forms from a cartilaginous phenotype that mineralises into calcified bone (Caira *et al.*, 2006). There are two possible pathways for calcification and ossification to occur in the diseased valves. Osteogenic cells derived from the bone marrow may enter the valves from the circulation to repair endothelial injury and cause heterotopic ossification (Egan *et al.*, 2011). Alternatively valve interstitial cells can differentiate into bone cells caused by abnormal biomechanical stress, reactive oxygen species, inflammation and disease (Rajamannan *et al.*, 2011). Calcium formation was confined in the posterior annulus in a study by Carpentier *et al.* (1996) which is in contrast to the data from the present study in which calcification was widespread and visible in both the anterior and posterior regions. A secondary limitation of using human heart tissue is its availability. In the UK there were 262 people on the heart transplant waiting list at the end of March 2015 but only 180 heart transplants during April 2014 to March 2015 (NHS Blood and Transplant, 2015). Donated human hearts can be used for heart transplantation or tissue can be harvested from the hearts to be used for homograft replacement or aortic valve and pulmonary valve replacements, where the tissue has been subjected to decellularisation treatment. If the decellularised annuloplasty

ring, using human tissue as the base material, was successfully taken to clinic the availability of human tissue would therefore also be a limiting factor in its use. Only when tissue is not suitable for clinical use is the heart tissue then used for research, which reduces the amount of tissue available. The close proximity of the aortic valve to the mitral valve means only one set of valves can be removed for research as the other valve will be damaged in the process, further reducing the number of mitral valves that can be utilised. Porcine tissue as an alternative is readily available and available at a low cost, which is a major advantage for this study.

3.5 Conclusion

One of the major aims of this part of the study was to determine whether human donor mitral valve annuli were suitable as a starting material for producing an acellular biological annulus for mitral valve annulus repair. The evidence of extensive calcification in the human donor mitral valves indicated that this was not a suitable way forward. Even if it was possible to decalcify the annuli prior to decellularisation processes, the evidence presented indicated that this would result in damaged tissue where the calcium deposits were present. The availability of the tissue is an additional limiting factor for human tissue use, which highlights the advantage that porcine tissue may have for this study.

Based on the comparison of the human and porcine mitral valve annuli it was considered that the porcine mitral valve annulus may be suited for development as an acellular biological annuloplasty ring. Whilst there were many similarities between species, there were some differences. The fibrosa of the human mitral valve was thicker, which may influence the biomechanical properties of the tissue and the trigones in the human annulus did not contain cartilage-like tissue, with a high GAG content, as found in the porcine trigones. The atrial side of the annulus in human tissue contained a larger proportion of adipose tissue compared to the porcine mitral valve which contained a larger proportion of atrial myocardium. The younger age of the porcine tissue and the older age of the human tissue may have contributed to some of the differences between species due to age related changes. The similarities between species included the anatomical size, posterior region and mitral-aortic continuum. Both species had a muscular posterior region, separated by a thin band of collagen formed from the fibrosa of the posterior leaflet, the anterior contained a

thicker band of collagen in the left and right trigones separated by the mitral to aortic continuum formed of a central core of dense fibrosa.

Due to the many similarities the porcine mitral valve annulus was found to share with the human mitral valve annulus the porcine annulus was used as the starting material for investigating decellularisation protocols developed at the University of Leeds, as the first step in creating an acellular biological annuloplasty ring device for mitral valve repair.

Chapter 4

Development of a decellularised porcine mitral valve annulus

4.1 Introduction

Protocols have been developed for the decellularisation of a range of tissues that have established that the natural structure of the ECM can be retained in order to provide a suitable environment for cellular adhesion and regeneration (Wilcox *et al.*, 2005; Mirsadraee *et al.*, 2006; Paniagua Gutierrez *et al.*, 2015). The mitral valve is inherently a complex structure, the leaflets are of different sizes, the chordae are numerous and have different mechanical characteristics (Ritchie *et al.*, 2005) and the annulus has heterogeneous properties (Walmsley, 1978, Angelini *et al.*, 1988; Berdajs *et al.*, 2007; McCarthy *et al.*, 2010). To date, attention has mainly centred on the development of tissue engineered chordae using directed collagen gel shrinkage (Shi & Vesely, 2004) and the use of pericardium for leaflet and annuloplasty repair, including autologous, glutaraldehyde treated human tissue (Chauvaud *et al.*, 1991; Muehrcke *et al.*, 1997; Ng *et al.*, 2001), glutaraldehyde treated bovine pericardium for closing perforations (Muehrcke *et al.*, 1997) and decellularised porcine tissue (Morticelli *et al.*, 2013). Recently a preliminary study has been undertaken for the decellularisation of the whole mitral valve complex in sheep (Iablonskii *et al.*, 2015). There have been no reports of research into annuloplasty repair using tissue engineered devices.

This study focuses on the decellularisation of the porcine mitral valve annulus with a view to clinical translation as an acellular biological annuloplasty ring replacement device. The porcine mitral valve has many similarities to the human mitral valve including anatomical dimensions and structure (Kunzelman *et al.*, 1994) albeit in the pig, the extent of the mitral to aortic continuity is reduced (Crick *et al.*, 1998). The major requirements of a successful decellularisation process for the porcine mitral valve annulus were that the ECM composition of tissue was retained and that the process had minimal effects on the biological, biochemical and biomechanical properties of the tissue whilst effectively removing the cells. It is hypothesised that if the acellular porcine annuloplasty ring was implanted into the heart, it would integrate into the surrounding tissue with cells penetrating the ring to provide remodelling and potential for repair.

Previous studies that have attempted to define an acellular tissue by quantifying the extent of decellularisation required to avoid adverse inflammatory reactions *in-vivo* whilst enabling constructive remodelling have led to the general acceptance of the following criteria:

- DNA content of less than 50 ng. mg⁻¹ dry weight (Crapo *et al.*, 2011).
- DNA fragment length of less than 180 base pairs for degradation in the lysosomes of macrophages (Nagata *et al.*, 2010).
- Nuclear material lacking in DAPI and H&E stained tissue sections (Crapo *et al.*, 2011).

The potential clinical use of decellularised porcine tissue may also carry the risk of disease transmission due to the presence of porcine endogenous retrovirus (PERV). It has been reported that the risk of transmission is removed if the DNA content post decellularisation is less than 2 % of native DNA per weight unit in porcine pulmonary artery scaffolds (Kallenbach *et al.*, 2004).

Decellularisation of tissues can be achieved using a range of chemical and mechanical processes. The majority of processes use a combination of methods to achieve successful decellularisation of tissue. Chemical processes include washing the tissue in non-ionic, ionic or zwitterionic detergents, enzymatic digestion using proteases and nucleases and washing using hypertonic and hypotonic buffers. Physical methods can include freeze thaw, sonification, agitation or direct pressure. The type and concentration of detergent used, process time, tissue type and age of the tissue are all factors that have been shown to be important considerations in the removal of cellular material, damage caused to the ECM (Cartmell & Dunn, 2000; Booth *et al.*, 2002; Schenke-Layland *et al.*, 2003; Woods & Gratzner, 2005; Gilbert *et al.*, 2006) and the remodelling response when implanted *in vivo* (Badylak, 2014). Previous studies have illustrated that successful decellularisation protocols hinge on many factors such as; the species from which the tissue is obtained, the age of the animal and the composition and density of the ECM. It will therefore be necessary to optimise the decellularisation protocol using chemical and physical methods for effective cell removal from the porcine mitral valve annulus.

4.1.1 Chemical methods used in tissue decellularisation

4.1.1.1 Biological agents

Nucleases are used to remove nuclear material from the tissues. Nucleases cleave the bonds of the subunits of DNA and RNA. DNase and RNase are endonucleases that cleave double and single stranded DNA and single stranded RNA but may cause an adverse immune reaction if they are from a bovine source (Gilbert *et al.*, 2006). Endonucleases, such as Benzonase have been reported to be more effective in removing DNA as they cause more efficient fragmentation of DNA material. Benzonase digests all nucleic acids into oligonucleotides of less than ten base pairs in length (Nestle & Roberts, 1969; Janning *et al.*, 1994) and rapidly hydrolyses DNA and RNA (Nestle & Roberts, 1969). Nucleases are used after the cell and nuclear membranes in tissues have been disrupted to ensure effective removal of nuclear material.

EDTA is a chelating agent, which is often incorporated into decellularisation processes. EDTA chelates calcium and magnesium ions which disrupts the cell-matrix interactions. By disrupting the attachment of cells to the ECM the level of cell removal can be improved (Klebe, 1974; Gailit & Ruoslahti, 1988).

Protease inhibitors such as aprotinin, phenylmethylsulfonyl fluoride and leupeptin have been used during decellularisation processes to prevent proteinases released from lysed cells degrading the proteins of the ECM. They have been reported to be useful in preventing damage to the ECM caused by proteases released by cells during the decellularisation process (Gilbert *et al.*, 2006).

The epitope α -gal is expressed widely on the cell surface glycoproteins and glycolipids of mammals except for humans, old world monkeys and apes. The presence of this epitope in implanted xenogeneic tissue causes hyperacute rejection and failure of the graft (Konakci *et al.*, 2005). Decellularisation processes may remove most of the α -gal epitopes but tissue can also be treated with α -galactosidase to reduce the content of the α -gal epitope within the decellularised tissue (Choi *et al.*, 2012).

4.1.1.2 Detergents

There are three types of detergent used for the decellularisation of tissue; non-ionic, ionic and zwitterionic. These operate by solubilising cell membranes and causing DNA dissociation from proteins (Crapo *et al.*, 2011). Detergents are often used near the start of the process to initiate the

disruption of the cell membranes but have been reported to cause ultrastructural damage to the ECM and growth factor removal (Booth *et al.*, 2002; Reing *et al.*, 2010).

Non-ionic detergents such as Triton X-100 disrupt lipid-lipid and lipid-protein interactions of the cells, caused by the uncharged hydrophilic head group on the detergents. Due to the disruption of the cell membranes, cell lysis is facilitated. The non-ionic detergents interact with the cell membrane and form micelles by penetrating between membrane bilayers when used at a suitable detergent concentration. They are advantageous for decellularisation due to their limited capacity for disrupting protein-protein interactions in the ECM. Non-ionic detergents, however have been reported to disrupt the basement membrane (Nakayama *et al.*, 2010), reduce GAG content (Vavken *et al.*, 2009) and change the ultrastructure of the tissue (Grauss *et al.*, 2005; Hyoungshin Park *et al.*, 2011) whilst complete decellularisation is not always achieved (Lumpkins *et al.*, 2008; Nakayama *et al.*, 2010).

Ionic detergents such as sodium dodecyl sulphate (SDS), sodium deoxycholate and Triton X-200 have hydrophobic head elements that solubilise and denature the membranes of the cells and nucleus. Such detergents have been shown to be successful in removing cell and nuclear elements from tissue but at certain concentrations have been found to remove essential ECM components such as collagen fibres, GAGs and growth factors (Gilbert *et al.*, 2006; Lumpkins *et al.*, 2008; Nakayama *et al.*, 2010; Stapleton *et al.*, 2008). Concentrations of SDS of 0.1% (w/v) facilitated the removal of cellular material without causing substantial damage to the ECM (Booth *et al.*, 2002). Concentrations of SDS of 1% (w/v) and higher have been found to change the biomechanical properties of tissues in some studies (Nakayama *et al.*, 2010) but have been reported to have no effect on the biomechanical properties of tissue in others (Lumpkins *et al.*, 2008).

Zwitterionic detergents, such as 3-[(3-cholamidopropyl)dimethylammonio]-1-propanesulfonate (CHAPS), combine the properties of non-ionic and ionic detergents, having both positive and negatively charged groups with an overall net charge of zero. Using CHAPS, Dahl *et al.* (2003) removed cells from the ECM of arteries but altered the biomechanical properties of the tissue.

It is important to include multiple wash cycles post detergent washes in the decellularisation process to remove any residual detergent. Detergents can be cytotoxic and prevent cells from integrating back into the ECM once

implanted (Booth *et al.*, 2002). This can be counteracted by introducing multiple wash cycles (Cebotari *et al.*, 2010).

4.1.1.3 Hypotonic/hypertonic buffers

Use of hypotonic and hypertonic buffers disrupts the osmotic balance of the cells. Exposure of cells to hypotonic solutions causes cell lysis by the movement of water into the cell and causes the cell to swell and burst. Hypertonic solutions help to dissociate DNA from proteins (Cox & Emili, 2006). These solutions are both commonly used during the decellularisation process and can be used to wash any cell debris out of the tissue.

4.1.1.4 Acids

Acids, such as peracetic acid (PAA), are often used at the end of the decellularisation process to disinfect the tissue whilst also aiding in the decellularisation process by removing nucleic acids. They play a role in decellularisation by helping to solubilise cellular components by hydrolytic degradation. Compared to gamma irradiation and ethylene oxide sterilisation methods, the use of PAA has been reported to give rise to improved cell attachment and increased matrix porosity without negatively affecting the mechanical properties of decellularised tissue (Woon *et al.*, 2011; Matuska & McFetridge, 2015).

4.1.2 Physical methods

Physical methods can be used to implement cell lysis and increase the permeability of tissue to allow chemical methods to work more effectively. Freeze thaw cycles can be used at the start of the decellularisation process to increase permeability of the ECM and cause cell lysis. Freeze/thaw cycles facilitate cell lysis and ECM permeability by the formation of ice crystals within the tissue and cells. Freeze/thaw cycles can have a negative effect on the ECM due to the ice crystal formation which may damage the matrix.

Another method that disrupts cells is sonification. Sonification generates ultrasound waves that cause disruption to the cell by cavitation. Bubbles form in the liquid which is subject to sonification which compress and decompress at high frequencies causing shock waves to the cell membrane, leading to cell lysis. Sonification has been used to create a more porous ECM in decellularised anterior cruciate ligament so that cells extrinsic to the tissue could migrate into the scaffold (Ingram *et al.*, 2007).

Abrasion is an alternative method that encourages the removal of cells by the application of direct force on the ECM but has been found to have a negative effect on the ECM (Hopkinson *et al.*, 2008).

4.2 Aims

The aim of this chapter was to optimise the decellularisation protocols developed by Booth *et al.* (2002) and Stapleton *et al.* (2008) for decellularisation of porcine aortic valves and menisci and adapt the approaches for porcine mitral annuli. The acellularity of the tissue during the development of the process was assessed, initially using histology and DNA content analysis. The process involved the optimisation of proprietary protocols previously developed at the University of Leeds using repeated cycles of low concentration SDS in the presence of proteinase inhibitors and hypotonic buffer.

4.3 Objectives

- To develop a decellularisation protocol to remove the cells and cell debris from the porcine mitral valve annulus without damaging the underlying the histioarchitecture
- Characterise the decellularised porcine mitral valve annulus and compare it to native porcine mitral annulus using the following techniques:
 - Histological characterisation looking at H&E, Sirius Red Millers and Alcian Blue staining and DAPI
 - Immunohistochemistry
 - DNA quantification

4.4 Methods

4.4.1 Decellularisation solutions

4.4.1.1 EDTA solution (10% w/v EDTA)

EDTA (10 g) was dissolved in 90 ml of distilled water with two sodium hydroxide pellets whilst being stirred and then the pH was adjusted to 8.0. The solution was topped up to 100 ml with distilled water and then autoclaved at 121°C. The solution was stored at room temperature for up to one month.

4.4.1.2 SDS solution (10%; w/v SDS)

Sodium dodecyl sulphate (10 g) was dissolved in 100 ml of distilled water using a magnetic stirrer. The solution was passed through a 0.2 µm filter into a sterile container in a class II safety cabinet and stored at room temperature for up to one month.

4.4.1.3 BSA solution (5 mg.ml⁻¹ BSA)

Bovine serum albumin (250 mg) was dissolved into 50 ml of distilled water using a magnetic stirrer. The solution was passed through a 0.2 µm filter into a sterile container in class II safety cabinet and used immediately or stored at -20°C for up to six months.

4.4.1.4 Magnesium Chloride (1M)

Magnesium chloride (2.03 g) was dissolved in 10 ml distilled water using a magnetic stirrer and then autoclaved at 121°C and stored at room temperature for up to one week.

4.4.1.5 Magnesium Chloride (10M)

Magnesium chloride (20.3 g) was dissolved in 10 ml distilled water using a magnetic stirrer and then autoclaved at 121°C and stored at room temperature for up to one week.

4.4.1.6 Hypertonic solution (50 mM tris, 1.5 M sodium chloride)

Sodium chloride (87.66 g) and 6.06 g of Tris was dissolved into 900 ml of distilled water and the pH was adjusted to 7.5 – 7.7. The volume was made up to 1000 ml using distilled water and autoclaved at 121°C and stored at room temperature for up to one week.

4.4.1.7 Hypotonic buffer (10 mM tris, 2.7 mM EDTA, 10 KIU.ml⁻¹ aprotinin)

Trizma base (1.21 g) and 1 g EDTA were dissolved into 450 ml of distilled water and the pH was adjusted to 8.0 – 8.2 using 6 M NaOH or 6 M HCL. The solution was made up to 1000 ml and autoclaved at 121 °C and stored at room temperature for up to one week. Prior to use 1 ml of aprotinin (10,000 KIU.ml⁻¹) was added aseptically.

4.4.1.8 SDS hypotonic buffer (0.1 %; w/v SDS, 2.7 mM EDTA, 10 KIU.ml⁻¹ aprotinin)

On the day of use, 5 ml of SDS solution was added to 495 ml of hypotonic buffer. Prior to use 0.5 ml of aprotinin (10,000 KIU.ml⁻¹) was added aseptically.

4.4.1.9 Nuclease solution 1 (50 mM Tris, 10 mM MgCl₂, 50 U.ml⁻¹ DNase, 1 U.ml⁻¹ RNase)

Trizma base (3.05 g) and 1.0 g of magnesium chloride were dissolved in 40 ml of distilled water and adjusted to pH 7.5 – 7.7 using 6 M NaOH or 6 M HCL. The solution was made up to 500 ml with distilled water and autoclaved at 121°C and stored at room temperature for up to one week. Ten minutes prior to use 1 ml of RNase stock (100U.ml⁻¹) and 0.5 ml DNase stock (10,000 U.ml⁻¹) were added aseptically.

4.4.1.10 Nuclease solution 2 (50 mM Tris, 10 mM MgCl₂ , 1 U.ml⁻¹ Benzonase)

Trizma base (6.1 g) and 2 g magnesium chloride were dissolved in 80 ml distilled water using a magnetic stirrer and stirrer bar. The pH was adjusted to 7.5 - 7.7 using 6 M NaOH or 6 M HCL. The volume was made up to 1000 ml with distilled water and autoclaved at 121 °C and stored at room temperature for up to one week. Prior to use 40 µl of Benzonase was added to 1000 ml of the buffer aseptically.

4.4.1.11 Nuclease solution 3 (50 mM Tris, 1 mM MgCl₂ , 10 U.ml⁻¹ Benzonase)

Trizma base (6.1 g) and 0.2 g magnesium chloride were dissolved in 80 ml distilled water using a magnetic stirrer and stirrer bar. The pH was adjusted to 7.5 - 7.7 using 6 M NaOH or 6 M HCL. The volume was made up to 1000 ml with distilled water and autoclaved at 121 °C and stored at room temperature for up to one week. Prior to use 400 µl of Benzonase was added to 1000 ml of the buffer aseptically.

Working solutions:

4.4.1.12 PBS

PBS was prepared in accordance with the protocol in Section 2.1.3.1 and stored at room temperature for up to one month.

4.4.1.13 PBS wash buffer with aprotinin (10 KIU.ml⁻¹ aprotinin)

Aprotinin (0.5ml, 10,000 KIU.ml⁻¹) was added aseptically to 499.5 ml of PBS and used within one hour of preparation.

4.4.1.14 Peracetic acid (PAA) solution (0.1 %; v/v)

PAA solution (1.57 ml) was added to 500 ml of autoclaved PBS aseptically and adjusted to pH 7.2 – 7.5 using 6 M NaOH or 6M HCL and used within one hour of preparation.

4.4.1.15 PBS wash buffer with EDTA, Aprotinin

EDTA (10%, 5ml) produced as described in Section 4.4.1.1 and 0.5 ml aprotinin (10,000 KIU.ml⁻¹) were aseptically added to 494.5 ml of PBS and used within one of preparation.

4.4.2. Decellularisation of the porcine mitral annulus

Several methods were tested for effectively removing cells and DNA from the porcine mitral valve annulus, as described below (Methods 1-8). For the application of each method, native porcine mitral annuli (n=3) were thawed from frozen storage at -20°C and each annulus initially placed into a 150 ml plastic pot after which 80 ml of solution was added and the pots were laid horizontally. Each wash was carried out at 240 rpm at 42 °C apart from the nuclease step which was carried out at 80 rpm at 37 °C and the post PAA (0.1 % w/v) washes which were carried out at 240 rpm at 4 °C. All wash solutions used were sterile as indicated above and pre-warmed to the correct temperature prior to use. All decellularisation methods were carried out aseptically with solution changes carried out in a class II safety cabinet.

4.4.2.1 Method 1 - 1 cycle SDS

Porcine mitral valve annuli were removed from porcine hearts and stored at -20°C on filter paper soaked in PBS until required, using the method described in Section 2.2.2.3. Each annulus was thawed for three hours at room temperature and placed into sterile 150 ml pots with 80 ml of hypotonic

Tris buffer (10 mM) at 42°C for 21 hours. The annuli were washed for a further 21 hours with SDS hypotonic buffer (0.1 % w/v SDS) at 42°C. Following this the annuli were washed thrice using PBS wash buffer with aprotinin for 30 minutes each at 42°C and then a further wash at 42°C for 66 hours. The annuli were then washed thrice using PBS wash buffer with aprotinin for 20 minutes each at 42°C and then a further wash for 24 hours. The annuli were washed in nuclease solution with magnesium chloride (10 mM) and Benzonase (1 U.ml⁻¹), twice for 2.5 hours at 37°C. They were then washed twice using PBS wash buffer for 20 minutes at 42°C and washed for a further 21 hours in PBS at 42°C. Following this the annuli were washed in hypertonic buffer for 21 hours at 42°C. The tissue was then washed twice in PBS for 15 minutes each at 42°C. The annuli were then disinfected using peracetic acid (0.1% v/v) solution for four hours at room temperature and washed three times using PBS for 30 minutes each at 42 °C and then washed for 66 hours at 42 °C. The annuli were stored in PBS without calcium and magnesium at 4°C for up to one week or used immediately for analysis as described in Section 4.4.3.

4.4.2.2 Method 2 – 2 cycles SDS

The process described in Method 1 was amended to include one extra cycle of hypotonic and SDS hypotonic buffer washes for 24 hours each, taking place directly after the first cycle.

4.4.2.3 Method 3 – 3 cycles SDS

The process in described in Method 1 was amended to include two extra cycles of hypotonic and SDS hypotonic buffer washes for 24 hours each, taking place directly after the first cycle.

4.4.2.4 Method 4 – RNase and DNase

The process described in Method 2 was altered by changing the Benzonase for RNase (1 U.ml⁻¹) and DNase (50 U.ml⁻¹) (Section 4.4.1.9) for the nuclease digestion step.

4.4.2.5 Method 5 - 2 cycles of SDS with freeze thaws

Extra steps of muscle removal were incorporated into the dissection process so that approximately 2-5 mm of muscle remained. The mitral annuli were thawed at 37°C for two hours and frozen at -20°C overnight, the tissue was then thawed at room temperature for three hours and then frozen at -20°C in hypotonic buffer overnight. The annuli were then subject to the process described in Method 2.

4.4.2.6 Method 6- Increased Benzoylase and reduced magnesium chloride concentration

Method 5 was used with the exception being that the Benzoylase concentration was increased to 10 U.ml⁻¹ and the magnesium chloride concentration was reduced to 1 mM. In addition, the decellularisation process was carried out in 250 ml pots with 150 ml of solutions throughout.

4.4.2.7 Method 7 - 6 x freeze thaw

Method 6 was applied following the addition of further cycles of freeze thaw. After the initial freeze thaw cycle the tissue was frozen at -20°C overnight, thawed at room temperature for three hours and then frozen at -20°C in hypotonic buffer overnight and thawed at room temperature, this was repeated for two more cycles. There were six freeze thaw cycles in total.

4.4.2.8 Method 8 - Multiple wash cycles

Method 6 was applied with the addition of further washes after the PAA step and 66 hour PBS wash. The annuli were washed thrice in PBS for 30 minutes each at 4 °C and washed for 24 hours in PBS, the tissue was washed thrice again in PBS at 4 °C for 30 minutes each and washed for 24 hours in PBS. Following this the annuli were subject to a final wash cycle of three PBS washes at 4 °C for 30 minutes each and one for 24 hours. The annuli were stored in PBS without calcium and magnesium at 4 °C and used for analysis as described in Section 4.4.3.

4.4.3 Determination of the effectiveness of the decellularisation methods (Methods 1-8)

In order to determine the effectiveness of each of the decellularisation protocols applied to the mitral annulus, following the application of each

method (Methods 1-8), porcine mitral valve annuli (n=3) were evaluated using histology to assess the extent of cell removal and any damage to the histoarchitecture. The total DNA content of the annuli (n=3) was also determined and compared to the total DNA content of native porcine mitral annuli to determine the extent of DNA removal.

The annuli were analysed in the two main regions, the anterior and posterior. For H&E and DAPI staining the two regions analysed were the left anterior trigone (Fig 4.1 S1) and posterior annulus (Fig 4.1 S2). For DNA quantification the annuli were split into the right anterior trigone (Fig 4.1 Adna) and the posterior annulus (Fig 4.1 Pdna) using the same tissue samples.

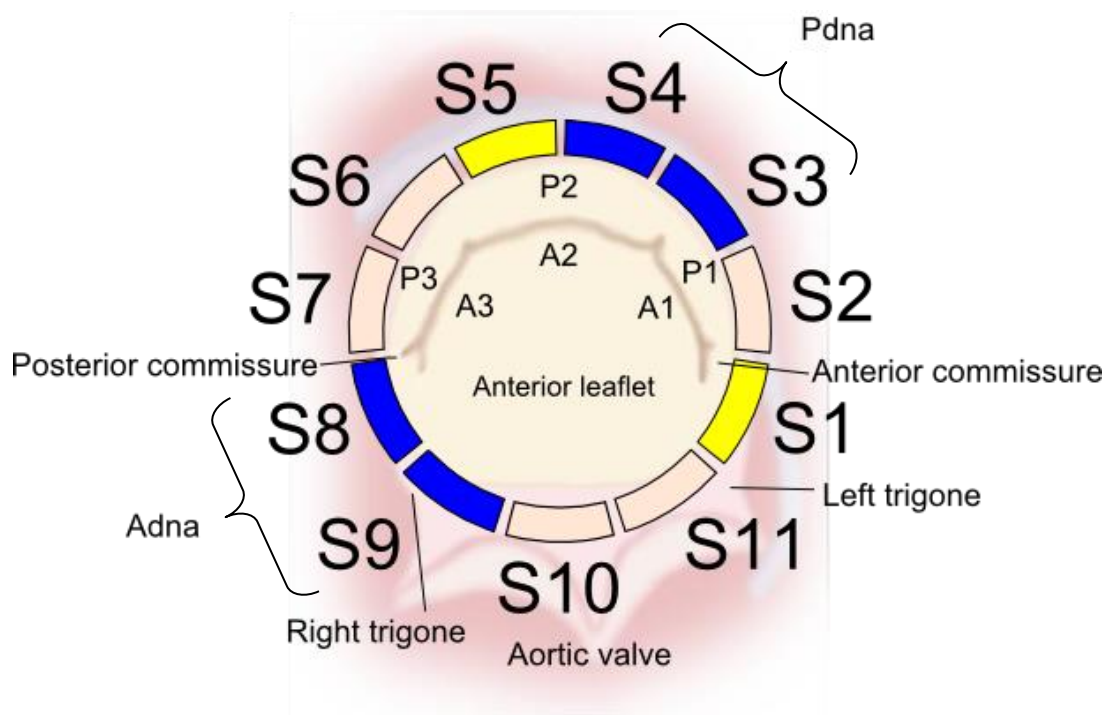


Fig 4.1 – Mitral valve annulus, following application of various decellularisation methods split into segments Regions selected for histological investigation of tissue sections using H&E, DAPI and DNA quantification. Histology: Anterior left trigone (S1. Yellow segment), Posterior right (S5. Yellow segment). DNA quantification: Posterior left (Pdna. S3-S4. Blue segment), Anterior right trigone (Adna. S8-S9. Blue segment).

4.4.3.1 Histological evaluation of the porcine mitral valve annuli following application of various decellularisation methods

The tissue specimens (n=3) were fixed in zinc for 24 hours and processed for standard histology as described in Section 2.2. Sections from the anterior

and posterior regions (Fig 4.1) were stained with H&E (Section 2.2.4.1) and DAPI (Section 2.2.4.4).

4.4.3.2 DNA quantification of the porcine mitral valve annuli following application of various decellularisation methods

Samples were processed for total DNA extraction by the DNeasy Blood & Tissue Kit (Qiagen, Texas, USA). Approximately 25 mg of native tissue (n=3) and 250 mg of processed tissue (n=3) was macerated and placed into sterile 2 ml microcentrifuge tubes. Proteinase K (20 µl) and 180 µl of Buffer ATL were added to each tube of fresh tissue and 40 µl of proteinase K and 360 µl of Buffer ATL was added to each tube of decellularised tissue. Samples were mixed by vortexing and incubated overnight at 56 °C in a water bath and vortexed to disperse the sample. Buffer AL (200 µl) and ethanol (200 µl) were mixed and added to the fresh samples and 400 µl of Buffer AL and 400 µl ethanol were mixed and added to the decellularised samples and then vortexed. From each sample, 600 µl was transferred to a DNeasy Mini spin column which was placed within a 2 ml collection tube and centrifuged at 6000 x g for one minute. The flow through was discarded and the process was repeated until no sample remained in the microcentrifuge tubes. The spin columns were placed into new 2 ml collection tubes and 500 µl of buffer AW1 was added to each sample and centrifuged at 6000 x g for one minute, discarding the flow through and collection tube. Each spin column was placed into a new collection tube and 500 µl of Buffer AW2 was added to each sample and centrifuged at 20000 x g for three minutes which dried the spin column membrane. The spin columns were placed into 2 ml microcentrifuge tubes and 200 µl of buffer AE was placed onto the spin column membrane and left to incubate at room temperature for one minute. The tubes were then centrifuged at 6000 x g for one minute to elute the substances from the membrane. The DNA samples were stored temporarily at 4°C and then quantified using a nanodrop spectrophotometer and checking for absorbance at 260 nm. Buffer AE was used as a blank.

4.5 Results

The extent of decellularisation for each method of decellularisation was examined by H&E for Method 1, H&E and DAPI for Methods 2-4 and H&E, DAPI and DNA quantification for Methods 5-8, with comparisons made to native porcine mitral valve annuli. The initial results of decellularisation using a single cycle of SDS followed by hypotonic SDS wash did not yield tissue void of cellular material. The protocol was altered in attempts to increase the removal of cells and nuclear material, as visualised in histological tissue sections stained with H&E. Once initial progress had been made subsequent tissues were analysed using DAPI stained histology sections for visual assessment of dsDNA remaining within the tissue. DNA quantification was then utilised once it was apparent that dsDNA was not visible with DAPI staining.

4.5.1 Method 1: One cycle of SDS

H&E stained sections of the tissue that had been subject to decellularisation Method 1 (Fig 4.2a; a, b) revealed the presence of cells and nuclear material in both the annulus and surrounding muscular tissue in all regions. Cells within the posterior region were elongated and had the appearance of fibroblasts elongated in the direction of collagen fibres. Cardiomyocytes were present in tissue surrounding the annulus with cell nuclei clearly visible. Cells appeared to be absent in the loose connective tissue bordering the myocardium. The general structure of the tissue was well maintained with no obvious signs of damage. No further analysis of the tissue was undertaken due to the failure to remove cellular material with this protocol.

4.5.2 Method 2: Two cycles of SDS

Following the addition of an extra cycle of hypotonic SDS washes the content of cellular material present had visibly reduced in the H&E stained tissue sections. Cellular material was present within the lacunae of the trigonal region (Fig 4.2a; c) which had the appearance of chondrocytes. H&E stained sections showed purple haematoxylin staining of the chondrocyte-like nuclear membrane with pink eosin staining within the nucleus, the cytoplasm appeared to have been removed. In the posterior region decellularisation appeared to be successful with no visible cell nuclei (Fig 4.2a; d) or fibroblasts. Observations of DAPI stained tissue sections revealed remnants of dsDNA, predominantly in the anterior annulus in the trigones (Fig 4.3 a).

4.5.3 Method 3: Three cycles of SDS

Following the addition of an extra two cycles of SDS washes to the decellularisation process the content of cellular material present within the tissue had reduced in H&E stained tissue sections compared Method 1. There was no visible difference in the results obtained using two SDS wash cycles (Fig 4.2b; e, f) compared to three SDS wash cycles. Interrogation of DAPI stained sections revealed staining for nuclear material in the anterior region in the trigones (Fig 4.3 b).

4.5.4 Method 4: RNase and DNase

Benzonase was replaced by RNase and DNase to establish if DNase was more effective at cleaving nuclear material from the lacunae present in the trigonal region. In H&E stained sections, cell nuclei were visible in both the anterior region (Fig 4.2b; g) within the lacunae and in the posterior region (Fig 4.2b; h) with the presence of fibroblast nuclei. Observations of DAPI stained sections showed an apparent lack of dsDNA in the tissues (Fig 4.3 c). Benzonase was retained for the nuclease step due to DNase and RNase offering no improvement in the removal of cellular material compared to the Benzonase. In H&E stained sections for the RNase and DNase treated tissue there was some nuclei visible in the posterior region which were absent with the Benzonase treated H&E stained sections.

4.5.5 Method 5: Two freeze thaw cycles

An extra freeze thaw cycle was added to the start of the decellularisation process in an attempt to open up the tissue structure and allow better diffusion of decellularisation solutions. Freeze thaw cycles might also increase damage inflicted on the cells prior to chemical decellularisation. Damage to the ECM ultrastructure was shown to be minimal in H&E stained tissue sections (Fig 4.2b; i, j) but nuclear debris remained within lacunae (Fig 4.2b; i). There was no visible positive staining with DAPI in tissue sections (Fig 4.3 d). DNA quantification revealed that there was $5.7 \pm 2.21 \text{ ng.mg}^{-1}$ of DNA per wet weight of tissue remaining in the anterior region, representing 94.6% removal of DNA compared to native tissue with $105.32 \pm 1.88 \text{ ng.mg}^{-1}$ of DNA per wet weight of tissue ($p < 0.05$) and $4.46 \pm 2.85 \text{ ng.mg}^{-1}$ per wet weight of tissue remaining in the posterior region equating to 97.5% removal of DNA compared to native tissue with $179.07 \pm 10.922 \text{ ng.mg}^{-1}$ of DNA per wet weight of tissue ($p < 0.05$) (Fig 4.4).

4.5.6 Method 6: Increased Benzonase and reduced magnesium chloride concentration

Method 5 was altered by changing the nuclease and magnesium concentrations in the nuclease treatment step in order to optimise the performance of the Benzonase enzyme and increasing the wash volumes to remove potentially toxic SDS remnants and enhance removal of cellular material. There were no visible nuclei in H&E stained sections of the posterior region (Fig 4.2c; l) but the lacunae in the anterior region (Fig 4.2c; k) had cellular debris remaining. There was no visible damage to the tissue structure and observations of DAPI stained sections showed no positive staining for dsDNA (Fig 4.3 e). DNA quantification revealed 1.05 ± 1.06 ng.mg⁻¹ of DNA remaining per wet weight of tissue in the anterior region, representing 99.14% removal of DNA with 122.42 ± 54.39 ng.mg⁻¹ of DNA per wet weight of tissue ($p < 0.05$) and 3.79 ± 1.2 ng.mg⁻¹ per wet weight of tissue remaining in the posterior region equating to 98.99% removal of DNA ($p < 0.05$) compared to native tissue with 374.21 ± 183.43 ng.mg⁻¹ of DNA per wet weight of tissue (Fig 4.4).

4.5.7 Method 7: Multiple freeze thaw cycles

Multiple freeze thaw cycles were added to the start of the decellularisation process. Multiple freeze thaw cycles might increase cell lysis and disrupt the ECM enabling solutions to diffuse into the tissue with greater effectiveness. Observations of H&E stained tissue sections revealed the presence of apparent cell debris remaining the lacunae of the anterior region of the annulus (Fig 4.2c; m). The morphology of the tissue appeared damaged compared to native tissue and all previous decellularisation methods. The muscular region (Fig 4.2c; n) and lacunae were visibly dilated with holes in the structure. Observations of DAPI stained sections of the processed tissue revealed the presence of dsDNA in the trigonal region where the lacunae resided (Fig 4.3 f). DNA quantification revealed 1.75 ± 1.46 ng.mg⁻¹ of DNA remaining in the anterior region per wet weight of tissue, representing 98.57% ($p < 0.05$) removal of DNA with 122.42 ± 54.39 ng.mg⁻¹ of DNA per wet weight of tissue and 3.18 ± 1.25 ng.mg⁻¹ per wet weight of tissue remaining in the posterior region equating to a 99.15 % removal of DNA ($p < 0.05$) compared to native tissue with 374.21 ± 183.43 ng.mg⁻¹ of DNA per wet weight of tissue (Fig 4.4).

4.5.8 Method 8: Multiple wash cycles post PAA sterilisation

In Method 8 multiple wash cycles were added to the process described as Method 6, after the PAA sterilisation step. Examination of H&E stained tissue samples revealed the tissue to be predominantly free of cellular material with improved removal of cellular debris from the lacunae region (Fig 4.2c; o) and no visible cells remaining in the posterior region (Fig 4.2c; p). Evaluation of DAPI stained sections did not reveal the presence of ds DNA (Fig 4.3 g). DNA quantification revealed 2.56 ± 0.73 ng.mg⁻¹ of DNA remaining per wet weight of tissue in the anterior region, 97.83 % removal of DNA with 155.76 ± 61.63 ng.mg⁻¹ of DNA per wet weight of tissue ($p < 0.05$) and 2.92 ± 2.11 ng.mg⁻¹ per wet weight of tissue remaining in the posterior region equating to a 99.07 % removal of DNA compared to the native tissue with 304.44 ± 164.72 ng.mg⁻¹ of DNA per wet weight of tissue ($p < 0.05$) (Fig 4.4).

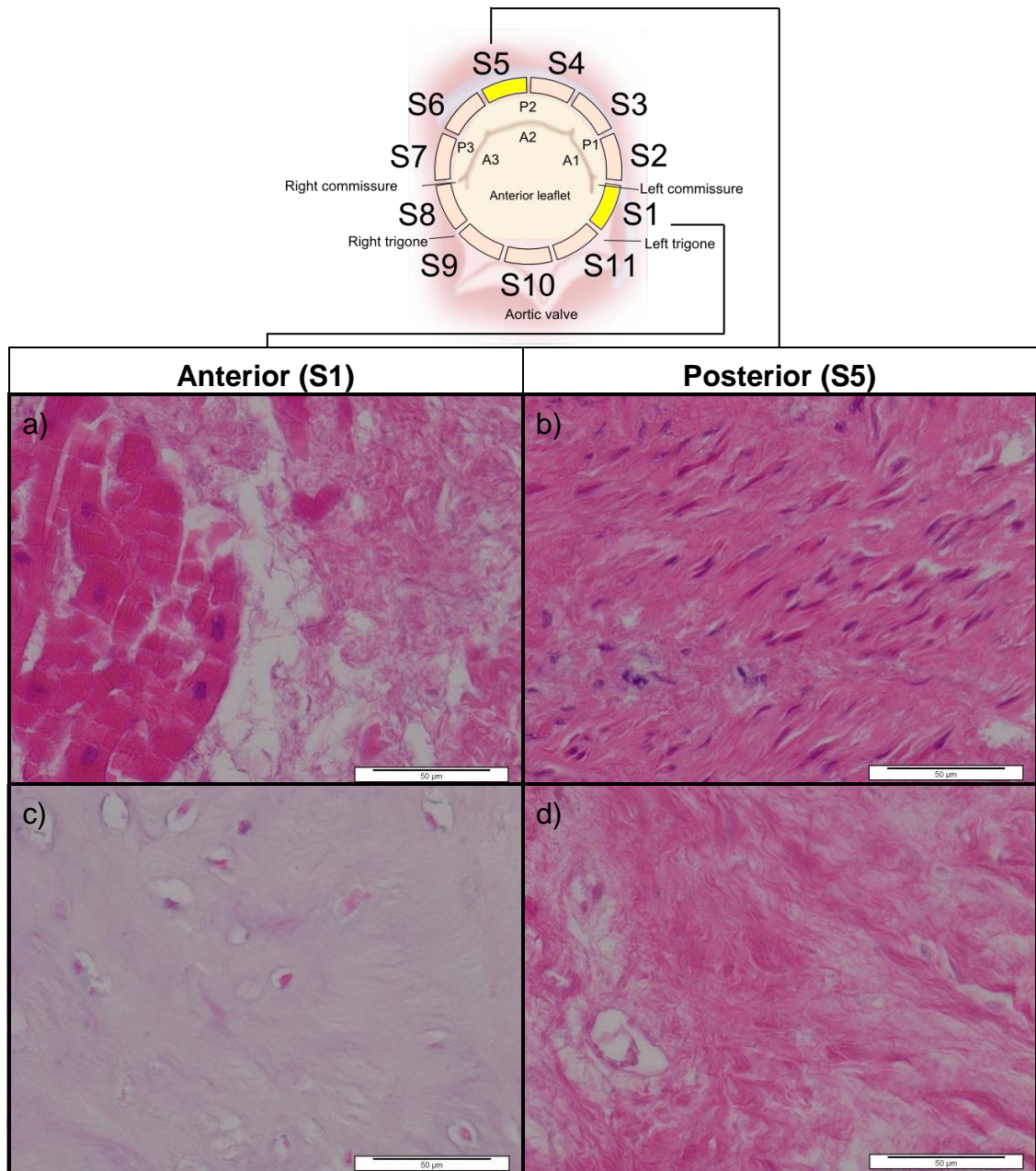


Fig 4.2a – Images of H&E stained sections from anterior and posterior segments of the porcine mitral valve annulus decellularised using different methods. Method 1 - Images of H&E stained sections of decellularised porcine mitral annulus using one cycle of SDS. Anterior region of annulus (a), Posterior part of the annulus (b). Method 2 - Two cycles of SDS. Anterior region of annulus (c), Posterior part of the annulus (d). Magnification x 200 unless stated otherwise. Images are representative of the results obtained from n = 3 annuli.

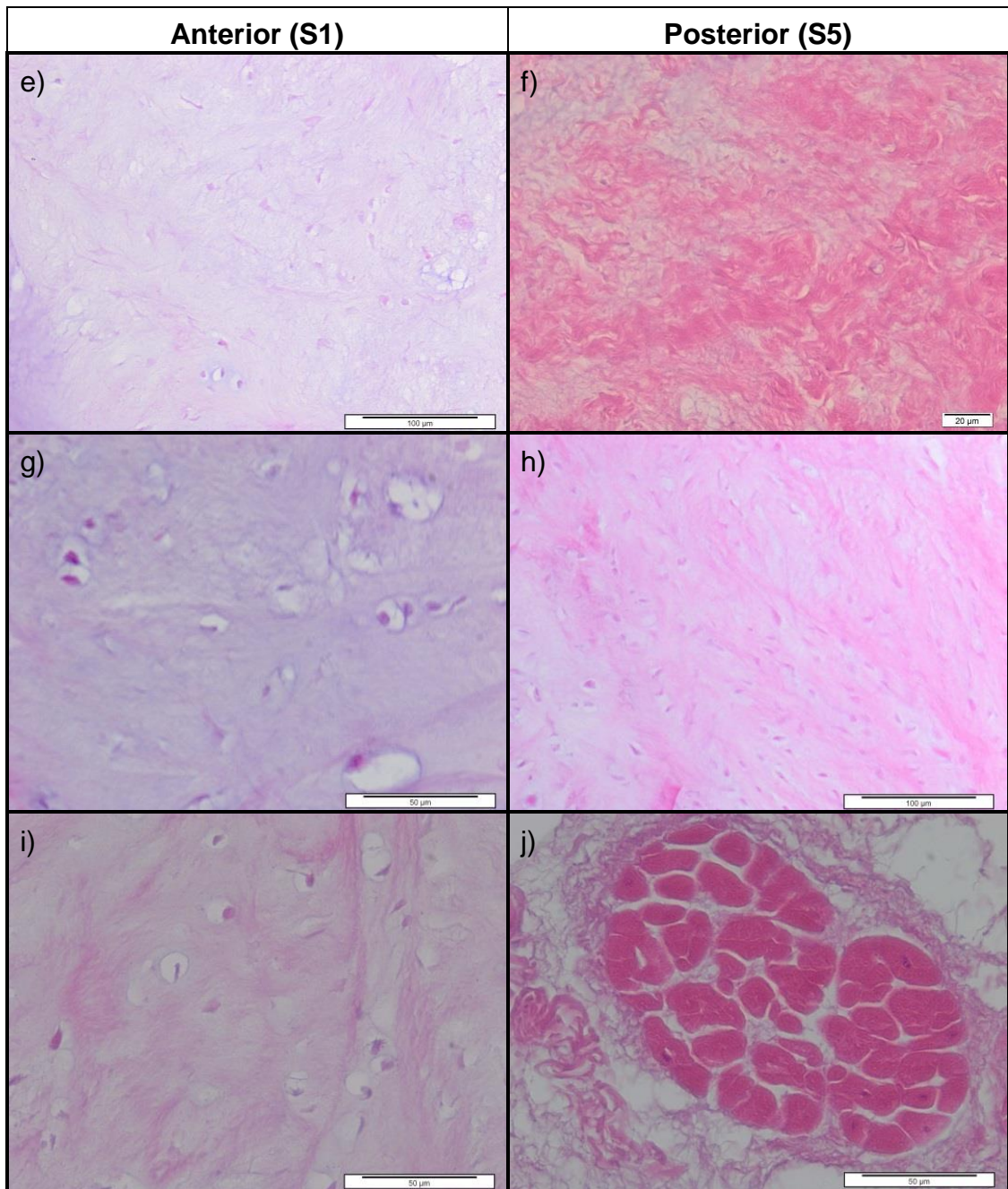


Fig 4.2b – Images of H&E stained sections from anterior and posterior segments of the porcine mitral valve annulus decellularised using different methods. Method 3 - Three cycles of SDS. Anterior region of annulus magnification x 100 (e), Posterior part of the annulus magnification x 400 (f). Method 4 - RNase and DNase. Anterior region of annulus (g), Posterior part of the annulus magnification x 100 (h). Method 5 -Two freeze thaw cycles and increased muscle removal. Anterior region of annulus (i), Posterior part of the annulus (j). Magnification x 200 unless stated otherwise. Images are representative of the results obtained from n = 3 annuli.

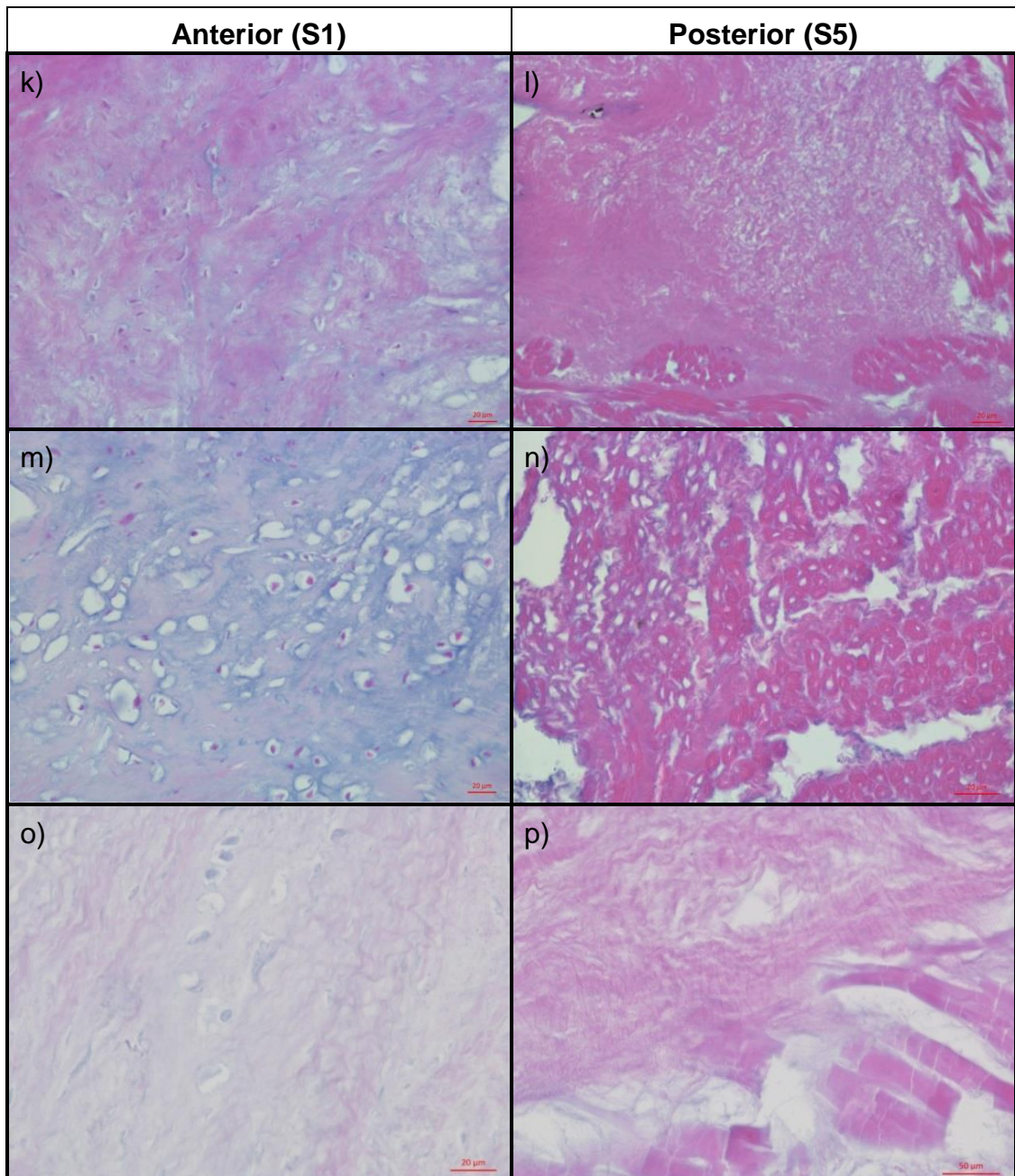


Fig 4.2c – Images of H&E stained sections from anterior and posterior segments of the porcine mitral valve annulus decellularised using different methods. Method 6 - Optimised nuclease concentration. Anterior region of annulus magnification x 400 (k), Posterior part of the annulus magnification x 400 (l). Method 7 - Six times freeze thaw cycles. Anterior region of annulus magnification x 400 (m), Posterior part of the annulus magnification x 400 (n). Method 8 - Final wash with multiple post PAA washes. Anterior region of annulus magnification x 400 (o), Posterior part of the annulus (p). Magnification x 200 unless stated otherwise. Images are representative of the results obtained from n = 3 annuli.

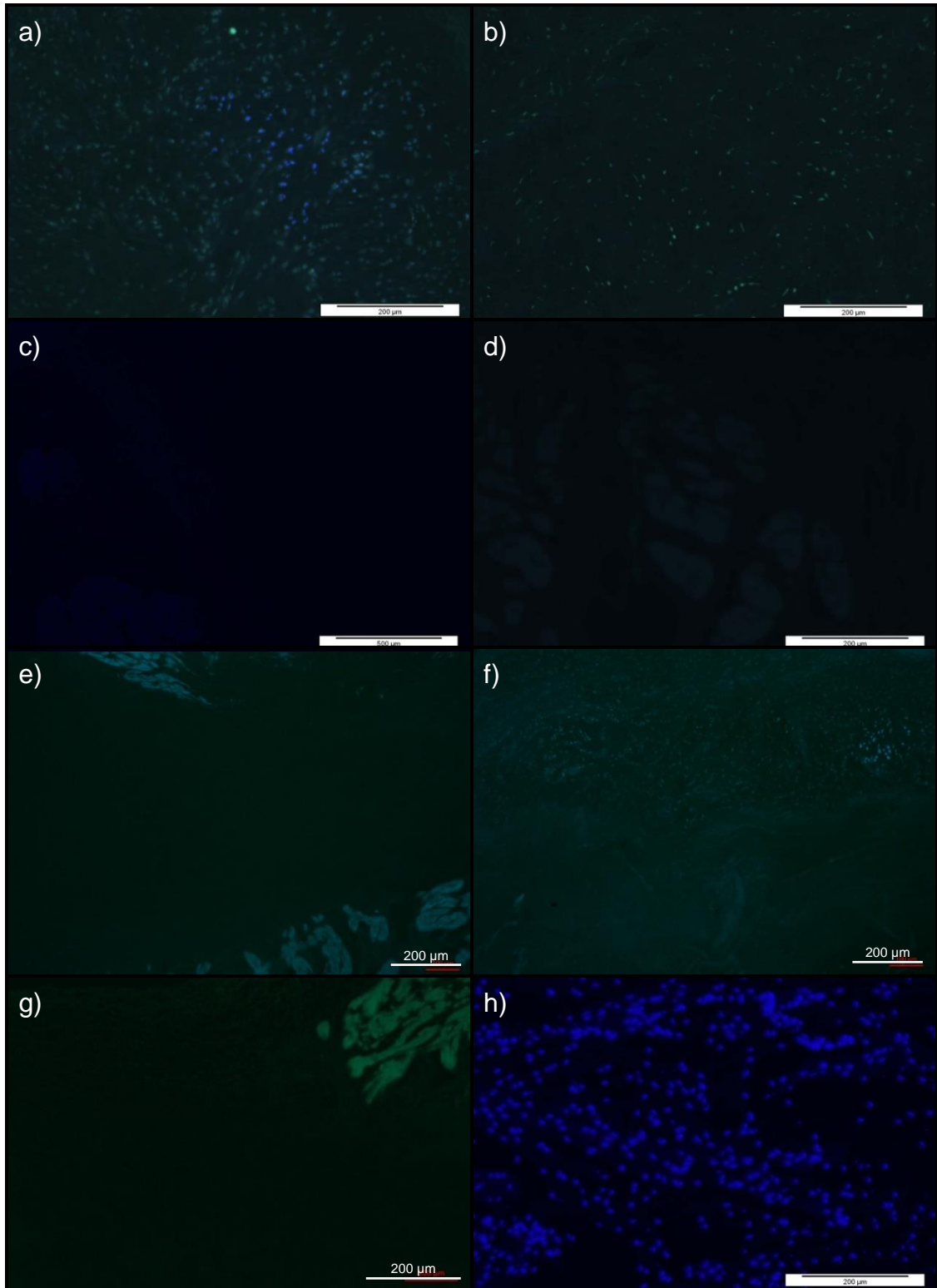


Fig 4.3 – Images of DAPI stained sections from segments of the porcine mitral valve annulus decellularised using alternative methods. Images of DAPI stained sections of decellularised porcine mitral valve annulus. Method 2 - Two cycles of SDS (a). Method 3 - Three cycles of SDS (b). Method 4 - RNase and DNase magnification x 20 (c). Method 5 - Two freeze thaw cycles and increased muscle removal (d). Method 6 - Optimised nuclease concentration (e). Method 7 - Six times freeze thaw cycles (f). Method 8 - Final wash with multiple post PAA washes (g). Fresh native control tissue (h). Magnification x50 unless stated otherwise. Images are representative of the results obtained from n = 3 annuli.

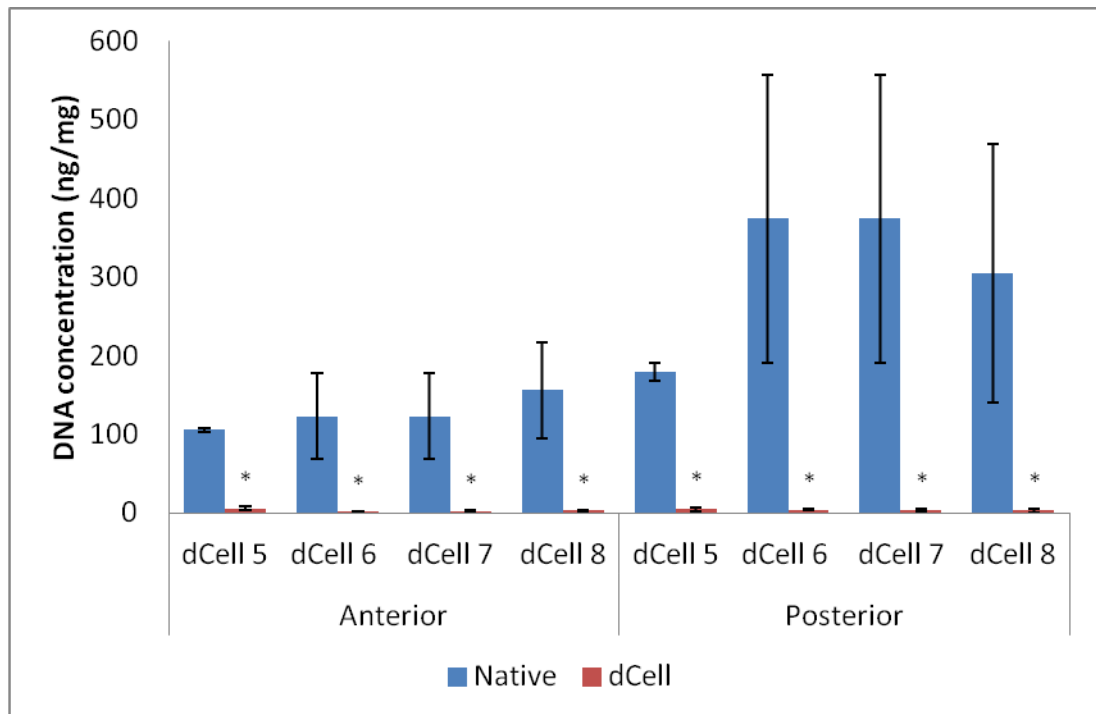


Fig 4.4 – DNA content of native and decellularised mitral valve annulus decellularised using Methods 5 to 8. Data is presented as the mean (n=3) \pm 95% C.I and was analysed by unpaired student's t-test (native vs dCELL for each method) that showed significant differences between all native and dCELL groups ($p < 0.05^*$).

4.6 Discussion

The aim of the research presented in this chapter was to develop a decellularisation method to remove the cell nuclei and cellular debris from the porcine mitral annulus, leaving only the ECM scaffold of the tissue and create a material free from the major immunogenic components. Extracellular matrix proteins that are conserved across higher mammalian species, such as collagens should not invoke an immune response in man since they would not be recognised as foreign. This initial protocol was based upon work previously completed by Booth *et al.* (2002) and Stapleton *et al.* (2008) for decellularisation of porcine aortic valves and menisci. Low concentrations of SDS were used to avoid possibly toxic levels that would prevent cell integration when used in vivo. Concentrations of SDS, when used in decellularisation protocols, of 1 % and above have been found to result in tissues which are toxic to cells and damage the collagen in the ECM (Booth *et al.*, 2002). The protease inhibitor aprotinin was included in the early stages of the decellularisation procedure to prevent breakdown of the ECM caused by release of proteases by the cells when being lysed.

The initial process using one cycle of SDS with hypotonic buffer was performed to establish if cells could be removed with minimal processing and damage to the ECM. Histological analysis of processed tissue revealed that the extent of cell removal when compared to native porcine mitral valve annuli was negligible, with visible cell nuclei remaining in both the annulus and muscle surrounding it. Increasing the number of SDS and hypotonic buffer cycles during tissue processing had a notable effect on cell removal with a decrease in visible cell nuclei in the annulus and myocardium although cell debris was still visible in the trigones whilst retaining the overall tissue structure. The use of two and three cycles of SDS washes in the decellularisation process were compared to ascertain the optimal number of cycles for cell removal. Histological evaluation of processed tissues revealed similar results using both methods with residual material present in the trigones and some evidence of cell nuclei in the myocardium. Further analysis was undertaken of DAPI stained tissue sections to visualise any remaining dsDNA in the decellularised tissue which showed no difference between methods. The lack of complete decellularisation suggested that increasing the number of SDS wash cycles alone was insufficient for complete removal of cellular material. Increased numbers of SDS washes also had the potential to increase damage to the ECM and cause cytotoxicity (Booth *et al.*, 2002; Elder *et al.*, 2009; Gilbert *et al.*, 2006; Hudson *et al.*; Lumpkins *et al.*, 2008; Nakayama *et al.*, 2010) so it was decided to use two cycles of SDS to reduce any potentially damaging effects it may cause.

The protocol was adjusted to use RNase and DNase in place of Benzonase in the nuclease digestion step to elucidate if the removal of cellular material could be improved. No improvement was seen between the use of Benzonase and RNase and DNase. The protocol was improved by increasing the number of freeze thaw cycles from one cycle to two cycles in hypotonic buffer. These freeze thaw cycles were used to increase the permeability of the tissue by the formation of ice crystals to dilate the tissue and damage cell membranes (Crapo *et al.*, 2011). Adding further freeze thaw cycles to the decellularisation process revealed that this resulted in damage the underlying structure of the tissue and hence this approach was abandoned. Moreover, it was clear that the addition of further freeze thaw cycles showed no improvement in the removal of nuclear material from the lacunae hence other approaches were required. It was hypothesised that residual SDS remaining in the tissue following the SDS washes may have been inhibitory to the action of the nuclease in the nuclease digestion step. SDS may denature enzymes such as Benzonase. The concentration of

Benzonase was increased to 10 U.ml^{-1} to compensate for any residual SDS. The concentration of the magnesium chloride in the nuclease digestion buffer was also changed from 10 to 1 mM. The magnesium chloride acts as a cofactor for nuclease enzymes but this is concentration dependent. The initial concentration of 10 mM magnesium chloride, whilst optimal for DNase activity was found to be above the recommended concentration for Benzonase (EMD Millipore Corporation, 2013), the concentration of magnesium chloride was reduced to 1mM to account for this. Histological analysis revealed that the cells were removed from the tissue in all regions although two regions appeared to contain residual cell debris; the myocardium and the cartilaginous region in the anterior part of the porcine mitral valve annulus. When the same regions were observed in DAPI stained sections there was no evidence of any positive staining for dsDNA. Moreover, the total DNA content of the processed tissue was below 3 ng.mg^{-1} of tissue, significantly lower than the 50 ng.mg^{-1} suggested (Crapo *et al.*, 2011). The content of DNA remaining in the tissue is important because the any remaining nuclear material can cause calcification (Spina *et al.*, 2003). Increased washes of PBS following the PAA cycles were carried out to improve the removal of cellular material and remove any potentially toxic solutions. Cell debris still remained within the lacunae even with multiple washes. It has been hypothesised that the cell remnants that appear in the anterior region could be ghost nuclei (Keller & Riley, 1976), these are the structural scaffold components of the nuclei without the presence of DNA. Further analysis of the changes to the histioarchitecture, cytotoxicity in the scaffold and changes to the biomechanical properties of the porcine mitral valve annulus, using the final decellularisation protocol, are investigated in the following chapter.

Chapter 5

Characterisation of the decellularised porcine mitral valve annulus

5.1 Introduction

In Chapter 4, a protocol for the decellularisation of the porcine mitral valve annulus was developed with a view to the future production of a biological acellular annuloplasty ring. The aims of the work described in this chapter, were to characterise further the acellular tissue using immunohistochemistry to detect key extracellular matrix proteins, biochemical assays to determine the extracellular matrix composition and biomechanical testing to determine whether the decellularisation process had any major effects on the biomechanical properties of the tissue compared to native porcine mitral valve annuli.

The extra cellular matrix (ECM) of a tissue is comprised of molecules that have been secreted by cells that reside in the tissue. These molecules form a large number of components which have a range of regulatory and structural functions. The components of the ECM can be categorised into three main classes: structural proteins such as collagen and elastin fibers, proteoglycans and specialist glycoproteins such as fibronectin and laminin. The molecules that assemble in the ECM are arranged in a 3D structure appropriate to the function of the tissue (Badylak *et al.*, 2009). The phenotype of a cell and the functions required of the tissues influence the composition and structure of the ECM (Badylak *et al.*, 2009). The process of decellularisation has been shown to deplete some structural components of the ECM. Studies in which 0.1 % (w/v) SDS and peracetic acid (PAA) have been used for effective tissue decellularisation have found depletion of components of the basement membrane, including fibronectin and collagen IV from porcine pulmonary valves (Luo *et al.*, 2014) and collagen IV and laminin from porcine bladder scaffold (Bolland *et al.*, 2007) with PAA being attributed to the loss of collagen IV from the matrix (Luo *et al.*, 2014). In the majority of studies that have used 0.1 % (w/v) SDS in the tissue decellularisation process, GAG content has been shown to be reduced in the decellularised scaffold compared to the fresh tissue, including in porcine pericardium (Morticelli *et al.*, 2013), porcine bladder (Bolland *et al.*, 2007), porcine medial meniscus (Stapleton *et al.*, 2008) and porcine pulmonary

valves (Luo *et al.*, 2014), the exception being in human pericardium (Mirsadraee *et al.*, 2006). Therefore, in this study it was important to determine whether the developed decellularisation process had any effects on the structural protein, glycoprotein and GAG content of the porcine mitral valve annulus.

Alpha-gal is an epitope found on cell membrane glycoproteins and glycolipids of all mammals excluding humans, apes and old world primates. The epitope is the major xenoantigen that causes hyperacute rejection in humans (Konakci *et al.*, 2005). Humans produce anti-gal antibody which interacts with the α -gal epitope present in xenografts. Up to 1 % of IgG antibodies and up to 8 % of IgM antibodies in humans can interact with this epitope (McMorrow *et al.*, 1997; Galili, 2001), the presence of the α -gal epitope in vascularised porcine tissue causes hyperacute rejection when implanted into humans (Kim *et al.*, 2007). In porcine tissue high amounts of α -gal are expressed on the surface of endothelial cells which promotes hyperacute rejection of vascularised organs (Sandrin & McKenzie, 1994). Other antigens may also lead to hyperacute rejection, including Hanganutziu–Deicher and Forssman antigens (Cooper, 1998). It was therefore important to determine if decellularisation of the porcine mitral valve annulus resulted in removal of the α -gal epitope from the scaffold.

The decellularisation process also uses chemicals that are potentially cytotoxic, in particular SDS (Sakai *et al.*, 1998; Caamaño *et al.*, 2009) and EDTA (Ballal *et al.*, 2009; Marins *et al.*, 2012), residual SDS or EDTA could prevent cells from attaching to and regenerating the decellularised scaffold both *in vitro* and *in vivo*. It was therefore important to assess the biocompatibility of the acellular porcine mitral valve annulus using contact and extract cytotoxicity assays.

Perhaps of most importance for any future consideration of the use of the acellular porcine mitral valve annulus in the clinic, it was important to determine any effects of the decellularisation process on the biomechanical properties of the scaffold. It has been shown in previous studies of cardiovascular tissue that treatment using 0.1 % (w/v) SDS can alter the biomechanical properties. Significant decreases in the elastin phase slope, increased transition stress (Korossis *et al.*, 2005; Luo *et al.*, 2014) along with increased extensibility (Korossis *et al.*, 2002; Mirsadraee *et al.*, 2006) and greater transition stress and strains (Morticelli *et al.*, 2013) were all found when compared to fresh tissue.

Few studies have investigated the biomechanical properties of the porcine mitral valve annulus. Biomechanical testing using uniaxial tensile testing was completed on native porcine mitral valve annuli by Gunning & Murphy (2014). The native porcine mitral valve annulus was split into regions, the anterior, left commissural, posterior and right commissural sections. The anterior region, defined as the mitral to aortic continuum situated between the trigones, was shown to have a significantly higher ($p < 0.05$) Young's modulus compared to the other regions of the porcine mitral valve annulus.

5.2 Aims

The aim of this chapter was to characterise the porcine mitral valve annulus that had been decellularised using Method 8 (Section 4.4.2.8) as outlined in Chapter 4.

5.3 Objectives

To characterise the decellularised porcine mitral valve annulus tissue using histological, immunohistochemical and biomechanical techniques and carry out a comparison with native tissue:

- To compare the GAG content of native and decellularised porcine mitral valve annulus tissue using histology with alcian blue staining
- To compare the orientation and localisation of collagen and elastin fibres of native and decellularised porcine mitral valve annulus using histology with Sirius red Miller's staining
- To compare the distribution of collagen I, II, III, IV, VI, and fibronectin, laminin and the α -gal epitope in sections of the native and decellularised porcine mitral valve annulus using immunohistochemistry.
- To determine the biocompatibility of the decellularised porcine mitral valve tissue using extract and contact cytotoxicity assays.
- Compare the quantitative biomechanical properties of the native and decellularised porcine mitral valve annulus using uniaxial tensile testing.

5.4 Methods

The decellularisation process (Method 8; developed in Chapter 4) used to prepare the acellular porcine mitral valve annulus for the analyses described below is summarised in Fig 5.1

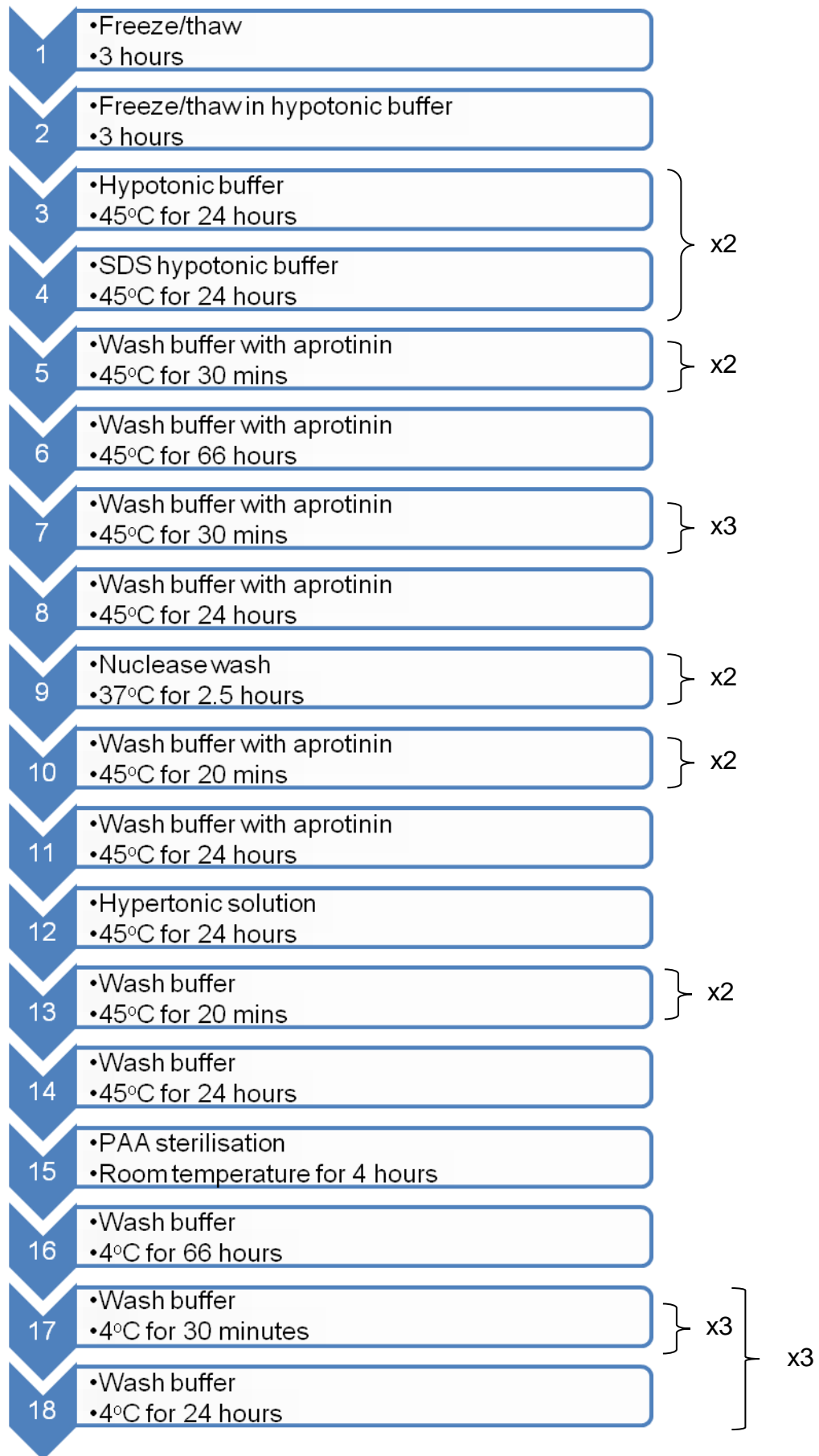


Fig 5.1 – Porcine mitral valve annulus decellularisation protocol

5.4.1 Analysis of the final decellularisation method (Method 8)

In order to determine the biological and biomechanical characteristics of the acellular porcine mitral valve annuli and to compare with the characteristics of native tissue, the annuli were evaluated using histology (n=3) and immunohistochemistry (n=3). This analysis was used to determine the extent of cell removal and any changes to the histoarchitecture of the tissue, including distribution of collagens, fibronectin and laminin. The biocompatibility of the decellularised porcine mitral annulus scaffold was evaluated using contact (n=3) and extract (n=3) cytotoxicity assays. The biomechanical characteristics of the annuli (n=12) were established by uniaxial tensile testing and compared to the biomechanical characteristics of the native mitral valve annuli (n=12) to determine if decellularisation caused any alterations in the mechanical properties of the tissue.

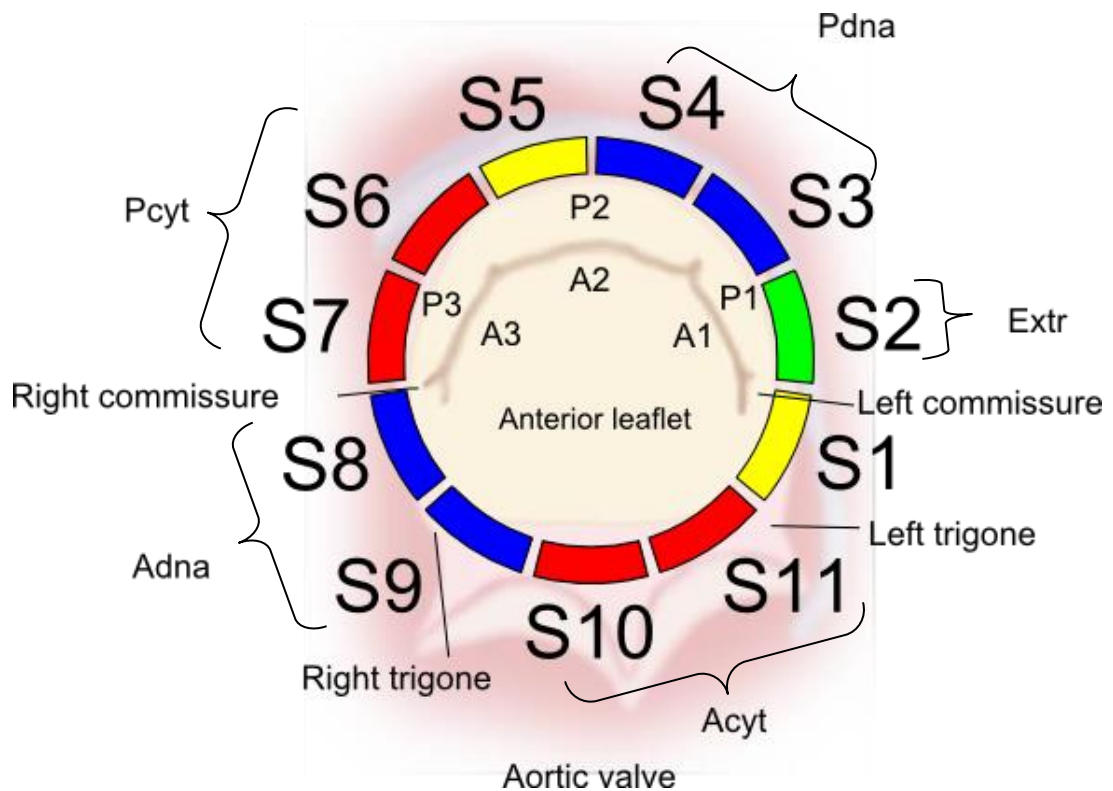


Fig 5.2 – Decellularised mitral valve annulus split into segments

Regions selected for histochemical investigation of tissue sections using Sirius red Miller's, alcian blue, immunohistochemistry, contact and extract cytotoxicity assays. Histology: Anterior left trigone (S1. Yellow), Posterior (S5. Yellow). DNA quantification: (Completed in Chapter 4) Anterior right trigone (Adna. Blue), Posterior (Pdna. Blue). Contact cytotoxicity assay: Anterior (Acyt. Red), Posterior right (Pcyt. Red). Extract cytotoxicity assay: Left commissure (Extr. Green).

The annuli were analysed in the two main regions, the anterior and posterior. For alcian blue and Sirius red Miller's staining and immunohistochemistry the

regions analysed were the anterior left trigone (Fig 5.2, S1) and the posterior annulus (Fig 5.2, S5). For the contact cytotoxicity assays the annuli were split into the anterior (Fig 5.2, Acyt S10-S11) and the posterior right annulus (Fig 5.2, Pcyt S6-S7) using the same tissue samples. For the extract cytotoxicity assays the annuli segment S2 was used (Fig 5.2, Extr S2). Separate annuli were used for biomechanical analysis and split four into regions using the protocol described in Chapter 2; Section 2.2.6.1.

5.4.2 Histological evaluation of the human and porcine mitral valve annulus

Tissue specimens (n = 3) were fixed in zinc for 24 hours and processed for standard histological treatment as described in Section 2.2. Sections from the anterior and posterior regions (Fig 5.2) were stained with Sirius red Miller's (Section 2.2.4.2) and alcian blue (Section 2.2.4.3).

5.4.3 Immunohistochemical analysis of the decellularised porcine valve annulus

To assess the extracellular matrix of the decellularised porcine mitral valve tissue, immunohistochemical analysis was undertaken using decellularised tissue sections and antibodies to collagens I, II, III, IV and VI along with fibronectin and laminin. The positive control sample for collagens I, III, IV, fibronectin and laminin was porcine common carotid artery whilst for collagens II and VI it was porcine articular cartilage. Samples were split into two regions, the anterior left trigone (Fig 5.2 S1) and the posterior annulus regions as shown in Fig 5.2 S5. The methods used for this part of the study can be found in Section 2.2.4.

5.4.4 Labelling the α -gal epitope using biotinylated GSL-1 lectin

GSL-1 lectin binds specifically to galactosyl residues and were used for labelling of α -gal epitopes in decellularised and native porcine mitral valve annulus tissue sections. Two controls were utilized: galactosidase treated tissue sections (negative control) and galactose-blocked lectin controls (negative control) to determine the specificity of the lectin binding to the α -gal epitope. Samples were split into two regions, the anterior left trigone (Fig 5.2 S1) and the posterior annulus regions (Fig 5.2 S5). The methods used for this part of the study can be found in Section 2.2.4.7

5.4.5 Extract cytotoxicity assay of the decellularised porcine valve annulus

To assess the biocompatibility of the decellularised mitral valve annuli, extract and contact cytotoxicity assays were undertaken to simulate what the direct and non-direct effects of the decellularised annuloplasty ring may be on cells in the body. Quantitative extract cytotoxicity was used for analysing the potential cytotoxic effects of any solutes from the decellularised annuloplasty rings on the cells. This assay determined the effect of soluble components from the decellularised porcine mitral valve annuli on L929 and BHK cell lines. Relative ATP levels were determined for the decellularised tissue, positive control and negative control. The relative ATP levels of cells following culture with tissue extracts were prepared from the decellularised porcine annuli taken from the left commissure (n=3) as shown in Fig 5.2 (S2). Cell culture medium with 40 % (v/v) DMSO was used as a positive control, as described in Chapter 2 Section 2.2.5 and the appropriate cell culture medium was used as a negative control. Baby hamster kidney cells (BHK) and murine adipose fibroblast cells (L929) were used. Samples of 300 mg tissue were macerated with a sterile scalpel blade and added to a bijoux with 3 ml of culture medium (1 ml per 100 mg tissue weight). Samples were incubated at 37°C for 72 hours with agitation of 240 rpm. The samples were checked for sterility by streaking onto agar plates containing nutrient agar, fresh blood agar and Sabouraud's agar. Extracts were then stored for up to one month at -20°C until tested. BHK cells were cultured (Section 2.2.5) and seeded at a density of 1×10^4 cells per well in a 96 well plate and cultured for 24 hours at 37°C in 5 % (v/v) CO₂ in air. L929 cells were cultured (Section 2.2.5) and seeded at a density of 2.5×10^4 cells per well in a 96 well plate and cultured for 24 hours at 37°C in 5 % (v/v) CO₂ in air. Extracts were thawed at 37 °C and the culture medium from each well was aspirated and replaced with 100 µl of test extract and 100 µl of culture medium containing 20% (v/v) FBS, 200 µl of the appropriate culture medium was added to the controls (n = 3) and the plates incubated for a further 24 hours under the same conditions.

The ATPLite-M assay (Perkin Elmer) was used as a measure of cell viability by determination of the adenosine triphosphate (ATP) content of the cells. All reagents were equilibrated to room temperature before carrying out the assay. Substrate buffer (25 ml) was added to a vial of lyophilised substrate solution. The culture medium from each well of the 96-well plate was

aspirated and replaced with 50 μ l culture medium along with 50 μ l of mammalian cell lysis solution, the well plate was shaken at 500 rpm for five minutes. Substrate (50 μ l) was added to each well and the plate was shaken at 500 rpm for five minutes. Luminescence was measured using Top Count NXT with the ATP2007 software, data (counts per second) was recorded and plotted using Microsoft Excel.

5.4.6 Contact cytotoxicity assay of the decellularised porcine valve annulus

Contact cytotoxicity assays were utilised to determine the effects of direct contact of the decellularised annuloplasty ring on cells. Contact cytotoxicity testing was undertaken as a qualitative assay in order to record the cell growth up to the tissue and morphology of the cells upon contact with the tissue. Anterior (Fig 5.2 S10-S11) and posterior regions (Fig 5.2 S6-S7) of decellularised mitral valve annuli (n=3) were aseptically dissected into 5 mm² sections and attached to a six well culture plate using steri-strips. A drop of cyanoacrylate contact adhesive was placed into one of the wells as a positive control (for cytotoxicity) and steri-strip was used as a negative control placed into the centre of a second well. All of the wells were washed using DPBS without calcium and magnesium, three times for ten minutes each. The cells were passaged and a cell count performed whilst the washes were taking place. The BHK and L929 cells were re-suspended in medium to a concentration of approximately 250,000 cells.ml⁻¹ of medium. Medium (2 ml) was added to the test and control wells, resulting in 500,000 cells per well. The plates were incubated for 48 hours in 5 % (v/v) CO₂ in air at 37 °C, with the plates examined at 24 hours and 48 hours. Any changes in the morphology, vacuolization, detachment, cell lysis and membrane integrity were recorded and images taken using phase contrast microscopy. The culture medium was aspirated from the plates and the surface gently washed using DPBS containing calcium and magnesium. Neutral buffered formalin (2 ml) was added to each well in a fume hood for ten minutes, the neutral buffered formalin was removed and discarded. Using a Pasteur pipette Giemsa stain was added onto the cell layer, ensuring that the stain covered the cell layer and left for five minutes before washing with tap water. The plates were air dried and viewed microscopically and changes to morphology, vacuolization, detachment, cell lysis and membrane integrity were recorded, images were taken using bright field microscopy.

5.4.7 Biomechanical testing of the native and decellularised porcine mitral valve annuli

The biomechanical properties of the native and decellularised porcine mitral valve annuli were examined using low strain rate to failure tensile testing. Decellularised porcine mitral valve annuli (n=12) were split into four regions and compared against fresh porcine mitral valve annuli (n=12) split into identical regions and tested using the protocol in Section 2.2.6.

5.5 Results

5.5.1 Histological and histochemical characterisation of decellularised porcine mitral valve annulus

Sirius red Miller's stain was used to highlight the collagen within sections of the decellularised porcine mitral valve annulus. When viewed under polarised light the Sirius red gave an indication of the collagen orientation. When viewed under bright field microscopy the elastin fibres stained blue and collagen fibres stained red. There appeared to be no loss of collagen or elastin fibres when decellularised porcine mitral annuli were stained with Sirius red Miller's. Similarly to native porcine mitral valve annulus, regions with lacunae type zones in the anterior annulus (Fig. 5.3a; S1a) were weakly birefringent with collagen fibres orientated isotropically (Fig. 5.3a; S1b). Elastin was prominent in the trigones surrounding the lacunae (Fig 5.3a; S1c), retaining the elastic cartilage-like characteristics of the native porcine mitral annulus (Fig 5.3a; S1 N). Collagen within this elastic zone was not birefringent under polarised light (Fig 5.3a; S1d) similar to that in native tissue in the same zone (Fig 5.3a; S1N b). Collagen fibres were prominent in the fibrosa of the posterior mitral valve leaflet and in the posterior annulus (Fig 5.3b; S5a, S5b, S5c) and comparable to fibres in the native posterior mitral valve annulus (Fig 5.3b; S5N a). The orientation of the fibres was isotropic with some fibres in the fibrosa and annulus orientated radially (Fig 5.3b; S5 c) but other fibres weakly birefringent with the orientation not detectable as also identified in the native posterior annulus under polarised light (Fig 5.3b; S5N b). Elastin, characterised by blue fibres, was visible in the atrialis of the leaflet and the endocardium of the mitral valve in the posterior annulus (Fig 5.3b; S5a).

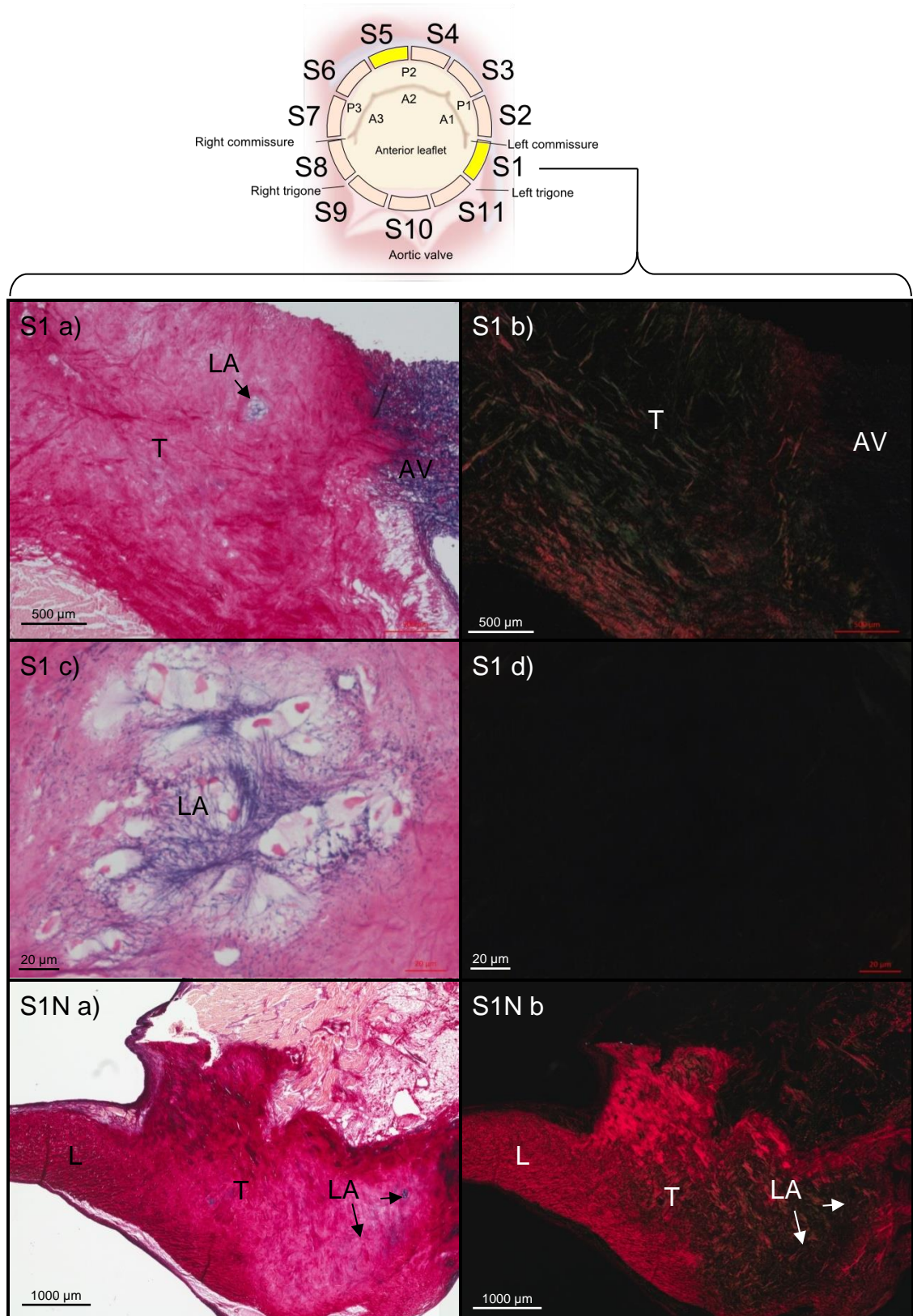


Fig 5.3a – Images of Sirius red Miller's stained sections from the anterior segments of the decellularised porcine mitral valve annulus viewed under polarised light microscopy and bright light microscopy. Annulus 1 (S1 a), Anterior polarised. Annulus 1 (S1 b), Anterior x 400 magnification (S1 c), Anterior polarised x 400 magnification (S1 d), Native anterior. Annulus 5 (S1N a), Native anterior polarised. Annulus 5 (S1N b). T: Trigone; LA: Lacunae; AV: Aortic Valve; L: Leaflet.

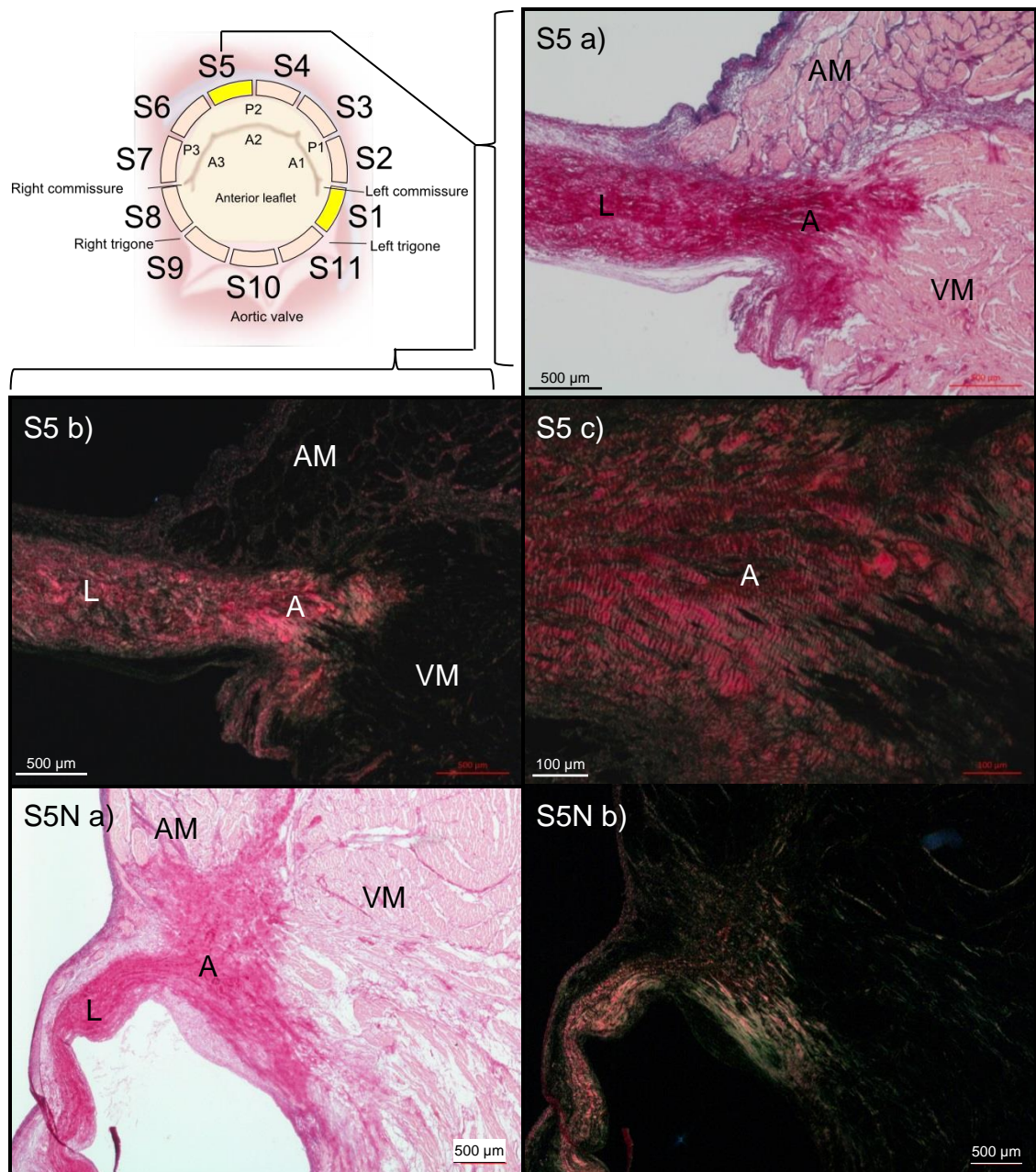


Fig 5.3b – Images of Sirius red Miller's stained sections from the posterior segments of the decellularised porcine mitral valve annulus viewed under polarised light microscopy and bright light microscopy. Annulus 1 (S5 a), posterior section polarised. Annulus 1 (S5 b), posterior section x 100 magnification (S5 c). Native posterior. Annulus 5 (S5N a), Native posterior polarised. Annulus 5 (S5N b). A: Annulus; T: Trigone; AM: Atrial Muscle; AV: Aortic Valve; AVL: Aortic Valve Leaflet; VM: Ventricular Muscle; L: Leaflet; LA: Lacunae. Images are representative of the results obtained from n = 3 annuli. Magnification x 20 unless stated otherwise.

In the anterior and posterior segments (S1, S5) of the decellularised porcine mitral valve annulus, sections were stained with alcian blue to determine the presence and abundance of GAGs. Alcian blue revealed that GAG concentration was reduced in both the anterior and posterior region compared to the native mitral valve annulus in the anterior (Fig 5.4 S1N) and the posterior region (Fig 5.4 S5N). The GAG content was higher in the anterior region where the trigones retained some of the GAGs (Fig 5.4 S1a, b) compared to that of the posterior region where the GAGs were removed at the hinge point (Fig 5.4 S5a, b), in contrast to GAGs present in the hinge point of the native tissue (Fig 5.4 S5N). Some GAGs remained in the spongiosa and ventricularis in the posterior of the decellularised tissue.

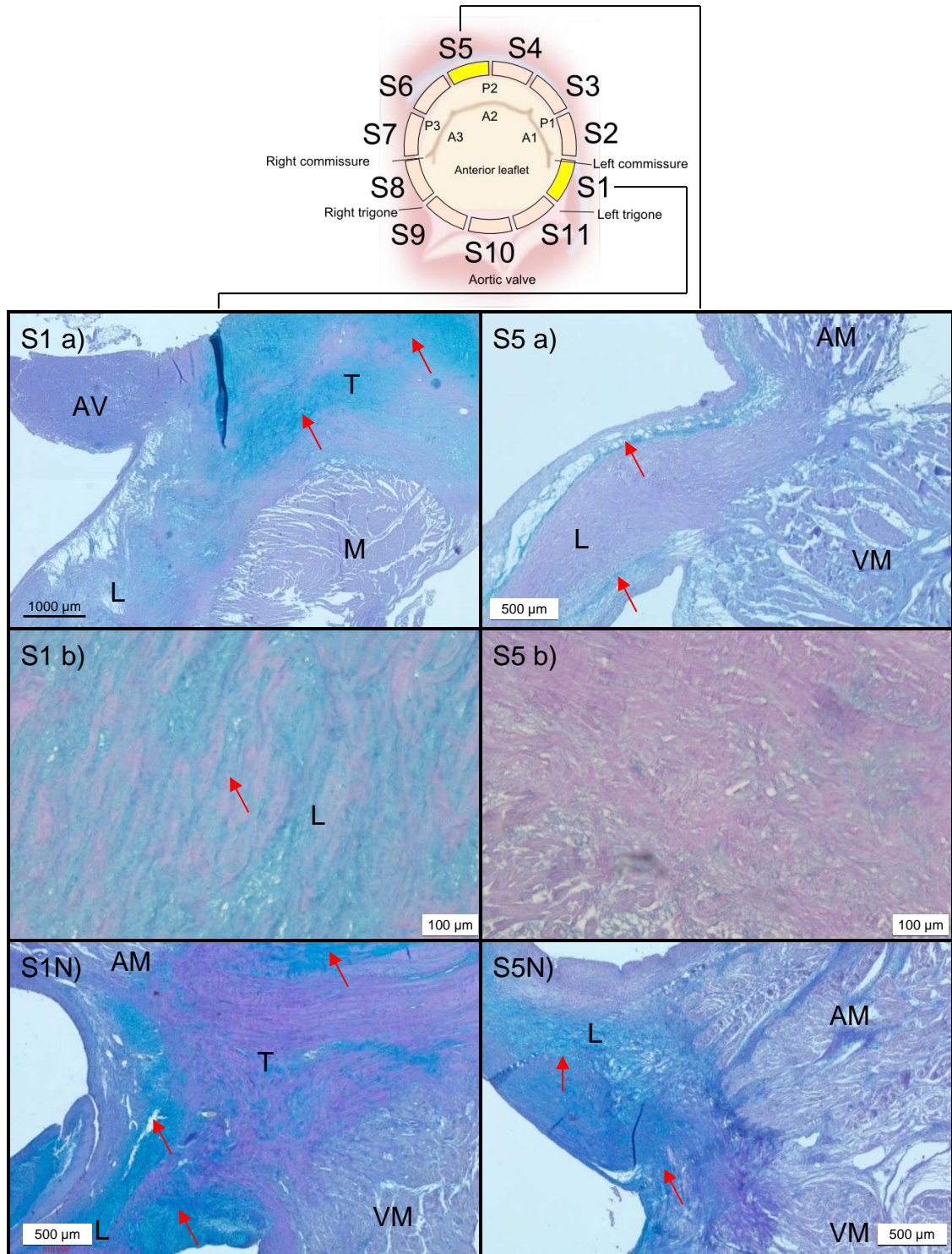


Fig 5.4 – Images of alcian blue stained sections from the anterior and posterior segments of the decellularised porcine mitral valve annulus. Images of alcian blue stained decellularised porcine mitral annulus to visualise GAG localisation, red arrows indicate regions of GAGs. Areas with GAG contain are stained blue. Decellularised anterior annulus stained with alcian blue. Annulus 1 (S1a), Anterior x 100 magnification (S1b), Decellularised posterior. Annulus 1 (S5a), Posterior x 100 magnification (S5b), Anterior x 100 magnification (S1b), Native anterior annulus. Annulus 1 (S1N), Native posterior annulus. Annulus 1 (S5N). A: Annulus; T: Trigone; AM: Atrial Muscle; AV: Aortic Valve; AVL: Aortic Valve Leaflet; VM: Ventricular Muscle; L: Leaflet. Images are representative of the results obtained from n = 3 annuli. Magnification x 20 unless stated otherwise.

5.5.2 Distribution of proteins in the extracellular matrix of decellularised porcine mitral annulus

The distribution of different structural proteins of the extracellular matrix of the decellularised porcine mitral valve annulus was investigated using immunohistochemistry.

5.5.2.1 Collagen I

Images of sections of the anterior and posterior regions (Fig. 5.5a) of the decellularised porcine mitral valve annulus labelled with the collagen I antibody showed that collagen I was distributed throughout the anterior (Fig 5.5a; S1) and posterior (Fig 5.5a; S5) regions. Positive staining was indicated by a dark brown stain and was more prominent in the posterior annulus compared to the anterior annulus. The level of collagen I in the decellularised tissue appeared to be similar to the native porcine mitral valve annuli, albeit staining appeared less prominent in the anterior decellularised section compared to the native anterior section (Fig 5.5a; S1, S1N). Limited background staining was observed in the control sections labelled with the isotype control antibody (Fig 5.5b; a) and diluent alone (Fig 5.5b; b).

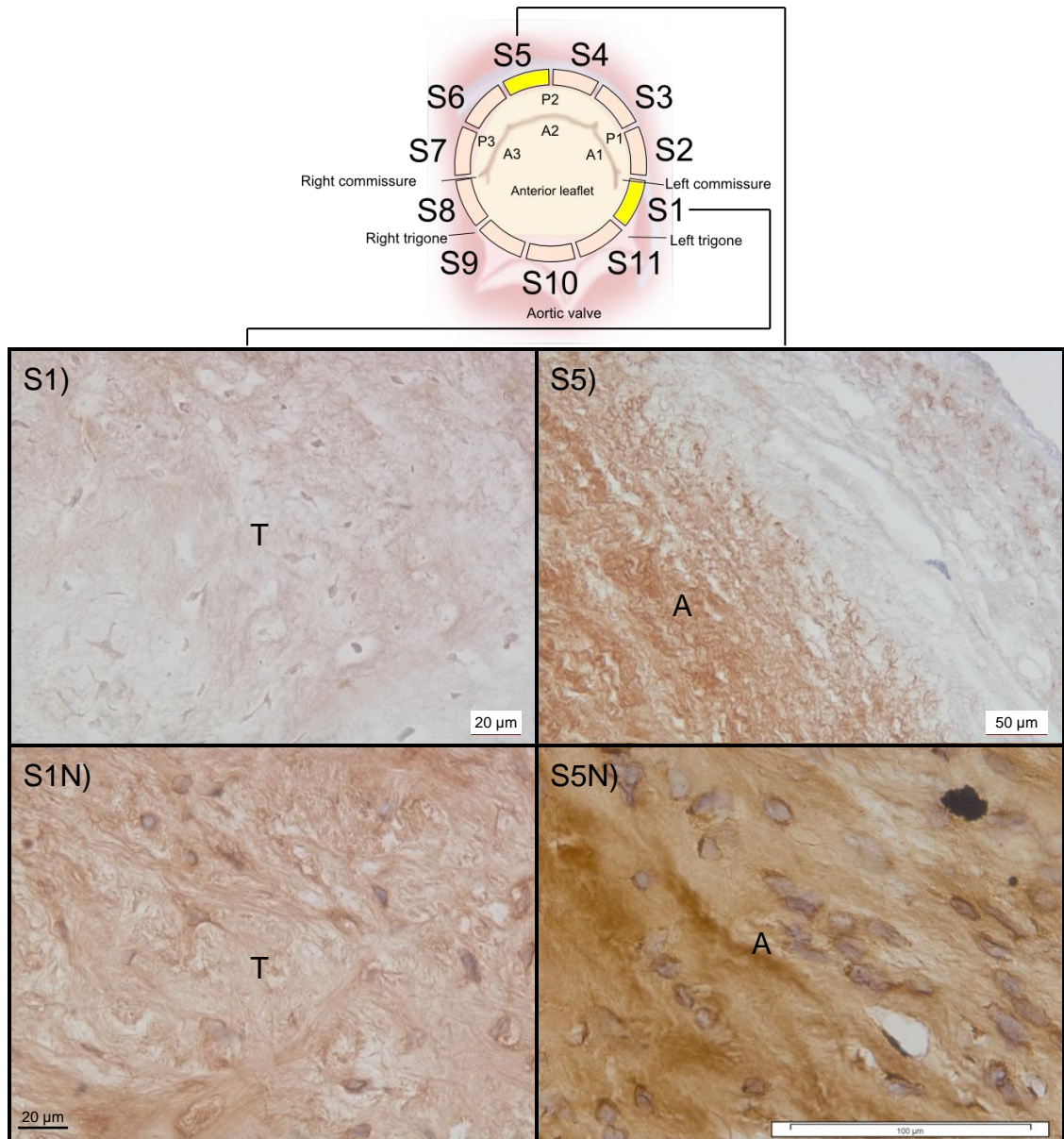


Fig 5.5a – Sections of decellularised porcine mitral valve annulus stained with antibodies to collagen I. Decellularised anterior region stained with antibodies to collagen I x 400 magnification. Annulus 3 (S1), Native anterior annulus x 200 magnification. Annulus 4 (S1N). Decellularised posterior region stained with antibodies to collagen I x 400 magnification. Annulus 1 (S5), Native posterior annulus x 400 magnification. Annulus 1 (S5N). A: Annulus; T: Trigone; AM: Atrial Muscle; AV: Aortic Valve; AVL: Aortic Valve Leaflet; VM: Ventricular Muscle; L: Leaflet. Images are representative of the results obtained from n = 3 annuli. Magnification x 20 unless stated otherwise.

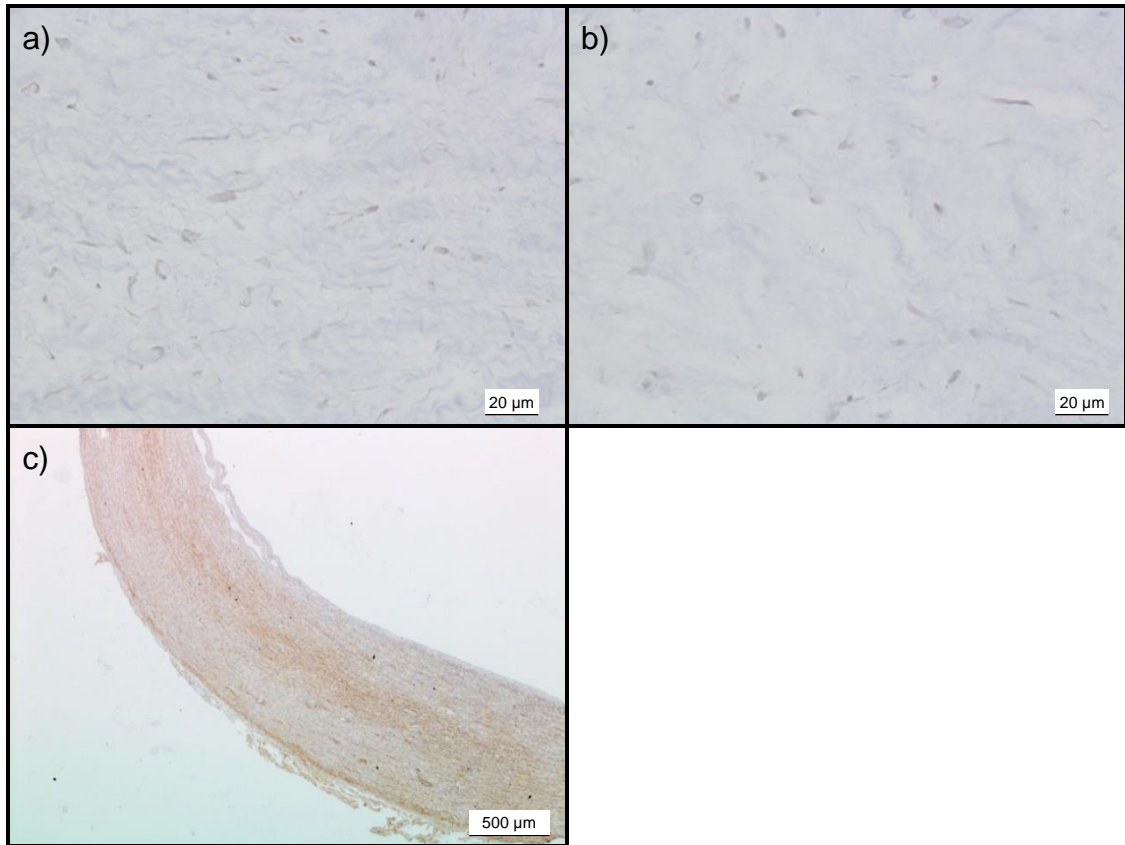


Fig 5.5b – Sections of decellularised porcine mitral valve annulus stained with antibodies to collagen I. Isotype control x 400 magnification (a). Diluent control x 400 magnification (b). Porcine common carotid artery positive control (c). A: Annulus; T: Trigone; AM: Atrial Muscle; AV: Aortic Valve; AVL: Aortic Valve Leaflet; VM: Ventricular Muscle; L: Leaflet. Images are representative of the results obtained from n = 3 annuli. Magnification x 20 unless stated otherwise.

5.5.2.2 Collagen II

Sections from the anterior and posterior regions (Fig 5.6a) of the decellularised porcine mitral valve annulus were labelled with antibodies to collagen II. Images of the sections showed staining in the anterior annulus (Fig 5.6a; S1) in the dense cartilage-like regions. Staining was not visible in the muscle surrounding the annulus or in the posterior annulus region (Fig 5.6a; S5). There was no visible reduction in staining when compared to the native porcine mitral annulus (Fig 5.6a; S1N, S5N). No staining was observed in sections stained with the antibody isotype control (Fig 5.6b; a) or diluent alone (Fig 5.6b; b).

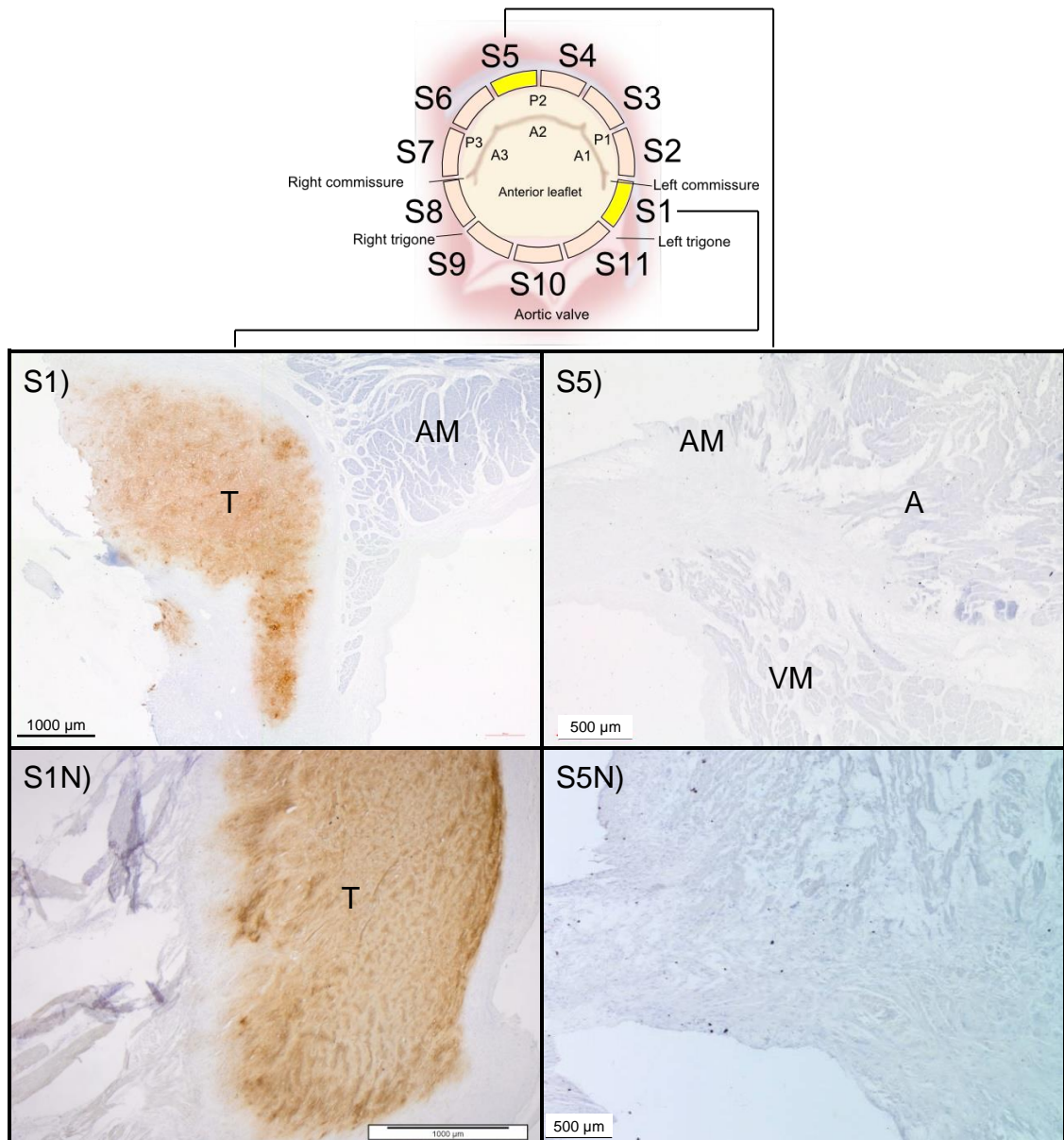


Fig 5.6a – Sections of decellularised porcine mitral valve annulus stained with antibodies to collagen II. Decellularised anterior region stained with antibodies to collagen II. Annulus 2 (S1), Native anterior region. Annulus 1 (S1N). Decellularised posterior region stained with antibodies to collagen II. Annulus 2 (S5), Native posterior region. Annulus 3 (S5N). A: Annulus; T: Trigone; AM: Atrial Muscle; AV: Aortic Valve; AVL: Aortic Valve Leaflet; VM: Ventricular Muscle; L: Leaflet. Images are representative of the results obtained from n = 3 annuli. Magnification x 20 unless stated otherwise.

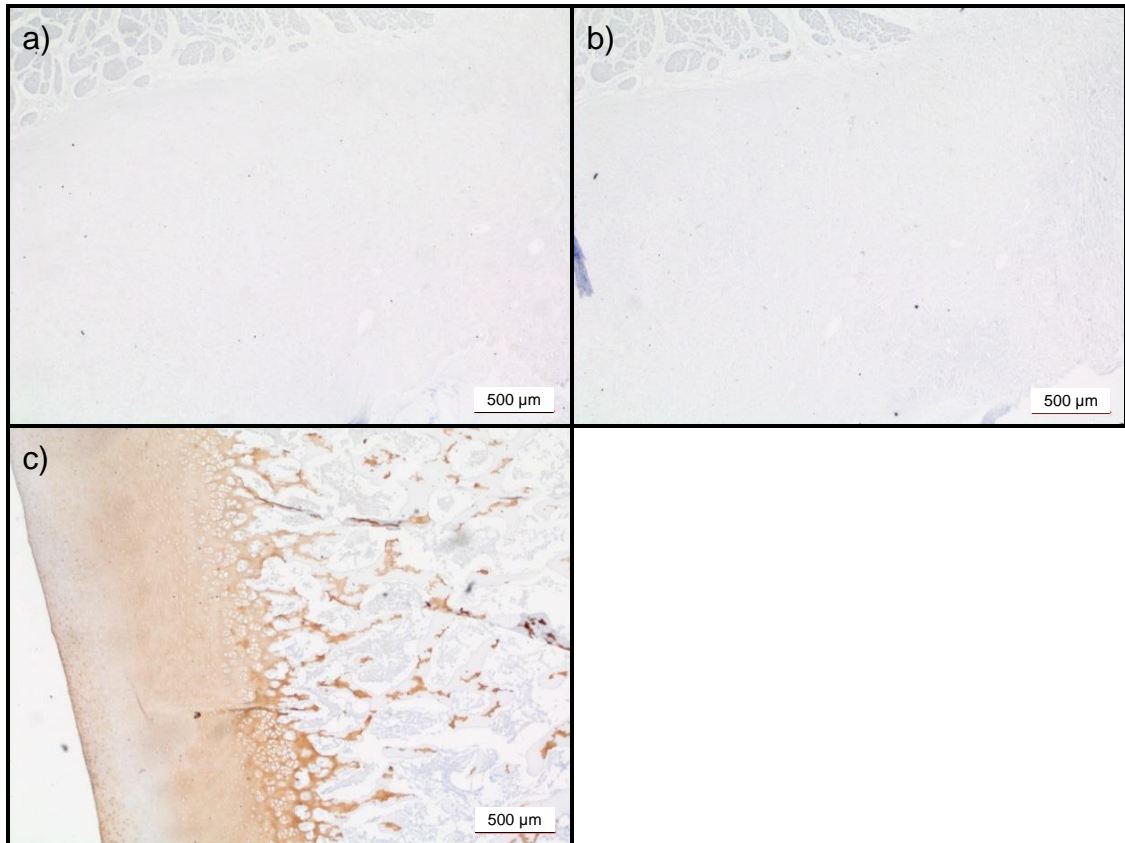


Fig 5.6b – Sections of decellularised porcine mitral valve annulus stained with antibodies to collagen II. Isotype control (a). Diluent control (b). Porcine articular cartilage positive control (c). A: Annulus; T: Trigone; AM: Atrial Muscle; AV: Aortic Valve; AVL: Aortic Valve Leaflet; VM: Ventricular Muscle; L: Leaflet. Images are representative of the results obtained from n = 3 annuli. Magnification x 20 unless stated otherwise.

5.5.2.3 Collagen III

Sections of decellularised porcine mitral valve annulus from both the anterior and posterior regions were stained with antibody to collagen III (Fig 5.7a). Images of the sections revealed positive staining in the annulus and atrial and ventricular myocardium in both the anterior and posterior regions of the decellularised annuli (Fig 5.7a; S1, S5). Staining was more prominent in the myocardium, endocardium and leaflet surfaces of the decellularised tissue compared to the collagenous annulus tissue. Similar amounts of staining were observed in the native annulus regions (Fig 5.7a; S1N, S5N) compared to the decellularised mitral valve annulus. No staining was observed in the sections stained with the antibody isotype control (Fig 5.7b; a) or diluent alone (Fig 5.7b; b).

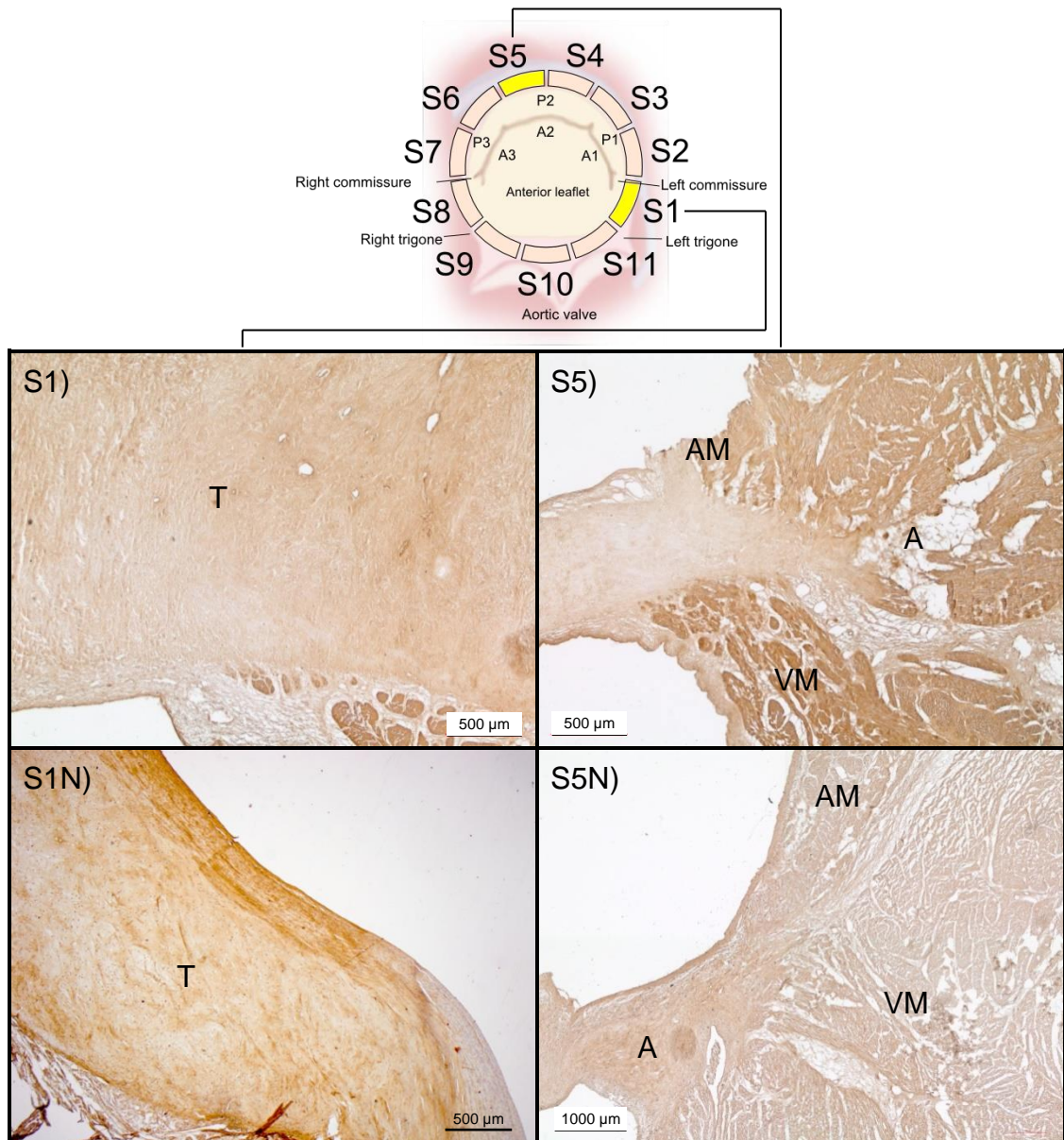


Fig 5.7a – Sections of decellularised porcine mitral valve annulus stained with antibodies to collagen III. Decellularised anterior region stained with antibodies to collagen III. Annulus 2 (S1). Native anterior annulus. Annulus 1 (S1 N). Decellularised posterior region stained with antibodies to collagen III. Annulus 2 (S5), Native posterior annulus. Annulus 4 (S5 N). A: Annulus; T: Trigone; AM: Atrial Muscle; AV: Aortic Valve; AVL: Aortic Valve Leaflet; VM: Ventricular Muscle; L: Leaflet. Images are representative of the results obtained from n = 3 annuli. Magnification x 20 unless stated otherwise.

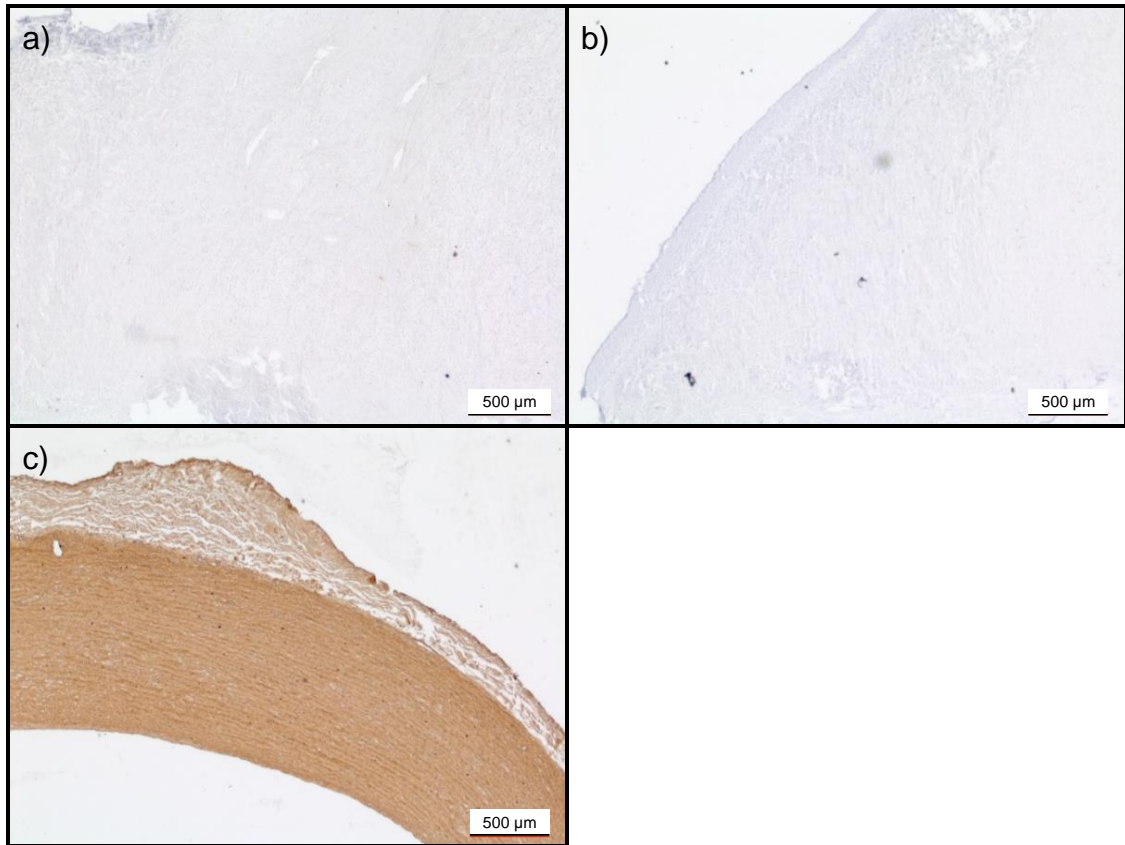


Fig 5.7b – Sections of decellularised porcine mitral valve annulus stained with antibodies to collagen III. Isotype control (a). Diluent control (b). Porcine common carotid artery positive control (c). A: Annulus; T: Trigone; AM: Atrial Muscle; AV: Aortic Valve; AVL: Aortic Valve Leaflet; VM: Ventricular Muscle; L: Leaflet. Images are representative of the results obtained from $n = 3$ annuli. Magnification $\times 20$ unless stated otherwise.

5.5.2.4 Collagen IV

Images of sections from the anterior and posterior regions of the decellularised porcine mitral valve annulus labelled with the collagen IV antibody are shown in Fig 5.8a. The anterior and posterior regions of the decellularised tissue were stained positive in the myocardium. Staining was strong in the atrial and ventricular myocardium and weak in the annulus and mitral valve leaflets. Staining in the decellularised annulus appeared diminished compared to the native porcine mitral valve annulus for both anterior (Fig 5.8a; S1N) and posterior (Fig 5.8a; S5 N) regions. There was some background staining observed in the sections stained with the antibody isotype control (Fig 5.8b; a) or diluent alone (Fig 5.8b; b)

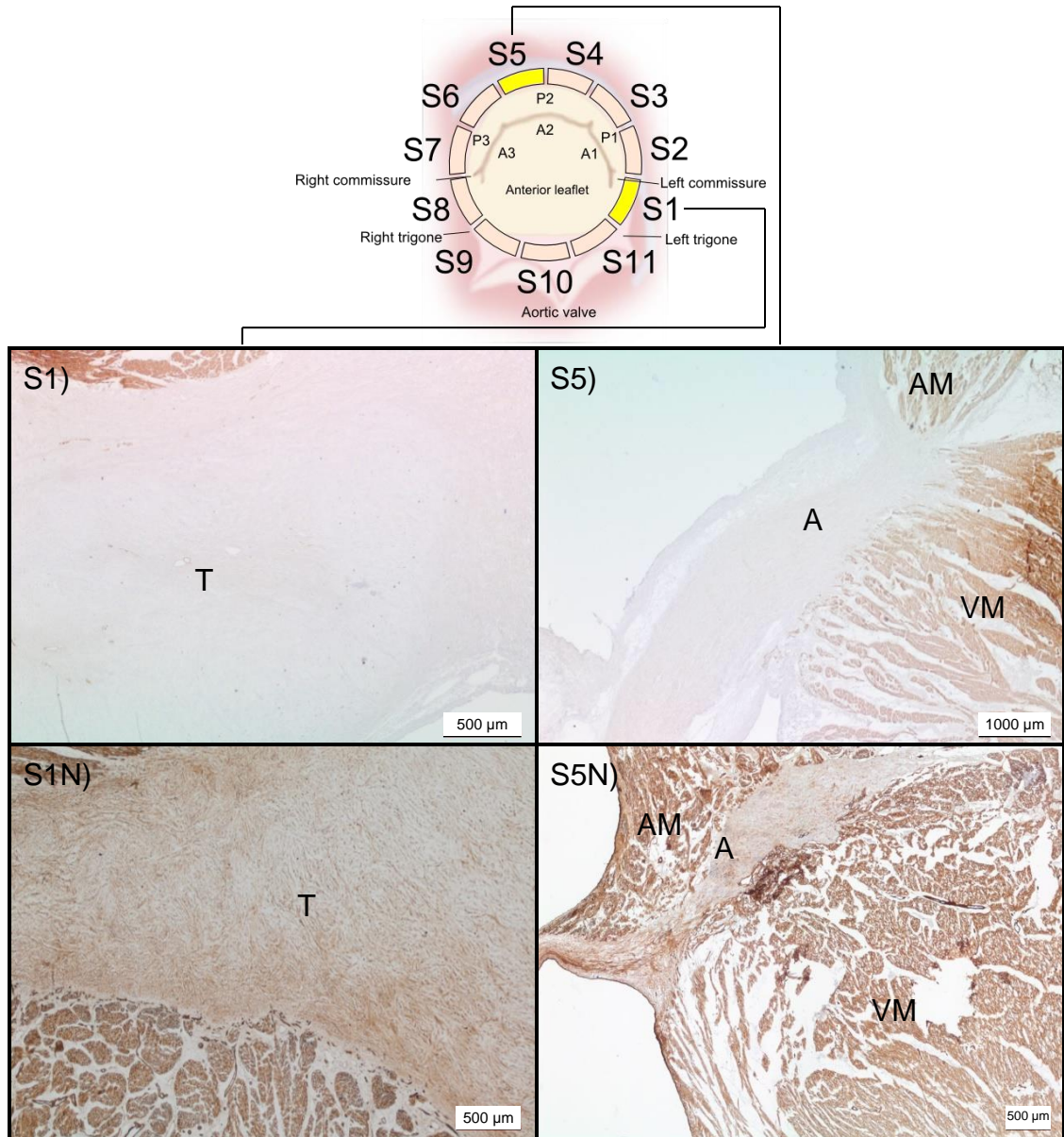


Fig 5.8a – Sections of decellularised porcine mitral valve annulus stained with antibodies to collagen IV. Decellularised anterior region. Annulus 1 (S1), Native anterior annulus. Annulus 4 (S1 N). Decellularised posterior region. Annulus 1 (S5), Native posterior annulus. Annulus 3 (S5 N). A: Annulus; T: Trigone; AM: Atrial Muscle; AV: Aortic Valve; AVL: Aortic Valve Leaflet; VM: Ventricular Muscle; L: Leaflet. Images are representative of the results obtained from n = 3 annuli. Magnification x 20 unless stated otherwise.

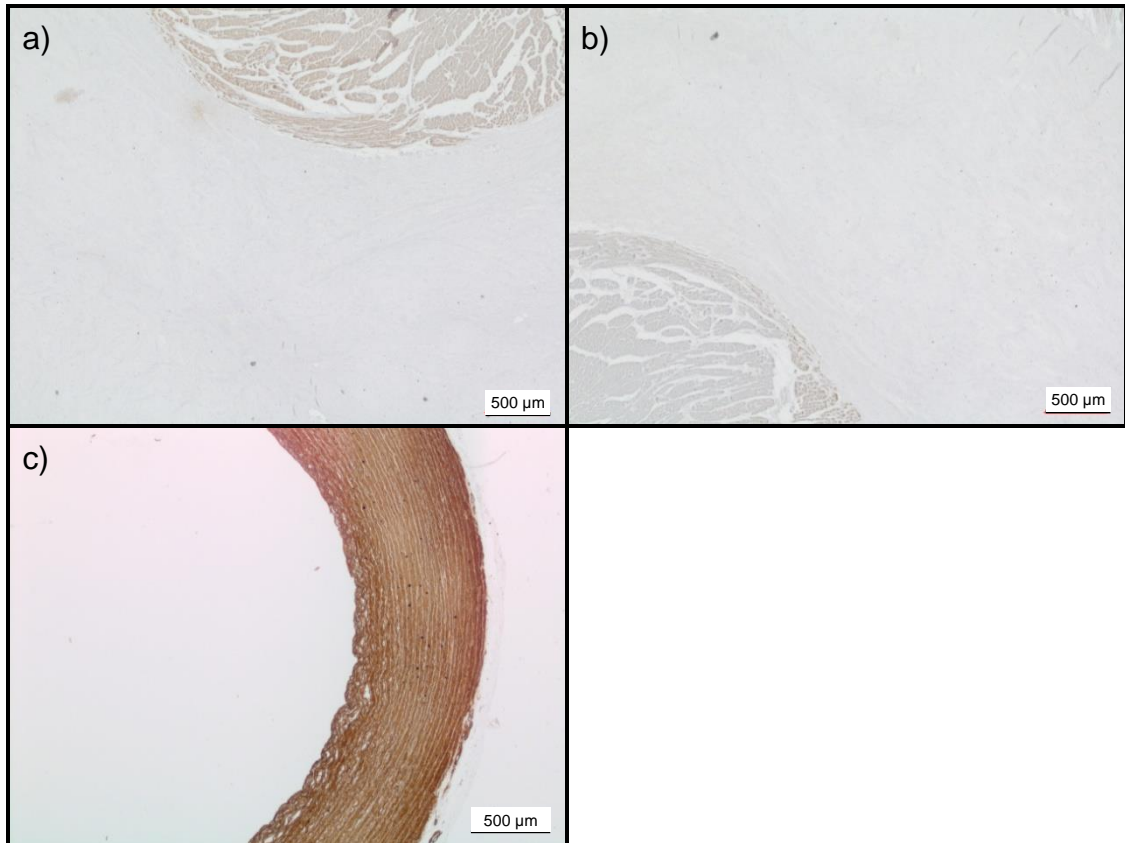


Fig 5.8b – Sections of decellularised porcine mitral valve annulus stained with antibodies to collagen IV. Isotype control (a). Diluent control (b). Porcine common carotid artery positive control (c). A: Annulus; T: Trigone; AM: Atrial Muscle; AV: Aortic Valve; AVL: Aortic Valve Leaflet; VM: Ventricular Muscle; L: Leaflet. Images are representative of the results obtained from n = 3 annuli. Magnification x 20 unless stated otherwise.

5.5.2.5 Collagen VI

Sections of the decellularised porcine mitral annulus from the anterior and posterior regions (Fig 5.9a) were labelled with antibody to collagen VI. Strong staining was observed primarily in the anterior annulus in the same region where the lacunae reside (Fig 5.9a; S1a, S1b). In the posterior region collagen VI was more prominent in the endocardium than the annulus (Fig 5.9a; S5). Compared to the native porcine mitral valve annulus in the anterior region, staining in the trigonal region was comparable (Fig 5.9a; S1N). In the posterior region staining appeared almost completely removed from the myocardium (Fig 5.9a; S5) compared to the native porcine mitral valve annulus in the same region (Fig 5.9a; S5N). No staining was observed in the sections stained with the antibody isotype control (Fig 5.9b; a) or diluent alone (Fig 5.9b; b).

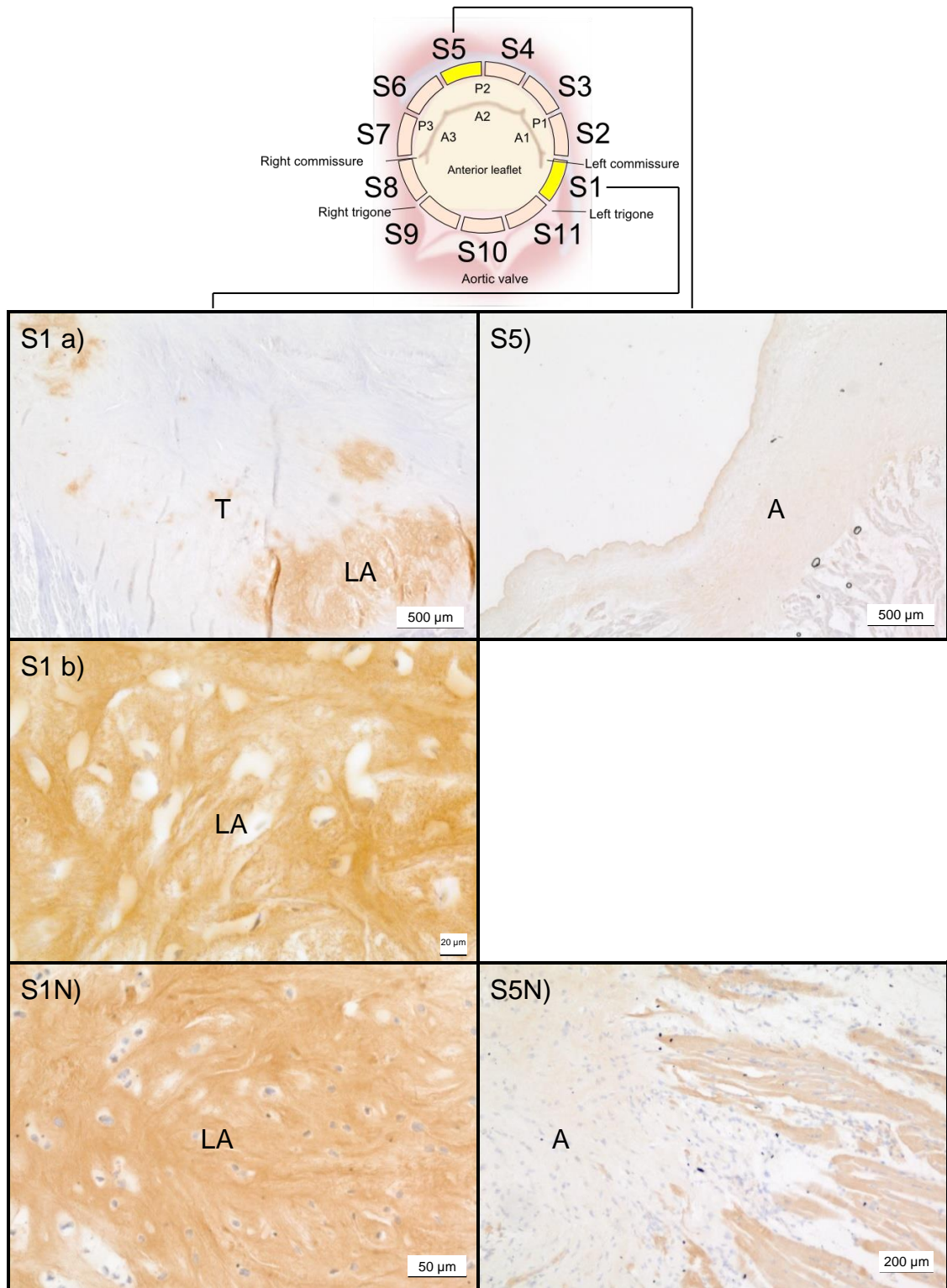


Fig 5.9a – Sections of decellularised porcine mitral valve annulus stained with antibodies to collagen VI. Decellularised anterior region stained with antibodies to collagen VI. Annulus 1 (S1 a), anterior region x 400 magnification. Annulus 1 (S1 b), Native anterior annulus x 200 magnification. Annulus 4 (S1 N). Decellularised posterior region stained with antibodies to collagen VI. Annulus 1 (S5), Native posterior annulus x 50 magnification. Annulus 4 (S5 N). A: Annulus; T: Trigone; AM: Atrial Muscle; AV: Aortic Valve; AVL: Aortic Valve Leaflet; VM: Ventricular Muscle; L: Leaflet; LA: Lacunae. Images are representative of the results obtained from n = 3 annuli. Magnification x 20 unless stated otherwise.

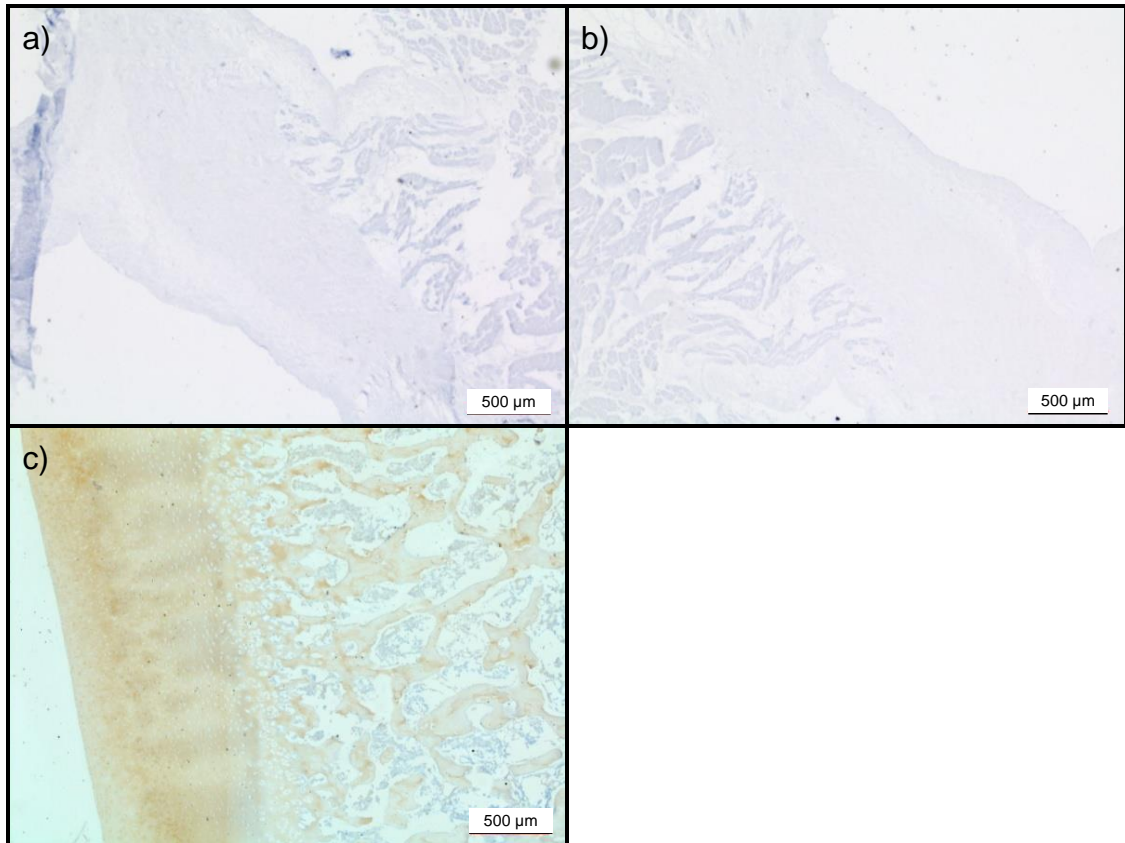


Fig 5.9b – Sections of decellularised porcine mitral valve annulus stained with antibodies to collagen VI. Isotype control (a). Diluent control (b). Porcine articular cartilage positive control (c). A: Annulus; T: Trigone; AM: Atrial Muscle; AV: Aortic Valve; AVL: Aortic Valve Leaflet; VM: Ventricular Muscle; L: Leaflet; LA: Lacunae. Images are representative of the results obtained from n = 3 annuli. Magnification x 20 unless stated otherwise.

5.5.2.6 Fibronectin

Images of sections of the anterior and posterior regions (Fig 5.10a, Fig 5.10b) of the decellularised porcine mitral annulus labelled with the fibronectin antibody show both regions were stained positive. Positive staining was indicated by a dark brown stain and was observed in the annulus and atrial and ventricular myocardium in all regions. Staining was more prominent in the myocardium compared to the annulus, endocardium and leaflet surfaces. Compared to the native porcine mitral valve annulus (Fig 5.10b; S1N, S5N) staining was weaker in both the anterior (Fig 5.10a; S1 a) and posterior (Fig 5.10a; S5 a) regions in the connective tissue of the annulus. Myocardium surrounding the annulus (Fig 5.10a; S5a) appeared the same as native (Fig 5.10b; S5N b) porcine mitral valve tissue. Limited background staining was observed in sections stained with the isotype control antibody (Fig 5.10c; a) or diluent alone (Fig 5.10c; b)

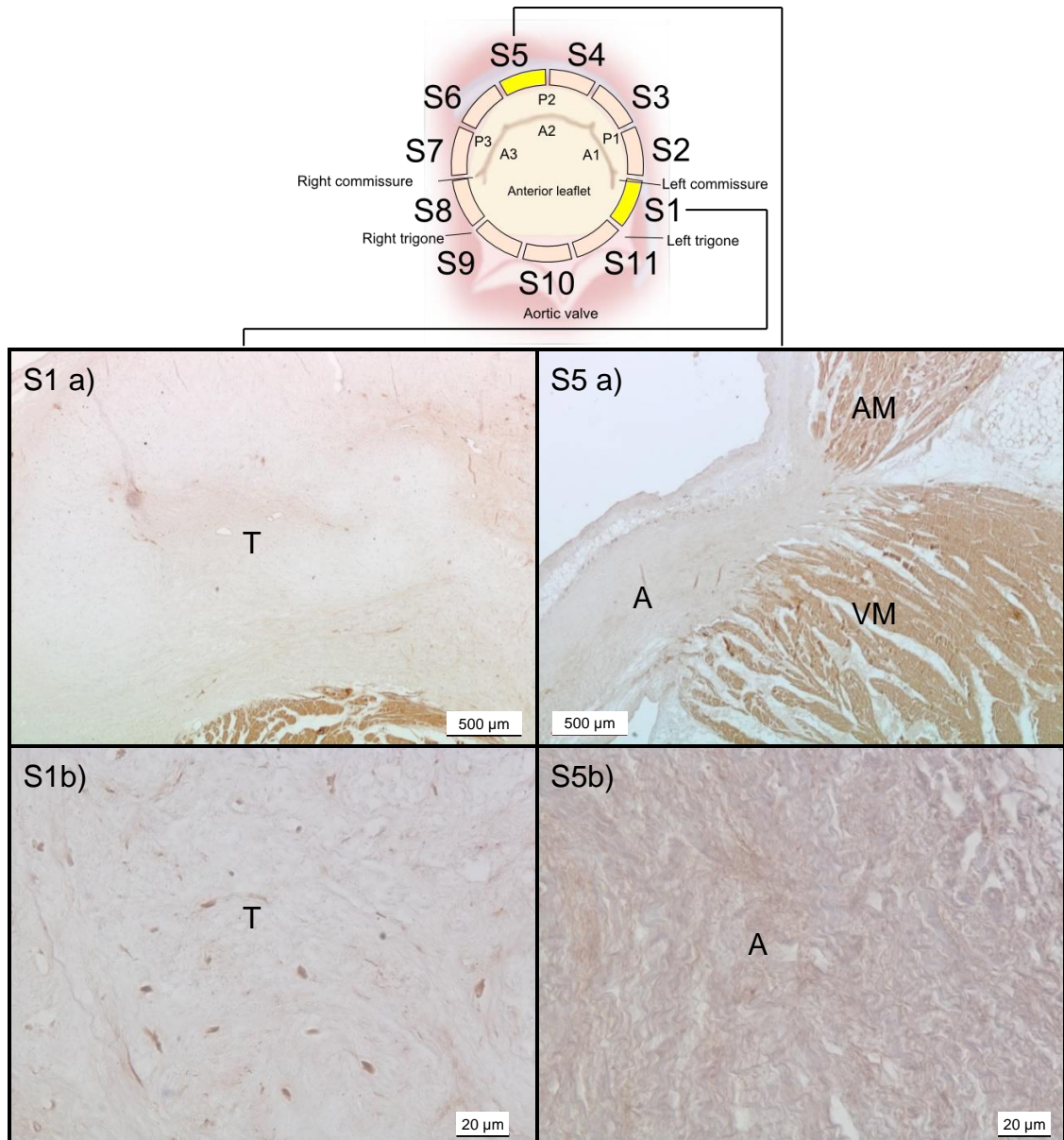


Fig 5.10a – Sections of decellularised porcine mitral valve annulus stained with antibodies to fibronectin. Decellularised anterior region stained with antibodies to fibronectin. Annulus 1 (S1 a), decellularised anterior region x 400 magnification (S1 b). Decellularised posterior region stained with antibodies to fibronectin. Annulus 1 (S5 a), decellularised posterior region x 400 magnification (S5 b). Native posterior annulus x 200 magnification. A: Annulus; T: Trigone; AM: Atrial Muscle; AV: Aortic Valve; AVL: Aortic Valve Leaflet; VM: Ventricular Muscle; L: Leaflet. Images are representative of the results obtained from n = 3 annuli. Magnification x 20 unless stated otherwise.

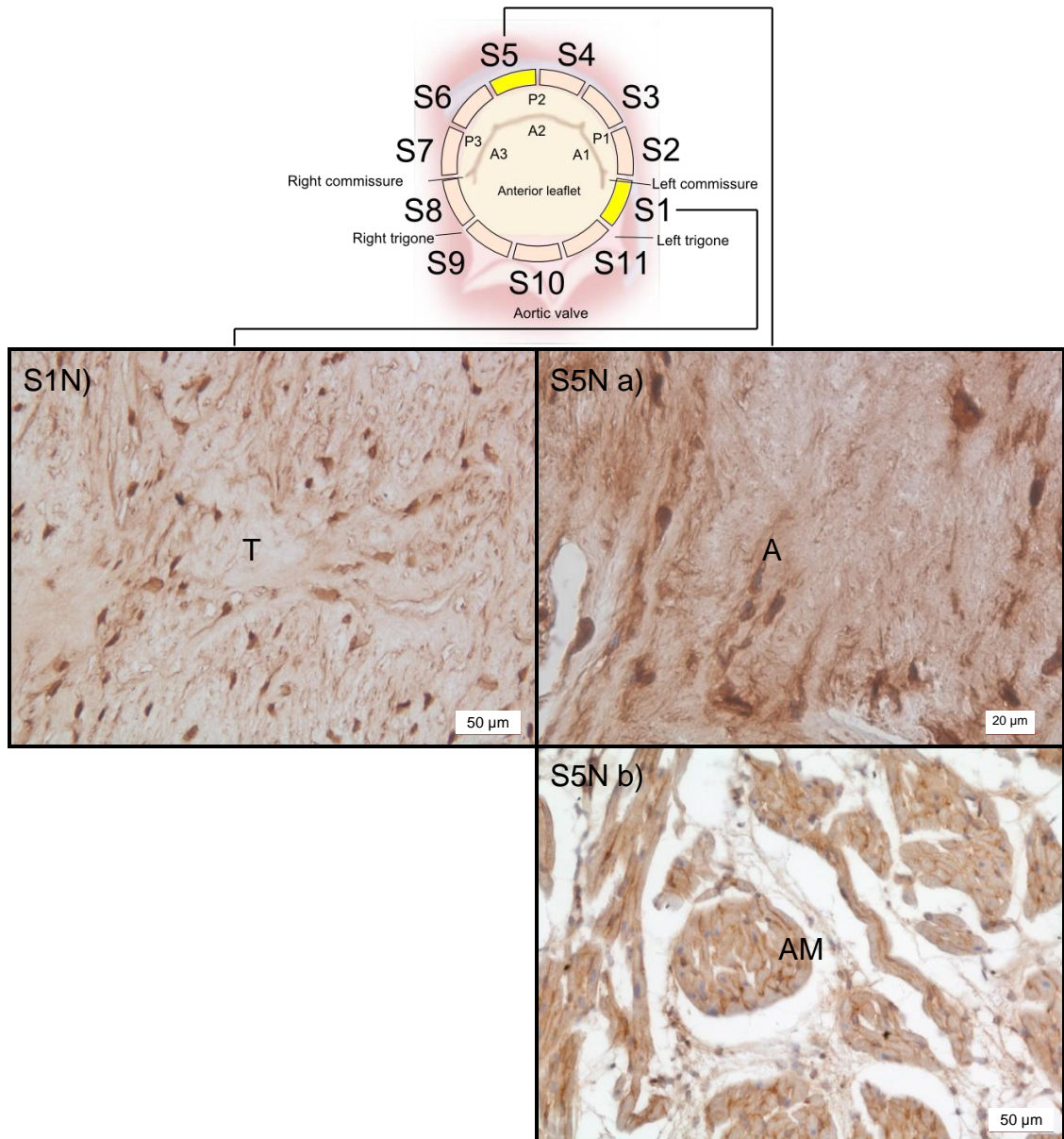


Fig 5.10b – Sections of decellularised porcine mitral valve annulus stained with antibodies to fibronectin. Decellularised anterior region stained with antibodies to fibronectin. Native anterior region x 200 magnification, Annulus 4 (S1 N). Decellularised posterior region stained with antibodies to fibronectin. Native posterior annulus x 200 magnification, Annulus 4 (S5N a). Native posterior region atrial myocardium x 200 magnification (S5N b). A: Annulus; T: Trigone; AM: Atrial Muscle; AV: Aortic Valve; AVL: Aortic Valve Leaflet; VM: Ventricular Muscle; L: Leaflet. Images are representative of the results obtained from n = 3 annuli. Magnification x 20 unless stated otherwise.

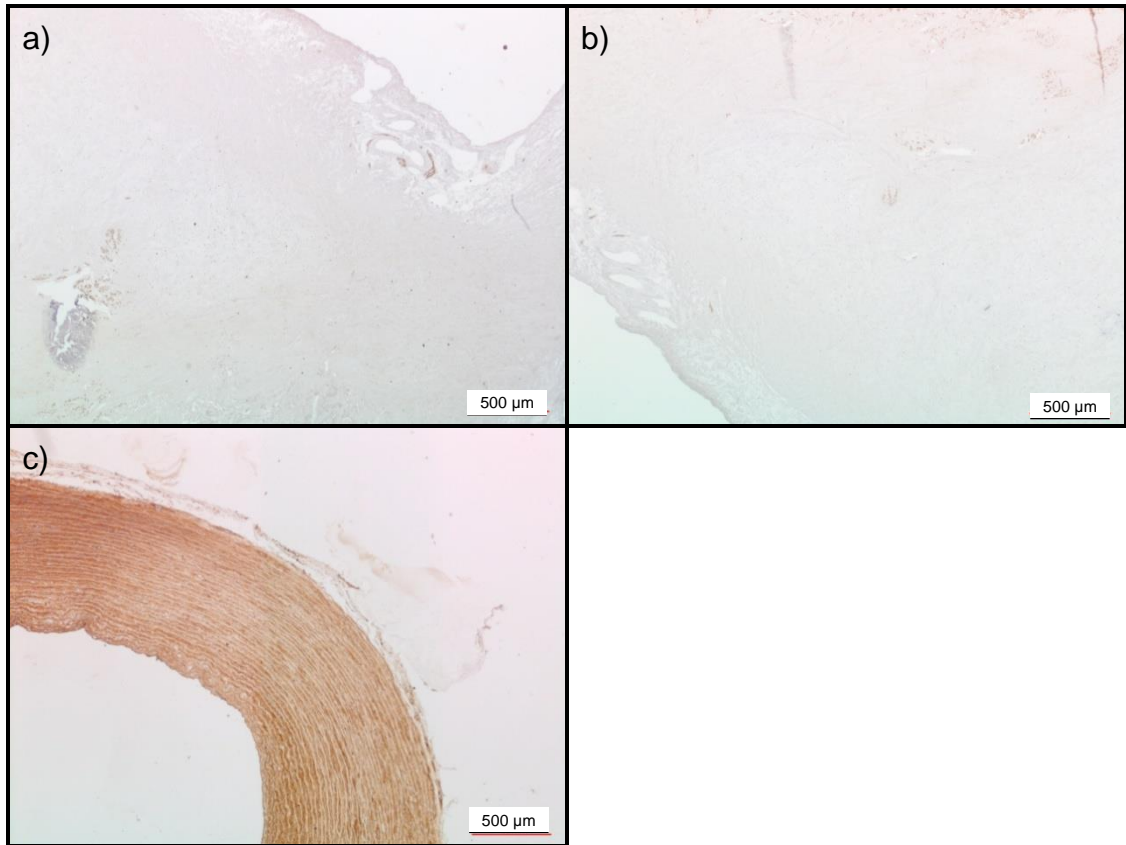


Fig 5.10c – Sections of decellularised porcine mitral valve annulus stained with antibodies to fibronectin. Isotype control (a). Diluent control (b). Porcine common carotid artery positive control (c). A: Annulus; T: Trigone; AM: Atrial Muscle; AV: Aortic Valve; AVL: Aortic Valve Leaflet; VM: Ventricular Muscle; L: Leaflet. Images are representative of the results obtained from n = 3 annuli. Magnification x 20 unless stated otherwise.

5.5.2.7 Laminin

Anterior and posterior sections of the decellularised porcine mitral valve annulus were labelled with antibodies to laminin. Images (Fig 5.11a; S1, S5) of the laminin labelled sections revealed absence of any staining. The decellularisation process appeared to have removed all laminin from the tissue which was prominent in the native porcine mitral valve annulus (Fig 5.11a; S1N, S5N). No staining was observed in the control sections labelled with the isotype control antibody (Fig 5.11b; a) and diluent alone (Fig 5.11b; b).

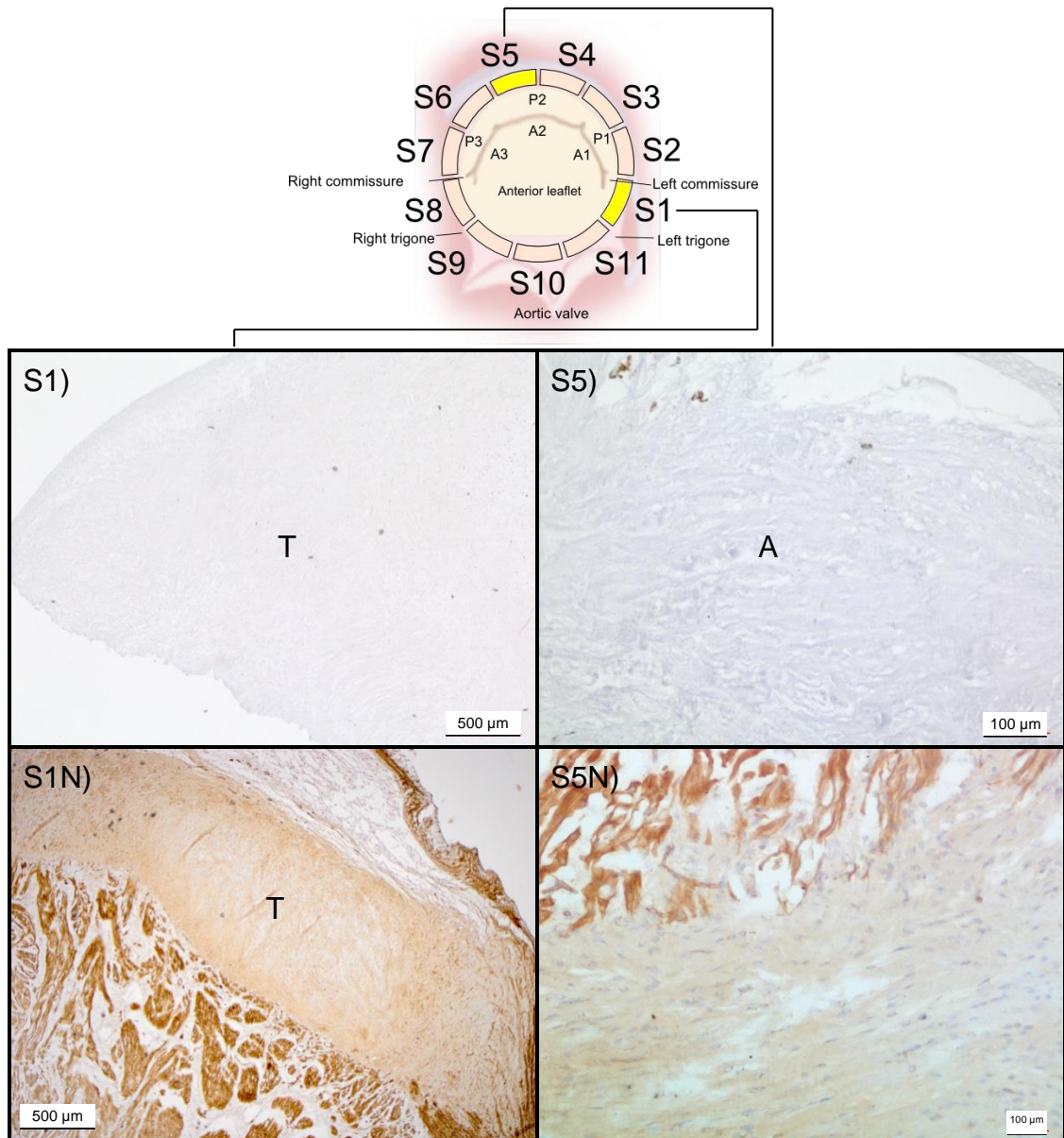


Fig 5.11a – Sections of decellularised porcine mitral valve annulus stained with antibodies to laminin. Decellularised anterior region stained with antibodies to laminin. Annulus 1 (S1), Native anterior region. Annulus 3 (S1N). Decellularised posterior region stained with laminin x 100 magnification. Annulus 3 (S5), Native posterior region. Annulus 3 x 100 magnification (S5N). A: Annulus; T: Trigone; AM: Atrial Muscle; AV: Aortic Valve; AVL: Aortic Valve Leaflet; VM: Ventricular Muscle; L: Leaflet. Images are representative of the results obtained from n = 3 annuli. Magnification x 20 unless stated otherwise.

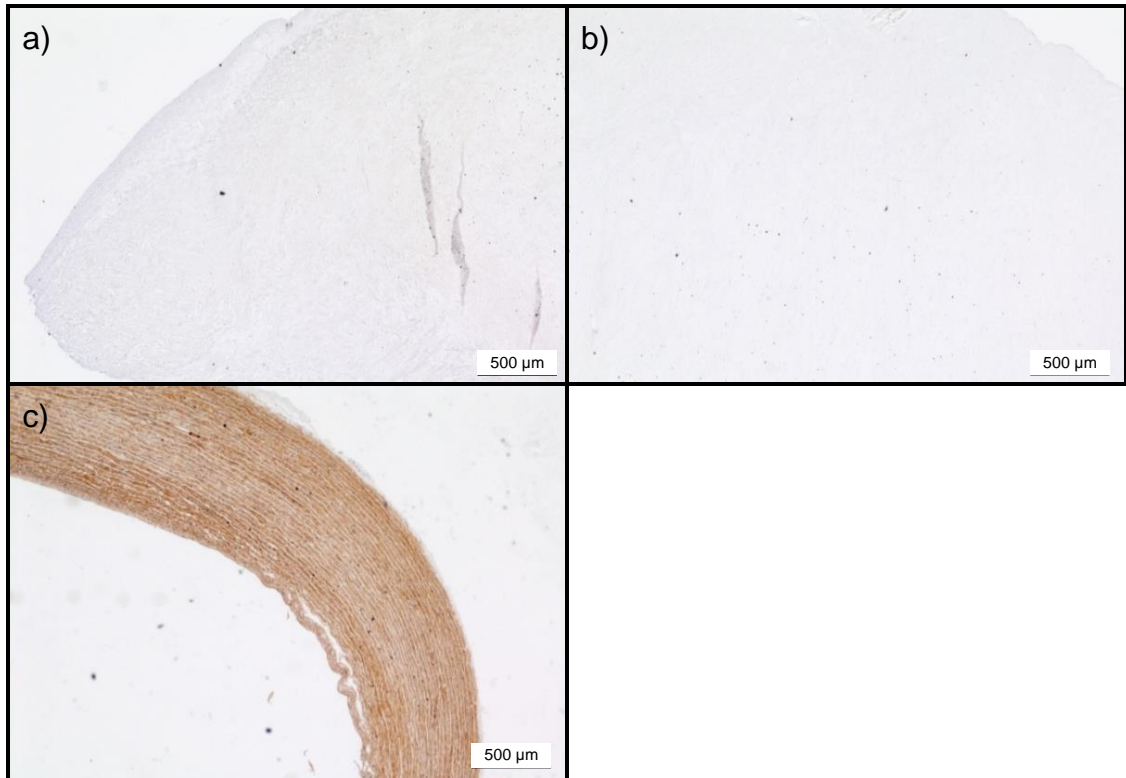


Fig 5.11b – Sections of decellularised porcine mitral valve annulus stained with antibodies to laminin. Decellularised anterior region stained with antibodies to laminin. Annulus 1 (S1), Native anterior region. Annulus 3 (S1N). Decellularised posterior region stained with laminin x 100 magnification. Annulus 3 (S5), Native posterior region. Annulus 3 x 100 magnification (S5N). Isotype control (a). Diluent control (b). Porcine common carotid artery positive control (c). A: Annulus; T: Trigone; AM: Atrial Muscle; AV: Aortic Valve; AVL: Aortic Valve Leaflet; VM: Ventricular Muscle; L: Leaflet. Images are representative of the results obtained from n = 3 annuli. Magnification x 20 unless stated otherwise.

5.5.2.8 Alpha-gal localisation using lectin

Images of sections of the anterior (Fig 5.12a; S1) and posterior regions (Fig 5.12a; S5) of the decellularised mitral valve annulus labelled with the lectin showed both regions stained positive for the α -gal epitope. Positive staining was indicated by a dark brown stain and was seen in the anterior annulus (Fig 5.12a; S1 a, S1 b) and myocardium (Fig 5.12a; S1 a, S1 c) and the posterior myocardium (Fig 5.12a; S5 a, S5 c). Staining was more prominent in the vasculature and muscle surrounding the annulus. Blood vessels and some of the cellular remnants in the anterior region stained positive. No staining was observed in the two control sections of galactosidase treated tissue (Fig 5.12b; a) and tissue stained with galactose-blocked lectin (Fig 5.12b; b) indicating specific staining. Lectin staining was noticeably reduced when compared to the native tissue, where staining was stronger in both the anterior (5.12b; c) and posterior (5.12b; d) annulus and surrounding myocardium.

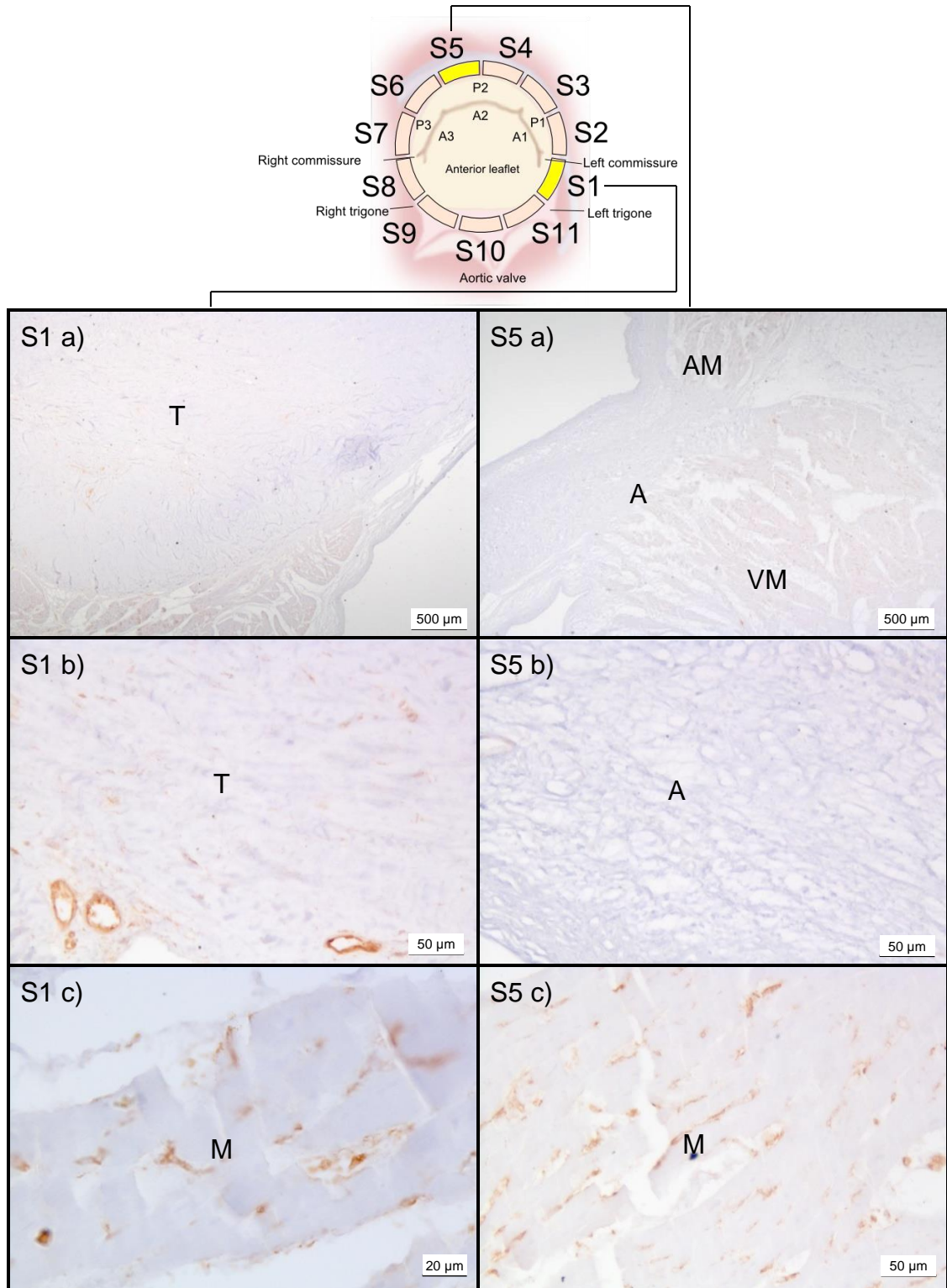


Fig 5.12a – Sections of decellularised porcine mitral valve annulus labelled with lectin. Sections labelled with lectin to identify α -gal epitopes. Decellularised anterior annulus region. Annulus 1 (S1a), decellularised anterior annulus x 200 magnification (S1b), decellularised anterior myocardium x 400 magnification (S1c). Decellularised posterior annulus region. Annulus 3 (S5a), decellularised posterior annulus x 200 magnification (S5b), decellularised posterior myocardium x 200 magnification (S5c). A: Annulus; T: Trigone; AM: Atrial Muscle; AV: Aortic Valve; M: Myocardium; VM: Ventricular Muscle; L: Leaflet. Images are representative of the results obtained from n = 3 annuli. Magnification x 20 unless stated otherwise.

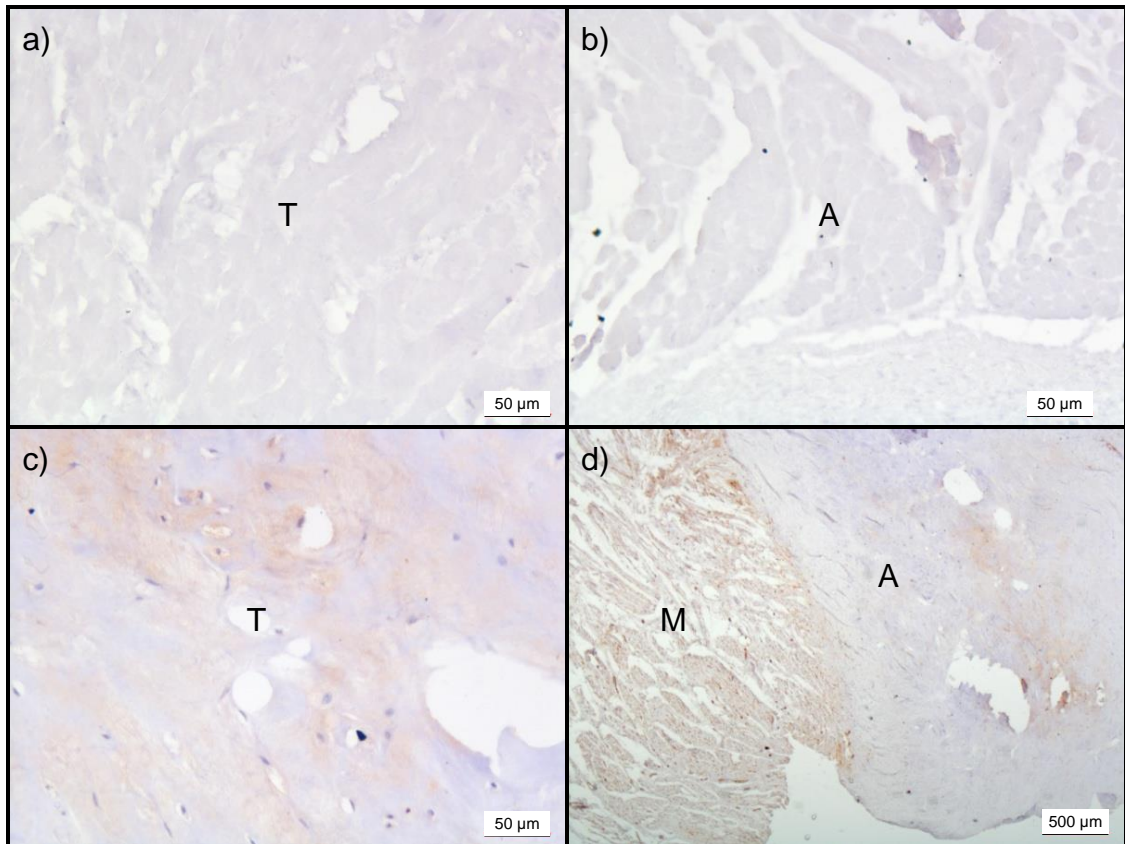


Fig 5.12b – Sections of decellularised porcine mitral valve annulus labelled with lectin. Galactosidase treated annulus section x 200 magnification (a), Galactose blocked lectin x 200 magnification (b), Native anterior porcine mitral valve annulus x 200 magnification (c), Native posterior porcine mitral valve annulus (d). A: Annulus; T: Trigone; AM: Atrial Muscle; AV: Aortic Valve; M: Myocardium; VM: Ventricular Muscle; L: Leaflet. Images are representative of the results obtained from n = 3 annuli. Magnification x 20 unless stated otherwise.

5.5.3 Extract cytotoxicity assays of decellularised porcine mitral valve annuli

The levels of ATP present in BHK and L929 cells following incubation with extracts of the decellularised annulus are illustrated in Fig 5.13 and Fig 5.14 respectively. There was no significant difference in the ATP levels of BHK cells incubated with the three decellularised annulus extracts compared to the negative control. BHK cells incubated with extract 3 had significantly lower levels of ATP compared to BHK cells incubated with extract 2 ($p < 0.05$; ANOVA). There was no significant difference in the ATP levels of L929 cells incubated with all three of the decellularised annulus extracts compared to the negative control. The ATP content of the L929 cells incubated with DMSO (positive control) was significantly lower than the extracts and the control ($p < 0.05$; ANOVA).

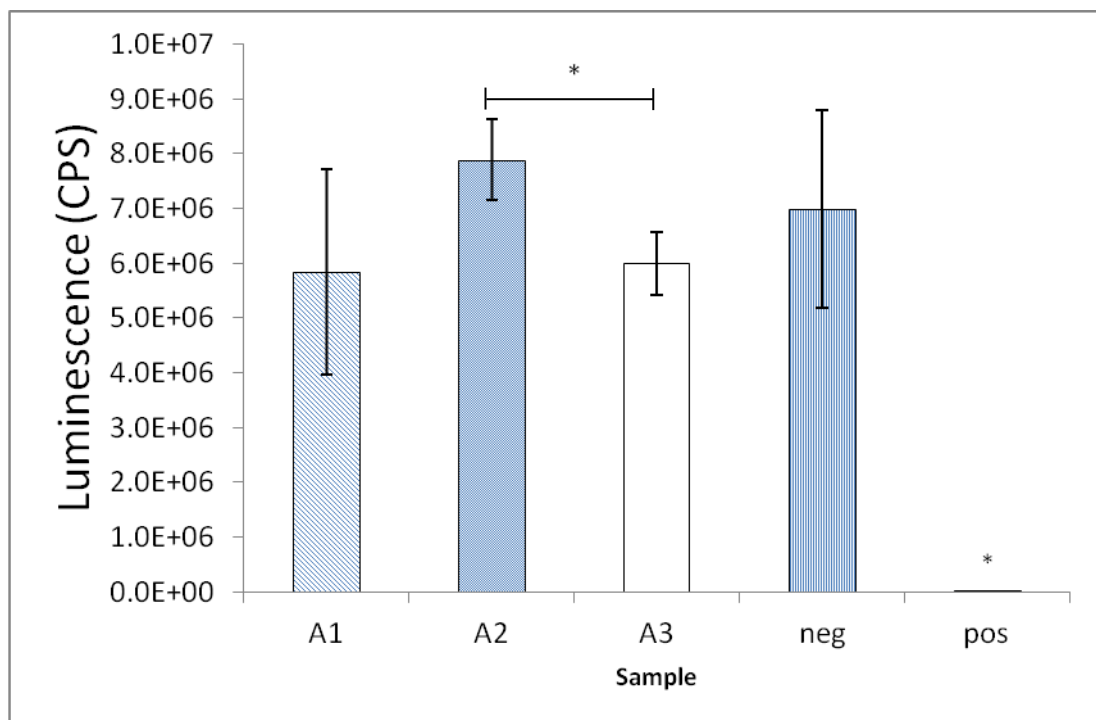


Fig 5.13 – ATP content of BHKs incubated with decellularised annulus extracts. Data is presented as the mean ($n = 3$) \pm 95 % CI. Data was analysed by one way ANOVA followed by calculation of MSD using the T-test. A1-A3 tissues extracts; Neg; Culture medium only; Pos; DMSO (40% v/v). Results showed a significant difference between extract A2 and extract A3 and between all tests and the positive control ($p < 0.05^*$)

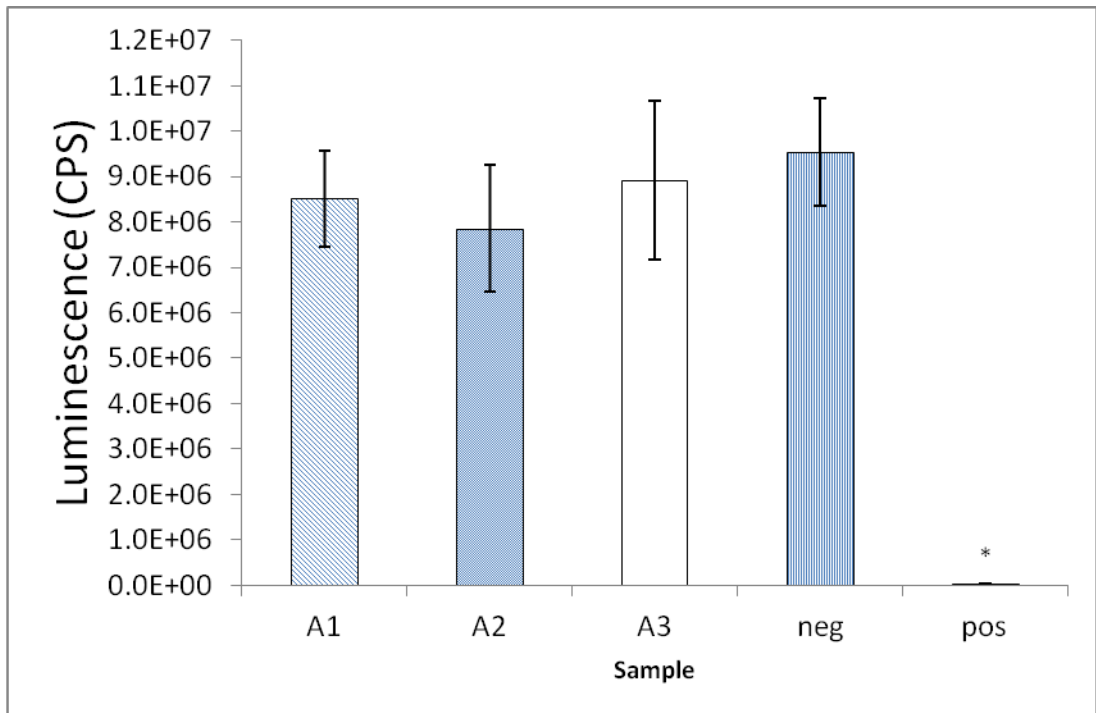


Fig 5.14 – ATP content of L929s incubated with acellular annulus extracts. Data is presented as the mean ($n = 3$) \pm 95 % CI. Data was analysed by one way ANOVA followed by calculation of MSD using the T-test. A1-A3 tissues extracts; Neg; Culture medium only; Pos; DMSO (40% v/v) Results showed a significant difference between the positive control and the extracts and the negative control ($p < 0.05^*$).

5.5.4 Contact cytotoxicity assays of decellularised porcine mitral valve annuli

The contact cytotoxicity results are shown in Fig 5.15 and Fig 5.16. Microscopic analysis of the contact cytotoxicity plates showed attachment and growth of both the BHK and L929 cells up to and onto the decellularised porcine mitral valve annulus tissues. There were no observed changes to the cell morphology of the BHK or L929 cells in the presence of tissues from the anterior (Fig 5.15c; Fig 5.16c) or posterior region (Fig 5.15d; Fig 5.16d) of the annulus or in the presence of the steri-strips used as negative controls (Fig 5.15b, Fig 5.16b). The scaffold appeared to be non-cytotoxic from these studies, the cyanoacrylate glue used as a positive control was cytotoxic to the cells (Fig 5.15a, Fig 5.16a).

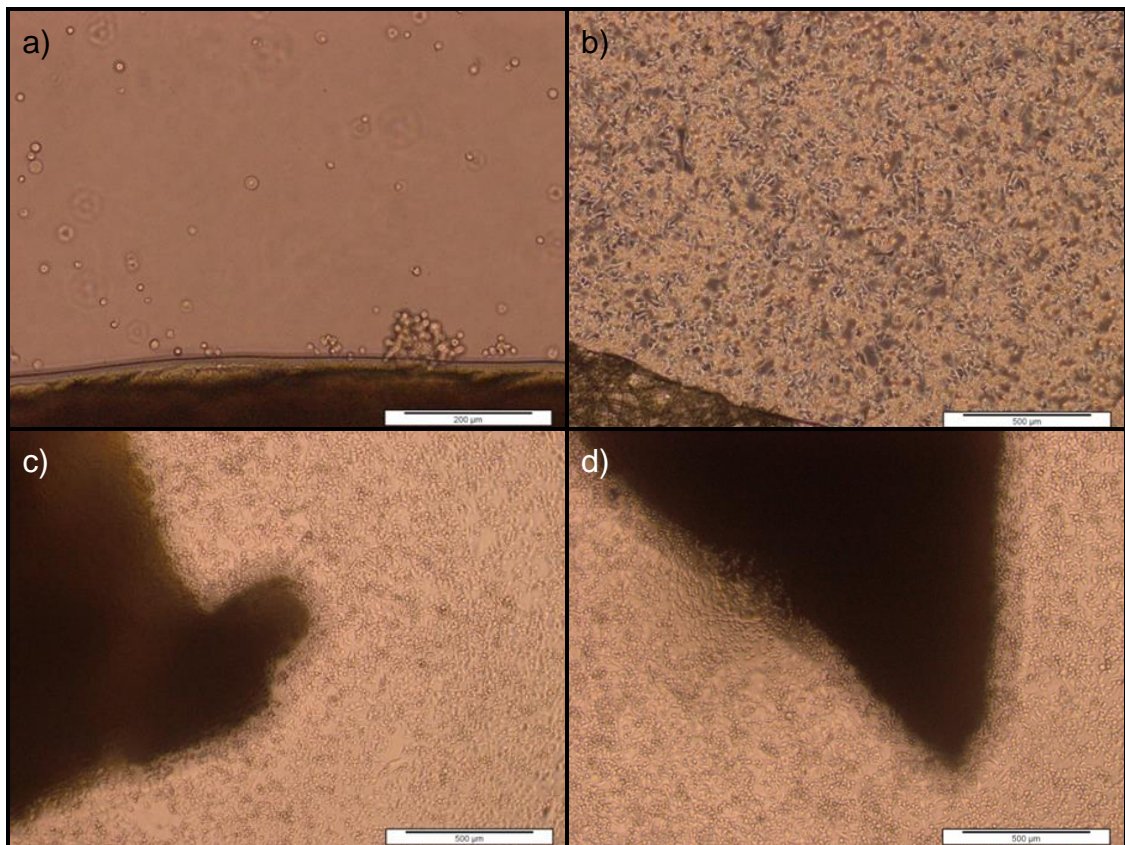


Fig 5.15 – Contact cytotoxicity of decellularised porcine mitral valve annulus tissues cultured with BHK cells. Images of BHK cells incubated with controls and decellularised porcine mitral annulus. Cyanoacrylate control x4 magnification (a), Steri-strip control (b), Anterior annulus 1 (c), Posterior annulus 1 (d). Images are representative of the results obtained from n = 3 annuli. Magnification x 20 unless stated otherwise.

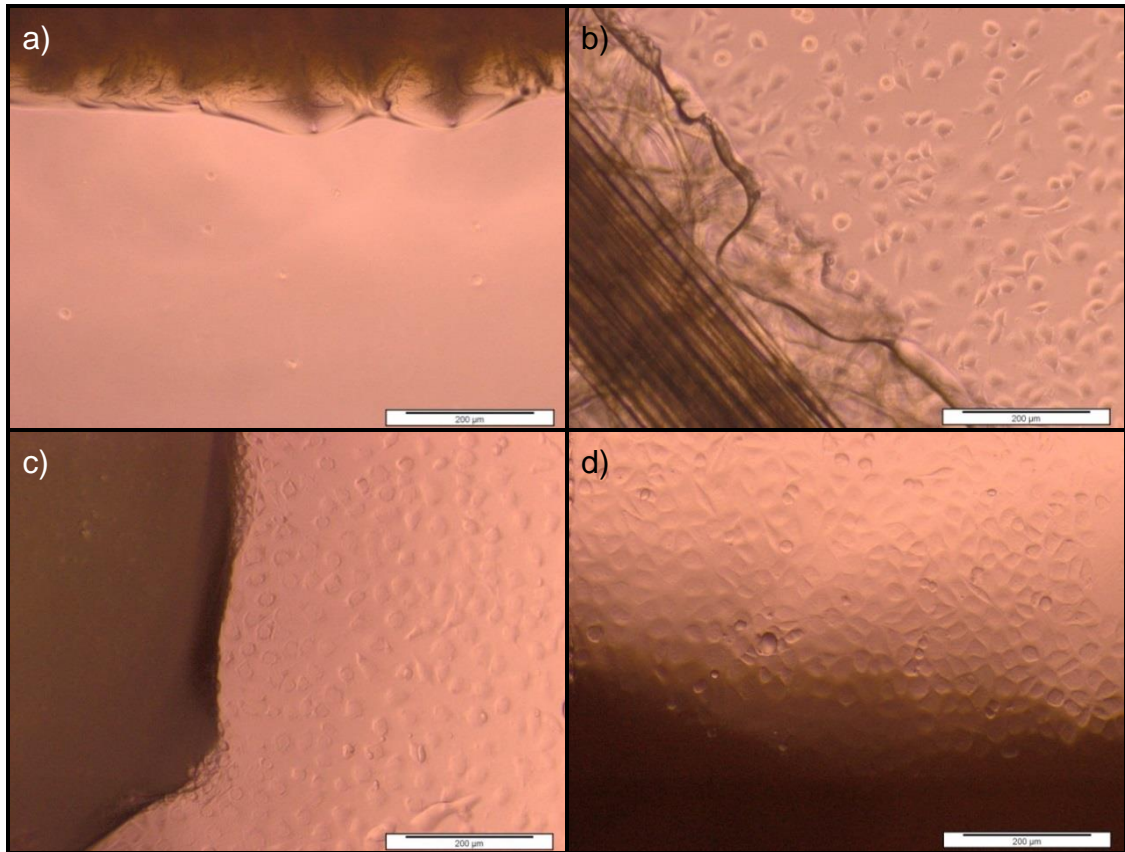


Fig 5.16 – Contact cytotoxicity of decellularised porcine mitral valve annuli cultured with L929 cells. Images of L929 cells incubated with controls and decellularised porcine mitral annulus. Cyanoacrylate control x 40 magnification (a), Steri-strip control x 40 magnification (b), Anterior annulus 1 x 40 magnification (c), Posterior annulus 1 x 40 magnification (d). Images are representative of the results obtained from n = 3 annuli. Magnification x 20 unless stated otherwise.

5.5.5 Biomechanical characterisation of native and decellularised porcine mitral valve annuli

For biomechanical testing the native and decellularised annuli (n=12) were split into four regions, these regions were identified as, R1: the posterior (between P2 segment of mitral leaflet), R3: anterior (left commissure to right commissure), R2: right commissure (P3 segment of mitral leaflet to right commissure) of the posterior annulus and R4: left commissure (P1 segment of mitral leaflet to left commissure) of the posterior annulus.

The stress-strain curves for the decellularised and native porcine mitral valve annuli for regions 1 to 4 are shown in Fig 5.17 to Fig 5.20. The stress strain curves for all the decellularised tissues from the four regions appeared to have larger variability compared to the native tissues. Comparing the slopes between regions for both the decellularised and native tissues it was apparent that region 3 had much greater ultimate tensile stresses and lower ultimate tensile strains compared to regions 1, 2 and 4.

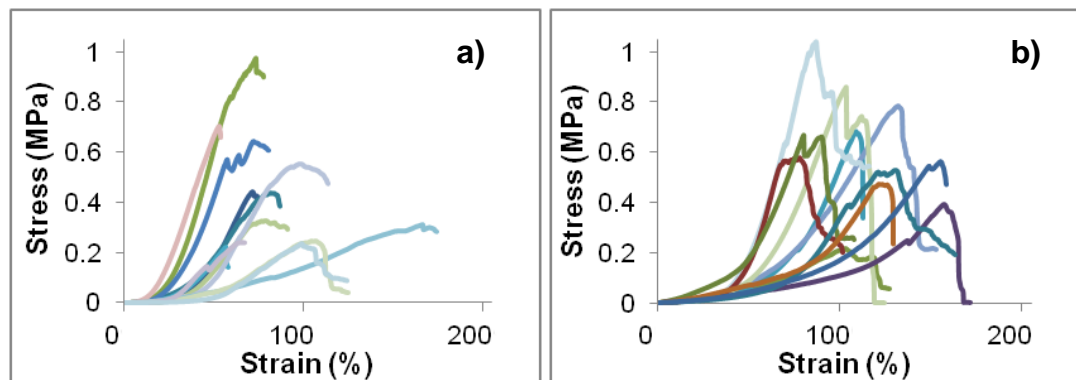


Fig 5.17 – Stress/strain curves for native and decellularised porcine mitral valve annuli in region 1 (posterior region). a) Native porcine mitral valve annulus region 1, b) Decellularised porcine mitral valve annulus region 1.

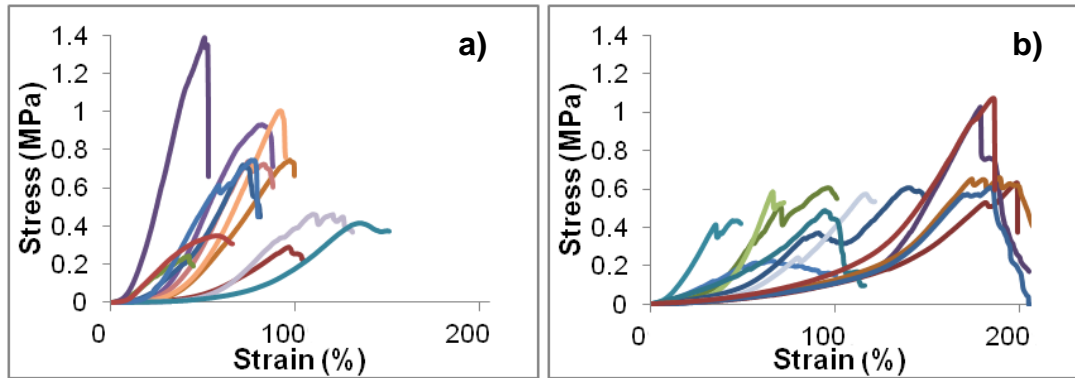


Fig 5.18 – Stress/strain curves for native and decellularised porcine mitral valve annuli in region 2 (right commissural region). a) Native porcine mitral valve annulus region 2, b) Decellularised porcine mitral valve annulus region 2.

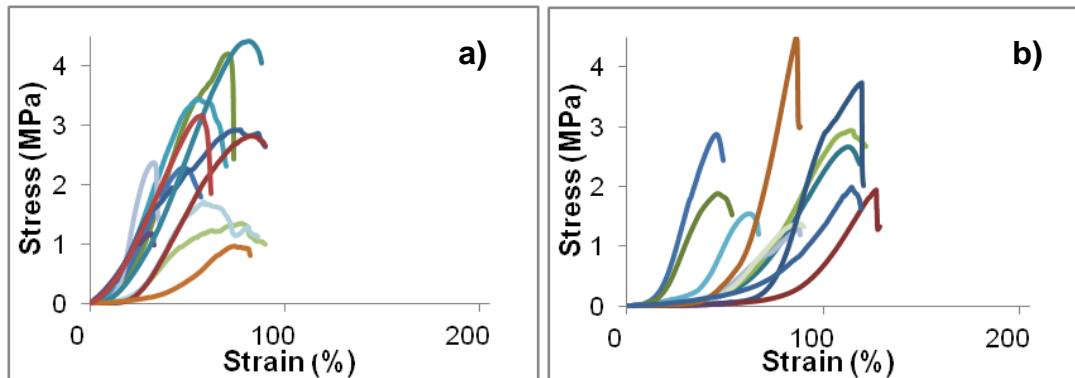


Fig 5.19 – Stress/strain curves for native and decellularised porcine mitral valve annuli in region 3 (anterior region). a) Native porcine mitral valve annulus region 3, b) Decellularised porcine mitral valve annulus region 3.

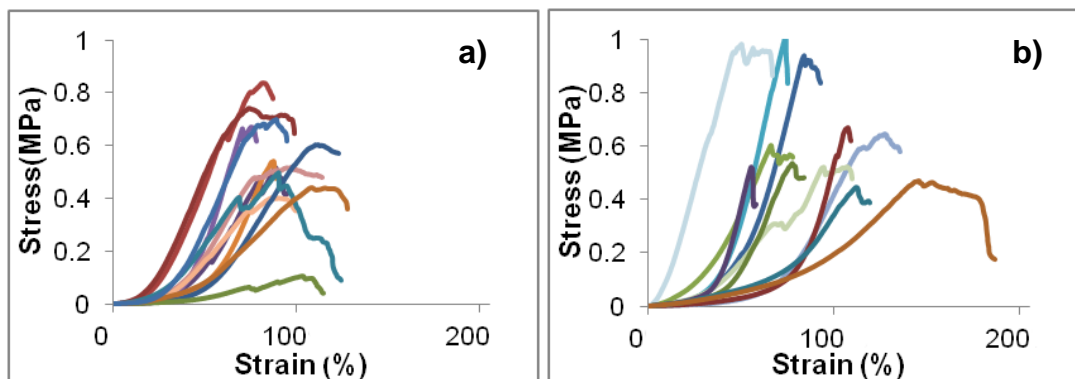


Fig 5.20 – Stress/strain curves for native and decellularised porcine mitral valve annuli in region 4 (left commissural region). a) Native porcine mitral valve annulus region 4, b) Decellularised porcine mitral valve annulus region 4.

The various biomechanical parameters (elastic phase modulus, collagen phase modulus, ultimate tensile stress, ultimate tensile strain, transition stress and transition strain) for the decellularised and native porcine mitral valve annulus tissues from regions 1 to 4 were extracted from the stress strain curves as described in Chapter 2, Section 2.2.6 and the mean (n=12) values are shown in Fig 5.21 to Fig 5.26.

The Young's modulus in the elastic region of the stress strain curves showed a high level of variation between the regions of the annulus in the native tissue, with a modulus of 0.83 MPa in region 3 compared to 0.05 MPa in region 1, 0.07 MPa in region 2 and 0.05 MPa in region 4. The Young's modulus in the elastic region of the stress strain curves for the decellularised tissues revealed that the modulus in region 3 was reduced to 0.12 MPa compared to native tissue with little effect of the decellularisation treatment on the elastic modulus in regions 1, 2 and 4. The data was analysed by two-way analysis of variance which revealed that the effect of decellularisation on Young's Modulus in the elastic phase of the stress-strain curve was dependent upon the region of the annulus (Fig 5.21). There was a significant interaction between the type of tissue (native versus decellularised) and the region of interest. This was the result of the differences in the Young's modulus in region 3 between the native and decellularised tissue but not for regions 1, 2 and 4. The Young's modulus for the native tissue in region 3 was significantly higher compared to native tissue in the other regions, whilst in the decellularised group there were no differences between regions. These results would seem to suggest that for region 3, decellularisation caused a reduction in Young's modulus in the elastic phase compared to the native tissue group.

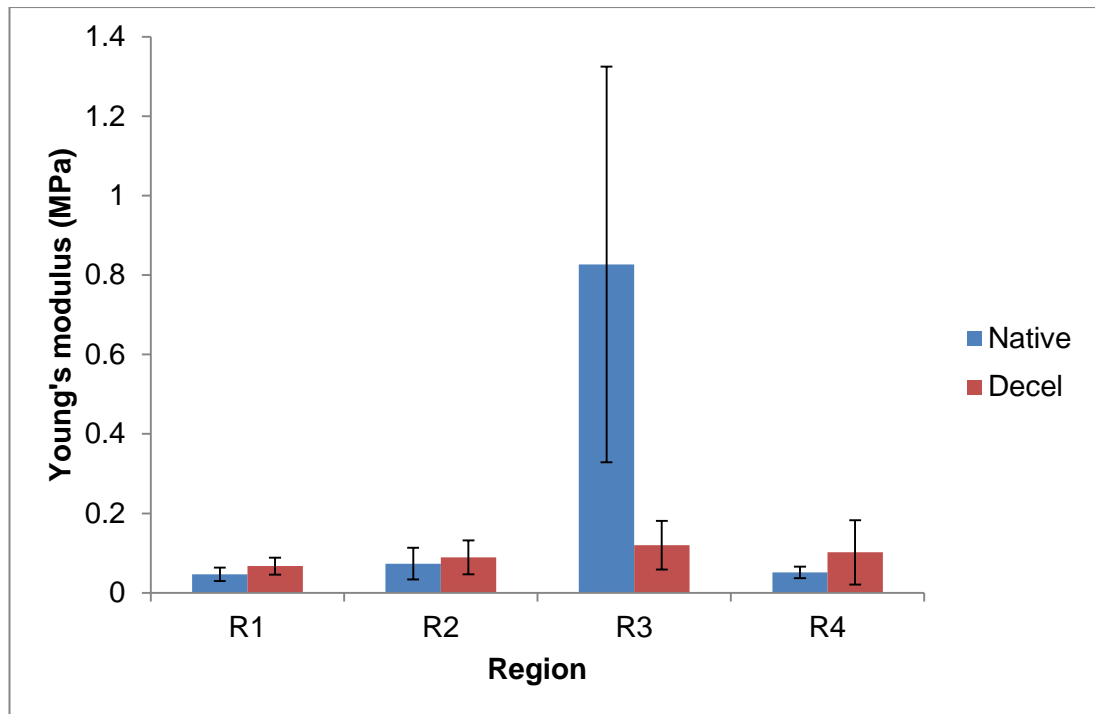


Fig 5.21 – The Young's Modulus in the elastic phase of each region of the native and decellularised porcine mitral valve annulus. Data is presented as the mean ($n = 12$) \pm 95 % CI. Data was analysed by two way ANOVA with replication that showed significant interaction between regions and the tissue, on the elastic phase modulus ($p < 0.05^*$). Perusal of the data revealed that this was due to a reduction in the modulus in region R3 following decellularisation. R1 = Posterior annulus, R2 = Right commissure, R3 = Anterior annulus, R4 = Left commissure.

The Young's modulus in the collagen region of the stress strain curves also showed a high level of variation between the regions of the annulus in the native tissue, with a modulus of 7.33 MPa in region 3 compared to 1.27 MPa in region 1, 2.17 MPa in region 2 and 1.23 MPa in region 4. The data for the Young's modulus in the collagen region of the stress strain curves for the decellularised tissues was similar to that of the native tissue in all four regions. The data was analysed by two-way analysis of variance which revealed that there was no effect of decellularisation on Young's modulus in the collagen phase of the stress-strain curve when compared to native tissue for the same mitral valve annulus region (Fig 5.22). Analysis of Young's modulus between regions showed that for both the decellularised and native porcine mitral valve annuli there were significant differences between region 3 and the other regions. Evaluation of the data revealed that the Young's modulus in the collagen phase for the native annuli was significantly higher in region 3 ($p < 0.05$; MSD = 2.32) compared to region 1, region 2 and region

4 and significantly higher for the decellularised mitral valve annuli in region 3 ($p < 0.05$; $MSD = 2.82$) compared to region 1, region 2, and region 4.

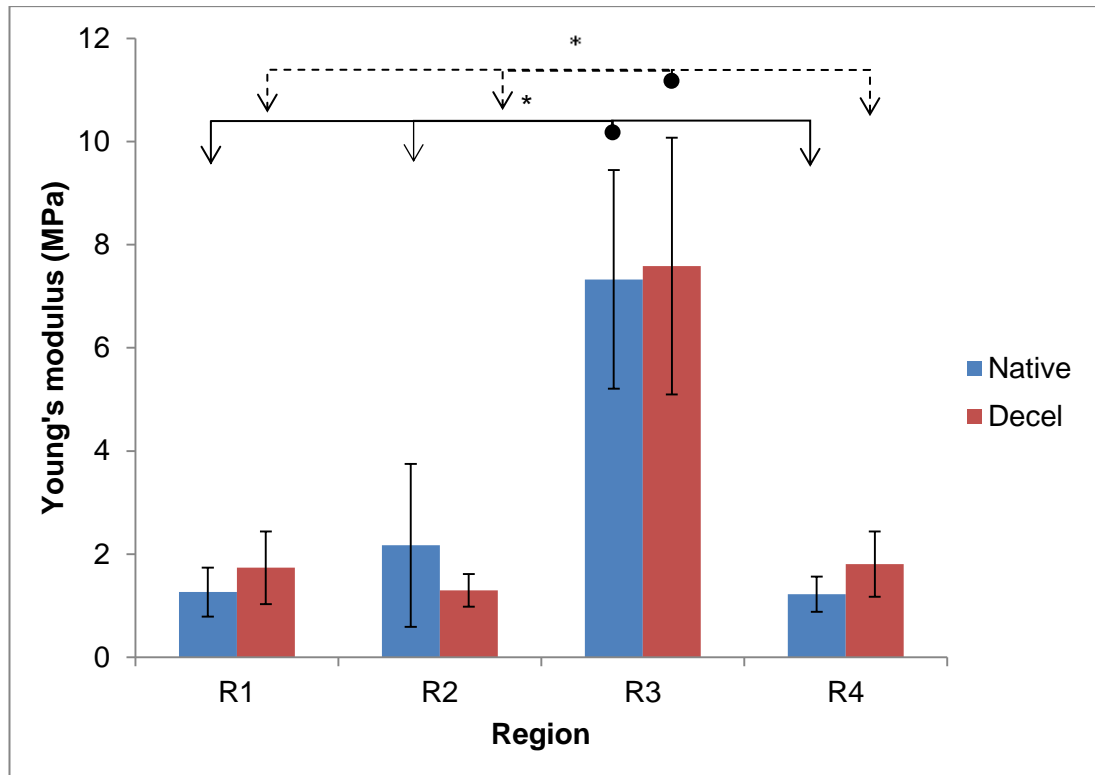


Fig 5.22 – The Young's Modulus in the collagen phase of each region of the native and decellularised porcine mitral valve annulus. Data is presented as the mean ($n = 12$) \pm 95 % CI. Data was analysed by two way ANOVA with replication followed by calculation of MSD using the T-test. Results showed significant differences between region 3 and the other regions for both native ($p < 0.05^*$; $MSD = 2.32$) and decellularised tissue ($p < 0.05^*$; $MSD = 2.82$) but not between the tissue types in the same region. R1 = Posterior annulus, R2 = Right commissure, R3 = Anterior annulus, R4 = Left commissure.

The data for the ultimate tensile stress of native and decellularised annuli in the four regions tested is presented in Fig 5.23. The ultimate tensile stress showed a high level of variation between the regions of the annulus in the native tissue, with a value of 2.55 MPa in region 3 compared to 0.63 MPa in region 1, 0.67 MPa in region 2 and 0.54 MPa in region 4. The data was analysed by two way analysis of variance. This revealed that there was no significant variation in the ultimate tensile stress between native and decellularised porcine mitral valve annuli for the same region (Fig 5.23). There were however significant differences in the ultimate tensile stress results between region 3 and the other regions for both the native and

decellularised porcine mitral valve annuli. Analysis of the data revealed that the ultimate tensile stress was significantly higher in region 3 ($p < 0.05$; $MSD = 0.70$) compared to region 1, region 2 and region 4 for the native porcine mitral valve annuli and significantly higher in region 3 ($p < 0.05$; $MSD = 0.63$) compared to region 1, region 2 and region 4 for the decellularised mitral valve annuli.

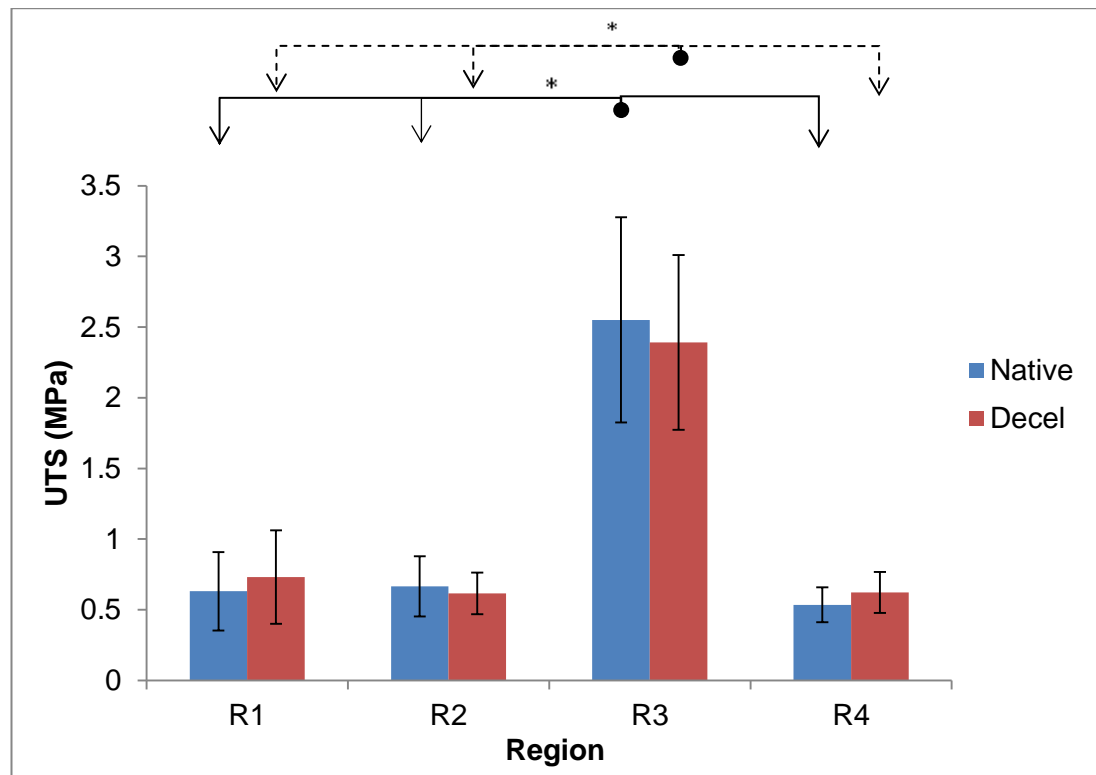


Fig 5.23 – The ultimate tensile stress in each region of the native and decellularised porcine mitral valve annulus. Data is presented as the mean ($n = 12$) \pm 95 % CI. Data was analysed by two way ANOVA with replication followed by calculation of MSD using the T-test. Results showed significant variation between region 3 and the other regions for both native ($p < 0.05^*$; $MSD = 0.70$) and decellularised tissue ($p < 0.05^*$; $MSD = 0.63$) but not between the tissue types in the same region. R1 = Posterior annulus, R2 = Right commissure, R3 = Anterior annulus, R4 = Left commissure.

The results for the ultimate tensile strain of native and decellularised annuli in the four regions tested is presented in Fig 5.24. The data showed little variation between the regions of the annulus in the native tissue, with values of 76.14 % in region 1, 81.65 % in region 2, 60.26 % in region 3 and 87.00 % in region 4. The data was analysed by two way analysis of variance. This revealed that the effect of decellularisation on the ultimate tensile strain was

dependent on the mitral valve annulus region. Further analysis of the data using the T-test revealed that the ultimate tensile strain of the decellularised tissue was higher than the native tissue in region 1, 2 and 3 ($p < 0.05$). The ultimate tensile strain for the native porcine mitral valve annuli in region 4 was significantly higher than region 3 ($p < 0.05$; $MSD = 21.95$), with no significant differences between the ultimate tensile strains in all regions for the decellularised porcine mitral valve annulus (Fig 5.24).

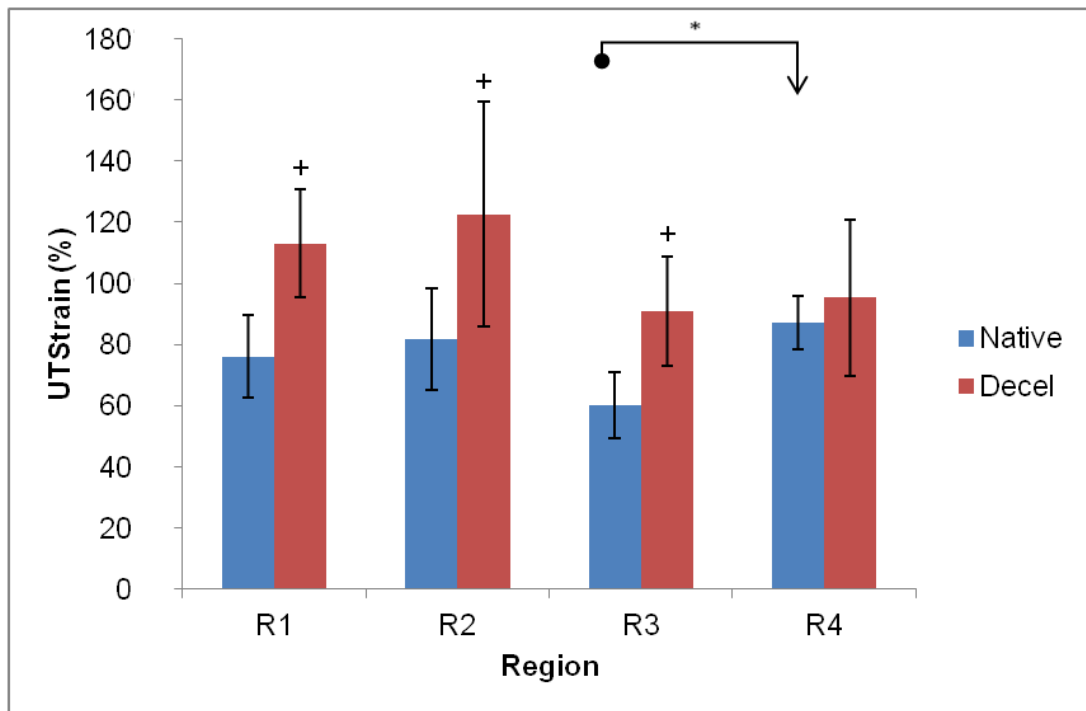


Fig 5.24 – The ultimate tensile strain in each region of the native and decellularised porcine mitral valve annulus. Data is presented as the mean ($n = 12$) \pm 95 % CI. Data was analysed by two way ANOVA with replication followed by calculation of MSD using the T-test. Analysis showed significant variation between regions 3 and 4 for the native tissue ($p < 0.05^*$; $MSD = 21.95$) and between the native and decellularised tissue types in regions 1, 2 and 3 ($p < 0.05^+$). R1 = Posterior annulus, R2 = Right commissure, R3 = Anterior annulus, R4 = Left commissure.

The data for the transition stress of native and decellularised annuli in the four regions tested is presented in Fig 5.25. The data showed a high level of variation between the regions of the annulus in the native tissue, with a value of 0.22 MPa in region 3 compared to 0.06 MPa in region 1, 0.07 MPa in region 2 and 0.07 MPa in region 4. The data was analysed by two-way analysis of variance which showed that the effect of decellularisation on the

transition stress depended upon the annulus region. There were differences in the transition stress in regions 1, 2 and 4 between the native and decellularised porcine mitral valve annulus but not for region 3. Evaluation of the data showed significantly higher transition stresses in the decellularised porcine mitral valve annulus compared to the native annulus for regions 1, 2 and 4 ($p < 0.05$). There were regional differences in the transition stresses for both the native and decellularised tissue groups. For the native porcine mitral valve annuli the transition stress between regions was significantly higher in region 3 compared to region 1, 2 and 4 ($p < 0.05$; MSD=0.06) and for the decellularised porcine mitral valve annulus, significantly higher in region 3 compared to regions 2 and 4 ($p < 0.05$; MSD=0.15).

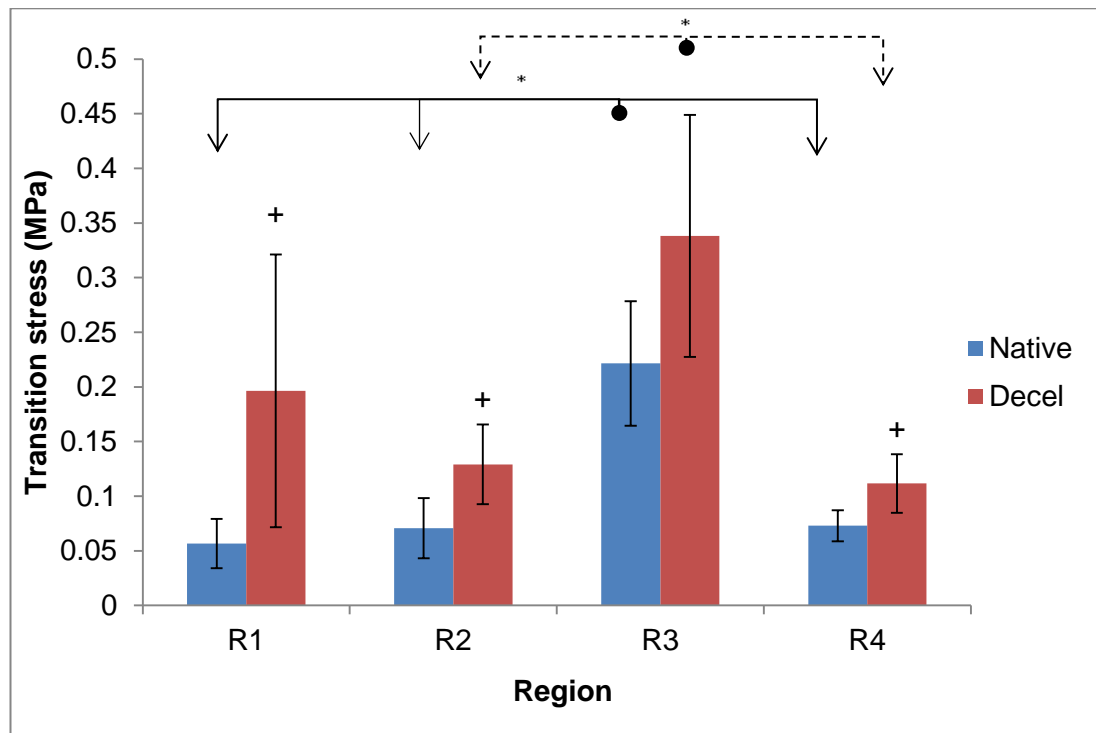


Fig 5.25 – The transition stress in each region of the native and decellularised porcine mitral valve annulus. Data is presented as the mean ($n = 12$) \pm 95 % CI. Data was analysed by two way ANOVA with replication followed by calculation of MSD using the T-test. Perusal of the data revealed that there was significant differences between region 3 and the other regions for the native tissue ($p < 0.05^*$; MSD=0.06) and between region 3 and regions 2 and 4 for decellularised tissue ($p < 0.05^*$; MSD=0.15). Significant differences were found between the native and decellularised tissue types in regions 1, 2 and 4 ($p < 0.05^+$). R1 = Posterior annulus, R2 = Right commissure, R3 = Anterior annulus, R4 = Left commissure.

The results for the transition strain of native and decellularised annuli in the four regions tested is presented in Fig 5.26. The data showed little variation between the regions of the annulus in the native tissue, with values of 36.14 % in region 1, 33.77 % in region 2, 23.86 % in region 3 and 36.23 % in region 4. The data was analysed by two-way analysis of variance which showed that the effect of decellularisation on the transition strain was similar in each annulus region. Data analysis revealed that there were significantly higher transition strains in the decellularised porcine mitral valve annuli compared to the native annuli for regions 1, 2, 3 and 4 ($p < 0.05$). There were no significant differences in the transition strains between regions for either the native or decellularised porcine mitral valve annulus tissue (Fig 5.26).

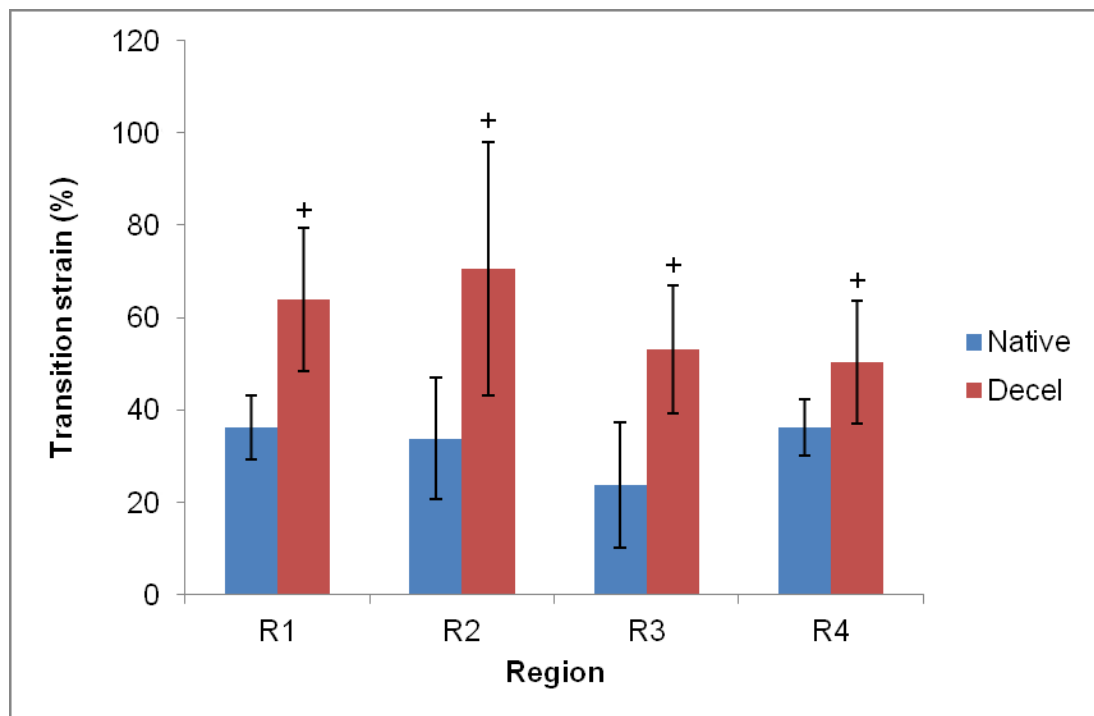


Fig 5.26 – The transition strain in each region of the native and decellularised porcine mitral valve annulus. Data is presented as the mean ($n = 12$) \pm 95 % CI. Data was analysed by two way ANOVA with replication followed by calculation of MSD using the T-test. Analysis of the data revealed significant differences ($p < 0.05^+$) between the native and decellularised tissue types in the same region. R1 = Posterior annulus, R2 = Right commissure, R3 = Anterior annulus, R4 = Left commissure.

5.6 Discussion

The aim of this chapter was to assess the biological and biomechanical properties of decellularised porcine mitral valve annuli and compare them to native porcine mitral valve annuli. Results from chapter 4 revealed that application of decellularisation Method 8 removed over 95% of DNA from all regions of the porcine mitral valve annulus, with residual cell fragments remaining in the lacunae of the trigones. In this chapter further studies were undertaken to determine the effects of the decellularisation process on the porcine mitral valve annulus including, effects on histoarchitecture (Sirius red Miller's), GAG distribution (alcian blue), ECM protein distribution (immunohistochemical staining), biocompatibility (cytotoxicity testing) and biomechanical properties (uniaxial tensile tests).

Decellularisation appeared to have no discernible effect on the histoarchitecture of collagen and elastin fibres, as revealed by Sirius red Miller's staining. The fibrosa layer of the leaflet formed into the annulus and the fibre density and orientation of the leaflet was comparable between the decellularised and native tissue. The trigonal region in the anterior annulus was also comparable between the native and decellularised annuli, with the cartilage-like lacunae being characterised by isotropic fibres.

There was a visible loss of GAGs from both the anterior and posterior regions of the decellularised annulus compared to the native annulus tissue in the same region. In the posterior region of the decellularised tissue the GAGs had been removed from the annular junction where the leaflet joins the annulus. GAGs were retained in the anterior annulus within the trigones but alcian blue staining was less intense within this region. The GAG content of the annulus is likely to contribute to the absorption of some of the forces generated by the heart during the cardiac cycle as reported in the leaflets and chordae of human mitral valves (Grande-Allen *et al.*, 2004). The removal of GAGs from the annular junction, at the region where the leaflets hinge, may have little effect due to the removal of the leaflets prior to the decellularisation of the mitral valve annulus, with the motion of the leaflets likely to contribute to the compressive forces in the annular junction. GAG removal from the trigones, as a result of decellularisation, would potentially affect the biomechanical characteristics, due to the retention of the trigones. However, GAGs were present in the trigonal regions after decellularisation but staining was reduced compared to the native porcine trigonal region. GAG removal from decellularised porcine tissue was also evident in previous studies carried out at the University of Leeds, including in pericardium

(Morticelli *et al.*, 2013), porcine bladder (Bolland *et al.*, 2007), porcine medial meniscus (Stapleton *et al.*, 2008) and porcine pulmonary valves (Luo *et al.*, 2014).

Immunohistochemical analysis of both the anterior and posterior regions revealed a loss of proteins associated with the basement membrane. Sections of decellularised porcine mitral valve annulus stained with antibodies to collagen IV and fibronectin revealed less intense staining in the annulus and leaflets, as well as the surrounding muscle compared to sections of the native porcine mitral valve annulus from the same regions, whilst there was reduced staining of sections labelled with antibodies to collagen VI in the myocardium. Sections of the decellularised annulus labelled with antibodies to laminin showed no positive staining, with laminin appearing to be completely removed by the decellularisation process. Removal of antibody staining of basement membrane proteins has been shown before in studies using similar decellularisation processes at the University of Leeds, for example removal of collagen IV and laminin in decellularised porcine bladder (Bolland *et al.*, 2007) and collagen IV in porcine pulmonary valves (Luo *et al.*, 2014). Recently it has been suggested that the PAA step of the decellularisation protocol is associated with removal of antibody staining of collagen IV in the basement membrane (Luo *et al.*, 2014). Whether the lack of immuno-staining for proteins such as collagen IV and laminin following decellularisation is due to a loss of the protein or a change in conformation of the protein leading to lack of antibody binding is not known. The presence of a functional basement membrane would be important for acellular biological scaffolds intended for certain applications requiring regeneration with epithelial cells, such as blood vessels. An acellular biological annular ring would reinforce mitral valve repair and reduce mitral valve orifice area, therefore retention of the collagen fibres involved with the biomechanical characteristics, such as collagens I and II, would be important, whereas retention of basement membrane components would be of no obvious value.

Whilst PAA has been cited as the chemical involved with removal of immunostaining for collagen IV in the basement membrane, studies have found that acellular human flexor tendon scaffolds treated with PAA showed improved cell attachment and increased matrix porosity (Woon *et al.*, 2011). This has also been reported for decellularised porcine temporomandibular joint discs, although PAA treatment did produce scaffolds with weaker compressive biomechanical properties (Matuska & McFetridge, 2015).

Immunohistochemical analysis of collagens I, II and III in the decellularised porcine mitral valve annulus tissue sections showed good retention of these structural proteins compared to the native tissue.

Biomechanical testing was completed on both the native and decellularised tissue in four regions of the porcine annulus. It was split into the anterior, left commissural, posterior and right commissural sections. The biomechanical parameters of the posterior region of the native annulus illustrated the lack of a dense collagen structure compared to the anterior region of the native annulus. The anterior annulus had a dense collagenous structure and biomechanical testing revealed that compared to the rest of the annulus this structure was associated with high Young's modulus and a tissue that withstood high load before failure. The anterior annulus attaches to the cardiac skeleton which provides a strong foundation to the whole of the heart; it ensures structural integrity for the mitral valve when it is functioning normally and elucidates the biomechanical requirements of the anterior annulus compared to the posterior annulus in the mitral valve. The posterior annulus undergoes up to 8% circumferential strain during the cardiac cycle, compared to 4% in the anterior (Timek *et al.*, 2003) in ovine hearts. This flexibility provides the primary mode of dilation and contraction of the annulus during the cardiac cycle (Eckert *et al.*, 2009). The ventricular and atrial myocardium were found to run in a circumferential orientation near to the annulus. The presence of the muscle close to the annulus may assist in leaflet coaptation during the systole phase of the cardiac cycle (Flachskampf *et al.*, 2000; Pai *et al.*, 2003). Gunning & Murphy (2014) undertook uniaxial tensile testing on porcine mitral valve annuli by segmenting the annulus into four regions: anterior, posterior, and left and right commissural sections. Tissue was preconditioned prior to uniaxial tensile testing, after which it was subjected to a strain rate of 2 mm/min up to a strain of 6 %. Moduli were calculated when the tissue had undergone 2 % and 6 % strain. The results for the native porcine mitral valve annulus in this study closely resembled the general outcomes from the study by Gunning & Murphy (2014). The anterior region tested between the trigones, had significantly higher ($p < 0.05$) Young's modulus compared to the other regions of the porcine mitral valve annulus. The modulus in the Gunning & Murphy study was only analysed at 2 % and 6 % strains, the tissue was preconditioned and the true stress and strain was calculated instead of the engineering stress and strain, so a direct comparison between studies cannot be made.

Compared to the native porcine mitral valve annulus the decellularised mitral valve annulus demonstrated larger ultimate tensile strains, transition strains and transition stresses. Ultimate tensile strains in all regions were significantly higher in the decellularised tissue compared to the native tissue, apart from region 4, the left commissure region, in which levels did not reach significance. These changes were comparable to alterations to biomechanical characteristics found in previous studies that have utilised 0.1 % (w/v) SDS during decellularisation. For example, the ultimate tensile strain was decreased in acellular porcine bladder matrix compared to native porcine bladder (Bolland *et al.*, 2007), whilst in decellularised human pericardium (Mirsadraee *et al.*, 2006) and decellularised porcine aortic leaflets (Korossis *et al.*, 2002) there was an increase in extensibility compared to native tissue. Transition stresses were all higher in the decellularised regions of the porcine mitral valve annuli compared to the same native tissue regions but significance was not reached in the anterior region, this has also been found in decellularised porcine pericardium (Morticelli *et al.*, 2013). Transition strains were all significantly higher in the decellularised mitral valve annulus compared to the native mitral valve annulus, similar results have been found in decellularised porcine aortic roots (Korossis *et al.*, 2005) and decellularised porcine pericardium (Morticelli *et al.*, 2013). Similar to the biomechanical results for decellularised porcine mitral valve annuli, there was no impact on the ultimate tensile strength of the various tissues studied previously, and apart from the study by Korossis *et al.* (2002) there has been found to be no impact on the collagen phase slope. The increased extensibility of decellularised porcine aortic roots was attributed to increased collagen crimping and disruption of the cells in the matrix. Treatment with low concentration SDS does seem to have different effects on the biomechanical characteristics depending on the types of tissues. For example, 0.1 % (w/v) SDS treatment resulted in an increased collagen phase slope and a significant decrease in failure strain for porcine bladder tissue (Bolland *et al.*, 2007), in contrast to findings with porcine cardiovascular tissues as discussed above. Decellularisation using SDS has also been reported to induce changes in collagen crimp pattern and tissue structure, leading to reduced cell attachment in ligamentous tissues (Gratzer *et al.*, 2006) and increased extensibility caused by the crimping and the removal of cells during the decellularisation protocol (Korossis *et al.*, 2002).

In the elastic phase of the stress-strain curve decellularisation caused a reduction in the Young's modulus only for region 3, the anterior region. The

other regions of the native tissue had lower Young's modulus compared to the native tissue region 3. After decellularisation the Young's modulus in region 3 was comparable to the other decellularised regions. This phase of the slope represents the region where the forces are distributed through the elastin fibres, which offer minimal resistance to elongation. A reduction of the Young's modulus in this region suggests that the elastin fibres offer less resistance to elongation compared to the native tissue in the same region and will be more compliant in the physiological range of the tissue. No changes were observed in the ultimate tensile stress or collagen phase slope, so the overall strength of this region did not appear to be affected. The other regions were not affected in the same way which is likely due to the different ECM characteristics identified in the histological and biomechanical studies of the native porcine annulus. The anterior annulus is in close proximity to the aortic and pulmonary walls which also exhibited similar changes in decellularisation studies, with a significant decrease in the elastin phase slope in the decellularised porcine aortic wall (Korossis *et al.*, 2005) and porcine pulmonary walls (Luo *et al.*, 2014).

When compared to the biomechanical characteristics of glutaraldehyde treated autologous pericardium (Ozolins *et al.*, 2008), the only other biological tissue used as an annuloplasty device (De La Zerda *et al.*, 2008), the decellularised porcine annulus provides a better match to the different regions of the collagenous anterior and more muscular posterior regions of the human annulus, with the structure of the porcine heart closely matching that of the human heart (Kunzelman *et al.*, 1994, Hearse & Sutherland, 2000).

Extract and contact cytotoxicity assays confirmed that the acellular porcine mitral valve annulus tissue was biocompatible. This inferred that potential toxic chemicals used during the decellularisation process, notably SDS has been adequately washed out. SDS is cytotoxic to cells so it is important that it has been removed from the scaffold (Caamaño *et al.*, 2009; Sakai *et al.*, 1998), BHK and L929 cells grew in contact with the scaffold and scaffold extracts demonstrating that a suitable number of wash cycles had been undertaken as the final step in the decellularisation protocol.

Lectin staining was undertaken to visualise α -gal distribution in the native and decellularised tissue. The α -gal distribution was reduced but not entirely removed from the tissue post decellularisation, the residual α -gal was primarily present within the muscle and not within the annulus. Alpha-gal is the target of pre-formed antibodies in humans and can cause hyperacute

reactions of vascularised tissues and organs (Konakci *et al.*, 2005). Rejection has been identified with antibodies binding to the α -gal epitope on the surface of endothelial cells (Liu *et al.*, 2002).

Whether the presence of residual α -gal in acellular biological scaffolds is a clinical concern is a matter for debate. However, biological scaffolds with residual α -gal have been implanted in millions of patients (D'Eredità, 2015; McPherson *et al.*, 2000; Mostow *et al.*, 2005). Alpha-gal epitopes have been found on commercially available glutaraldehyde fixed bioprosthetic heart valves, although patients implanted with these valves exhibited increased titres of anti-gal antibodies (Konakci *et al.*, 2005). The elimination of the α -gal epitopes on the decellularised tissue could be achieved using α -galactosidase. This has already been used to remove α -gal on porcine aortic valve and pericardial tissue (Park *et al.*, 2009) without detrimental effects on the biomechanical properties (Choi *et al.*, 2012) or by using endo-beta-galactosidase C as used to remove the α -gal epitope from porcine kidneys (Liu *et al.*, 2002).

The results of the biological and biomechanical characterisation of the decellularised porcine mitral valve annulus illustrate that the scaffold could be suitable for use as clinical product. The functional capabilities of the ring will be investigated in the next chapter to determine if it could be considered for future use as a biological acellular annuloplasty ring.

Chapter 6

In vitro evaluation of decellularised porcine mitral annulus for annuloplasty repair

6.1 Introduction

To evaluate the biological acellular annuloplasty ring for use in annuloplasty repair it was necessary to develop an explanted porcine heart model. The gold standard for mitral valve repair is synthetic ring annuloplasty (Fundarò *et al.*, 2007) which necessitated the development of a suitable procedure to compare synthetic rings with the biological acellular annuloplasty ring developed in the previous chapter. Developing a medical device for heart valve repair can be complex, costly and require ethical approval if performing animal trials (Perry, 2007). To reduce this burden a preclinical *in vitro* explanted heart static pressure model was developed to test annuloplasty rings for repair.

In a study by Richards *et al.* (2009), an *in vitro* dynamic heart system was developed in which saline was pumped through the left atrium of porcine hearts at physiological pressures and heart rates. Regurgitation was induced in the hearts by manually dilating the mitral valve annulus and severing chordae tendinae connecting the P2 leaflet to the papillary muscles. For the present study, a static system was proposed rather than a dynamic system as it provided a simple system to measure the rate of regurgitation at maximum normal valve pressures of 120 mmHg. Clinically, annuloplasty repairs are tested by re-pressurising the valve with saline solution to check that the valves are competent before completing the repair procedure. The static method offered an analogous method to *in-vivo* repair whilst ensuring pressures were controlled to the maximum expected during systole, when the mitral valve leaflets are closed and regurgitation occurs. The American Society of Echocardiography defines the rate of regurgitation as mild when regurgitation is less than 30 ml.beat⁻¹, moderate when it is between 30 and 59 ml.beat⁻¹ and severe when regurgitation is more than 59 ml.beat⁻¹ (Zoghbi, 2003).

The model to be developed to test the decellularised porcine annuloplasty rings therefore had the following requirements:

- Be able to achieve repeatable regurgitation volumes at correct pressures that are significantly higher than normal heart regurgitation rates
- To be quick to manufacture
- To be cost effective
- To be suitable for undertaking annuloplasty repair using synthetic and decellularised annuloplasty rings

To reproduce mitral valve regurgitation, porcine hearts were obtained from a local abattoir and the mitral valve complex, which includes the mitral valve leaflets, chordae, papillary muscle and the annulus, was tested under various regurgitation scenarios in a static heart rig.

The main causes of mitral valve regurgitation are ischaemic and non-ischaemic mitral valve disease. These are further subcategorised as functional, which includes ventricular remodelling, or organic, which only involves the mitral valve complex (Enriquez-Sarano *et al.*, 2009).

Remodelling of the heart due to ischaemic mitral valve disease can cause annulus dilation (Boltwood *et al.*, 1983; Kaplan *et al.*, 2000; Mihalatos *et al.*, 2007), whilst non-ischaemic regurgitation tends to be caused by myxomatous mitral valve disease in which the connective tissue is weakened causing valve prolapse and mitral annular dilation (Bulkley & Roberts, 1975; Ormiston *et al.*, 1982; Mihalatos *et al.*, 2007). It has also been reported that annular dilation can occur independently of mitral valve prolapse and left ventricular remodelling (Mihalatos *et al.*, 2007) although this finding is controversial with other studies reporting that this is not the case (Otsuji *et al.*, 2002). Other causes of mitral regurgitation include endocarditis, chordae rupture due to myxomatous valve disease, papillary muscle rupture due to myocardial infarction (Stout & Verrier, 2009) and annulus dilation alongside mitral valve prolapse, due to rheumatic mitral valve disease (Marcus, 1994). It was therefore logical to investigate models that were representative of these modes of mitral valve regurgitation. Previous methods of inducing regurgitation *in-vivo* in the mitral valve include chordal rupture in dogs (Urabe *et al.*, 1992, Pat *et al.*, 2010) and the application of collagenase in the hearts of dogs (Fujiki *et al.*, 2000). *In-vitro* methods used chordal rupture alongside annular dilation in porcine hearts (Richards *et al.*, 2009). The protocol that provided repeatable rates of regurgitation whilst being suitable for annuloplasty repair would be developed and utilised as the regurgitation model for testing the rings.

6.1.1 Aims and objectives

Aims:

The aim of this chapter was to establish methods for invoking regurgitation in the mitral valve of porcine hearts and to undertake a comparative *in-vitro* evaluation of biological acellular rings to synthetic annuloplasty rings currently used for valve repair due to mitral valve regurgitation.

Objectives:

To perform *in-vitro* evaluation of the acellular annuloplasty rings by comparing the decellularised annuloplasty rings with synthetic rings using an explanted porcine heart regurgitation model:

- To develop a method for producing regurgitant porcine hearts *in-vitro*
- To repair the regurgitant porcine hearts using synthetic annuloplasty rings
- To repair the regurgitant porcine hearts using decellularised annuloplasty rings
- To compare the decrease in regurgitant volume as a result of repair using decellularised porcine mitral valve annuli vs synthetic annuloplasty rings.

6.2 Material and methods

6.2.1 Working solutions

6.2.1.1 PBS wash buffer with EDTA (0.1 % w/v), Aprotinin (10 KIU.ml⁻¹ aprotinin)

Ten Oxoid Dulbecco PBS tablets were dissolved in 1 L of distilled water and pH adjusted to 7.2 – 7.4. EDTA (1 g) was added to the solution with 1 ml of aprotinin (10000 KIU.ml⁻¹).

6.2.1.2 Transport medium

Aprotinin (1 ml, 10,000 KIU.ml⁻¹) and HEPES (5 ml, 1M) was added into 500 ml of HBSS and made up for each heart.

6.2.1.3 Trypsin (11250 U.ml⁻¹) solution

Trypsin (1 g) was added to 15 ml of PBS and mixed using a magnetic stirrer.

6.2.2 Static regurgitation testing of porcine mitral valves

To compare the functional repair capabilities of the decellularised annuloplasty rings compared to synthetic annuloplasty rings, regurgitation testing of the porcine mitral valve was undertaken using a static heart test rig. The tests quantified the regurgitant volumes under four different scenarios:

1. Normal healthy mitral valve
2. Valve with induced mitral regurgitation
3. Repaired mitral valve using synthetic annuloplasty rings
4. Repaired mitral valve using biological acellular annuloplasty rings

Two controls were used for the testing. The negative controls were fresh porcine hearts without any induced regurgitation. Positive controls were hearts with a hole punched in the anterior leaflet to invoke regurgitation at clinically relevant levels of 100 ml.s⁻¹. The time taken for the pressure to drop from 120 mmHg to 100 mmHg and from 120 mmHg to 80 mmHg was recorded and used to calculate leakage rates. Leakage rates were converted from ml.s⁻¹ to ml.beat⁻¹ by equating one beat to 0.3 seconds which is equivalent to the time period of the systolic contraction of the heart (Weissler *et al.*, 1961).

6.2.2.1 Fresh porcine heart preparation

Fresh porcine hearts were supplied by local abattoirs. These had been removed from Large White pigs approximately 24-26 weeks old which had been slaughtered within 24 hours of transport to the laboratory. Excess non-heart tissue and pericardium was removed (Fig 6.1a) and an incision was made around the aorta, where it branches to the brachiocephalic artery, the left common carotid artery and the left subclavian artery, preserving the ascending aorta (Fig 6.1b). The pulmonary and aortic roots were separated via the membrane connecting them. Using scissors, an incision was made in the membrane and the roots were separated (Fig 6.1b). An incision was made in the left auricle just above its junction with the left ventricle and the left auricle was removed to reveal the left atrium (Fig 6.1c). Aortic leaflets were removed by holding each leaflet in a tissue clamp and carefully cutting it with scissors (Fig 6.1d). The right coronary artery branching from the aorta was identified, adipose tissue surrounding the right coronary artery was removed with scissors. Sutures (size 3-0) were tied around the artery to prevent saline flowing to the myocardial tissue, tissue clamps were also used to clamp the artery. The left coronary artery branching from the aorta was identified. Adipose tissue surrounding the left coronary artery was removed with scissors. Sutures (size 3-0) were tied around the artery to prevent saline flowing to the myocardial tissue, tissue clamps were also used to clamp the left coronary artery. The prepared hearts were washed in PBS wash buffer with EDTA and aprotinin for 30 minutes three times at room temperature and then stored overnight in transport medium at 4 °C.

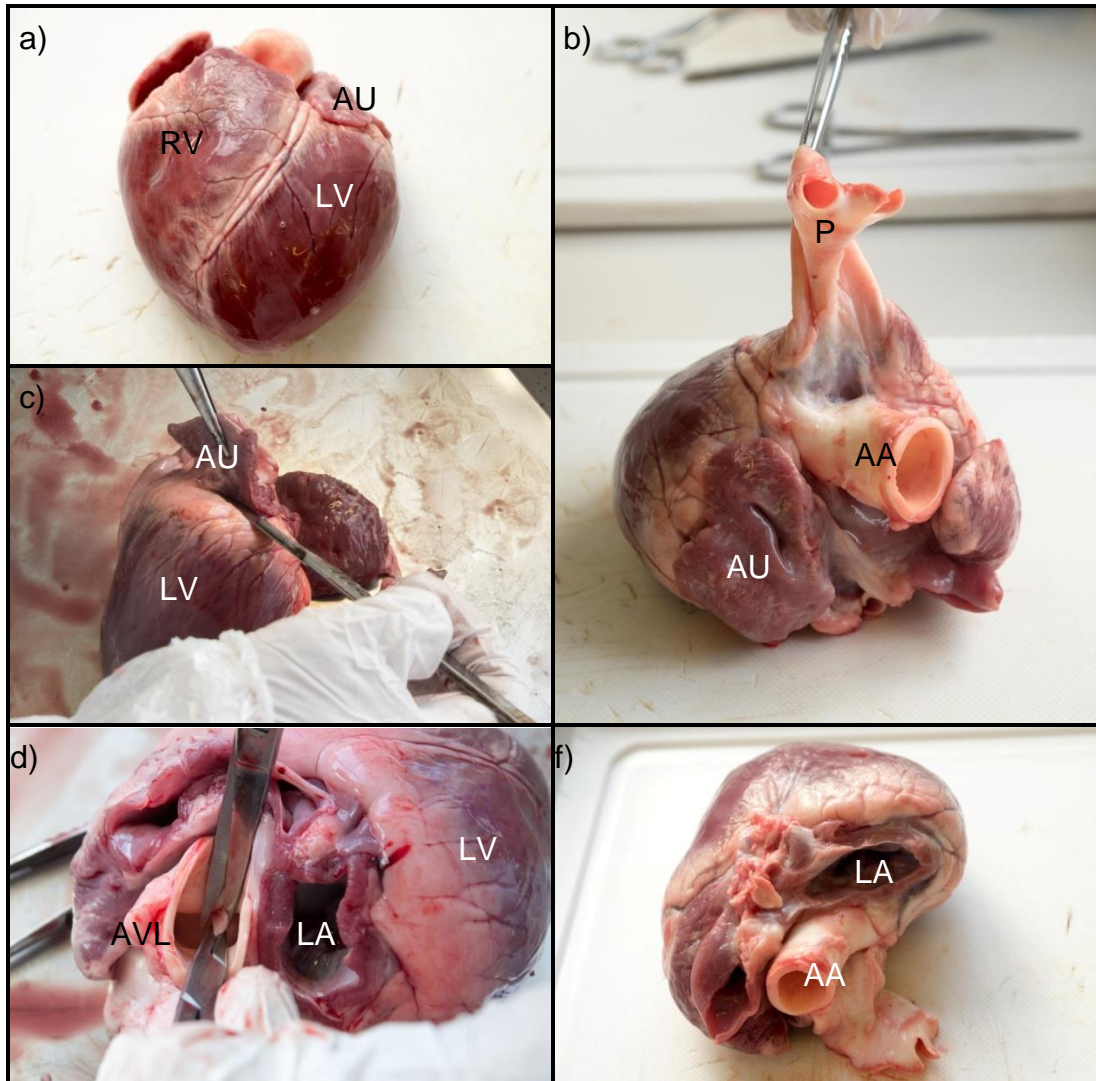


Fig 6.1 – Preparation of porcine tissue for static testing. Whole heart (a), splitting of aorta and pulmonary valve (b), removal of left auricle (c), cutting of aortic valve leaflets (d). AA: Ascending aorta, AU: Left auricle, AVL: Aortic valve leaflet, LA: Left atrium, LV: Left ventricle, RV: Right ventricle.

6.2.2.2 Static test rig preparation

A Perspex column 1832 mm high was used to create a pressure head of 120 mmHg for testing the hearts (Fig 6.2). The test rig was marked with pressures in 20 mmHg intervals up to 120 mmHg and could be drained via an outlet drainage pipe at the base. A valve mounting block was attached to the column at the base where the hearts were cannulised by a spigot. The test rig was placed into a large plastic container and secured to the bench with a clamp (Fig 6.3a). Hearts were attached to the static test rig via a medium sized spigot, 'o' rings were placed on either side of the spigot and inserted together into the valve mounting block (Fig 6.3b). The assembly

was fixed into position by a Perspex plate attached by three bolts. The spigot was cannulised via the aorta and secured by cable ties (Fig 6.3b).

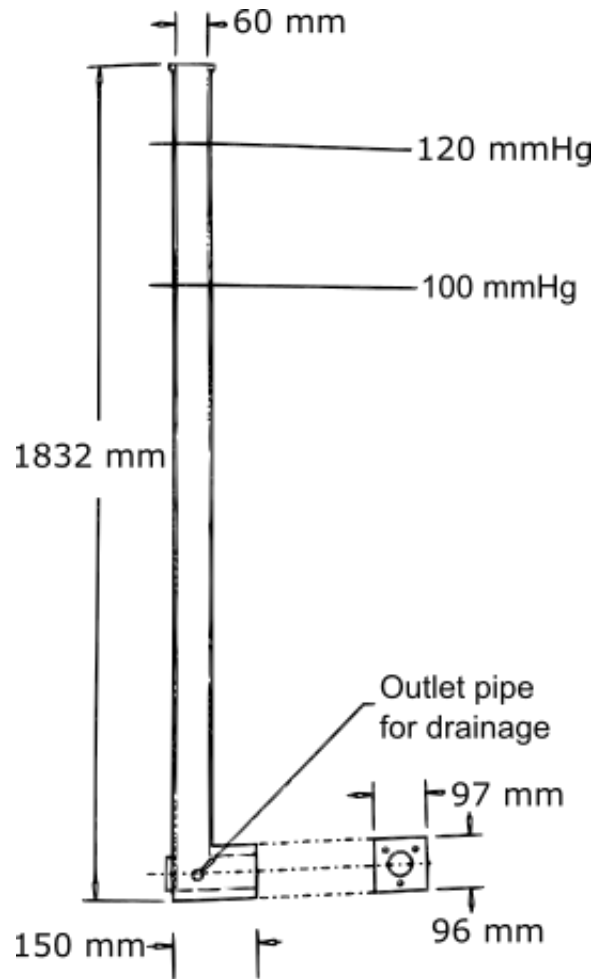


Fig 6.2 – Side profile of static test rig Static test rig to test regurgitation on porcine hearts using a column of saline to pressurise the left ventricle.

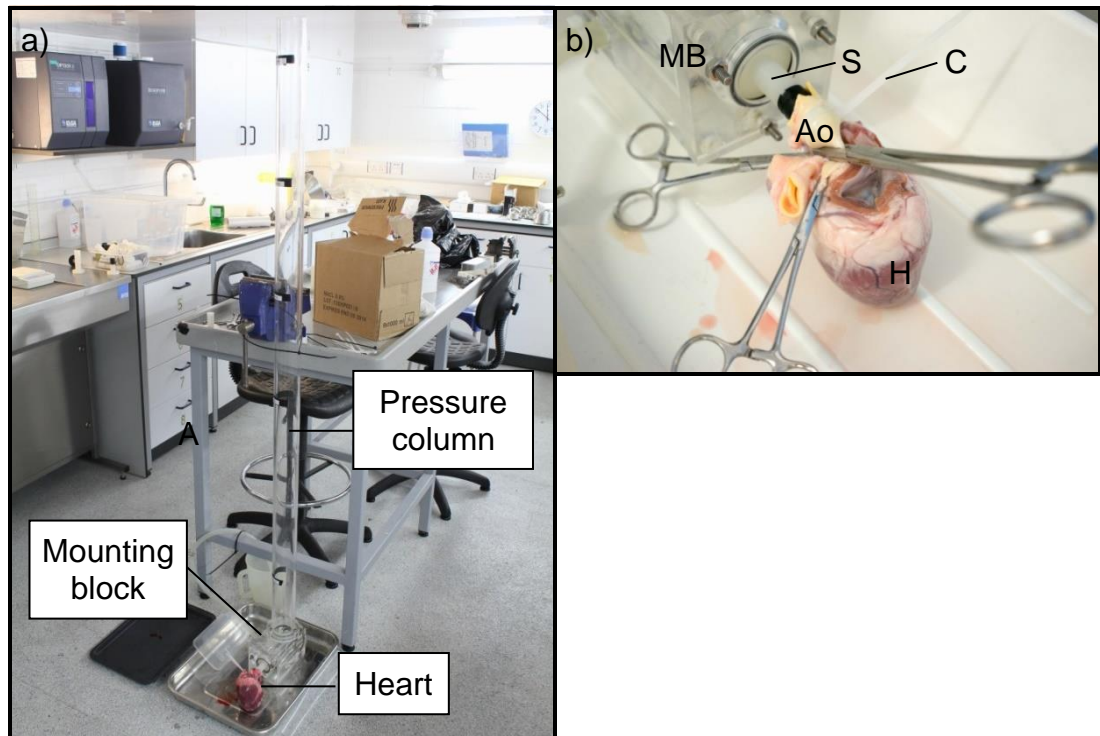


Fig 6.3 – Porcine heart attachment to the static test rig Fresh porcine hearts were cannulated to the static test rig (a) via a spigot and fastened using a cable tie (b). Anterior and posterior coronary arteries were closed using tissue clamps. Ao: Aorta, C: Cable tie, H: Heart, MB: Mounting Block, S: Spigot.

Prior to testing, the aorta was clamped to prevent saline from entering the heart before the timer was started (Fig 6.3b). The column was filled to the 120 mmHg mark using 0.9% (w/v) saline. At the beginning of the test the clamp was removed from the aorta and the heart checked for leaks from regions other than the mitral valve. The primary cause of leaks was from the coronary arteries. This was resolved using sutures or tissue clamps to tie off the arteries. Once leaks were stopped the aorta was clamped and the column was re-filled to 120 mmHg. Hearts were covered with a plastic container to prevent the saline from spraying during the test. Each test started with the removal of the clamp and a stop watch started.

6.2.2.3 Healthy heart model

The time for the column to drop from 120-100 mmHg and 120-80 mmHg was recorded. The valve was considered to be competent if the pressure head did not drop from 120 mmHg to 80 mmHg after a period of 20 minutes.

6.2.2.4 Positive control heart model

A hole was punched in the A2 cleft of the anterior leaflet. The diameter of the hole required to cause moderate regurgitation was estimated using the Bernoulli equation (Eq 6.1) and the equation for flow rate through a pipe (Eq 6.2):

$$P_1 + 0.5 \times \rho \times v_1^2 + h_1 \rho g = P_2 + 0.5 \times \rho \times v_2^2 + h_2 \rho g \quad (6.1)$$

$$\text{Pipe diameter} = \sqrt{\frac{4 \times f_1}{\pi \times v^2}} \quad (6.2)$$

Where:

$$P_1 = \text{Max pressure (Kg.m}^{-2}\text{)}$$

$$h_2 = \text{height at puncture hole (m)}$$

$$P_1 =$$

$$h_2 = 0.1 \text{ m}$$

$$16000 \text{ (Kg.m}^{-2}\text{) (120 mmHg)}$$

$$P_2 = \text{Pressure in atrium (Kg.m}^{-2}\text{)}$$

$$v_1 = \text{velocity at } h_1 \text{ (m.s}^{-1}\text{)}$$

$$P_2 = 0 \text{ (Kg.m}^{-2}\text{)}$$

$$v_1 = 0 \text{ m.s}^{-1}$$

$$p = \text{Density of saline (Kg.m}^{-2}\text{)}$$

$$v_2 = \text{velocity at hole (m.s}^{-1}\text{)}$$

$$p = 1004.6 \text{ (Kg.m}^{-2}\text{)}$$

$$f_1 = \text{required flow rate (m}^3\text{.s}^{-1}\text{)}$$

$$h_1 = \text{reference height (m)}$$

$$f_1 = 0.0001 \text{ m}^3\text{.s}^{-1} \text{ for moderate regurgitation}$$

$$h_1 = 0 \text{ m}$$

$$16000 + (0.5 \times 1004.6 \times 0) + 0$$

$$= 0 + (0.5 \times 1004.6 \times v_2^2) + 0.1 \times 1004.6 \times 9.81$$

$$16000 = (502.3 \times v_2^2) + 985.5$$

$$v_2 = \sqrt{\frac{15014.5}{502.3}}$$

$$v_2 = 5.47 \text{ m.s}^{-1}$$

$$\text{Hole diameter} = \sqrt{\frac{4 \times 0.0001}{\pi \times 5.47}}$$

$$\text{Hole diameter} = 4.82 \text{ mm}$$

A hole 4.82 mm in diameter was required to cause a moderate rate of regurgitation of 100 ml.s^{-1} . Using a 5 mm biopsy punch a hole was punched into the A2 cleft of the anterior leaflet (Fig 6.4), ensuring that the part of the leaflet punched did not fold into another cleft on the posterior leaflet during coaptation and prevent leakage.

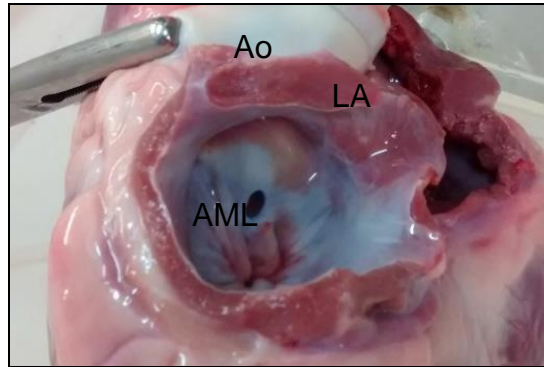


Fig 6.4 – Positive control for the regurgitant porcine heart model. Holes of 5 mm were punched into the A2 cleft of the anterior leaflet using a 5 mm biopsy punch. Ao: Aorta, AU: Left auricle, AML: Anterior mitral valve leaflet, LA: Left atrium, LV: Left ventricle, RV: Right ventricle.

6.2.2.5 Regurgitant porcine heart model

The regurgitant model was designed to permit backflow of saline solution through the mitral valve. Various methods, described below, were assessed to establish a protocol that would provide a repeatable and appropriate rate of regurgitation whilst being suitable for repair.

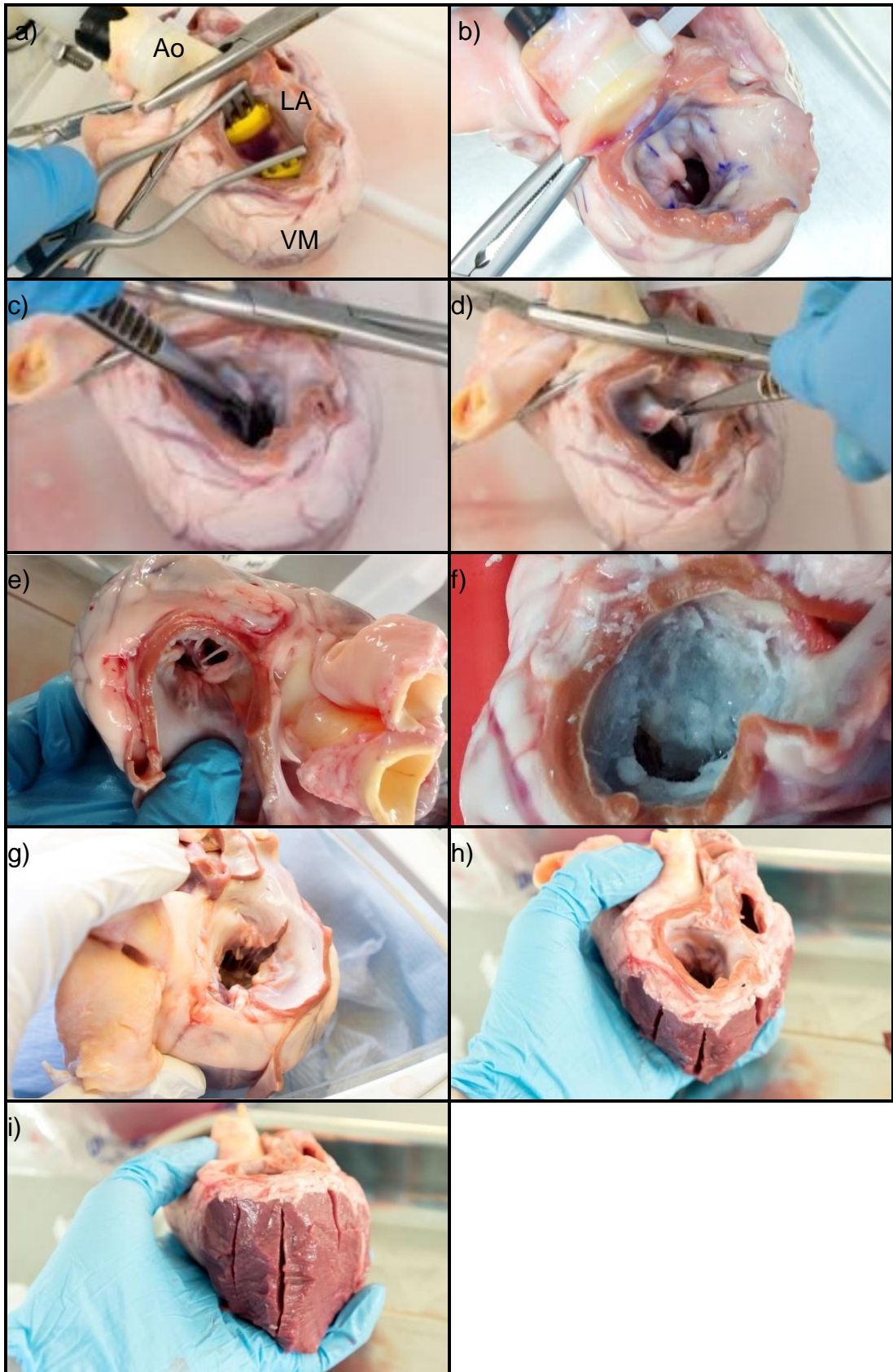


Fig 6.5 – Different methods of inducing mitral valve regurgitation in the porcine heart. Stretch (a), Trypsin treatment (b), Chordae cutting (c, d), Papillary muscle elongation (e), Cyanoacrylate glue (f), Annulus cutting (g), Ventricular muscle trimming (h, i). Ao: Aorta, AU: Left auricle, LA: Left atrium, LV: Left ventricle, RV: Right ventricle.

Methods used to replicate physiological causes of mitral valve regurgitation

For each method tested to replicate mitral valve regurgitation, n=3 hearts were tested using the protocol for measuring regurgitation described in Section 6.2.2.2. If the method resulted in tests that met the criteria of having repeatable regurgitation volumes significantly higher than normal heart regurgitation rates then a further n=3 hearts were subject to the tests.

6.2.2.5.1 Stretching the annulus using retractors

Clinically, the mitral valve annulus dilates in the anterior to posterior dimension up to 25 % which can cause regurgitation. The aim was to replicate this process using this method. Medical grade self-retaining retractors were used to gradually increase the size of the mitral valve orifice by stretching in the anterior to posterior dimension (Fig 6.5a). The dimensions of the valve in the anterior to posterior dimensions were measured using Vernier callipers with the hearts at a pressure of 120 mmHg, hearts were clamped at the aorta to prevent backflow of saline through the mitral valve whilst the valve was stretched. The retractors were opened until the anterior to posterior dimensions were increased by 25 %. Retractors were left in position for ten minutes. The dimensions of the annulus were measured after stretching the tissue and the saline column re-pressurised to 120 mmHg, the retractors were removed before measurement and testing. Hearts were then tested for regurgitation using the method described in Section 6.2.2.2. If sufficient regurgitation had not occurred the aorta was clamped and the annulus was stretched further. The process was repeated until moderate regurgitation occurred or the open limits of the retractors had been met.

6.2.2.5.2 Injecting trypsin around the mitral valve annulus with annulus dilation

Myxomatous mitral valve disease can cause weakening of the mitral valve connective tissue which can lead to regurgitation. To replicate this mode of regurgitation, trypsin (11250 U.ml^{-1}) was applied via injection around the mitral valve annulus of the porcine mitral valve (Fig 6.5b). The points of injection (Fig 6.6) were marked on the valve using surgical marker pen. Trypsin volumes of 0.25 ml were used for each injection site. The trypsin was injected in parallel to the circumference of the annulus, uniformly distributing the trypsin around the annulus. To ensure the trypsin was as uniformly distributed as possible the needle was inserted 5 mm prior to the

injection point and moved into the tissue until the needle tip lined up with the marker. Trypsin (0.125 ml) was injected at the marker and 0.125ml injected gradually as the needle was pulled out.

The trypsin treated tissue was incubated in a humidified container at 37°C for two hours with transport medium surrounding the hearts and padded with tissue paper to stop the hearts falling over, after two hours the trypsin (11250 U.ml^{-1}) was reapplied and the hearts again incubated in a humidified container at 37°C for two hours in transport medium. The hearts were removed from the container and stored in transport medium overnight at 4°C until testing the next day.

Prior to testing, the hearts were stretched by 25 % to increase in anterior – posterior diameter, following the method outlined in Section 6.2.2.5.1.

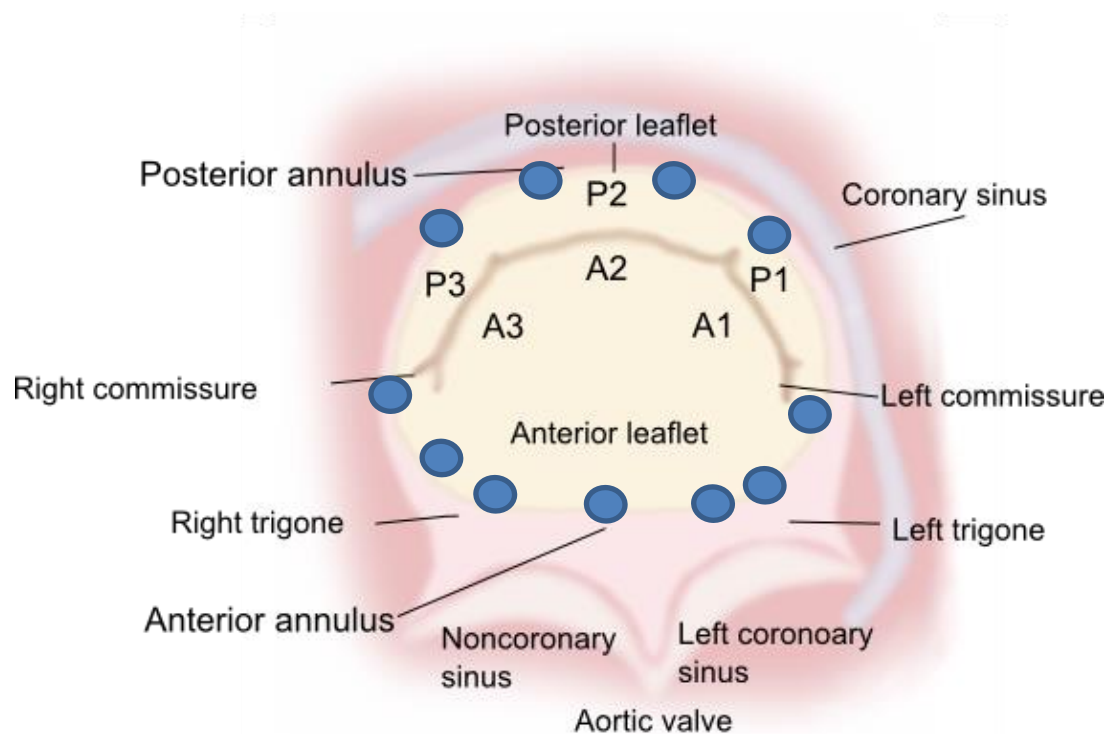


Fig 6.6 – Injection sites for trypsin Syringes were inserted at the blue dot and pushed 5 mm into the annulus in parallel to the circumference.

6.2.2.5.3 Rupturing chordae with annulus dilation

Acute mitral valve regurgitation can be caused by chordal rupture. The chordae attached at the free edge of the A2 leaflet in the mitral valve was identified and cut (Fig 6.5c-d). The method described in Section 6.2.2.5.1 was followed until 25% dilation had occurred to the porcine mitral valve annulus in the anterior to posterior direction, under a pressure of 120 mmHg.

6.2.2.5.4 Papillary muscle dilation with annulus dilation

The chordae can elongate due to myxomatous mitral valve disease. In order to replicate the elongation and subsequent mitral valve prolapse the papillary muscles were partially ruptured. The partial rupture simulated elongation of the chordae. The anterolateral papillary muscle was identified in mitral valve of the porcine heart (Fig 6.5e). Using scissors, the muscle was cut behind the chordae attachment to the muscle until the leaflet attached to the chordae of the muscle displayed signs of prolapse, being careful not to remove the muscle fully from the left ventricular wall. Following papillary muscle partial rupture the annulus was dilated by 25% in the anterior to posterior direction following the protocol described in Section 6.2.2.5.1.

6.2.2.5.5 Super gluing the annulus and leaflets alongside annulus dilation

Endocarditis and rheumatic mitral valve disease can cause the mitral valve to form fibrinous vegetations. Superglue was applied to the mitral valve leaflets to replicate this process. The aorta was clamped and saline solution was removed from the left atrium and left ventricle, using tissue paper to absorb excess solution around the mitral valve. Drops of ethyl cyanoacrylate were applied around the annulus using the insertion points shown in Fig 6.6 for the application points. Drops of ethyl cyanoacrylate were then applied to the atrial surface of the anterior and posterior leaflets ensuring the glue had dried before any tests were conducted. Prior to application of the glue the annulus was dilated by 25 % in the anterior to posterior direction following the protocol described in Section 6.2.2.5.1.

6.2.2.5.6 Trimming the muscle of the left ventricular

Ischaemic mitral valve disease causes the left ventricle to dilate. In order to simulate that effect, the majority of the muscle of the left ventricle was removed. The muscle of the left ventricle was removed until there was approximately 10 mm of muscle remaining between the endocardium and epicardial side of the left ventricle. Muscle was removed from around the annulus in the atrial and ventricular myocardium to increase annulus dilation, until the thickness of the myocardium was approximately 5 mm. The circumferential fibres of the left ventricle were cut axially from the epicardial side of the annulus down towards the apex of the heart in three equally spaced regions (Fig 6.5h-i) to further increase dilation. Following myocardial removal the annulus was dilated by 25% in the anterior to posterior direction following the protocol described in Section 6.2.2.5.1.

6.2.2.5.7 Bisecting the mitral valve annulus at the left commissure

To increase the circumference of the mitral valve annulus and simulate mitral valve dilation, the annulus was bisected. The annulus of each heart was cut at the left commissure where the leaflet length from the annulus was the smallest. It was cut at this point to prevent leakage occurring through the leaflet which would require a more complex repair. The cut intersected the annulus and partially into the muscle wall which also permitted some regurgitation through the cut.

Non-physiological causes of regurgitation

6.2.2.5.8 Cauterising the mitral valve leaflets

Anterior and posterior leaflets were reduced using medium temperature, thick tipped cauterisers. The anterior leaflet was heated until the leaflet shrunk back until no more shrinking occurred. The posterior leaflet of the mitral valve was also heated using cauterisers, until no further shrinkage was visible.

6.2.2.5.9 Zinc fixing the porcine mitral valve complex

Zinc fixative was prepared as described in Chapter 2, Section 2.2.3.1. The left ventricle of each heart was filled with zinc fixative until it covered the mitral valve leaflets. Each heart was placed into a plastic container and the container was padded with tissue paper to keep the hearts upright. The hearts were immersed in transport medium and kept at 4°C for 16 hours overnight. Hearts were then washed in PBS for 30 minutes and placed into transport medium for storage before testing.

6.2.2.6 Repaired heart model

The final method chosen to induce regurgitation in the porcine mitral valve annulus was the method in Section 6.2.2.5.7 in which the annulus was cut in the left commissure. This caused annular dilation, alongside regurgitation through the perforation. For each test using the synthetic or decellularised porcine mitral valve annulus rings for repair n=5 hearts were used. Prior to the insertion of the annuloplasty rings the perforation was closed using 3-0 sutures (Fig 6.7a) and then the synthetic or decellularised porcine annuloplasty ring was used to reinforce the repair. Training was provided by Dr Rodolfo Paniagua to Dr Tayyeb Vafae and myself to demonstrate the correct clinical procedure for suturing the synthetic rings to the mitral valve. In the subsequent repairs of the mitral valves all repairs, both with synthetic and biological annuloplasty rings were carried out by Dr Tayyeb Vafae.

6.2.2.6.1 Synthetic annuloplasty rings

A Carpentier-Edwards classic annuloplasty ring was used for each repair. This device consisted of a solid titanium core with a polyester knit fabric with commissure markers for ease of insertion. To insert the annuloplasty ring, fresh porcine hearts were first prepared as described in Section 6.2.2.1 and then placed into a heart holder (Fig 6.7b). To secure the hearts in the holder, sutures (3-0) were inserted into remaining left auricle tissue and secured into the heart holder on three sides. The annuloplasty ring was sized for the heart by stretching the anterior leaflet across the plane of the annuloplasty ring and ensuring that the leaflet covered the whole area of the annuloplasty ring (Fig 6.7c). The left and right trigones were identified as the primary anchoring points for the annuloplasty ring. Using the markers for the trigones on the ring, the first suture was threaded through the ring at the marker and then through the annulus at the right trigone and back through the annuloplasty ring a second time. A second suture was then placed through the annuloplasty ring at the left trigone marker and threaded through the left trigone and back through the ring (Fig 6.7d). Two further sutures were inserted horizontally into the annuloplasty ring at the fibrous mitral to aortic continuum. In the posterior region four sutures were inserted spread evenly across the posterior annulus. Each suture was threaded through the annuloplasty ring and into the annulus, carefully threading the suture behind the leaflet and back up into the annulus and through the annuloplasty ring (Fig 6.7e). Once all the sutures were inserted into the annulus the annuloplasty ring was lowered into the mitral valve and all the sutures tied and cut (Fig 6.7f).

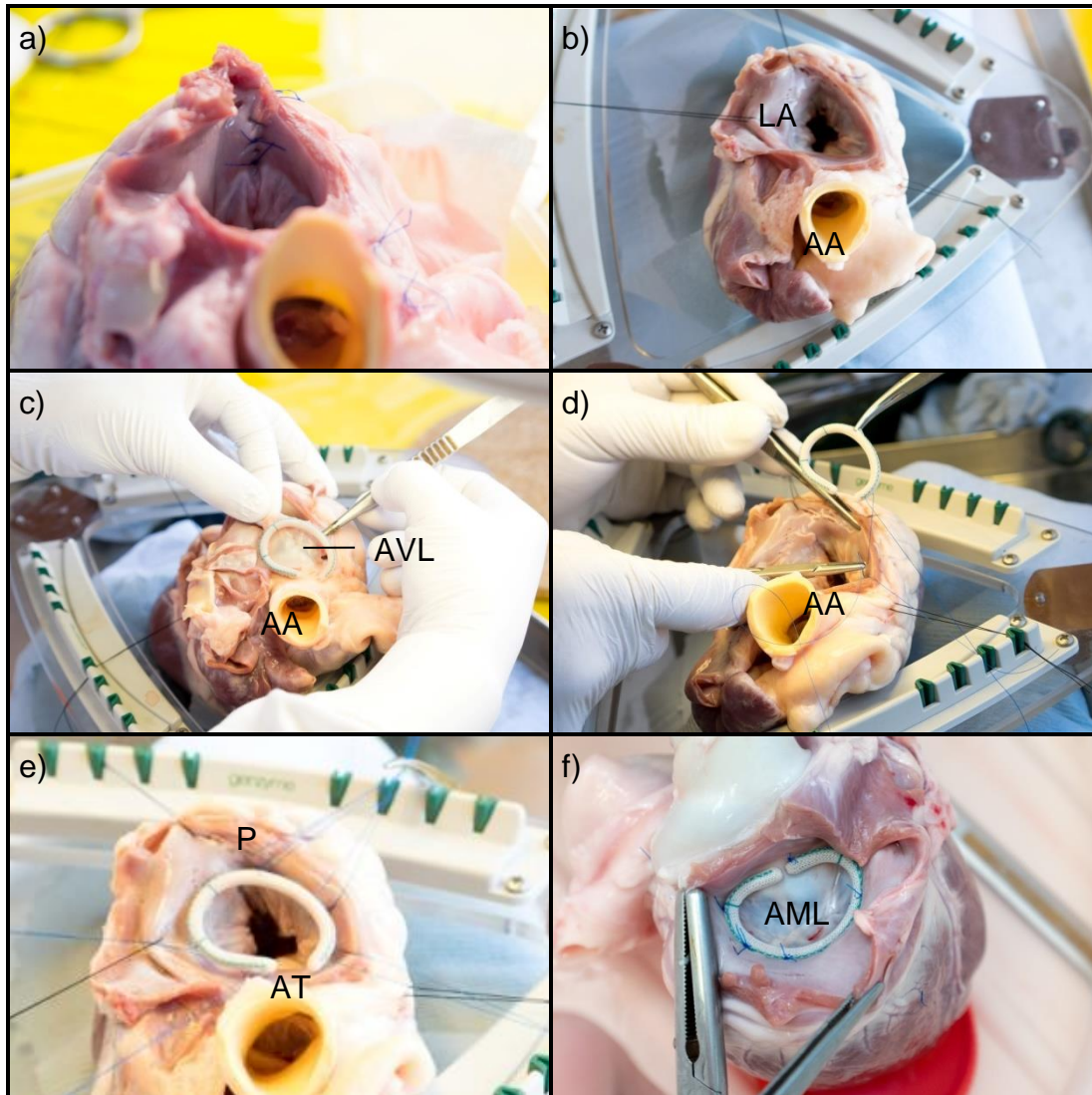


Fig 6.7 – Preparation of porcine heart tissue repaired with synthetic annuloplasty ring for static testing. Sutures were inserted into the mitral valve annulus to repair the cut created in the left commissure (a), whole heart fixed into position with sutures into the heart holder (b), sizing of the annuloplasty ring using the anterior mitral valve leaflet for reference (c), attaching the mitral valve annuloplasty ring into position using the left and right trigones as anchoring points (d), annuloplasty ring lowered into position in the porcine mitral valve (e), sutures tied off and cut to secure the annuloplasty ring into position in the porcine mitral valve (f). AA: Ascending aorta, AML: Anterior mitral valve leaflet, LA: Left atrium, AT: Anterior annulus, P: Posterior mitral valve.

6.2.1.6.2 Decellularised porcine mitral valve annuloplasty ring

The annuloplasty rings were tested in the physiological orientation, in which each trigone in the decellularised annuloplasty ring matched up with the trigone in the fresh porcine heart. A reverse annuloplasty ring was also tested, the ring was reversed so that the left trigone matched up with the P1 cleft on the posterior leaflet and the right trigone matched up with the P3 on the posterior leaflet.

Decellularised porcine mitral valve annuloplasty rings (n=5) processed using Method 8 as described in Chapter 4, Section 4.5.8 were used for each orientation. To insert the decellularised annuloplasty rings, fresh porcine hearts were first prepared as described in Section 6.2.2.1 and then placed into a heart holder, if required, to aid annuloplasty insertion. The annuloplasty ring was sized for the heart by stretching the anterior leaflet across the plane of the annuloplasty ring and ensuring that the leaflet covered the whole area of the annuloplasty ring. The left and right trigones were identified as the primary anchoring point for the decellularised annuloplasty ring (Fig 6.8b).

Physiological orientation

Using the trigonal regions on the decellularised annuloplasty ring as markers the first suture was threaded through the annuloplasty ring at the right trigone (Fig 6.8a) and then through the annulus of the heart at the right trigone and back through the annuloplasty ring a second time. A second suture was then placed through the decellularised annuloplasty ring at the left trigone and threaded through the left trigone in the heart and back through the ring. Two further sutures were inserted horizontally into the annuloplasty ring at the fibrous mitral to aortic continuum. In the posterior region four sutures were inserted spread evenly across the posterior annulus. Each suture was threaded through the annuloplasty ring and into the annulus, carefully threading the suture behind the leaflet and back up into the annulus and through the annuloplasty ring. Once all the sutures were inserted into the annulus the annuloplasty ring was lowered into the mitral valve and all the sutures were tied and cut (Fig 6.8d).

Reverse orientation

Using the trigonal regions on the fresh porcine heart as an anchor, the annuloplasty ring was inserted as described for the physiological ring orientation but in reverse, so that the anterior region of the annuloplasty ring was inserted into the posterior annulus in the heart (Fig 6.8 e).

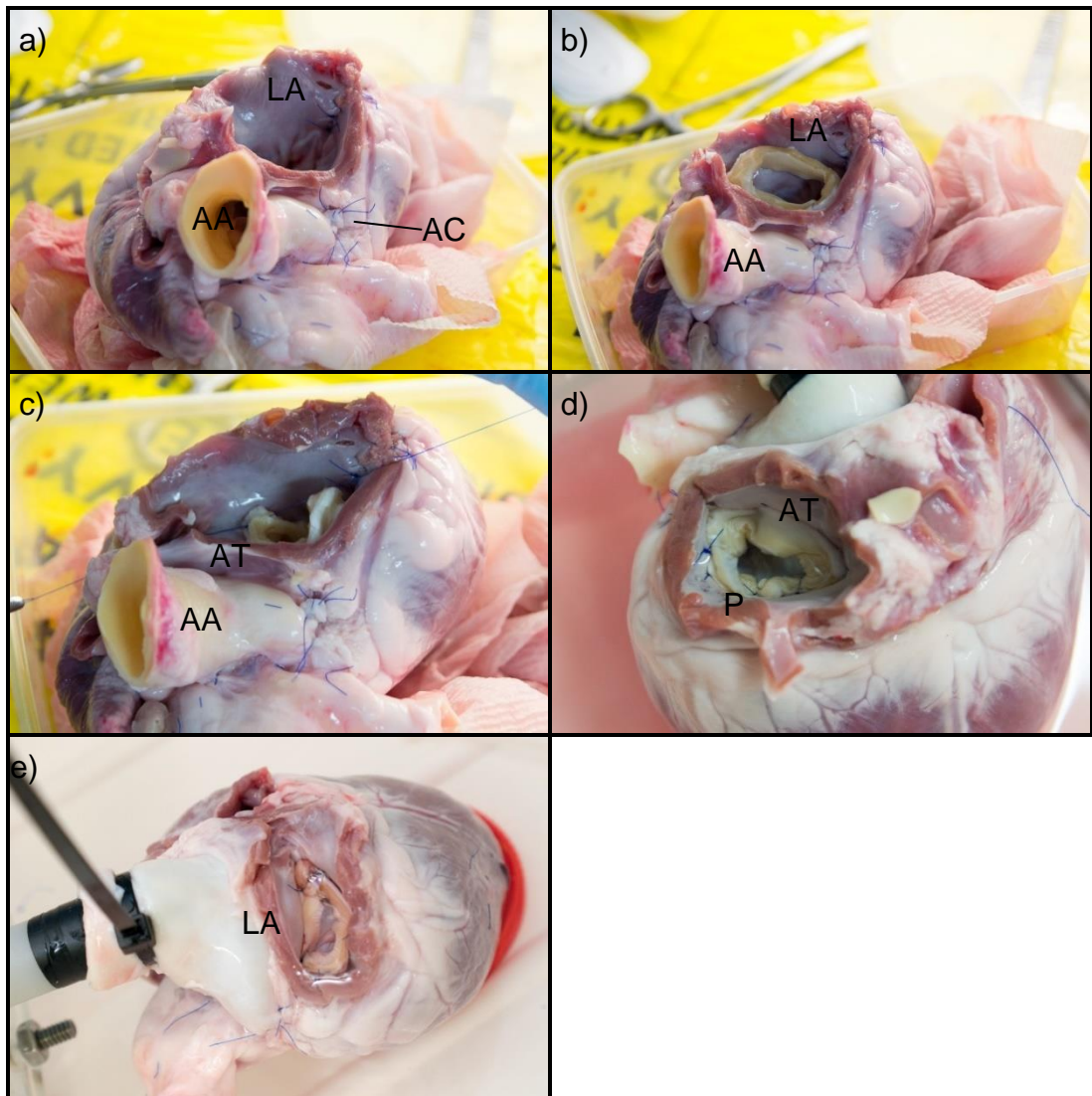


Fig 6.8 Preparation of porcine heart tissue repaired with decellularised porcine mitral valve annuloplasty ring for tissue for static testing. Fresh porcine heart with sutures in anterior and posterior coronary artery (a), orientation of the decellularised annuloplasty ring into the porcine heart using the left and right trigones on the annuloplasty ring as reference (c), sutures tied off and cut to secure the annuloplasty ring into position in the porcine mitral valve (d), sutures tied off and cut to secure the annuloplasty ring into a reverse position in the porcine mitral valve (e). AA: Ascending aorta, AC: Anterior coronary artery, AVL: Anterior mitral valve leaflet, LA: Left atrium, AT: Anterior annulus, P: Posterior mitral valve.

6.3 Results

6.3.1 Healthy porcine heart model

The results of regurgitation testing of the healthy porcine heart model are displayed in Table 6.1. There were very mild rates of regurgitation occurring through the mitral valve of the hearts when there was no intervention to induce regurgitation. The average time for columns of saline to drop from 120 to 80 mmHg was not recorded as none of the hearts reached the 80 mmHg level in 20 minutes. The average regurgitation rate was 0.05 ± 0.05 ml.beat⁻¹, calculated from the difference in volume of saline solution in the column from 120 mmHg to the level of the pressure column head measured at 20 minutes.

Table 6.1 – Regurgitation rates for mitral valves of healthy porcine hearts

Heart	Average regurgitation rate (ml.s ⁻¹)	Average regurgitation rate (ml.beat ⁻¹)	Class
1	0.36	0.11	Mild
2	0.35	0.11	Mild
3	0.16	0.05	Mild
4	0.06	0.02	Mild
5	0.02	0.01	Mild
6	0.06	0.02	Mild
Average	0.17	0.05	Mild
95% CI	0.16	0.05	

6.3.2 Positive control heart model

The results for the regurgitation testing of the positive control porcine heart model are displayed in Table 6.2. There were mild to moderate rates of leakage through the 5 mm hole punctured in the anterior leaflet.

The average time for the column to drop from 120 to 80 mmHg was 16.79 ± 5.54 s which was equivalent to a rate of 30.51 ± 12.72 ml.beat⁻¹.

Table 6.2 – Regurgitation rates for mitral valves of positive control hearts

Heart	Time of column leak 120 – 80 mmHg (s)	Rate to 80 mmHg (ml.s ⁻¹)	Rate to 80 mmHg (ml.beat ⁻¹)	Class
1	8.72	176.39	52.92	Moderate
2	19.54	78.72	23.62	Mild
3	20.09	76.56	22.97	Mild
4	13.63	112.85	33.85	Moderate
5	15.37	100.07	30.02	Moderate
6	23.41	65.70	19.71	Mild
Average	16.79	101.72	30.51	Moderate
95 %CI	5.54	42.40	12.72	

6.3.3 Regurgitant models

6.3.3.1 Stretched annulus

When the porcine heart annulus was stretched using retractors, there was no leakage in two of the three hearts and mild leakage in one heart. The

average time for the column to drop from 120 to 80 mmHg was 675.20 s which was equivalent to an average rate of 5.24 ml.beat⁻¹. The range of leakage rates meant that this method would not deliver repeatable regurgitation rates required for the final regurgitation model.

6.3.3.2 Trypsin injection around the mitral valve annulus

The treatment of the porcine mitral valve annulus with trypsin produced only mild rates of leakage through the leaflets of mitral valves. The average time for the column to drop from 120 to 80 mmHg was 531 s which was equivalent to a rate of 2.58 ml.beat⁻¹. The limited regurgitation together with extended preparation time compared to other methods meant this method was not suitable for the final regurgitation model.

6.3.3.3 Ruptured chordae

The results for hearts with their chordae ruptured are displayed in Table 6.3. There were mild to severe rates of regurgitation through the anterior leaflet. The average time for the column to drop from 120 to 80 mmHg was 41.82 ± 75.15 s which was equivalent to a rate of 48.53 ± 55.29 ml.beat⁻¹.

Table 6.3 – Regurgitation rates for porcine mitral valves with ruptured chordae

	Time of column leak 120 – 80 mmHg (s)	Rate to 80 mmHg (ml.s⁻¹)	Rate to 80 mmHg (ml.beat⁻¹)	Class
1	187.42	8.21	2.46	Mild
2	17.28	89.01	26.70	Mild/ Moderate
3	19.83	77.57	23.27	Mild
4	15.54	98.98	29.69	Moderate
5	3.09	497.77	149.33	Severe

6	7.73	198.98	59.69	Severe
Average	41.82	161.75	48.53	Moderate
95 % CI	75.15	184.29	55.29	

6.3.3.4 Papillary muscle dilation

Three hearts were tested using papillary muscle dilation. There were mild rates of leakage through a prolapsed leaflet caused by the dilation. One heart failed due to complete dissection of the papillary muscle. The average time for the column to drop from 120 to 80 mmHg was 38.73 s which was equivalent to a rate of 12.84 ml.beat⁻¹. No further testing was completed due to the poor reproducibility of the test procedure including the complete failure of the papillary muscle.

6.3.3.5 Super glued leaflets and annulus

Three hearts were tested using the method of coating the top leaflet surfaces and annulus with superglue. There were mild rates of leakage that occurred where the anterior and posterior leaflets closed together at the coaptation point. The average time for the column to drop from 120 to 80 mmHg was 95.88 s which was equivalent to a rate of 5.49 ml.beat⁻¹. It was determined that due to the difficulty in repairing the lesions created using this method, that no additional tests with this method would be completed.

6.3.3.6 Trimmed left ventricular myocardium

Three hearts with ventricular muscle removed were tested for mitral valve regurgitation. There were mild rates of leakage in hearts with simulated left ventricular dilation. The average time for the column to drop from 120 to 80 mmHg was 954 s which was equivalent to a rate of 0.58 ml.beat⁻¹. No further testing was completed due to the poor leakage rates.

6.3.3.7 Bisected mitral valve annulus at the left commissure

The results for the hearts with the annuli cut at the left commissure are displayed in Table 6.4. There were mild rates of leakage through the valves. The average time for the column to drop from 120 to 100 mmHg for all hearts was 54.04 ± 23.74 s which was equivalent to a rate of 4.36 ± 1.90 ml.beat⁻¹.

Table 6.4 – Regurgitation rates for porcine mitral valves with bisected mitral valve annuli

	Time of column leak 120 – 80 mmHg (s)	Rate to 80 mmHg (ml.s ⁻¹)	Rate to 80 mmHg (ml.beat ⁻¹)	Class
1	150.53	10.22	3.07	Mild
2	126.11	12.2	3.66	Mild
3	85.69	17.95	5.38	Mild
4	104	14.79	4.44	Mild
5	202	7.61	2.28	Mild
6	62.84	24.48	7.34	Mild
Average	121.86	14.54	4.36	Mild
95 % CI	52.20	6.34	1.90	

6.3.3.8 Cauterising the mitral valve leaflets

There were mild rates of leakage through the valves of hearts in which the leaflets had been cauterised. One heart did not reach 80 mmHg in the time limit of 20 minutes and so it met the criteria for no regurgitation. The average time for the column to drop from 120 to 100 mmHg for all hearts was 649 s

which was equivalent to a rate of $0.99 \text{ ml.beat}^{-1}$. The minimal rate of regurgitation meant that this test would not be suitable for the final regurgitation model and no additional tests were performed.

6.3.3.9 Zinc fixed mitral valve

The zinc fixed hearts used in this test failed prior to the test or during the test procedure. Due to these failures no extra hearts were tested due to the poor reliability of the procedure.

6.3.4 Mitral valve repair

The disease model that produced replicable rates of mitral valve regurgitation as well as being simple to repair with an annuloplasty ring was the method Section 6.2.2.5.7, the bisection of the mitral valve annulus. Hearts were first tested for regurgitation with the cut in the annulus at the left commissure as described in Section 6.2.2.5.7 and then repaired with either a synthetic annuloplasty ring or decellularised porcine mitral valve annuloplasty rings. In the disease model before the annulus was repaired with a synthetic ring there was a regurgitation rate of $4.33 \pm 2.51 \text{ ml.beat}^{-1}$, after the annulus had been repaired with a synthetic annuloplasty ring there was a regurgitation rate of $0.41 \pm 0.49 \text{ ml.beat}^{-1}$ ($p < 0.05$) (Fig 6.7) and a reduction in regurgitation of 90.60% (Fig 6.10).

In the disease model for the biological acellular annuloplasty rings, inserted in a physiological orientation, there was a regurgitation rate of $4.55 \pm 2.23 \text{ ml.beat}^{-1}$ and with post annuloplasty repair there was a regurgitation rate of $0.42 \pm 0.30 \text{ ml.beat}^{-1}$ ($p < 0.05$) (Fig 6.9) and a reduction in regurgitation of 90.74% (Fig 6.10). In the disease model for the biological acellular annuloplasty rings, inserted in a reverse orientation to the physiological makeup, there was a regurgitation rate of $5.10 \pm 1.96 \text{ ml.beat}^{-1}$ and with annuloplasty repair in the reverse orientation there was a regurgitation rate of $0.55 \pm 0.52 \text{ ml.beat}^{-1}$ ($p < 0.05$) (Fig 6.9) and a reduction in regurgitation of 89.20% (Fig 6.10). There was no statistical significance found between repair groups.

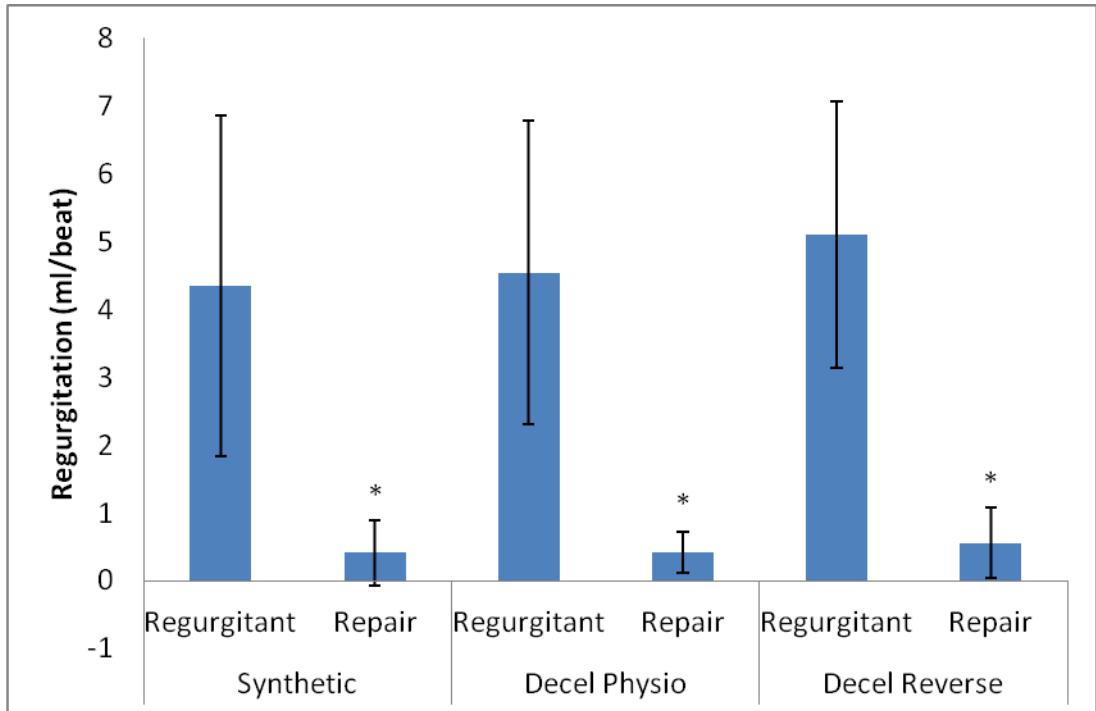


Fig 6.9 – Regurgitation testing of porcine hearts using synthetic and decellularised annuloplasty rings. Data is presented as the mean (n=5) ± 95% C.I and was analysed by paired student's t-test that showed significant difference between groups ($p < 0.05^*$).

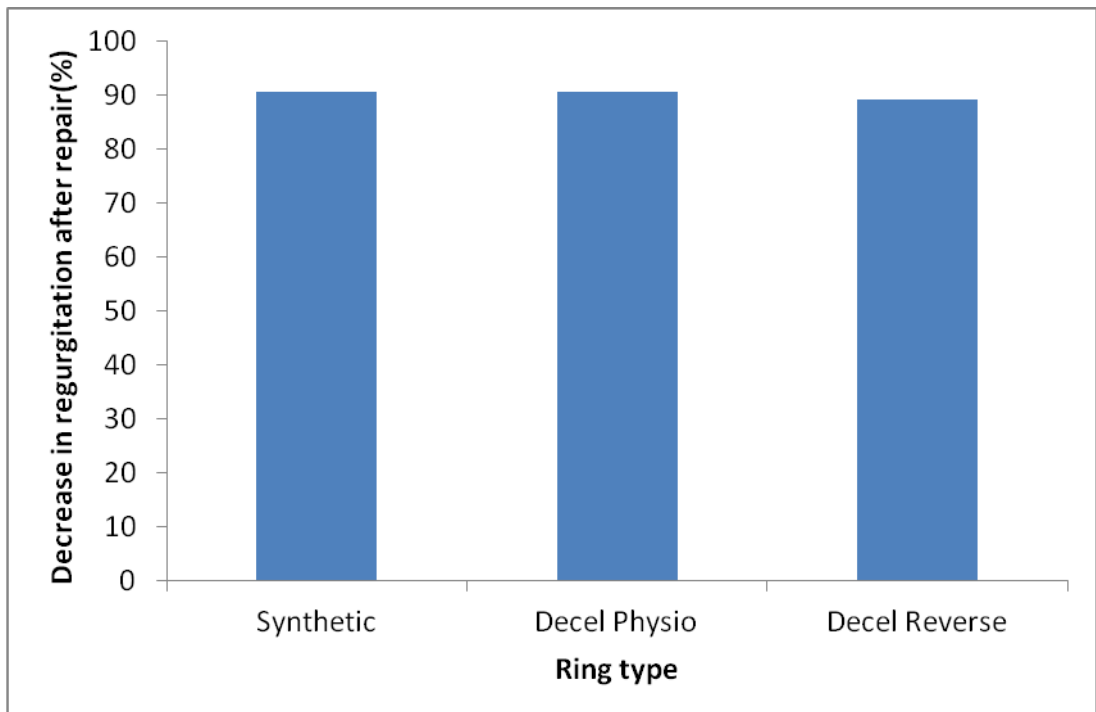


Fig 6.10 – Percentage decrease in regurgitation after repair with an annuloplasty ring (n=5). Data is presented as the mean decrease in regurgitation rate after repair compared to the rate before repair (n=5).

6.4 Discussion

The aim of the research described in this chapter was to assess the functional capabilities of the decellularised mitral valve annulus for use as an annuloplasty ring. Porcine decellularised mitral valve annuli were implanted into an explanted porcine heart with induced regurgitation and tested under static pressure. Synthetic annuloplasty rings were implanted under the same conditions and compared against the decellularised porcine mitral valve annuli. Numerous methods to invoke mitral regurgitation were initially attempted. The ideal outcome for these tests were regurgitation volumes that replicated moderate to severe regurgitation *in-vivo* which would warrant the insertion of an annuloplasty ring. All procedures tested apart from chordae rupture with annulus dilation resulted in mild rates of regurgitation. Whilst the chordae rupture model was considered for final testing purposes it was decided that chordae resection alone would likely contribute to successful reduction in regurgitation without the requirement for annuloplasty. Of all the methods tested, annulus bisection was considered to be simple to replicate with repeatable results and provided a suitable repair choice for annuloplasty.

Previous methods of inducing regurgitation *in-vivo* in the mitral valve include chordal rupture in dogs (Urabe et al., 1992, Pat et al., 2010) and the application of collagenase in the hearts of dogs (Fujiki *et al.*, 2000). For explanted heart models chordal rupture alongside annular dilation has been carried out (Richards *et al.*, 2009). A similar method designed to digest collagen in the heart was attempted in this study. Trypsin treatment was used in an attempt to replicate some of the effects of myxomatous mitral valve disease. The trypsin was only applied to the mitral annulus rather than the whole of the mitral valve complex, possibly limiting the effectiveness of this approach. Trypsin treatment was combined with annular dilation but proved ineffective at producing moderate regurgitation and results were also quite variable. The *in-vivo* model by Fujiki *et al.*, (2000) permitted long term changes to take place in the heart which produced ventricular dilation and remodelling which was possibly the major factor why this type of model did not work *in-vitro*. Chordal rupture was successful in producing mitral valve regurgitation, regurgitation was caused by leaflet prolapse into the left atrium. The ruptured chordae model was the only model that produced moderate and severe rates of mitral valve regurgitation with results closest to regurgitation rates in the positive controls. Consultation with a

cardiovascular surgeon revealed that this type of repair would be better suited to chordae resection and might not offer insight into the effectiveness of mitral annular repair using the decellularised porcine mitral valve annuloplasty ring compared to a synthetic ring. Inducing regurgitation with mitral annular dilation alone produced mild regurgitation and variable results. Isolated mitral annular dilation can cause mitral valve regurgitation (Mihalatos *et al.*, 2007) but other factors may prevent regurgitation when annular dilation is present. The main factor preventing a moderate rate of regurgitation appears to be the redundant leaflet coaptation area present in the mitral valve (Kunzelman *et al.*, 1994), allowing appropriate leaflet coaptation even with increased dilation. Other unsuccessful methods to invoke repeatable rates of regurgitation included papillary muscle dilation to replicate chordae elongation and coating the leaflets with cyanoacrylate to replicate leaflet vegetation caused by endocarditis and rheumatic mitral valve disease. Some of the methods had very little effect on regurgitation, these included cauterising the leaflets and removal of left ventricular muscle and left atrial muscle.

The only model that produced results that were repeatable whilst also being suitable for the assessment of annuloplasty repair was the cutting of the mitral annulus at the left commissure. The main limitation of this method was the mild rates of regurgitation achieved. After consultation with a cardiovascular surgeon it was decided that this method would be the most suitable for providing a regurgitant valve model that could be used for comparing repairs using synthetic and decellularised porcine mitral valve annuloplasty rings. All repairs, using both the synthetic and decellularised annuloplasty rings produced significantly lower regurgitation rates compared to the hearts with induced regurgitation. No difference was found between groups. Static testing did not allow the comparison of the dynamic performance of each type of annuloplasty ring as experienced by the mitral valve during the cardiac cycle. There were limitations to the method of inducing regurgitation in the static test rig; alongside the annuloplasty, suture repair was carried out on the annulus tear. It was decided that the repair *in vivo* would necessitate the use of annuloplasty to ensure sufficient reinforcement for the repair, as it is unlikely that sutures would hold in this area alone.

Failure to invoke moderate regurgitation using some of the methods may be explained from studies of mitral valve regurgitation. Valves that have fibrinous vegetation such as with rheumatic heart disease show few signs of regurgitation with acute episodes (Veasy & Tani, 2005), only in chronic rheumatic heart disease does mitral valve regurgitation usually occur. Annular dilation is present in acute rheumatic heart disease but only in chronic rheumatic valve disease does mitral regurgitation increase. This occurs when the left ventricle and left atrium dilate and remodel due to long term regurgitation, causing annular dilation, chordal elongation and leaflet prolapse (Marcus, 1994). Other studies have identified mitral annular dilation contributing to only modest rates of regurgitation, the contributing factor leading to significant mitral valve regurgitation was papillary muscle tethering caused by left ventricular dilation and dysfunction (Otsuji *et al.*, 2002). It appears that only acute forms of mitral regurgitation, such as with sudden chordae or papillary muscle rupture due to myocardial infarction or annular bisection, would provide for a sufficient model for testing regurgitation volumes that would warrant mitral valve repair when using a static heart regurgitation model, unless pigs had regurgitation induced 6-12 months prior to slaughter to replicate some of the chronic effects of the disease, as described by Urabe *et al.* (1992) Fujiki *et al.* (2000) and Pat *et al.* (2010).

The static pressure test rig was designed to keep costs and complexity low as a precursor to animal trials. The advantage of the design allows multiple trials to be undertaken whilst maintaining low development and time costs. Porcine hearts are available from the local abattoirs with a cost of £5 per heart which can be tested under multiple test methods with little effect on cost or time involved. The major limitation of this model was that annuloplasty rings could not be tested dynamically. Valves tested dynamically would reduce variability in the regurgitation for each sample and provide a system capable of testing the durability of repair. A dynamic system would also permit the calculation of regurgitation fraction which would give a better understanding of the functional implications of a repair on the heart valve by normalising the regurgitation results for the size of each individual heart.

An array of dynamic models have been used previously, in two different studies the mitral valve complex was excised, including the papillary muscles, from the heart (Arita *et al.*, 2004; He *et al.*, 1997) whilst one model retained the whole heart taken from pigs (Richards *et al.*, 2009), both of

which used a pulsatile flow system. Whilst the first models provided some advantages in allowing more control over test parameters such as papillary muscle placement, the similarities to the *in vivo* environment were reduced. The whole heart model comprised of a pulsatile flow system simulating some of the physiological type conditions seen *in vivo* in the left ventricle and atrium by permitting physiological pressure waveforms and flow rates. More complex solutions have been utilised by maintaining the contractile properties of excised porcine hearts *ex vivo* using chemical techniques (Araki *et al.*, 2005; Chinchoy *et al.*, 2000). This required increased preparation time, costs, access to laboratory animals as well as knowledge of the correct transplantation procedures which would negate many of the benefits associated with using *ex vivo* hearts, when attempting to remove the use of laboratory animals in testing.

There are advantages of fully beating heart models as they maintain the contractile muscle properties of the left ventricle and papillary muscles which would permit the change of left ventricular volumes during the cardiac cycle. The contractile elements of this model would include the geometric changes to the mitral valve annulus which cannot be replicated with the other models mentioned. This would allow an improved comparison between the decellularised annuloplasty ring and the synthetic ring and establish if the annuloplasty ring improved the dynamic performance compared to synthetic rings. Synthetic rings can impede the dynamic motion of the annulus *in vivo* by abolishing changes to the mitral annular area and annular circumference during the cardiac cycle (Dagum *et al.*, 2001; Glasson *et al.*, 1999) as well as restricting leaflet motion during the cardiac cycle (Green *et al.*, 1999).

The simplicity of the static system used in this study provided control over all test conditions whilst maintaining the natural heart structure and allowed regurgitation to be easily quantified by measuring the volume change in the column of saline. Future studies can be compared against this study using the same criteria making this process highly repeatable.

Chapter 7 Discussion

7.1 General Discussion

Every year more than 300,000 people undergo open heart surgery for treatment of mitral valve disease worldwide (Bonow *et al.*, 2006), with mitral valve regurgitation being the second most common form of valve disease in Europe (Iung *et al.*, 2003). In the United States 1.7% of the population suffer from mitral valve regurgitation (Nkomo *et al.*, 2006). In a healthy heart, the mitral valve leaflets coapt in apposition to each other which prevents regurgitation. The mitral annulus in the healthy valve is of the best possible size to ensure correct leaflet closure whilst being optimally shaped to reduce leaflet stresses across the valve (Salgo, 2002). The chordae and papillary muscles work in tandem to prevent restricted leaflet motion or leaflet prolapse which are governed by the forces generated during contraction of the myocardium during the cardiac cycle. The continual relationship between all these components is therefore paramount for normal valve performance (Van Mieghem *et al.*, 2010).

Current treatment strategies include mitral valve repair and mitral valve replacement, with repair offering the advantage of preserving left ventricular systolic function. Repair also avoids the requirement for lifelong anticoagulation treatment and offers improved survival compared to mitral valve replacement (Otto, 2003; Enriquez-Sarano *et al.*, 2009), with mitral valve annuloplasty being the most common repair procedure. Current annuloplasty rings can change annular dynamics, geometry and force distribution of the mitral valve (Glasson *et al.*, 1999; Jensen *et al.*, 2008; Yamaura *et al.*, 1997) whilst the motion of the posterior leaflet can be restricted (Green *et al.*, 1999; Timek *et al.*, 2002; Zhu *et al.*, 2005). In children, the use of annuloplasty rings is not recommended as it can cause secondary mitral valve stenosis as the heart of the child grows. Long term results show that significant regurgitation can reoccur in patients that have mitral valve repair using rigid or flexible annuloplasty rings, although reoperation rates are quite low (Chang *et al.*, 2007). Pericardium has also been used as an annuloplasty device in both adults and children, permitting the growth of the mitral valve in children whilst correcting the mitral valve regurgitation (Delmo Walter *et al.*, 2010; Miura *et al.*, 2012; Bruno *et al.*,

2013; Salvador *et al.*, 2014). An acellular biological scaffold approach has the potential to overcome the problems with synthetic rings, particularly for paediatric patients, whilst offering advantages over autologous pericardium such as being readily available, retaining the pericardium, removal of additional risk associated with removing the pericardium and possessing biological and biomechanical similarities to the mitral valve region.

The overall aim of this study was therefore to explore the potential for annuloplasty repair utilising decellularised tissues. Human and porcine mitral valve annuli were initially considered as the primary source materials due to their similar macroscopic characteristics, of which the porcine mitral valve annulus was identified as a suitable candidate. Human tissue was rejected as a suitable tissue because of heavy calcification in the tissue that was obtained and the limited availability of human tissue for use in the research and possible future use in the clinic. The use of a cell seeded strategy was avoided as it was envisaged that, following implantation resident cells in the patient would integrate and gradually regenerate and remodel the donor scaffold over time. Development costs and complexity would also be reduced as well as minimising regulatory hurdles necessary for taking the concept to market.

Decellularisation protocols for the porcine mitral valve annuli were adapted from methods developed by Booth *et al.* (2002) and Stapleton *et al.* (2008) for the decellularisation of porcine aortic valves and menisci. The process involved the optimisation of protocols developed and patented at the University of Leeds using repeated cycles of low concentration SDS in the presence of proteinase inhibitors and hypotonic buffer wash cycles. The removal of cellular components during the development of the decellularisation of the mitral valve annulus was assessed using histology, DAPI staining of tissue sections and total DNA quantification until a suitable protocol had been established. Further analysis of the acellular tissue produced by optimised process was then undertaken using histochemistry, immunohistochemistry and biomechanical tests to determine any changes in the overall composition and structure compared to native porcine mitral valve annuli. The decellularised porcine mitral valve annuli were then functionally tested using a static test rig to investigate the effectiveness of *in-vitro* mitral valve repair. Synthetic annuloplasty rings were compared to decellularised annuloplasty rings when used to repair explanted regurgitant porcine hearts.

Histological characterisation of human and porcine mitral valve annuli revealed some differences between species. Collagen II was isolated to the trigones in the porcine tissue whilst collagen II presence in human annuli was likely due to disease. GAG distribution differed in the trigones between species but similarities between species existed for GAG distribution in the posterior annulus at the annular junction. Further differences in the trigones were found between species, the human trigones were absent of the cartilaginous tissue identified in the porcine mitral valve and the human fibrosa was thicker, with an increase in the deposition of adipose tissue surrounding the human annulus. Histological characterisation of both species revealed that on the whole there were similar macroscopic and microscopic features in both the anterior and posterior annulus. The anterior mitral valve annulus consisted of a dense collagenous mitral- aortic continuum bordered by thick trigones on the right and left sides of the annulus. Towards the posterior, the fibrosa layer of the posterior leaflet in both species formed into a thin collagenous annulus region that separated the atrial and ventricular myocardium. Immunohistochemical staining of tissue sections showed that the distribution of collagens in the porcine and human annulus and surrounding regions were comparable, with the exception of collagen II. Overall, the results indicated that the porcine mitral valve annulus would be suitable as a start material for the development of a decellularised annuloplasty ring. Human mitral valve annuli were not further investigated for the development of a decellularised annuloplasty device because the donated human tissue was heavily calcified and exhibited some signs of ossification. The human tissue was obtained from older donors, due to the limited supply of tissue from younger donors. The incidence of valve calcification and mitral valve thickness increases with age (Kitzman & Edwards, 1990). Hence, it is likely mitral valves taken from younger donors would be more comparable to the porcine tissue whilst also being absent of calcification and ossification, therefore suitable to be investigated for use as an acellular annuloplasty ring.

Following histological characterisation the biomechanical properties of the porcine mitral valve annulus were investigated using uniaxial tensile testing. The biomechanical characteristics of the native porcine mitral valve regions illustrated the difference in the biomechanical properties between the anterior region of the mitral annulus and the posterior regions. The anterior region was stiffer and underwent a higher load before failure compared to the posterior regions. This was likely because the anterior region forms part of the cardiac skeleton that supports and anchors the valve, whereas the

posterior region undergoes the majority of contraction and dilation during the cardiac cycle (Eckert et al., 2009). The biomechanical characteristics of the anterior and posterior regions of the mitral annulus can be attributed to the underlying histoarchitecture, with a dense fibrosa that forms into the annulus in the anterior region alongside thick cartilaginous regions in the trigones and a thin fibrosa surrounded by myocardium in the posterior region. The biomechanical properties of the human tissue that was available for study was not established due to the calcification.

Histological analysis of the porcine mitral valve annulus post decellularisation revealed that the structural components of the extracellular matrix were largely retained, although there was a reduction in the distribution of GAGs and collagens associated with the basement membrane following decellularisation. The collagen and elastin fibres appeared intact following decellularisation when analysed with Sirius red Miller's stain. The thick fibrosa layer formed into the annulus in both the native and decellularised tissue, with the density and fibre orientation comparable. The trigonal region of the anterior annulus was similar when compared using histological analysis, with cartilage-like tissue characterised by lacunae. Sirius red Miller's staining of the decellularised tissue sections showed the retention of the elastic cartilage-like tissue found in the native tissue sections. The structural collagens I and II were maintained following decellularisation but changes were identified in mitral valve annulus sections labelled with collagen IV, collagen VI, fibronectin and laminin. The basement membrane proteins of collagen IV, fibronectin and laminin were most affected by the decellularisation procedure. It is thought that SDS removes these components of the ECM apart from collagen IV which has been reported to be altered by the use of PAA during the sterilisation step of the decellularisation protocol (Luo *et al.*, 2014).

Following the application of the final decellularisation protocol to the porcine mitral valve annuli a reduction in total DNA content of over 95 % was achieved in both the anterior and posterior regions, however histological evaluation revealed residual "nuclear ghosts" in the lacunae of the trigones. In future studies it would be important to analyse these structures in more detail. This could be carried out using laser capture microdissection of tissue sections to extract the nuclear remnants in the trigones. This would allow the DNA content of the cellular remnants to be analysed using quantitative DNA analysis and determination of the size of any DNA fragments present. The results could then be compared to extracts from the lacunae of native tissue

in the same region. The current literature suggests that DNA fragments less than 180 base pairs in length (Nagata *et al.*, 2010) should not cause an immune response, hence fragments less than this length found present in the lacunae of the decellularised tissue would not be an issue. *In-vitro* cytotoxicity assays showed that BHKs and L929s grew up to the acellular porcine mitral valve tissue in contact assays and were not inhibited when grown in extracts of the decellularised tissue, illustrating that the post wash cycles of PBS removed any potentially cytotoxic chemicals from the scaffolds.

Biomechanical testing of the decellularised tissue revealed larger ultimate tensile strains, transition stresses and transition strains compared to the native porcine mitral valve annulus tested in the same regions. The increase in ultimate tensile strain of the tissue following decellularisation was similar to results for other cardiovascular tissues in other studies using 0.1 % (w/v) SDS combined with hypotonic buffer washes (Korossis *et al.*, 2002; Mirsadraee *et al.*, 2006). Transition stresses and transitions strains were larger in all regions of the decellularised porcine mitral valve annuli compared to that of the native tissue which corresponded with previous studies in which decellularisation protocols were performed using 0.1 % SDS and hypotonic buffer washes (Korossis *et al.*, 2002; Morticelli *et al.*, 2013). The changes in the biomechanical properties of tissues following decellularisation have been attributed to the use of SDS detergent (Gratzer *et al.*, 2006), hypotonic buffer washes and the removal of cells (Korossis *et al.*, 2002). GAG removal was also evident in the decellularised porcine annulus trigones. In order to determine if the removal of GAGs has any effects on the biomechanical characteristics of the porcine mitral valve trigones, future studies should use indentation testing to evaluate the compressive stiffness of this region compared to native porcine mitral valve annuli. Whilst such studies would determine the changes in the porcine tissue due to the decellularisation process, these studies would not however determine any differences between the properties of the human and porcine mitral valve. It would be important to determine whether the properties of the acellular porcine mitral trigones were matched with those of human tissue. To establish the biomechanical characteristics of the human trigones it would be important to use healthy human tissue without the associated calcification found in the older heart tissue, thereby requiring younger human hearts.

Flexible, semi rigid and rigid annuloplasty rings have all been shown to reduce annular dynamics and may partially obstruct the aortic outflow tract (Dagum et al., 2001). The region of the acellular ring that will be closest to the outflow tract is the mitral to aortic continuum. The similarities in the underlying architecture between human and decellularised porcine mitral valve annuli may extend to the biomechanical characteristics in this region. These similarities may help reduce any obstruction that normally occurs when synthetic rings are used. The changes caused to the porcine tissue due to the decellularisation process may also be an advantages because of the reduction in the elastic phase Young's modulus in the mitral to aortic continuum, making the tissue more compliant in this region. Thus, there will be less resistance to elongation and any obstruction of the aortic outflow tract will be decreased compared to the native porcine tissue. Future biomechanical testing of the healthy native human annulus would be required to understand any differences in mechanical properties between the different tissue species. Functional assessment of the obstruction to the outflow track would also offer further insights into any advantages the decellularised ring would offer compared to synthetic rings in reducing any obstruction at the aortic outflow tract.

In-vitro functionality testing of the decellularised annuloplasty rings was undertaken as a pre-clinical test. The aim was to compare the decellularised rings with the current gold standard for mitral valve repair, synthetic annuloplasty rings, by repairing explanted porcine hearts in which mitral regurgitation had been induced. Decellularised annuloplasty rings inserted in physiological and reverse positions showed similar reduction in regurgitation compared to the synthetic ring. There were two main limitations of this *in-vitro* model; the testing utilised statically pressurised hearts rather than dynamically pressurised hearts and the porcine hearts were healthy and so regurgitation was artificially induced. Previous studies have used dynamic explanted heart models, including a pulsatile flow model (Richards *et al.*, 2009) and a working heart model that kept the heart pumping post explantation (Chinchoy *et al.*, 2000; Araki *et al.*, 2005). These models would have increased complexity, time to delivery, time for each test and increased cost. The advantage is that the use of the dynamic models would have permitted the calculation of regurgitation fractions and enabled better assessment of the durability of the decellularised rings compared to the synthetic rings. With further time and funding it would have been beneficial to develop a dynamic pressure pulsatile heart model as described by Richards *et al.* (2009) to allow these parameters to be determined. A

dynamic pressure pulsatile heart model could also be used for testing devices in other regions of the heart such as in the aortic and pulmonary valves. Working heart models that retain the cardiac function of the porcine hearts would require in-depth knowledge of heart transplant techniques and awareness of procedures required to maintain physiological activity whilst also demanding high costs. Whilst such models would have many advantages for the physiological testing of annuloplasty rings they would negate advantages of using *in-vitro* models as a pre-cursor to studies in living large animal models.

For the functional tests regurgitation was induced artificially because it was not possible to obtain porcine hearts which were regurgitant due to disease. Previous methods of inducing regurgitation *in-vivo* include chordal rupture in dogs (Urabe et al., 1992, Pat et al., 2010), the application of collagenase in the hearts of dogs (Fujiki et al., 2000) and causing ischaemic mitral regurgitation by restricting blood flow to the myocardium (Cui et al., 2014), all of which were performed long term and had effects on the left ventricle and diastolic volume, left atrial volume and stroke volume. The problems encountered in the present study in obtaining moderate to severe rates of mitral valve regurgitation in the functional testing of the annuloplasty rings may have been caused by the lack of long term remodelling that commonly occurs with mitral valve regurgitation. Porcine hearts with regurgitation induced prior to explantation would have been useful for this study to enable the long term effects of mitral regurgitation on the hearts to be taken into account. There are disadvantages associated with this process because the function of the heart could only be assessed immediately after repair, long term remodelling and changes to cardiac function post repair could not be evaluated.

In children, mitral valve repair is recommended because left ventricle function is better preserved by retaining the mitral valve complex making congenital repair a well-established procedure. Mitral valve replacement in children tends to occur because either the repair has failed or the valve is comprehensively damaged. Compared to repair, replacement of the mitral valve is associated with poor long term survival (Caldarone et al., 2001; Ackermann et al., 2007; Beierlein et al., 2007; Selamet Tierney et al., 2008; Alsoufi et al., 2009) as well as there being limited options for replacement valves due to lack of appropriate valve sizes for children (Lee et al., 2010). Children who undergo replacement will require secondary replacement later in life to account for the growth of the heart. Whilst repair offers better long

term survival in children, challenges remain due to the growth of the mitral valve region in children, various pathologies causing MR and the fragility of the paediatric valve (Oppido *et al.*, 2008; Curi-Curi *et al.*, 2010; Stellin *et al.*, 2010). Children who have their heart valves repaired only have annuloplasty rings implanted if the mitral valve is large enough to accommodate an adult size annuloplasty ring due to the risk of stenosis. The smallest ring available is usually about 26 mm in diameter. It has been suggested that biomaterials for annuloplasty repair, that can be absorbed whilst permitting growth of the valve should be developed (Quinonez & Del Nido, 2015). A decellularised annuloplasty ring of the correct size for the child's heart would permit the growth of the mitral valve annulus over time whilst reducing regurgitation. Due to the ability of the decellularised ring to integrate with the mitral valve it will avoid the risk of mitral valve stenosis as the heart grows. A decellularised annuloplasty ring device also has the potential to remove the requirement of reoperation later in life by avoiding stenosis associated with synthetic annuloplasty repairs and mitral valve replacement.

Pericardium is an example of a biological device being used to enable growth of the mitral valve long term. Glutaraldehyde treated (Borghetti *et al.*, 2000; De La Zerda *et al.*, 2008; Ng *et al.*, 2001; Roshanali *et al.*, 2012; Salvador *et al.*, 2014) and untreated (Salati *et al.*, 1991) autologous pericardium has been used as an annuloplasty repair device to stabilise the posterior annulus in children and adults, providing an insight into the possible benefits of biological rings compared to synthetic rings. Pericardial annuloplasty prevents further posterior annulus dilation whilst allowing growth of the anterior annulus in relation to the body over time and preserves the flexible properties of the mitral valve annulus when used in children (Delmo Walter *et al.*, 2010). Studies have established that it is a durable solution whilst being superior to rigid prosthetic rings by offering improved mitral annulus dynamics and preserved left ventricular function (Borghetti *et al.*, 2000). It is also superior to the use of flexible rings in some areas by offering improved left ventricular function under stress conditions (Roshanali *et al.*, 2012) without signs of long term degeneration. Furthermore, long term it has been reported that glutaraldehyde treated pericardial annuloplasty, combined with neochordal implantation, was safe, offered long term durability with high survival rates and low rates of reoperation. At reoperation, it has been shown that the pericardium is covered with an endocardial like covering and is not in contact with the flow of blood (Salvador *et al.*, 2014) with the covering being indistinguishable from the atrial endocardium (Delmo Walter *et al.*, 2010). A study by

Bevilacqua *et al.*, (2003) was less favourable, they found that glutaraldehyde treated pericardial annuloplasty was a risk factor for repair failure and reoperation whilst it did not offer durable remodelling of the annulus. This study included a limited number of patients with limited follow-up periods and used different techniques which may have contributed to the poor outcomes.

Repair of mitral regurgitation with an acellular biological annuloplasty ring may provide a superior repair to pericardial repair and consequently synthetic ring repair. Pericardial repair often only involves posterior annuloplasty which does not include the anterior annulus, even though the fibrous anterior annulus can undergo dilation due to mitral valve disease, just like the posterior annulus (Kwan, 2003; Tibayan *et al.*, 2003; Kaji *et al.*, 2005). The primary aim of annuloplasty repair is to reinforce and stabilise the annulus whilst reducing leaflet stresses, along with correcting and preventing annular dilation whilst reintroducing leaflet coaptation. The acellular porcine mitral valve annulus has the potential to provide anchor points at the left and right trigones which might reinforce the repair and improve durability as well as absorbing some of the forces generated during the cardiac cycle, which are largest at the trigones (Kunzelman *et al.*, 2007). The decellularised porcine annuloplasty ring closely resembles the histoarchitecture of the native human annulus, therefore should provide a suitable environment for cell attachment and integration thereby enhancing durability of the repair.

Traditional methods of mitral valve repair involve open heart surgery, but the age of the patient, expertise of the surgeon and comorbidities can prevent patients having this type of surgery. In these cases the emergence of transcatheter techniques becomes valuable. Existing technology includes direct and indirect methods of transcatheter repair (Van Mieghem *et al.*, 2010). Direct methods of transcatheter annuloplasty involve the manipulation of the mitral valve annulus via catheter insertion through the left atrium or left ventricle which avoids the requirement of cardiopulmonary bypass. Indirect methods involve manipulating the orifice area from outside the mitral valve. A decellularised ring would only be suitable for direct transcatheter repair. However, current strategies using this technique have avoided annuloplasty using complete rings and have instead focussed on inserting pledgets into the annulus and reducing the length of small sections of the annulus, such as with the Mitralign system (Mitralign, Inc., Tewksbury, Massachusetts) and Accucinch (Guided Delivery Systems, Inc., Santa Clara, California). As further techniques are developed for direct transcatheter annuloplasty, the use of decellularised mitral valve annuli may become more feasible in this

emerging field. The major obstacles to the potential use of direct transcatheter repair would be suturing of the decellularised annuloplasty ring to the annulus and the size of the porcine annuloplasty ring for insertion via a catheter.

One of the main advantages of the decellularised annuloplasty ring compared to a synthetic alternative is that the biological device has the potential to provide a biocompatible supporting structure to the mitral valve annulus that can integrate with the endogenous tissue and cells at the repair site and regenerate over time. Durability may, however be affected by the lack of functional cells within the implanted decellularised annuloplasty ring immediately following repair. This may lead to degradation of the extracellular matrix due to cycling loading on the ring during the cardiac cycle. Future studies could also consider seeding cells into the decellularised ring prior to implantation so that remodelling might occur immediately upon implantation of the device. It is critical with the cell seeding approach that a sufficient oxygen supply reaches the cells in the scaffold once implanted, this can often impair the use of cell seeding prior to implantation as lack of oxygen and nutrients can lead to cell death resulting in matrix degradation caused by the release of enzymes by the cells (Martin *et al.*, 2004).

In addition to the biocompatibility testing of the decellularised annuloplasty rings *in-vitro*, it will be important to determine whether the acellular tissue elicits an immune response *in-vivo* using a small animal model, for example subcutaneous implantation in mice. Adverse reactions to the implanted scaffolds could be analysed using histology and immunohistochemistry of the explants, enabling the evaluation of cell integration. Various regions of the decellularised annuloplasty ring could be tested so that regional differences in the decellularised rings could be evaluated, this would be important for the trigonal region where the presence of “nuclear ghosts” might provoke an immune response. Further optimisation of the process to produce the decellularised annuloplasty ring would be necessary if there were adverse host responses.

To assess the remodelling of the porcine mitral valve annulus *in-vivo* and to determine functional performance as an annuloplasty repair device it will be necessary to implant the acellular annuloplasty ring in a large animal model. Sheep are often the animal model of choice for the assessment of cardiac valves (Ali *et al.*, 1996). Sheep hearts closely match human hearts in regards to the mechanical properties and haemodynamics (Rashid *et al.*,

2004) whilst they also grow less rapidly compared to other species such as calves and pigs, making studies easier to control (Ali *et al.*, 1996; Rashid *et al.*, 2004). Due to accelerated calcification in juvenile sheep they have also become a standard model for assessing calcification (Ali *et al.*, 1996) which means implanted devices can be studied for signs of calcification in relatively short time periods (Paniagua Gutierrez *et al.*, 2015). For a sheep model to provide useful data, it would be necessary to induce mitral valve regurgitation in the animals up to 6 months before the implantation of the acellular biological annuloplasty rings in order to evaluate the effects of the repair in a chronic mitral valve regurgitation model. The study would need to be performed over a period of 6 months in order to provide information on functional performance, remodelling, any local immune response and regeneration of the acellular tissue over the course of the study. Explant analysis at various time points would enable investigations using histology, immunohistochemistry, biochemical assays and biomechanical testing to assess any changes in the structure, composition, cellularity and biomechanical properties of the scaffold.

Studies of long term outcomes after mitral valve repair have shown that significant levels of mitral regurgitation can reoccur after the initial repair (Gillinov *et al.*, 1998; Flameng *et al.*, 2003; Chang *et al.*, 2007). Durability of the repair is one of the main factors in failure and understanding the complex relationship between all components of the mitral valve complex is cited as one of the main solutions to reducing this problem. Chronic mitral valve regurgitation causes left ventricular remodelling which enlarges the ventricle and alters the position of the components of the valve, including annular dilation and papillary muscle contraction. It has been suggested that superior outcomes may be obtained by repairing the whole of the mitral valve, not just the annulus (McGee *et al.*, 2004). The maintenance of the full mitral valve complex using mitral valve repair has been reported to offer superior outcomes compared to replacement (David, 1994). Preservation of the whole mitral valve may not be feasible due to calcification, fibrosis and surgical experience, amongst other reasons. It has been suggested that components that cannot be retained, such as chordae should be replaced by artificial chordae to maintain the mitral valve complex (David, 1994). The preservation of the full mitral valve complex, by retaining the link between the mitral valve annulus and the left ventricle wall via the leaflets, chordae and papillary muscles has been reported to be essential for recovery of myocardial function following the correction of mitral valve regurgitation (Ishihara *et al.*, 1992; Moon *et al.*, 1999). Disruption of these links has been

shown to cause myocardial systolic deformation and inferior outcomes (Moon *et al.*, 1999). Studies have shown that following the preservation of mitral valve components, such as the chordae, ventricular contraction returns, even if the mitral valve is replaced by a mechanical or bioprosthetic valve rather than being repaired (Ishihara *et al.*, 1992). Following on from the development of an acellular biological mitral valve annulus repair device, as described here, it may be possible to produce an acellular mitral valve complex. This would comprise the mitral valve annulus, mitral valve leaflets, chordae and the chordal attachment to the papillary muscles. This would offer further options for repair of the mitral valve and provide an alternative to mitral valve replacement using mechanical and bioprosthetic devices. The combined use of a glutaraldehyde treated pericardial annuloplasty repair alongside neochordal implantation was found to have high survival rates and low rates of reoperation after long term follow up (Salvador *et al.*, 2014). This study provides evidence of the potential to improve outcomes by use of a decellularised mitral valve complex compared to annuloplasty alone. In children chordal repair techniques are not recommended because the native chordae are thin and can break when sutured (Quinonez & Del Nido, 2015). In valves that require annuloplasty repair and chordal shortening a complete mitral valve replacement using a decellularised mitral valve complex could potentially offer an alternative solution. A recent study by Iablonskii *et al.* (2015) undertook preliminary research into a decellularised ovine mitral valve which showed cell removal and favourable leaflet characteristics.

The decellularised annuloplasty ring described here was developed with a view to creating a device that would be clinically relevant and a potential candidate for commercial development as a medical device for annuloplasty repair. Following successful large animal studies in the university, the next step in the development of the biological acellular annuloplasty ring would be to transfer the technology to an industrial partner to initiate the procedures for obtaining a CE mark so the device can be sold in Europe. In order to follow the correct route to market the porcine mitral valve annuloplasty ring would need to meet the requirements set out in the European Council Directive 93/42/EEC which applies to medical devices. These directives categorise the decellularised annuloplasty ring as a Class III medical device which is identified as high risk as a result of being derived from porcine tissue and implantable into the body. To gain approval for being placed on the European market and be awarded a CE mark the device would need to meet the guidelines set out in the directives. Acellular devices such as the decellularised mitral valve annuloplasty ring however avoid the complex

regulatory hurdles faced by cellular technologies as they are classed as medical devices rather than Advanced Therapy Medicinal Products.

The process of obtaining a CE mark would involve meeting all the essential requirements set out in the directives including following the appropriate quality management system for medical devices, ISO 13485:2003 and establishing that the device was safe and works as intended by following the harmonised standard for risk assessments, ISO 14971:2007. Clinical data forms a major component of gaining regulatory approval for a Class III device such as the annuloplasty ring; this data may be obtained from similar devices that exist in the literature or from data collected from a clinical trial. In the UK any devices that are placed onto the European market are regulated by the Medicines and Healthcare Regulatory Agency (MHRA), the MHRA designate notified bodies to carry out audits of facilities and product information before awarding a CE mark. Upon passing the audit the manufacturer of the annuloplasty ring would declare that the device meets the provisions of the appropriate Directives and could be sold on the European market.

7.2 Conclusion

In conclusion, this study has described the initial research towards development of a novel decellularised annuloplasty ring for potential use in mitral valve repair. It has been shown that it is possible to decellularise the porcine mitral valve annulus without substantial changes to the biological structure and biomechanical properties. The acellular tissue contained less than 50 ng.mg⁻¹ wet weight residual DNA in all regions representing over 95 % of DNA removal. Functional assessment of the acellular biological rings compared to synthetic annuloplasty rings demonstrated that acellular biological annuloplasty rings performed as well as synthetic rings in *in vitro* tests, however further functional tests need to be performed. Future studies should focus on evaluation of the durability of annuloplasty repair using the decellularised porcine mitral valve annulus in a physiologically relevant large animal model to establish the potential of the device for commercial development.

References

- Acar, C., de Ibarra, J. S. & Lansac, E. (2004). Anterior leaflet augmentation with autologous pericardium for mitral repair in rheumatic valve insufficiency. *J Heart Valve Dis* 13, 741–6.
- Ackermann, K., Balling, G., Eicken, A., Günther, T., Schreiber, C., Hess, J. & Gunther, T. (2007). Replacement of the systemic atrioventricular valve with a mechanical prosthesis in children aged less than 6 years: late clinical results of survival and subsequent replacement. *J Thorac Cardiovasc Surg* 134, 750–6.
- Ahmad, R. M., Gillinov, a M., McCarthy, P. M., Blackstone, E. H., Apperson-Hansen, C., Qin, J. X., Agler, D., Shiota, T. & Cosgrove, D. M. (2004). Annular geometry and motion in human ischemic mitral regurgitation: novel assessment with three-dimensional echocardiography and computer reconstruction. *Ann Thorac Surg* 78, 2063–8; discussion 2068.
- Alexander, H. & Brunski, J. (1996). Classes of materials used in medicine. *An Introd to Mater Med*.
- Ali, M. L., Kumar, S. P., Bjornstad, K. & Duran, C. M. (1996). The sheep as an animal model for heart valve research. *Cardiovasc Surg* 4, 543–9.
- Allen, R. A., Seltz, L. M., Jiang, H., Kasick, R. T., Sellaro, T. L., Badylak, S. F. & Ogilvie, J. B. (2010). Adrenal extracellular matrix scaffolds support adrenocortical cell proliferation and function in vitro. *Tissue Eng Part A* 16, 3363–74.
- Allison, M. A., Cheung, P., Criqui, M. H., Langer, R. D. & Wright, C. M. (2006). Mitral and aortic annular calcification are highly associated with systemic calcified atherosclerosis. *Circulation* 113, 861–6.
- Alsoufi, B., Manlihot, C., McCrindle, B. W., Canver, C. C., Sallehuddin, A., Al-Oufi, S., Joufan, M. & Al-Halees, Z. (2009). Aortic and mitral valve replacement in children: is there any role for biologic and bioprosthetic substitutes? *Eur J Cardiothorac Surg* 36, 84–90; discussion 90.
- Andrus, B. W. & Baldwin, J. C. (2006). Chronic Mitral Regurgitation. In *Valvular Hear Dis*, 1st edn., p. 176. London.
- Angelini, A., Ho, S. Y., Anderson, R. H., Davies, M. J. & Becker, A. E. (1988). A histological study of the atrioventricular junction in hearts with normal and prolapsed leaflets of the mitral valve. *Heart* 59, 712–716.

- Anyanwu, A. C. & Adams, D. H. (2007). Etiologic classification of degenerative mitral valve disease: Barlow's disease and fibroelastic deficiency. *Semin Thorac Cardiovasc Surg* 19, 90–6.
- Araki, Y., Usui, A., Kawaguchi, O., Saito, S., Song, M.-H., Akita, T. & Ueda, Y. (2005). Pressure-volume relationship in isolated working heart with crystalloid perfusate in swine and imaging the valve motion. *Eur J Cardiothorac Surg* 28, 435–42. Oxford University Press.
- Arita, M., Kasegawa, H. & Umezu, M. (2004). Static analysis of annuloplasty rings sutured on an annulus model of the mitral valve: comparison between the Duran ring and the Carpentier Classic ring. *J Artif Organs* 7, 30–6.
- Aumailley, M. & Timpl, R. (1986). Attachment of cells to basement membrane collagen type IV. *J Cell Biol* 103, 1569–75.
- Bader, A., Schilling, T., Teebken, O. E., Brandes, G., Herden, T., Steinhoff, G. & Haverich, A. (1998). Tissue engineering of heart valves--human endothelial cell seeding of detergent acellularized porcine valves. *Eur J Cardiothorac Surg* 14, 279–84.
- Bader, A., Steinhoff, G., Strobl, K., Schilling, T., Brandes, G., Mertsching, H., Tsikas, D., Froelich, J. & Haverich, A. (2000). Engineering of human vascular aortic tissue based on a xenogeneic starter matrix. *Transplantation* 70, 7–14.
- Badylak, S. F. (2002). The extracellular matrix as a scaffold for tissue reconstruction. *Semin Cell Dev Biol* 13, 377–383.
- Badylak, S. F. (2014). Decellularized allogeneic and xenogeneic tissue as a bioscaffold for regenerative medicine: factors that influence the host response. *Ann Biomed Eng* 42, 1517–27.
- Badylak, S. F., Freytes, D. O. & Gilbert, T. W. (2009). Extracellular matrix as a biological scaffold material: Structure and function. *Acta Biomater* 5, 1–13. Acta Materialia Inc.
- Ballal, N. V., Kundabala, M., Bhat, S., Rao, N. & Rao, B. S. S. (2009). A comparative in vitro evaluation of cytotoxic effects of EDTA and maleic acid: root canal irrigants. *Oral Surg Oral Med Oral Pathol Oral Radiol Endod* 108, 633–8.
- Barkan, D., Green, J. E. & Chambers, A. F. (2010). Extracellular matrix: a gatekeeper in the transition from dormancy to metastatic growth. *Eur J Cancer* 46, 1181–8.
- Bashey, R. I., Martinez-Hernandez, A. & Jimenez, S. A. (1992). Isolation, characterization, and localization of cardiac collagen type VI. Associations with other extracellular matrix components. *Circ Res* 70, 1006–1017.

- Bateman, M. G., Hill, A. J., Quill, J. L. & Iazzo, P. A. (2013). The clinical anatomy and pathology of the human arterial valves: implications for repair or replacement. *J Cardiovasc Transl Res* 6, 166–75.
- Bechtel, J. F. M., Gellissen, J., Erasmi, A. W., Petersen, M., Hiob, A., Stierle, U. & Sievers, H.-H. (2005). Mid-term findings on echocardiography and computed tomography after RVOT-reconstruction: comparison of decellularized (SynerGraft) and conventional allografts. *Eur J Cardiothorac Surg* 27, 410–5; discussion 415.
- Beckstead, J. H. (1994). A simple technique for preservation of fixation-sensitive antigens in paraffin-embedded tissues. *J Histochem Cytochem* 42, 1127–34.
- Beierlein, W., Becker, V., Yates, R., Tsang, V., Elliott, M., de Leval, M. & van Doorn, C. (2007). Long-term follow-up after mitral valve replacement in childhood: poor event-free survival in the young child. *Eur J Cardio-Thoracic Surg* 31, 860.
- Berdajs, D., Zünd, G., Camenisch, C., Schurr, U., Turina, M. I. & Genoni, M. (2007). Annulus fibrosus of the mitral valve: reality or myth. *J Card Surg* 22, 406–9.
- Bernacca, G. M., Straub, I. & Wheatley, D. J. (2002). Mechanical and morphological study of biostable polyurethane heart valve leaflets explanted from sheep. *J Biomed Mater Res* 61, 138–45.
- Bevilacqua, S., Cerillo, A. G., Gianetti, J., Paradossi, U., Mariani, M., Matteucci, S., Kallushi, E. & Glauber, M. (2003). Mitral valve repair for degenerative disease: is pericardial posterior annuloplasty a durable option? *Eur J Cardio-Thoracic Surg* 23, 552–559.
- Bolland, F., Korossis, S., Wilshaw, S.-P., Ingham, E., Fisher, J., Kearney, J. N. & Southgate, J. (2007). Development and characterisation of a full-thickness acellular porcine bladder matrix for tissue engineering. *Biomaterials* 28, 1061–70.
- Bloori Zadeh, P., Corbett, S. C. & Nayeb-Hashemi, H. (2013). Effects of fluid flow shear rate and surface roughness on the calcification of polymeric heart valve leaflet. *Mater Sci Eng C Mater Biol Appl* 33, 2770–5.
- Boltwood, C. M., Tei, C., Wong, M. & Shah, P. M. (1983). Quantitative echocardiography of the mitral complex in dilated cardiomyopathy: the mechanism of functional mitral regurgitation. *Circulation* 68, 498–508.
- Bonow, R. O., Carabello, B., de Leon, A. C., Edmunds, L. H., Fedderly, B. J., Freed, M. D., Gaasch, W. H., McKay, C. R., Nishimura, R. A. & other authors. (1998). Guidelines for the management of patients with valvular heart disease: executive summary. A report of the American College of Cardiology/American Heart Association Task Force on Practice

- Guidelines (Committee on Management of Patients with Valvular Heart . *Circulation* 98, 1949–84.
- Bonow, R. O., Carabello, B. A., Chatterjee, K., de Leon, A. C., Faxon, D. P., Freed, M. D., Gaasch, W. H., Lytle, B. W., Nishimura, R. A. & other authors. (2006). ACC/AHA 2006 guidelines for the management of patients with valvular heart disease: a report of the American College of Cardiology/American Heart Association Task Force on Practice Guidelines (writing Committee to Revise the 1998 guidelines for the manage. *J Am Coll Cardiol* 48, e1–148.
- Booth, C., Korossis, S. A., Wilcox, H. E., Watterson, K. G., Kearney, J. N., Fisher, J. & Ingham, E. (2002). Tissue engineering of cardiac valve prostheses I: development and histological characterization of an acellular porcine scaffold. *J Heart Valve Dis* 11, 457–62.
- Borghetti, V., Campana, M., Scotti, C., Domenighini, D., Totaro, P., Coletti, G., Pagani, M. & Lorusso, R. (2000). Biological versus prosthetic ring in mitral-valve repair: enhancement of mitral annulus dynamics and left-ventricular function with pericardial annuloplasty at long term. *Eur J Cardiothorac Surg* 17, 431–9.
- Bornstein, P. & Sage, E. H. (2002). Matricellular proteins: extracellular modulators of cell function. *Curr Opin Cell Biol* 14, 608–16.
- Bothe, W., Kvitting, J.-P. E., Swanson, J. C., Hartnett, S., Ingels, N. B. & Miller, D. C. (2010a). Effects of different annuloplasty rings on anterior mitral leaflet dimensions. *J Thorac Cardiovasc Surg* 139, 1114–22. The American Association for Thoracic Surgery.
- Bothe, W., Kvitting, J.-P. E., Swanson, J. C., Göktepe, S., Vo, K. N., Ingels, N. B. & Miller, D. C. (2010b). How do annuloplasty rings affect mitral leaflet dynamic motion? *Eur J Cardiothorac Surg* 38, 340–9.
- Boucek, R. J., Boucková, B. & Levy, S. (1978). Anatomical arrangement of muscle tissue in the anterior mitral leaflet in man. *Cardiovasc Res* 12, 675–80.
- Broom, N. D. & Myers, D. B. (1980). A study of the structural response of wet hyaline cartilage to various loading situations. *Connect Tissue Res* 7, 227–37.
- Brown, B. N., Barnes, C. a, Kasick, R. T., Michel, R., Gilbert, T. W., Beer-Stolz, D., Castner, D. G., Ratner, B. D. & Badylak, S. F. (2010a). Surface characterization of extracellular matrix scaffolds. *Biomaterials* 31, 428–37. Elsevier Ltd.
- Brown, J. W., Elkins, R. C., Clarke, D. R., Tweddell, J. S., Huddleston, C. B., Doty, J. R., Fehrenbacher, J. W. & Takkenberg, J. J. M. (2010b). Performance of the CryoValve SG human decellularized pulmonary valve in 342 patients relative to the conventional CryoValve at a mean

- follow-up of four years. *J Thorac Cardiovasc Surg* 139, 339–48. Elsevier.
- Bruckner, P. & van der Rest, M. (1994). Structure and function of cartilage collagens. *Microsc Res Tech* 28, 378–84.
- Bruno, P. G., Leva, C., Santambrogio, L., Lazzarini, I., Musazzi, G., Del Rosso, G. & Di Credico, G. (2009). Early clinical experience and echocardiographic results with a new semirigid mitral annuloplasty ring: the Sorin Memo 3D. *Ann Thorac Surg* 88, 1492–8.
- Bruno, V. D., Zebele, C., Chivasso, P., Sedmakov, H. & Ascione, R. (2013). Pericardial versus artificial ring remodeling annuloplasty for surgical repair of degenerative mitral valve disease: a propensity score analysis. *Eur Heart J* 34, P5374–P5374.
- Bulkley, B. H. & Roberts, W. C. (1975). Dilatation of the mitral anulus. *Am J Med* 59, 457–463.
- Burch, P. T., Kaza, A. K., Lambert, L. M., Holubkov, R., Shaddy, R. E. & Hawkins, J. A. (2010). Clinical performance of decellularized cryopreserved valved allografts compared with standard allografts in the right ventricular outflow tract. *Ann Thorac Surg* 90, 1301–5; discussion 1306. Elsevier.
- Burns, A. T., McDonald, I. G., Thomas, J. D., Macisaac, A. & Prior, D. (2008). Doin' the twist: new tools for an old concept of myocardial function. *Heart* 94, 978–83.
- Caamaño, S., Shiori, A., Strauss, S. H. & Orton, E. C. (2009). Does sodium dodecyl sulfate wash out of detergent-treated bovine pericardium at cytotoxic concentrations? *J Heart Valve Dis* 18, 101–5.
- Caira, F. C., Stock, S. R., Gleason, T. G., McGee, E. C., Huang, J., Bonow, R. O., Spelsberg, T. C., McCarthy, P. M., Rahimtoola, S. H. & Rajamannan, N. M. (2006). Human degenerative valve disease is associated with up-regulation of low-density lipoprotein receptor-related protein 5 receptor-mediated bone formation. *J Am Coll Cardiol* 47, 1707–12. Journal of the American College of Cardiology.
- Caldarone, C. A., Raghuvver, G., Hills, C. B., Atkins, D. L., Burns, T. L., Behrendt, D. M. & Moller, J. H. (2001). Long-Term Survival After Mitral Valve Replacement in Children Aged <5 Years. *Circulation* 104, I–143–I–147.
- Carpentier, A. (1983). Cardiac valve surgery--the 'French correction'. *J Thorac Cardiovasc Surg* 86, 323–37.
- Carpentier, a F., Lessana, a, Relland, J. Y., Belli, E., Mihaileanu, S., Berrebi, a J., Palsky, E. & Loulmet, D. F. (1995). The 'physio-ring': an advanced

concept in mitral valve annuloplasty. *Ann Thorac Surg* 60, 1177–85; discussion 1185–6.

- Carpentier, A. F., Pellerin, M., Fuzellier, J. F. & Relland, J. Y. (1996). Extensive calcification of the mitral valve anulus: pathology and surgical management. *J Thorac Cardiovasc Surg* 111, 718–29; discussion 729–30.
- Cartmell, J. S. & Dunn, M. G. (2000). Effect of chemical treatments on tendon cellularity and mechanical properties. *J Biomed Mater Res* 49, 134–40.
- Cebotari, S., Tudorache, I., Jaekel, T., Hilfiker, A., Dorfman, S., Ternes, W., Haverich, A. & Lichtenberg, A. (2010). Detergent decellularization of heart valves for tissue engineering: toxicological effects of residual detergents on human endothelial cells. *Artif Organs* 34, 206–10.
- Chang, B.-C., Youn, Y.-N., Ha, J.-W., Lim, S.-H., Hong, Y.-S. & Chung, N. (2007). Long-term clinical results of mitral valvuloplasty using flexible and rigid rings: a prospective and randomized study. *J Thorac Cardiovasc Surg* 133, 995–1003.
- Charonis, A. S., Tsilibary, E. C., Yurchenco, P. D. & Furthmayr, H. (1985). Binding of laminin to type IV collagen: a morphological study. *J Cell Biol* 100, 1848–53.
- Chauvaud, S., Jebara, V., Chachques, J. C., el Asmar, B., Mihaileanu, S., Perier, P., Dreyfus, G., Relland, J., Couetil, J. P. & Carpentier, A. (1991). Valve extension with glutaraldehyde-preserved autologous pericardium. Results in mitral valve repair. *J Thorac Cardiovasc Surg* 102, 171–7; discussion 177–8.
- Chee, T., Haston, R., Togo, A. & Raja, S. G. (2008). Is a flexible mitral annuloplasty ring superior to a semi-rigid or rigid ring in terms of improvement in symptoms and survival? *Interact Cardiovasc Thorac Surg* 7, 477–84.
- Chinchoy, E., Soule, C. L., Houlton, A. J., Gallagher, W. J., Hjelle, M. A., Laske, T. G., Morissette, J. J., Iuzzo, P. A. & Mark, A. (2000). Isolated four-chamber working swine heart model. *Ann Thorac Surg* 70, 1607–1614.
- Choi, S.-Y., Jeong, H.-J., Lim, H.-G., Park, S.-S., Kim, S.-H. & Kim, Y. J. (2012). Elimination of alpha-gal xenoreactive epitope: alpha-galactosidase treatment of porcine heart valves. *J Heart Valve Dis* 21, 387–97.
- Cicha, I., Rüffer, A., Cesnjevar, R., Glöckler, M., Agaimy, A., Daniel, W. G., Garlichs, C. D. & Dittrich, S. (2011). Early obstruction of decellularized xenogenic valves in pediatric patients: involvement of inflammatory and fibroproliferative processes. *Cardiovasc Pathol* 20, 222–31.

- Cima, L. G., Vacanti, J. P., Vacanti, C., Ingber, D., Mooney, D. & Langer, R. (1991). Tissue Engineering by Cell Transplantation Using Degradable Polymer Substrates. *J Biomech Eng* 113, 143. American Society of Mechanical Engineers.
- Cochran, R. P., Kunzelman, K. S., Chuong, C. J., Sacks, M. S. & Eberhart, R. C. (1991). Nondestructive analysis of mitral valve collagen fiber orientation. *ASAIO Trans* 37, M447–8.
- Cole, W. G., Chan, D., Hickey, A. J. & Wilcken, D. E. (1984). Collagen composition of normal and myxomatous human mitral heart valves. *Biochem J* 219, 451–60.
- Combs, M. D. & Yutzey, K. E. (2009). Heart valve development: regulatory networks in development and disease. *Circ Res* 105, 408–21.
- Cooper, D. K. (1998). Xenoantigens and xenoantibodies. *Xenotransplantation* 5, 6–17.
- Cortiella, J., Niles, J., Cantu, A., Brettler, A., Pham, A., Vargas, G., Winston, S., Wang, J., Walls, S. & Nichols, J. E. (2010). Influence of acellular natural lung matrix on murine embryonic stem cell differentiation and tissue formation. *Tissue Eng Part A* 16, 2565–80.
- Cosgrove, D. M., Arcidi, J. M., Rodriguez, L., Stewart, W. J., Powell, K. & Thomas, J. D. (1995). Initial experience with the Cosgrove-Edwards Annuloplasty System. *Ann Thorac Surg* 60, 499–503; discussion 503–4.
- Da Costa, F. D. A., Santos, L. R., Collatusso, C., Matsuda, C. N., Lopes, S. A. V., Cauduro, S., Roderjan, J. G. & Ingham, E. (2009). Thirteen years' experience with the Ross Operation. *J Heart Valve Dis* 18, 84–94.
- Da Costa, F. D. A., Costa, A. C. B. A., Prestes, R., Domanski, A. C., Balbi, E. M., Ferreira, A. D. A. & Lopes, S. V. (2010). The early and midterm function of decellularized aortic valve allografts. *Ann Thorac Surg* 90, 1854–60. Elsevier.
- Cox, B. & Emili, A. (2006). Tissue subcellular fractionation and protein extraction for use in mass-spectrometry-based proteomics. *Nat Protoc* 1, 1872–8. Nature Publishing Group.
- Crapo, P. M., Gilbert, T. W. & Badylak, S. F. (2011). An overview of tissue and whole organ decellularization processes. *Biomaterials* 32, 3233–43.
- Crick, S. J., Sheppard, M. N., Ho, S. Y., Gebstein, L. & Anderson, R. H. (1998). Anatomy of the pig heart: comparisons with normal human cardiac structure. *J Anat* 193 (Pt 1, 105–19.
- Cui, Y.-C., Li, K., Tian, Y., Yuan, W.-M., Peng, P., Yang, J.-Z., Zhang, B.-J., Zhang, H.-D., Wu, A.-L. & Tang, Y. (2014). A pig model of ischemic

mitral regurgitation induced by mitral chordae tendinae rupture and implantation of an ameroid constrictor. *PLoS One* 9, e111689.

Culav, E. M., Clark, C. H. & Merrilees, M. J. (1999). Connective Tissues: Matrix Composition and Its Relevance to Physical Therapy. *Phys Ther* 79, 308–319.

Curi-Curi, P., Ramírez-Marroquín, S., Cervantes-Salazar, J., Soulé, M., Erdmenger, J. & Calderón-Colmenero, J. (2010). Surgical repair of congenital mitral valve malformations. *Arch Cardiol México* 80, 87–94. Elsevier.

Curtil, A., Pegg, D. E. & Wilson, A. (1997). Repopulation of freeze-dried porcine valves with human fibroblasts and endothelial cells. *J Heart Valve Dis* 6, 296–306.

D'Eredità, R. (2015). Porcine small intestinal submucosa (SIS) myringoplasty in children: A randomized controlled study. *Int J Pediatr Otorhinolaryngol*.

Daebritz, S. H., Sachweh, J. S., Hermanns, B., Fausten, B., Franke, A., Groetzner, J., Klosterhalfen, B. & Messmer, B. J. (2003). Introduction of a flexible polymeric heart valve prosthesis with special design for mitral position. *Circulation* 108 Suppl , II134–9.

Dagum, P., Timek, T., Green, G. R., Daughters, G. T., Liang, D., Ingels, N. B. & Miller, D. C. (2001). Three-dimensional geometric comparison of partial and complete flexible mitral annuloplasty rings. *J Thorac Cardiovasc Surg* 122, 665–73.

Dahl, S. L. M., Koh, J., Prabhakar, V. & Niklason, L. E. (2003). Decellularized native and engineered arterial scaffolds for transplantation. *Cell Transplant* 12, 659–66.

Daimon, M., Fukuda, S., Adams, D. H., McCarthy, P. M., Gillinov, a M., Carpentier, A., Filsoufi, F., Abascal, V. M., Rigolin, V. H. & other authors. (2006). Mitral valve repair with Carpentier-McCarthy-Adams IMR ETlogix annuloplasty ring for ischemic mitral regurgitation: early echocardiographic results from a multi-center study. *Circulation* 114, I588–93.

David, T. E. (1994). Papillary muscle-annular continuity: is it important? *J Card Surg* 9, 252–4.

Delmo Walter, E. M., Siniawski, H., Ovroutski, S. & Hetzer, R. (2010). Mitral valve growth after posterior annular stabilization with untreated autologous pericardial strip in children with mitral valve insufficiency. *Ann Thorac Surg* 90, 1577–85; discussion 1585. Elsevier Inc.

- Dohmen, P. M., Lembcke, A., Holinski, S., Pruss, A. & Konertz, W. (2011). Ten years of clinical results with a tissue-engineered pulmonary valve. *Ann Thorac Surg* 92, 1308–14. Elsevier.
- Duan, B., Hockaday, L. A., Kang, K. H. & Butcher, J. T. (2013). 3D bioprinting of heterogeneous aortic valve conduits with alginate/gelatin hydrogels. *J Biomed Mater Res A* 101, 1255–64.
- Eckert, C. E., Zubiate, B., Vergnat, M., Gorman, J. H., Gorman, R. C. & Sacks, M. S. (2009). In vivo dynamic deformation of the mitral valve annulus. *Ann Biomed Eng* 37, 1757–71.
- Egan, K. P., Kim, J.-H., Mohler, E. R. & Pignolo, R. J. (2011). Role for circulating osteogenic precursor cells in aortic valvular disease. *Arterioscler Thromb Vasc Biol* 31, 2965–71.
- Elder, B. D., Eleswarapu, S. V & Athanasiou, K. A. (2009). Extraction techniques for the decellularization of tissue engineered articular cartilage constructs. *Biomaterials* 30, 3749–56.
- EMD Millipore Corporation. (2013). Benzoylase endonuclease. Billerica, MA, USA.
- Enriquez-Sarano, M., Akins, C. W. & Vahanian, A. (2009). Mitral regurgitation. *Lancet* 373, 1382–94. Elsevier Ltd.
- Erdbrügger, W., Konertz, W., Dohmen, P. M., Posner, S., Ellerbrok, H., Brodde, O.-E., Robenek, H., Modersohn, D., Pruss, A. & other authors. (2006). Decellularized xenogenic heart valves reveal remodeling and growth potential in vivo. *Tissue Eng* 12, 2059–68.
- Etchells, E., Bell, C. & Robb, K. (1997). Does this patient have an abnormal systolic murmur? *JAMA* 277, 564–71.
- Fedak, P. W. M., McCarthy, P. M. & Bonow, R. O. (2008). Evolving concepts and technologies in mitral valve repair. *Circulation* 117, 963–74.
- Flachskampf, F. A., Chandra, S., Gaddipatti, A., Levine, R. A., Weyman, A. E., Ameling, W., Hanrath, P. & Thomas, J. D. (2000). Analysis of shape and motion of the mitral annulus in subjects with and without cardiomyopathy by echocardiographic 3-dimensional reconstruction. *J Am Soc Echocardiogr* 13, 277–87.
- Flameng, W., Herijgers, P. & Bogaerts, K. (2003). Recurrence of mitral valve regurgitation after mitral valve repair in degenerative valve disease. *Circulation* 107, 1609–13.
- Flanagan, T. C. & Pandit, a. (2003). Living artificial heart valve alternatives: a review. *Eur Cell Mater* 6, 28–45; discussion 45.

- Flanagan, T. C., Cornelissen, C., Koch, S., Tschoeke, B., Sachweh, J. S., Schmitz-Rode, T. & Jockenhoevel, S. (2007). The in vitro development of autologous fibrin-based tissue-engineered heart valves through optimised dynamic conditioning. *Biomaterials* 28, 3388–97.
- Fratzl, P. (2008). *Collagen: Structure and Mechanics (Google eBook)*. Springer.
- Fujiki, M., Misumi, K. & Sakamoto, H. (2000). Evaluation of collagenase-induced mitral valve regurgitation in dogs. *Am J Vet Res* 61, 1593–8.
- Fundarò, P., Tartara, P. M., Villa, E., Fratto, P., Campisi, S. & Vitali, E. O. (2007). Mitral valve repair: is there still a place for suture annuloplasty? *Asian Cardiovasc Thorac Ann* 15, 351–8.
- Gailit, J. & Ruoslahti, E. (1988). Regulation of the fibronectin receptor affinity by divalent cations. *J Biol Chem* 263, 12927–12932.
- Galili, U. (2001). The α -gal epitope (Gal α 1-3Gal β 1-4GlcNAc-R) in xenotransplantation. *Biochimie* 83, 557–563.
- Gelse, K., Pöschl, E. & Aigner, T. (2003). Collagens--structure, function, and biosynthesis. *Adv Drug Deliv Rev* 55, 1531–46.
- Ghanbari, H., Viatge, H., Kidane, A. G., Burriesci, G., Tavakoli, M. & Seifalian, A. M. (2009). Polymeric heart valves: new materials, emerging hopes. *Trends Biotechnol* 27, 359–67.
- Gilbert, T. W., Sellaro, T. L. & Badylak, S. F. (2006). Decellularization of tissues and organs. *Biomaterials* 27, 3675–83.
- Gillinov, a M., Cosgrove, D. M., Blackstone, E. H., Diaz, R., Arnold, J. H., Lytle, B. W., Smedira, N. G., Sabik, J. F., McCarthy, P. M. & Loop, F. D. (1998). Durability of mitral valve repair for degenerative disease. *J Thorac Cardiovasc Surg* 116, 734–43.
- Gillinov, a M., Wierup, P. N., Blackstone, E. H., Bishay, E. S., Cosgrove, D. M., White, J., Lytle, B. W. & McCarthy, P. M. (2001). Is repair preferable to replacement for ischemic mitral regurgitation? *J Thorac Cardiovasc Surg* 122, 1125–41.
- Glasson, J. R., Green, G. R., Nistal, J. F., Dagum, P., Komeda, M., Daughters, G. T., Bolger, a F., Foppiano, L. E., Ingels, N. B. & Miller, D. C. (1999). Mitral annular size and shape in sheep with annuloplasty rings. *J Thorac Cardiovasc Surg* 117, 302–9.
- Glasson, J. R., Komeda, M., Daughters, G. T., Niczyporuk, M. A., Bolger, A. F., Ingels, N. B. & Miller, D. C. (1996). THREE-DIMENSIONAL REGIONAL DYNAMICS OF THE NORMAL MITRAL ANULUS DURING LEFT VENTRICULAR EJECTION. *J Thorac Cardiovasc Surg* 111, 574–585.

- Goldstein, S., Clarke, D. R., Walsh, S. P., Black, K. S. & O'Brien, M. F. (2000). Transpecies heart valve transplant: advanced studies of a bioengineered xeno-autograft. *Ann Thorac Surg* 70, 1962–9.
- Grande-Allen, K. J., Calabro, A., Gupta, V., Wight, T. N., Hascall, V. C. & Vesely, I. (2004). Glycosaminoglycans and proteoglycans in normal mitral valve leaflets and chordae: association with regions of tensile and compressive loading. *Glycobiology* 14, 621–33.
- Grande-Allen, K. J., Borowski, A. G., Troughton, R. W., Houghtaling, P. L., Dipaola, N. R., Moravec, C. S., Vesely, I. & Griffin, B. P. (2005). Apparently normal mitral valves in patients with heart failure demonstrate biochemical and structural derangements: an extracellular matrix and echocardiographic study. *J Am Coll Cardiol* 45, 54–61.
- Grande-Allen, K. J., Griffin, B. P., Ratliff, N. B., Cosgrove, D. M. & Vesely, I. (2003). Glycosaminoglycan profiles of myxomatous mitral leaflets and chordae parallel the severity of mechanical alterations. *J Am Coll Cardiol* 42, 271–277.
- Gratzer, P. F., Harrison, R. D. & Woods, T. (2006). Matrix alteration and not residual sodium dodecyl sulfate cytotoxicity affects the cellular repopulation of a decellularized matrix. *Tissue Eng* 12, 2975–83.
- Grauss, R. W., Hazekamp, M. G., Oppenhuizen, F., van Munsteren, C. J., Gittenberger-de Groot, A. C. & DeRuiter, M. C. (2005). Histological evaluation of decellularised porcine aortic valves: matrix changes due to different decellularisation methods. *Eur J Cardiothorac Surg* 27, 566–71.
- Green, G. R., Dagum, P., Glasson, J. R., Nistal, J. F., Daughters, G. T., Ingels, N. B. & Miller, D. C. (1999). Restricted posterior leaflet motion after mitral ring annuloplasty. *Ann Thorac Surg* 68, 2100–6.
- Grinnell, F. (2003). Fibroblast biology in three-dimensional collagen matrices. *Trends Cell Biol* 13, 264–9.
- Gross, L. & Kugel, M. A. (1931). Topographic Anatomy and Histology of the Valves in the Human Heart. *Am J Pathol* 7, 445–474.7.
- Grossi, E. a, Goldberg, J. D., LaPietra, a, Ye, X., Zakow, P., Sussman, M., Delianides, J., Culliford, a T., Esposito, R. a & other authors. (2001). Ischemic mitral valve reconstruction and replacement: comparison of long-term survival and complications. *J Thorac Cardiovasc Surg* 122, 1107–24.
- Güden, M., Kazimoğlu, K., Sanisoğlu, Y., Sağbaş, E., Yaman, R. & Akpınar, B. (2004). The use of autologous pericardium for complicated mitral valve annulus. *Asian Cardiovasc Thorac Ann* 12, 7–10.

- Gunning, G. M. & Murphy, B. P. (2014). Determination of the tensile mechanical properties of the segmented mitral valve annulus. *J Biomech* 47, 334–40. Elsevier.
- Gupta, V., Barzilla, J. E., Mendez, J. S., Stephens, E. H., Lee, E. L., Collard, C. D., Laucirica, R., Weigel, P. H. & Grande-Allen, K. J. (2009). Abundance and location of proteoglycans and hyaluronan within normal and myxomatous mitral valves. *Cardiovasc Pathol* 18, 191–7. Elsevier Inc.
- Hammer, D., Leier, C. V, Baba, N., Vasko, J. S., Wooley, C. F. & Pinnell, S. R. (1979). Altered collagen composition in a prolapsing mitral valve with ruptured chordae tendineae. *Am J Med* 67, 863–6.
- Hammermeister, K. E., Sethi, G. K., Henderson, W. G., Oprian, C., Kim, T. & Rahimtoola, S. (1993). A comparison of outcomes in men 11 years after heart-valve replacement with a mechanical valve or bioprosthesis. Veterans Affairs Cooperative Study on Valvular Heart Disease. *N Engl J Med* 328, 1289–96.
- Hawkins, J. A., Hillman, N. D., Lambert, L. M., Jones, J., Di Russo, G. B., Profaizer, T., Fuller, T. C., Minich, L. L., Williams, R. V & Shaddy, R. E. (2003). Immunogenicity of decellularized cryopreserved allografts in pediatric cardiac surgery: comparison with standard cryopreserved allografts. *J Thorac Cardiovasc Surg* 126, 247–52; discussion 252–3.
- He, S., Fontaine, A. A., Schwammenthal, E., Yoganathan, A. P. & Levine, R. A. (1997). Integrated mechanism for functional mitral regurgitation: leaflet restriction versus coapting force: in vitro studies. *Circulation* 96, 1826–34.
- He, Z. & Bhattacharya, S. (2008). Papillary muscle and annulus size effect on anterior and posterior annulus tension of the mitral valve: an insight into annulus dilatation. *J Biomech* 41, 2524–32.
- Hearse, D. J. & Sutherland, F. J. (2000). Experimental models for the study of cardiovascular function and disease. *Pharmacol Res* 41, 597–603.
- Hiemann, N. E., Mani, M., Huebler, M., Meyer, R., Hetzer, R., Thieme, R. & Bethge, C. (2010). Complete destruction of a tissue-engineered porcine xenograft in pulmonary valve position after the Ross procedure. *J Thorac Cardiovasc Surg* 139, e67–8. Elsevier.
- Hill, R. B. (1986). Bloom and Fawcett: A Textbook of Histology. *JAMA J Am Med Assoc* 256, 1366. American Medical Association.
- Hillman, N. D., Tani, L. Y., Veasy, L. G., Lambert, L. L., Di Russo, G. B., Doty, D. B., McGough, E. C. & Hawkins, J. a. (2004). Current status of surgery for rheumatic carditis in children. *Ann Thorac Surg* 78, 1403–8.
- Ho, S. Y. (2002). Anatomy of the mitral valve. *Heart* 88 Suppl 4, iv5–10.

- Ho, S. Y. (2009). Anatomy and myoarchitecture of the left ventricular wall in normal and in disease. *Eur J Echocardiogr* 10, iii3–7. Oxford University Press.
- Hoerstrup, S. P., Sodian, R., Daebritz, S., Wang, J., Bacha, E. A., Martin, D. P., Moran, A. M., Guleserian, K. J., Sperling, J. S. & other authors. (2000). Functional Living Trileaflet Heart Valves Grown In Vitro. *Circulation* 102, III–44–III–49.
- Hoerstrup, S. P., Kadner, A., Melnitchouk, S., Trojan, A., Eid, K., Tracy, J., Sodian, R., Visjager, J. F., Kolb, S. A. & other authors. (2002). Tissue engineering of functional trileaflet heart valves from human marrow stromal cells. *Circulation* 106.
- Hopkinson, A., Shanmuganathan, V. A., Gray, T., Yeung, A. M., Lowe, J., James, D. K. & Dua, H. S. (2008). Optimization of amniotic membrane (AM) denuding for tissue engineering. *Tissue Eng Part C Methods* 14, 371–81. Mary Ann Liebert, Inc. 140 Huguenot Street, 3rd Floor New Rochelle, NY 10801 USA.
- Hu, X. & Zhao, Q. (2011). Systematic evaluation of the flexible and rigid annuloplasty ring after mitral valve repair for mitral regurgitation. *Eur J Cardiothorac Surg* 40, 480–7.
- Hubbell, J. A., Massia, S. P., Desai, N. P. & Drumheller, P. D. (1991). Endothelial cell-selective materials for tissue engineering in the vascular graft via a new receptor. *Nat Biotechnol* 9, 568–572.
- Hudson, T. W., Liu, S. Y. & Schmidt, C. E. Engineering an improved acellular nerve graft via optimized chemical processing. *Tissue Eng* 10, 1346–58.
- Hueb, A. C., Jatene, F. B., Moreira, L. F. P., Pomerantzeff, P. M., Kallás, E. & de Oliveira, S. A. (2002). Ventricular remodeling and mitral valve modifications in dilated cardiomyopathy: new insights from anatomic study. *J Thorac Cardiovasc Surg* 124, 1216–24.
- Hyoungshin Park , Milica Radisic , Jeong Ok Lim , Bong Hyun Chang, G. (2011). A Novel Composite Scaffold for Cardiac Tissue Engineering Author (s): Hyoungshin Park , Milica Radisic , Jeong Ok Lim , Bong Hyun Chang , Gordana Source : In Vitro Cellular & Developmental Biology . Animal , Vol . 41 , No . 7 (Jul . - Aug . , 2005), Pu. *In Vitro* 41, 188–196.
- lablonskii, P., Cebotari, S., Tudorache, I., Granados, M., Morticelli, L., Goecke, T., Klein, N., Korossis, S., Hilfiker, A. & Haverich, A. (2015). Tissue-engineered mitral valve: morphology and biomechanics †. *Interact Cardiovasc Thorac Surg* 20, 712–9.
- Ingram, J. H., Korossis, S., Howling, G., Fisher, J. & Ingham, E. (2007). The use of ultrasonication to aid recellularization of acellular natural tissue

- scaffolds for use in anterior cruciate ligament reconstruction. *Tissue Eng* 13, 1561–72.
- Iozzo, P. (2011). Myocardial, perivascular, and epicardial fat. *Diabetes Care* 34 Suppl 2, S371–9.
- Ishihara, K., Zile, M. R., Kanazawa, S., Tsutsui, H., Urabe, Y., DeFreyte, G. & Carabello, B. A. (1992). Left ventricular mechanics and myocyte function after correction of experimental chronic mitral regurgitation by combined mitral valve replacement and preservation of the native mitral valve apparatus. *Circulation* 86, 1116–25.
- lung, B. (2003). Management of ischaemic mitral regurgitation. *Heart* 89, 459–464.
- lung, B., Baron, G., Butchart, E. G., Delahaye, F., Gohlke-Bärwolf, C., Levang, O. W., Tornos, P., Vanoverschelde, J.-L., Vermeer, F. & other authors. (2003). A prospective survey of patients with valvular heart disease in Europe: The Euro Heart Survey on Valvular Heart Disease. *Eur Heart J* 24, 1231–1243.
- lung, B., Baron, G., Tornos, P., Gohlke-Bärwolf, C., Butchart, E. G. & Vahanian, A. (2007). Valvular heart disease in the community: a European experience. *Curr Probl Cardiol* 32, 609–61.
- Janning, P., Schrader, W. & Linscheid, M. (1994). A new mass spectrometric approach to detect modifications in DNA. *Rapid Commun Mass Spectrom* 8, 1035–40.
- Jensen, M. O., Jensen, H., Smerup, M., Levine, R. A., Yoganathan, A. P., Nygaard, H., Hasenkam, J. M., Nielsen, S. L. & Ajit, P. (2008). Saddle-shaped mitral valve annuloplasty rings experience lower forces compared with flat rings. *Circulation* 118, S250–5.
- Jensen, M. O., Jensen, H., Levine, R. a, Yoganathan, A. P., Andersen, N. T., Nygaard, H., Hasenkam, J. M. & Nielsen, S. L. (2011). Saddle-shaped mitral valve annuloplasty rings improve leaflet coaptation geometry. *J Thorac Cardiovasc Surg* 142, 697–703. The American Association for Thoracic Surgery.
- Jensen, U. B., Owens, D. M., Pedersen, S. & Christensen, R. (2010). Zinc fixation preserves flow cytometry scatter and fluorescence parameters and allows simultaneous analysis of DNA content and synthesis, and intracellular and surface epitopes. *Cytometry A* 77, 798–804.
- Jimenez, J., Soerensen, D., He, Z., Ritchie, J., Yoganathan, A. & Engineering, B. (2005). Mitral Valve Function and Chordal Force Distribution Using a Flexible Annulus Model: An In Vitro Study. *Ann Biomed Eng* 33, 557–566.

- Jimenez, J. H., Soerensen, D. D., He, Z., He, S. & Yoganathan, A. P. (2003). Effects of a Saddle Shaped Annulus on Mitral Valve Function and Chordal Force Distribution: An In Vitro Study. *Ann Biomed Eng* 31, 1171. Springer Netherlands.
- Jimenez, J. H., Liou, S. W., Padala, M., He, Z., Sacks, M., Gorman, R. C., Gorman, J. H. & Yoganathan, A. P. (2007). A saddle-shaped annulus reduces systolic strain on the central region of the mitral valve anterior leaflet. *J Thorac Cardiovasc Surg* 134, 1562–8.
- Jockenhoevel, S. (2001). Fibrin gel – advantages of a new scaffold in cardiovascular tissue engineering. *Eur J Cardio-Thoracic Surg* 19, 424–430.
- Jones, E. L. (1994). Mitral valve replacement: indications, choice of valve prosthesis, results, and long-term morbidity of porcine and mechanical valves. *J Card Surg* 9, 218–21.
- Kadler, K. E., Baldock, C., Bella, J. & Boot-Handford, R. P. (2007). Collagens at a glance. *J Cell Sci* 120, 1955–8.
- Kaji, S., Nasu, M., Yamamuro, A., Tanabe, K., Nagai, K., Tani, T., Tamita, K., Shiratori, K., Kinoshita, M. & other authors. (2005). Annular geometry in patients with chronic ischemic mitral regurgitation: three-dimensional magnetic resonance imaging study. *Circulation* 112, 1409–14.
- Kalangos, A. (2006). Polydioxanone Polymers for Annuloplasty in Valve Repair 81–83.
- Kallenbach, K., Leyh, R. G., Lefik, E., Walles, T., Wilhelmi, M., Cebotari, S., Schmiedl, A., Haverich, A. & Mertsching, H. (2004). Guided tissue regeneration: porcine matrix does not transmit PERV. *Biomaterials* 25, 3613–20.
- Kaplan, S. I. L., Bashein, G., Sheehan, F. H., Atch, M. & Martin, R. W. (2000). Three-dimensional of annular shape regurgitant mitral echocardiographic assessment changes in the normal and valve. *Heart*.
- Keene, D. R., Engvall, E. & Glanville, R. W. (1988). Ultrastructure of type VI collagen in human skin and cartilage suggests an anchoring function for this filamentous network. *J Cell Biol* 107, 1995–2006.
- Keller, J. & Riley, D. (1976). Nuclear ghosts: a nonmembranous structural component of mammalian cell nuclei. *Science (80-)* 193, 399–401.
- Keren, G., Sonnenblick, E. H. & LeJemtel, T. H. (1988). Mitral anulus motion. Relation to pulmonary venous and transmitral flows in normal subjects and in patients with dilated cardiomyopathy. *Circulation* 78, 621–9.

- Khalil, S. & Sun, W. (2007). Biopolymer deposition for freeform fabrication of hydrogel tissue constructs. *Mater Sci Eng C* 27, 469–478.
- Kheradvar, A. & Gharib, M. (2007). Influence of Ventricular Pressure Drop on Mitral Annulus Dynamics Through the Process of Vortex Ring Formation. *Ann Biomed Eng* 35, 2050–2064. Springer Netherlands.
- Khoshnoodi, J., Pedchenko, V. & Hudson, B. G. (2008). Mammalian collagen IV. *Microsc Res Tech* 71, 357–70.
- Kim, N. Y., Jung, W.-W., Oh, Y.-K., Chun, T., Park, H.-Y., Lee, H.-T., Han, I.-K., Yang, J. M. & Kim, Y. B. (2007). Natural protection from zoonosis by alpha-gal epitopes on virus particles in xenotransmission. *Xenotransplantation* 14, 104–11.
- Kitzman, D. W. & Edwards, W. D. (1990). Age-Related Changes in the Anatomy of the Normal Human Heart. *J Gerontol* 45, M33–M39.
- Klabunde, R. E. (2011). Pressure Gradients.
- Klebe, R. J. (1974). Isolation of a collagen-dependent cell attachment factor. *Nature* 250, 248–51.
- Konakci, K. Z., Bohle, B., Blumer, R., Hoetzenecker, W., Roth, G., Moser, B., Boltz-Nitulescu, G., Gorlitzer, M., Klepetko, W. & other authors. (2005). Alpha-Gal on bioprostheses: xenograft immune response in cardiac surgery. *Eur J Clin Invest* 35, 17–23.
- Konertz, W., Dohmen, P. M., Liu, J., Beholz, S., Dushe, S., Posner, S., Lembcke, A. & Erdbrügger, W. (2005). Hemodynamic characteristics of the Matrix P decellularized xenograft for pulmonary valve replacement during the Ross operation. *J Heart Valve Dis* 14, 78–81.
- Konuma, T., Devaney, E. J., Bove, E. L., Gelehrter, S., Hirsch, J. C., Tavakkol, Z. & Ohye, R. G. (2009). Performance of CryoValve SG decellularized pulmonary allografts compared with standard cryopreserved allografts. *Ann Thorac Surg* 88, 849–54; discussion 554–5. Elsevier.
- Korossis, S. A., Wilcox, H. E., Watterson, K. G., Kearney, J. N., Ingham, E. & Fisher, J. (2005). In-vitro assessment of the functional performance of the decellularized intact porcine aortic root. *J Heart Valve Dis* 14, 408–21; discussion 422.
- Korossis, S. A., Booth, C., Wilcox, H. E., Watterson, K. G., Kearney, J. N., Fisher, J. & Ingham, E. (2002). Tissue engineering of cardiac valve prostheses II: biomechanical characterization of decellularized porcine aortic heart valves. *J Heart Valve Dis* 11, 463–71.

- Kron, I. L., Green, G. R. & Cope, J. T. (2002). Surgical relocation of the posterior papillary muscle in chronic ischemic mitral regurgitation. *Ann Thorac Surg* 74, 600–601.
- Kumar, A. S., Talwar, S. & Gupta, A. (2009). Mitral valve replacement with the pulmonary autograft: midterm results. *J Thorac Cardiovasc Surg* 138, 359–64.
- Kunzelman, K. (1997). Annular dilatation increases stress in the mitral valve and delays coaptation: a finite element computer model. *Cardiovasc Surg* 5, 427–434.
- Kunzelman, K. S., Cochran, R. P., Murphree, S. S., Ring, W. S., Verrier, E. D. & Eberhart, R. C. (1993). Differential collagen distribution in the mitral valve and its influence on biomechanical behaviour. *J Heart Valve Dis* 2, 236–44.
- Kunzelman, K. S., Cochran, R. P., Verrier, E. D. & Eberhart, R. C. (1994). Anatomic basis for mitral valve modelling. *J Heart Valve Dis* 3, 491–6.
- Kunzelman, K. S., Reimink, M. S. & Cochran, R. P. (1998a). Flexible versus rigid ring annuloplasty for mitral valve annular dilatation: a finite element model. *J Heart Valve Dis* 7, 108–16.
- Kunzelman, K. S., Einstein, D. R. & Cochran, R. P. (2007). Fluid-structure interaction models of the mitral valve: function in normal and pathological states. *Philos Trans R Soc Lond B Biol Sci* 362, 1393–406.
- Kunzelman, K. S., Quick, D. W. & Cochran, R. P. (1998b). Altered collagen concentration in mitral valve leaflets: biochemical and finite element analysis. *Ann Thorac Surg* 66, S198–S205.
- Kunzelman, K. S. & Cochran, R. P. (1992). Stress/Strain Characteristics of Porcine Mitral Valve Tissue: Parallel Versus Perpendicular Collagen Orientation. *J Card Surg* 7, 71–78.
- Kwan, J. (2003). Geometric Differences of the Mitral Apparatus Between Ischemic and Dilated Cardiomyopathy With Significant Mitral Regurgitation: Real-Time Three-Dimensional Echocardiography Study. *Circulation* 107, 1135–1140.
- De La Zerda, D. J., Cohen, O., Marelli, D., Esmailian, F., Hekmat, D. & Laks, H. (2008). Long-term results of mitral valve repair using autologous pericardium annuloplasty. *J Heart Valve Dis* 17, 10–5.
- Lam, J. H. C., Ranganathan, N., Wigle, E. D. & Silver, M. D. (1970). Morphology of the Human Mitral Valve: I. Chordae Tendineae: A New Classification. *Circulation* 41, 449–458.

- Lansac, E., Lim, K. H., Shomura, Y., Goetz, W. A., Lim, H. Sen, Rice, N. T., Saber, H. & Duran, C. M. G. (2002). Dynamic balance of the aortomitral junction. *J Thorac Cardiovasc Surg* 123, 911–8.
- Laskey, W. K., Plappert, T. A. & Sutton, M. G. S. J. (2007). Left ventricular mechanical load and contractile function in patients with chronic mitral regurgitation. *J Heart Valve Dis* 16, 247–54.
- Lee, C.-H. C., Kwak, J. G., Park, C. S., Kim, S.-J., Song, J. Y. & Shim, W.-S. (2010). Long-term results after mitral valve repair in children. *Eur J Cardiothorac Surg* 37, 267–72.
- Levine, R. A., Triulzi, M. O., Harrigan, P. & Weyman, A. E. (1987). The relationship of mitral annular shape to the diagnosis of mitral valve prolapse. *Circulation* 75, 756–67.
- Levine, R. A., Handschumacher, M. D., Sanfilippo, A. J., Hagege, A. A., Harrigan, P., Marshall, J. E. & Weyman, A. E. (1989). Three-dimensional echocardiographic reconstruction of the mitral valve, with implications for the diagnosis of mitral valve prolapse. *Circulation* 80, 589–98.
- Liao, J. & Vesely, I. (2003). A structural basis for the size-related mechanical properties of mitral valve chordae tendineae. *J Biomech* 36, 1125–33.
- Lim, K. H., Yeo, J. H. & Duran, C. M. G. (2005). Three-dimensional asymmetrical modeling of the mitral valve: a finite element study with dynamic boundaries. *J Heart Valve Dis* 14, 386–92.
- Liu, D., Kobayashi, T., Yokoyama, I., Ogawa, H., Nagasaka, T., Muramatsu, H., Kadomatsu, K., Oikawa, T., Shimano, Y. & other authors. (2002). Enzymatic removal of alphaGal antigen in pig kidneys by ex vivo and in vivo administration of endo-beta-galactosidase C. *Xenotransplantation* 9, 228–36.
- López, D., Durán, A. C. & Sans-Coma, V. (2000). Formation of cartilage in cardiac semilunar valves of chick and quail. *Ann Anat* 182, 349–59.
- López, D., Fernández, M. C., Durán, A. C. & Sans-Coma, V. (2001). Cartilage in pulmonary valves of Syrian hamsters. *Ann Anat* 183, 383–8.
- López, D., Durán, A. C., de Andrés, A. V., Guerrero, A., Blasco, M. & Sans-Coma, V. (2003). Formation of cartilage in the heart of the Spanish terrapin, *Mauremys leprosa* (Reptilia, Chelonia). *J Morphol* 258, 97–105.
- Lovekamp, J. J., Simionescu, D. T., Mercuri, J. J., Zubiarte, B., Sacks, M. S. & Vyavahare, N. R. (2006). Stability and function of glycosaminoglycans in porcine bioprosthetic heart valves. *Biomaterials* 27, 1507–18. NIH Public Access.

- Lumpkins, S. B., Pierre, N. & McFetridge, P. S. (2008). A mechanical evaluation of three decellularization methods in the design of a xenogeneic scaffold for tissue engineering the temporomandibular joint disc. *Acta Biomater* 4, 808–16.
- Luo, J., Korossis, S. A., Wilshaw, S.-P., Jennings, L. M., Fisher, J. & Ingham, E. (2014). Development and characterization of acellular porcine pulmonary valve scaffolds for tissue engineering. *Tissue Eng Part A* 20, 2963–74.
- Marchington, J. M., Mattacks, C. A. & Pond, C. M. (1989). Adipose tissue in the mammalian heart and pericardium: structure, foetal development and biochemical properties. *Comp Biochem Physiol B* 94, 225–32.
- Marcus, R. H. (1994). The Spectrum of Severe Rheumatic Mitral Valve Disease in a Developing Country: Correlations among Clinical Presentation, Surgical Pathologic Findings, and Hemodynamic Sequelae. *Ann Intern Med* 120, 177. American College of Physicians.
- Maria, P., Pomerantzeff, A., Manuel, C., Brandão, D. A., Albuquerque, M. A., Pomerantzeff, P. Y., Takeda, F., Oliveira, S. A., Pma, P. & other authors. (2005). ORIGINAL RESEARCH MITRAL VALVE ANNULOPLASTY WITH A BOVINE PERICARDIAL STRIP - 18-YEAR RESULTS. *Heart* 60, 305–310.
- Marins, J. S. R., Sassone, L. M., Fidel, S. R. & Ribeiro, D. A. (2012). In vitro genotoxicity and cytotoxicity in murine fibroblasts exposed to EDTA, NaOCl, MTAD and citric acid. *Braz Dent J* 23, 527–33.
- Martin, I., Wendt, D. & Heberer, M. (2004). The role of bioreactors in tissue engineering. *Trends Biotechnol* 22, 80–6.
- Masoumi, N., Annabi, N., Assmann, A., Larson, B. L., Hjortnaes, J., Alemdar, N., Kharaziha, M., Manning, K. B., Mayer, J. E. & Khademhosseini, A. (2014). Tri-layered elastomeric scaffolds for engineering heart valve leaflets. *Biomaterials* 35, 7774–85.
- Matuska, A. M. & McFetridge, P. S. (2015). The effect of terminal sterilization on structural and biophysical properties of a decellularized collagen-based scaffold; implications for stem cell adhesion. *J Biomed Mater Res B Appl Biomater* 103, 397–406.
- Mayne, R. (1989). Cartilage collagens. What Is Their Function, and Are They Involved in Articular Disease? *Arthritis Rheum* 32, 241–246.
- McCarthy, K. P., Ring, L. & Rana, B. S. (2010). Anatomy of the mitral valve: understanding the mitral valve complex in mitral regurgitation. *Eur J Echocardiogr* 11, i3–9.

- McDevitt, C. A., Wildey, G. M. & Cutrone, R. M. (2003). Transforming growth factor-beta1 in a sterilized tissue derived from the pig small intestine submucosa. *J Biomed Mater Res A* 67, 637–40.
- McGee, E. C., Gillinov, A. M., Blackstone, E. H., Rajeswaran, J., Cohen, G., Najam, F., Shiota, T., Sabik, J. F., Lytle, B. W. & other authors. (2004). Recurrent mitral regurgitation after annuloplasty for functional ischemic mitral regurgitation. *J Thorac Cardiovasc Surg* 128, 916–24.
- McLeod, O., Dunér, P., Samnegård, A., Tornvall, P., Nilsson, J., Hamsten, A. & Bengtsson, E. (2015). Autoantibodies against basement membrane collagen type IV are associated with myocardial infarction. *IJC Hear Vasc* 6, 42–47.
- McMorrow, I. M., Comrack, C. A., Sachs, D. H. & DerSimonian, H. (1997). Heterogeneity of human anti-pig natural antibodies cross-reactive with the Gal(alpha1,3)Galactose epitope. *Transplantation* 64, 501–10.
- McPherson, T. B., Liang, H., Record, R. D. & Badylak, S. F. (2000). Galalpha(1,3)Gal epitope in porcine small intestinal submucosa. *Tissue Eng* 6, 233–9. Mary Ann Liebert, Inc.
- Mendoza-Novelo, B., Avila, E. E., Cauich-Rodríguez, J. V, Jorge-Herrero, E., Rojo, F. J., Guinea, G. V & Mata-Mata, J. L. (2011). Decellularization of pericardial tissue and its impact on tensile viscoelasticity and glycosaminoglycan content. *Acta Biomater* 7, 1241–8.
- Merryman, W. D., Engelmayr, G. C., Liao, J. & Sacks, M. S. (2006). Defining biomechanical endpoints for tissue engineered heart valve leaflets from native leaflet properties. *Prog Pediatr Cardiol* 21, 153–160.
- Messas, E., Guerrero, J. L., Handschumacher, M. D., Conrad, C., Chow, C. M., Sullivan, S., Yoganathan, A. P. & Levine, R. A. (2001). Chordal cutting: a new therapeutic approach for ischemic mitral regurgitation. *Circulation* 104, 1958–63.
- Van Mieghem, N. M., Piazza, N., Anderson, R. H., Tzikas, A., Nieman, K., De Laet, L. E., McGhie, J. S., Geleijnse, M. L., Feldman, T. & other authors. (2010). Anatomy of the mitral valvular complex and its implications for transcatheter interventions for mitral regurgitation. *J Am Coll Cardiol* 56, 617–26.
- Mihalatos, D. G., Joseph, S., Gopal, A., Bercow, N., Toole, R., Passick, M., Grimson, R., Norales, A. & Reichek, N. (2007). Mitral annular remodeling with varying degrees and mechanisms of chronic mitral regurgitation. *J Am Soc Echocardiogr* 20, 397–404.
- Millington-Sanders, C., Meir, A., Lawrence, L. & Stolinski, C. (1998). Structure of chordae tendineae in the left ventricle of the human heart. *J Anat* 192 (Pt 4, 573–81.

- Mirsadraee, S., Wilcox, H. E., Korossis, S. a, Kearney, J. N., Watterson, K. G., Fisher, J. & Ingham, E. (2006). Development and characterization of an acellular human pericardial matrix for tissue engineering. *Tissue Eng* 12, 763–73. Mary Ann Liebert, Inc. 2 Madison Avenue Larchmont, NY 10538 USA.
- Miura, T., Eishi, K., Sakamoto, I., Yamachika, S., Hashizume, K., Yamane, K., Tanigawa, K., Matsukuma, S. & Nakaji, S. (2012). Time-dependent change in fresh autologous pericardium applied for posterior mitral annuloplasty: degree of calcification and its influence on the repaired mitral valve. *Gen Thorac Cardiovasc Surg* 60, 334–40.
- Mohammadi, H. & Mequanint, K. (2011). Prosthetic aortic heart valves: modeling and design. *Med Eng Phys* 33, 131–47. Institute of Physics and Engineering in Medicine.
- Mohler, E. R., Gannon, F., Reynolds, C., Zimmerman, R., Keane, M. G. & Kaplan, F. S. (2001). Bone Formation and Inflammation in Cardiac Valves. *Circulation* 103, 1522–1528.
- Moon, M. R., DeAnda, A., Daughters, G. T., Ingels, N. B. & Miller, D. C. (1999). Effects of mitral valve replacement on regional left ventricular systolic strain. *Ann Thorac Surg* 68, 894–902.
- Morticelli, L., Thomas, D., Roberts, N., Ingham, E. & Korossis, S. (2013). Investigation of the suitability of decellularized porcine pericardium in mitral valve reconstruction. *J Heart Valve Dis* 22, 340–53.
- Mostow, E. N., Haraway, G. D., Dalsing, M., Hodde, J. P. & King, D. (2005). Effectiveness of an extracellular matrix graft (OASIS Wound Matrix) in the treatment of chronic leg ulcers: a randomized clinical trial. *J Vasc Surg* 41, 837–43.
- Muehrcke, D. D., Cosgrove, D. M., Lytle, B. W., Taylor, P. C., Burgar, BS, A. M., Durnwald, BS, C. P. & Loop, F. D. (1997). Is There an Advantage to Repairing Infected Mitral Valves? *Ann Thorac Surg* 63, 1718–1724. Elsevier.
- Nagata, S., Hanayama, R. & Kawane, K. (2010). Autoimmunity and the clearance of dead cells. *Cell* 140, 619–30.
- Nakayama, K. H., Batchelder, C. A., Lee, C. I. & Tarantal, A. F. (2010). Decellularized rhesus monkey kidney as a three-dimensional scaffold for renal tissue engineering. *Tissue Eng Part A* 16, 2207–16.
- Naugle, J. E., Olson, E. R., Zhang, X., Mase, S. E., Pilati, C. F., Maron, M. B., Folkesson, H. G., Horne, W. I., Doane, K. J. & Meszaros, J. G. (2006). Type VI collagen induces cardiac myofibroblast differentiation: implications for postinfarction remodeling. *Am J Physiol Heart Circ Physiol* 290, H323–30.

- Nestle, M. & Roberts, W. K. (1969). An extracellular nuclease from *Serratia marcescens*. II. Specificity of the enzyme. *J Biol Chem* 244, 5219–25.
- Neuenschwander, S. & Hoerstrup, S. P. (2004). Heart valve tissue engineering. *Transpl Immunol* 12, 359–65.
- Ng, C., Nesser, J., Punzengruber, C., Pachinger, O., Auer, J., Franke, H. & Hartl, P. (2001). Autologous Pericardium in Patients With Complex. *Ann Thorac Surgery*, 4975, 1–8.
- Nguyen, T. C., Itoh, A., Carlhäll, C. J., Bothe, W., Timek, T. a, Ennis, D. B., Oakes, R. a, Liang, D., Daughters, G. T. & other authors. (2008). The effect of pure mitral regurgitation on mitral annular geometry and three-dimensional saddle shape. *J Thorac Cardiovasc Surg* 136, 557–65.
- NHS Blood and Transplant. (2015). *Organ Donation and Transplantation Activity Data: UNITED KINGDOM*.
- Nkomo, V. T., Gardin, J. M., Skelton, T. N., Gottdiener, J. S., Scott, C. G. & Enriquez-Sarano, M. (2006). Burden of valvular heart diseases: a population-based study. *Lancet* 368, 1005–11.
- Odell, J. A., Schaff, H. V & Orszulak, T. A. (1995). Early results of a simplified method of mitral valve annuloplasty. *Circulation* 92, 1150–4.
- Oliveira, J. M. F. De & Antunes, M. J. (2006). Mitral valve repair: better than replacement. *Heart* 92, 275–81.
- Onorati, F., Rubino, A. S., Marturano, D., Pasceri, E., Mascaro, G., Zinzi, S., Serraino, F. & Renzulli, A. (2009). Mid-term echocardiographic results with different rings following restrictive mitral annuloplasty for ischaemic cardiomyopathy. *Eur J Cardiothorac Surg* 36, 250–60; discussion 260.
- Oppido, G., Davies, B., McMullan, D. M., Cochrane, A. D., Cheung, M. M. H., d'Udekem, Y. & Brizard, C. P. (2008). Surgical treatment of congenital mitral valve disease: Midterm results of a repair-oriented policy. *J Thorac Cardiovasc Surg* 135, 1313–1321.e4. Elsevier.
- Ormiston, J. a, Shah, P. M., Tei, C. & Wong, M. (1981). Size and motion of the mitral valve annulus in man. I. A two-dimensional echocardiographic method and findings in normal subjects. *Circulation* 64, 113–20.
- Ormiston, J. a, Shah, P. M., Tei, C. & Wong, M. (1982). Size and motion of the mitral valve annulus in man. II. Abnormalities in mitral valve prolapse. *Circulation* 65, 713–9.
- Otsuji, Y., Kumanohoso, T., Yoshifuku, S., Matsukida, K., Koriyama, C., Kisanuki, A., Minagoe, S., Levine, R. A. & Tei, C. (2002). Isolated annular dilation does not usually cause important functional mitral regurgitation. *J Am Coll Cardiol* 39, 1651–1656. Journal of the American College of Cardiology.

- Ottani, V., Raspanti, M. & Ruggeri, A. (2001). Collagen structure and functional implications. *Micron* 32, 251–260.
- Otto, C. M. (2003). Timing of surgery in mitral regurgitation. *Heart* 89, 100–5.
- Ozolins, V., Ozolanta, I., Smits, L., Lacis, A. & Kasyanov, V. (2008). Biomechanical Properties of Glutaraldehyde Treated Human Pericardium. In *14th Nord Conf Biomed Eng Med Phys*, pp. 143–145.
- Padala, M., Hutchison, R. a, Croft, L. R., Jimenez, J. H., Gorman, R. C., Gorman, J. H., Sacks, M. S. & Yoganathan, A. P. (2009). Saddle shape of the mitral annulus reduces systolic strains on the P2 segment of the posterior mitral leaflet. *Ann Thorac Surg* 88, 1499–504. Elsevier Inc.
- Pai, R. G., Varadarajan, P. & Tanimoto, M. (2003). Effect of atrial fibrillation on the dynamics of mitral annular area. *J Heart Valve Dis* 12, 31–7.
- Paniagua Gutierrez, J. R., Berry, H., Korossis, S., Mirsadraee, S., Lopes, S. V., da Costa, F., Kearney, J., Watterson, K., Fisher, J. & Ingham, E. (2015). Regenerative potential of low-concentration SDS-decellularized porcine aortic valved conduits in vivo. *Tissue Eng Part A* 21, 332–42.
- Parekh, A., Mantle, B., Banks, J., Swarts, J. D., Badylak, S. F., Dohar, J. E. & Hebda, P. A. (2009). Repair of the tympanic membrane with urinary bladder matrix. *Laryngoscope* 119, 1206–13.
- Park, S., Kim, W.-H., Choi, S.-Y. & Kim, Y.-J. (2009). Removal of alpha-Gal epitopes from porcine aortic valve and pericardium using recombinant human alpha galactosidase A. *J Korean Med Sci* 24, 1126–31.
- Pat, B., Chen, Y., Killingsworth, C., Gladden, J. D., Shi, K., Zheng, J., Powell, P. C., Walcott, G., Ahmed, M. I. & other authors. (2010). Chymase inhibition prevents fibronectin and myofibrillar loss and improves cardiomyocyte function and LV torsion angle in dogs with isolated mitral regurgitation. *Circulation* 122, 1488–95.
- Pektok, E., Sierra, J., Cikirikcioglu, M., Müller, H., Myers, P. O. & Kalangos, A. (2010). Midterm results of valve repair with a biodegradable annuloplasty ring for acute endocarditis. *Ann Thorac Surg* 89, 1180–5. Elsevier Inc.
- Perry, P. (2007). The Ethics of Animal Research: A UK Perspective. *ILAR J* 48, 42–46.
- Petrofsky, J. (2008). The effect of the subcutaneous fat on the transfer of current through skin and into muscle. *Med Eng Phys* 30, 1168–76.
- Du Plessis, M., Blaak, C., Tubbs, R. S. & Loukas, M. (2014). Unraveling the anatomy of the cardiac skeleton of the heart (913.6). *FASEB J* 28.

- Poole, C. A., Ayad, S. & Gilbert, R. T. (1992). Chondrons from articular cartilage. V. Immunohistochemical evaluation of type VI collagen organisation in isolated chondrons by light, confocal and electron microscopy. *J Cell Sci* 103 (Pt 4, 1101–10.
- Quick, D. W., Kunzelman, K. S., Kneebone, J. M. & Cochran, R. P. (1997). Collagen synthesis is upregulated in mitral valves subjected to altered stress. *ASAIO J* 43, 181–6.
- Quinonez, L. G. & Del Nido, P. J. (2015). Valve reconstruction for congenital mitral valve disease. *Multimed Man Cardiothorac Surg MMCTS / Eur Assoc Cardio-Thoracic Surg* 2015, mmv007–.
- Rabkin-Aikawa, E., Farber, M., Aikawa, M. & Schoen, F. J. (2004). Dynamic and reversible changes of interstitial cell phenotype during remodeling of cardiac valves. *J Heart Valve Dis* 13, 841–7.
- Raffoul, R., Uva, M. S., Rescigno, G., Belli, E., Scorsin, M., Pouillart, F. & Lessana, a. (1998). Clinical Evaluation of the Physio Annuloplasty Ring. *Chest* 113, 1296–1301.
- Rajamannan, N. M., Evans, F. J., Aikawa, E., Grande-Allen, K. J., Demer, L. L., Heistad, D. D., Simmons, C. A., Masters, K. S., Mathieu, P. & other authors. (2011). Calcific aortic valve disease: not simply a degenerative process: A review and agenda for research from the National Heart and Lung and Blood Institute Aortic Stenosis Working Group. Executive summary: Calcific aortic valve disease-2011 update. *Circulation* 124, 1783–91.
- Ramamurthi, A. & Vesely, I. (2005). Evaluation of the matrix-synthesis potential of crosslinked hyaluronan gels for tissue engineering of aortic heart valves. *Biomaterials* 26, 999–1010.
- Ranganathan, N., Lam, J. H. C., Wigle, E. D. & Silver, M. D. (1970). Morphology of the Human Mitral Valve: II. The Valve Leaflets. *Circulation* 41, 459–467.
- Rashid, S. T., Salacinski, H. J., Hamilton, G. & Seifalian, A. M. (2004). The use of animal models in developing the discipline of cardiovascular tissue engineering: a review. *Biomaterials* 25, 1627–1637.
- Rausch, M. K., Bothe, W., Kvitting, J.-P. E., Swanson, J. C., Ingels, N. B., Miller, D. C. & Kuhl, E. (2011). Characterization of mitral valve annular dynamics in the beating heart. *Ann Biomed Eng* 39, 1690–702. Springer Netherlands.
- Rausch, M. K., Bothe, W., Kvitting, J.-P. E., Swanson, J. C., Miller, D. C. & Kuhl, E. (2012). Mitral valve annuloplasty: a quantitative clinical and mechanical comparison of different annuloplasty devices. *Ann Biomed Eng* 40, 750–61. Springer Netherlands.

- Von Rechenberg, B., Akens, M. ., Nadler, D., Bittmann, P., Zlinszky, K., Kutter, A., Poole, A. . & Auer, J. . (2003). Changes in subchondral bone in cartilage resurfacing—an experimental study in sheep using different types of osteochondral grafts. *Osteoarthr Cartil* 11, 265–277.
- Reing, J. E., Brown, B. N., Daly, K. A., Freund, J. M., Gilbert, T. W., Hsiong, S. X., Huber, A., Kullas, K. E., Tottey, S. & other authors. (2010). The effects of processing methods upon mechanical and biologic properties of porcine dermal extracellular matrix scaffolds. *Biomaterials* 31, 8626–33.
- Richards, A. L. R., Cook, R. C. C., Bolotin, G. B. & Buckner, G. D. B. (2009). A Dynamic Heart System to Facilitate the Development of Mitral Valve Repair Techniques. *Ann Biomed Eng* 37, 651–660.
- Van Rijk-Zwikker, G. L., Mast, F., Schipperheyn, J. J., Huysmans, H. A. & Brusckhe, A. V. (1990). Comparison of rigid and flexible rings for annuloplasty of the porcine mitral valve. *Circulation* 82, IV58–64.
- Rijk-Zwikker, G. L., Delemarre, B. J. & Huysmans, H. A. (1994). Mitral Valve Anatomy and Morphology: Relevance to Mitral Valve Replacement and Valve Reconstruction. *J Card Surg* 9, 255–261.
- Ritchie, J., Warnock, J. N. & Yoganathan, A. P. (2005). Structural characterization of the chordae tendineae in native porcine mitral valves. *Ann Thorac Surg* 80, 189–97.
- Roshanali, F., Vedadian, A., Shoar, S., Sandoughdaran, S., Naderan, M. & Mandegar, M. H. (2012). The viable mitral annular dynamics and left ventricular function after mitral valve repair by biological rings. *Int Cardiovasc Res J* 6, 118–23.
- Rumberger, J. A. (1994). Ventricular dilatation and remodeling after myocardial infarction. *Mayo Clin Proc* 69, 664–74.
- Ruzmetov, M., Shah, J. J., Geiss, D. M. & Fortuna, R. S. (2012). Decellularized versus standard cryopreserved valve allografts for right ventricular outflow tract reconstruction: a single-institution comparison. *J Thorac Cardiovasc Surg* 143, 543–9. Elsevier.
- Ryan, M., Antony, J. & Gratten-Smith, P. (2000). Sydenham's chorea: a resurgence in the 1990s? *J Paediatr Child Health* 36, 94–95.
- Sacks, M. S., David Merryman, W. & Schmidt, D. E. (2009). On the biomechanics of heart valve function. *J Biomech* 42, 1804–24.
- Sakai, M., Imai, T., Ohtake, H. & Otagiri, M. (1998). Cytotoxicity of absorption enhancers in Caco-2 cell monolayers. *J Pharm Pharmacol* 50, 1101–8.

- Salati, M., Scrofani, R. & Santoli, C. (1991). Posterior pericardial annuloplasty: a physiological correction? *Eur J Cardiothorac Surg* 5, 226–9; discussion 229.
- Salgo, I. S. (2002). Effect of Annular Shape on Leaflet Curvature in Reducing Mitral Leaflet Stress. *Circulation* 106, 711–717.
- Salvador, L., Cavarretta, E., Minniti, G., Di Angelantonio, E., Salandin, V., Frati, G., Polesel, E. & Valfrè, C. (2014). Autologous pericardium annuloplasty: a 'physiological' mitral valve repair. *J Cardiovasc Surg (Torino)* 55, 831–9.
- Sanders, T. & Scanlon, D. V. (1997). *Understanding Human Structure and Function*. F.A. Davis Company.
- Sandrin, M. & Mckenzie, I. F. C. (1994). Galalpha(1,3)Gal, the Major Xenoantigen(s) Recognised in Pigs by Human Natural Antibodies. *Immunol Rev* 141, 169–190.
- Sans-Coma, V., Franco, D., Durán, A. C., Arqué, J. M., Cardo, M. & Fernandez, B. (1994). Cartilage in the Aortic Valve and Its Relationship with the Aortic Valve Morphology in Syrian Hamsters. *Cells Tissues Organs* 149, 255–263. Karger Publishers.
- Schenke-Layland, K., Vasilevski, O., Opitz, F., König, K., Riemann, I., Halbhuber, K. J., Wahlers, T. & Stock, U. A. (2003). Impact of decellularization of xenogeneic tissue on extracellular matrix integrity for tissue engineering of heart valves. *J Struct Biol* 143, 201–208.
- Schmitto, J. D., Lee, L. S., Mokashi, S. a, Bolman, R. M., Cohn, L. H. & Chen, F. Y. (2010). Functional mitral regurgitation. *Cardiol Rev* 18, 285–91.
- Schoen, F. J. & Levy, R. J. (1999). Founder's Award, 25th Annual Meeting of the Society for Biomaterials, perspectives. Providence, RI, April 28-May 2, 1999. Tissue heart valves: current challenges and future research perspectives. *J Biomed Mater Res* 47, 439–65.
- Schoen, F. J. (2008). Evolving concepts of cardiac valve dynamics: the continuum of development, functional structure, pathobiology, and tissue engineering. *Circulation* 118, 1864–80.
- Scrofani, R., Moriggia, S., Salati, M., Fundaro, P., Danna, P. & Santoli, C. (1996). Mitral valve remodeling: long-term results with posterior pericardial annuloplasty. *Ann Thorac Surg* 61, 895–9.
- Selamet Tierney, E. S., Pigula, F. a, Berul, C. I., Lock, J. E., del Nido, P. J. & McElhinney, D. B. (2008). Mitral valve replacement in infants and children 5 years of age or younger: evolution in practice and outcome over three decades with a focus on supra-annular prosthesis

- implantation. *J Thorac Cardiovasc Surg* 136, 954–61, 961.e1–3. The American Association for Thoracic Surgery.
- Selevsek, N., Rival, S., Tholey, A., Heinzle, E., Heinz, U., Hemmingsen, L. & Adolph, H. W. (2009). Zinc ion-induced domain organization in metallo-beta-lactamases: a flexible 'zinc arm' for rapid metal ion transfer? *J Biol Chem* 284, 16419–31.
- Sheridan, M. ., Shea, L. ., Peters, M. . & Mooney, D. . (2000). Bioabsorbable polymer scaffolds for tissue engineering capable of sustained growth factor delivery. *J Control Release* 64, 91–102.
- Shi, Y. & Vesely, I. (2004). Characterization of statically loaded tissue-engineered mitral valve chordae tendineae. *J Biomed Mater Res A* 69, 26–39.
- Shi, Y., Ramamurthi, A. & Vesely, I. (2002). Towards tissue engineering of a composite aortic valve. *Biomed Sci Instrum* 38, 35–40.
- Shinn, S. H., Sung, K., Park, P. W., Lee, Y. T., Kim, W. S., Yang, J.-H., Jun, T.-G., Lee, S.-C. & Park, S. W. (2009). Results of annular reconstruction with a pericardial patch in active infective endocarditis. *J Heart Valve Dis* 18, 315–20.
- Shinoka, T., Ma, P. X., Shum-Tim, D., Breuer, C. K., Cusick, R. A., Zund, G., Langer, R., Vacanti, J. P. & Mayer, J. E. (1996). Tissue-engineered heart valves. Autologous valve leaflet replacement study in a lamb model. *Circulation* 94, 1164–8.
- Shinoka, T., Breuer, C. K., Tanel, R. E., Zund, G., Miura, T., Ma, P. X., Langer, R., Vacanti, J. P. & Mayer, J. E. (1995). Tissue engineering heart valves: Valve leaflet replacement study in a lamb model. *Ann Thorac Surg* 60, S513–S516.
- Shrivastava, S. (2003). Medical device materials: proceedings from the Materials & Processes for Medical Devices Conference 2003. ASM International.
- Silberman, S., Klutstein, M. W., Sabag, T., Oren, A., Fink, D., Merin, O. & Bitran, D. (2009). Repair of ischemic mitral regurgitation: comparison between flexible and rigid annuloplasty rings. *Ann Thorac Surg* 87, 1721–6; discussion 1726–7. Elsevier.
- Silbiger, J. J. & Bazaz, R. (2009). Contemporary insights into the functional anatomy of the mitral valve. *Am Heart J* 158, 887–95. Mosby, Inc.
- Simionescu, D. T., Chen, J., Jaeggli, M., Wang, B. & Liao, J. (2012). Form Follows Function: Advances in Trilayered Structure Replication for Aortic Heart Valve Tissue Engineering. *J Healthc Eng* 3, 179–202.

- Simon, P., Kasimir, M. T., Seebacher, G., Weigel, G., Ullrich, R., Salzer-Muhar, U., Rieder, E. & Wolner, E. (2003). Early failure of the tissue engineered porcine heart valve SYNERGRAFT in pediatric patients. *Eur J Cardiothorac Surg* 23, 1002–6; discussion 1006.
- Sodian, R., Schaefermeier, P., Abegg-Zips, S., Kuebler, W. M., Shakibaei, M., Daebritz, S., Ziegelmueller, J., Schmitz, C. & Reichart, B. (2010). Use of human umbilical cord blood-derived progenitor cells for tissue-engineered heart valves. *Ann Thorac Surg* 89, 819–28. Elsevier.
- Spina, M., Ortolani, F., El Messlemani, A., Gandaglia, A., Bujan, J., Garcia-Honduvilla, N., Vesely, I., Gerosa, G., Casarotto, D. & other authors. (2003). Isolation of intact aortic valve scaffolds for heart-valve bioprostheses: extracellular matrix structure, prevention from calcification, and cell repopulation features. *J Biomed Mater Res A* 67, 1338–50.
- Stapleton, T. W., Ingram, J., Katta, J., Knight, R., Korossis, S., Fisher, J. & Ingham, E. (2008). Development and characterization of an acellular porcine medial meniscus for use in tissue engineering. *Tissue Eng Part A* 14, 505–18. Mary Ann Liebert, Inc. 140 Huguenot Street, 3rd Floor New Rochelle, NY 10801 USA.
- Steinhoff, G., Stock, U., Karim, N., Mertsching, H., Timke, A., Meliss, R. R., Pethig, K., Haverich, A. & Bader, A. (2000). Tissue engineering of pulmonary heart valves on allogenic acellular matrix conduits: in vivo restoration of valve tissue. *Circulation* 102, III50–5.
- Stellin, G., Padalino, M. A., Vida, V. L., Boccuzzo, G., Orrù, E., Biffanti, R., Milanese, O. & Mazzucco, A. (2010). Surgical repair of congenital mitral valve malformations in infancy and childhood: A single-center 36-year experience. *J Thorac Cardiovasc Surg* 140, 1238–1244. Elsevier.
- Stephens, E. H., Nguyen, T. C., Itoh, A., Ingels, N. B., Miller, D. C. & Grande-Allen, K. J. (2008). The effects of mitral regurgitation alone are sufficient for leaflet remodeling. *Circulation* 118, S243–9.
- Stout, K. K. & Verrier, E. D. (2009). Acute valvular regurgitation. *Circulation* 119, 3232–41.
- Tahta, S. A., Oury, J. H., Maxwell, J. M., Hiro, S. P. & Duran, C. M. G. (2002). Outcome after mitral valve repair for functional ischemic mitral regurgitation. *J Heart Valve Dis* 11, 11–8; discussion 18–9.
- Tamariz, E. & Grinnell, F. (2002). Modulation of fibroblast morphology and adhesion during collagen matrix remodeling. *Mol Biol Cell* 13, 3915–29.
- Tanemoto, K. (2005). Surgical treatment of ischemic mitral valve regurgitation. *Ann Thorac Cardiovasc Surg* 11, 228–31.

- Tavakkol, Z., Gelehrter, S., Goldberg, C. S., Bove, E. L., Devaney, E. J. & Ohye, R. G. (2005). Superior durability of SynerGraft pulmonary allografts compared with standard cryopreserved allografts. *Ann Thorac Surg* 80, 1610–4. Elsevier.
- Tedder, M. E., Simionescu, A., Chen, J., Liao, J. & Simionescu, D. T. (2011). Assembly and testing of stem cell-seeded layered collagen constructs for heart valve tissue engineering. *Tissue Eng Part A* 17, 25–36.
- Teebken, O. E., Pichlmaier, a M. & Haverich, a. (2001). Cell seeded decellularised allogeneic matrix grafts and biodegradable polydioxanone-prostheses compared with arterial autografts in a porcine model. *Eur J Vasc Endovasc Surg* 22, 139–45.
- Tibayan, F. a, Rodriguez, F., Langer, F., Zasio, M. K., Bailey, L., Liang, D., Daughters, G. T., Ingels, N. B. & Miller, D. C. (2003). Annular Remodeling in Chronic Ischemic Mitral Regurgitation: Ring Selection Implications. *Ann Thorac Surg* 76, 1549–1555.
- Tibayan, F. a, Rodriguez, F., Langer, F., Zasio, M. K., Bailey, L., Liang, D., Daughters, G. T., Ingels, N. B. & Miller, D. C. (2004). Does septal-lateral annular cinching work for chronic ischemic mitral regurgitation? *J Thorac Cardiovasc Surg* 127, 654–63.
- Timek, T. A., Lai, D. T., Dagum, P., Tibayan, F., Daughters, G. T., Liang, D., Berry, G. J., Miller, D. C. & Ingels, N. B. (2003). Ablation of mitral annular and leaflet muscle: effects on annular and leaflet dynamics. *Am J Physiol Heart Circ Physiol* 285, H1668–74.
- Timek, T. a, Glasson, J. R., Lai, D. T., Liang, D., Daughters, G. T., Ingels, N. B. & Miller, D. C. (2005). Annular height-to-commissural width ratio of annuloplasty rings in vivo. *Circulation* 112, 1423–8.
- Timek, T. A., Dagum, P., Lai, D. T., Tibayan, F., Liang, D., Daughters, G. T., Hayase, M., Ingels, N. B. & Miller, D. C. (2002). Will a Partial Posterior Annuloplasty Ring Prevent Acute Ischemic Mitral Regurgitation? *Circulation* 106, I–33–39.
- Toumanidis, S. T., Sideris, D. A., Papamichael, C. M. & Mouloupoulos, S. D. (1992). The role of mitral annulus motion in left ventricular function. *Acta Cardiol* 47, 331–48.
- Tranquillo, R. T., Durrani, M. A. & Moon, A. G. (1992). Tissue engineering science: consequences of cell traction force. *Cytotechnology* 10, 225–50.
- Urabe, Y., Mann, D. L., Kent, R. L., Nakano, K., Tomanek, R. J., Carabello, B. A. & Cooper, G. (1992). Cellular and ventricular contractile dysfunction in experimental canine mitral regurgitation. *Circ Res* 70, 131–147.

- Valentin, J. E., Turner, N. J., Gilbert, T. W. & Badylak, S. F. (2010). Functional skeletal muscle formation with a biologic scaffold. *Biomaterials* 31, 7475–84.
- Vavken, P., Joshi, S. & Murray, M. M. (2009). TRITON-X is most effective among three decellularization agents for ACL tissue engineering. *J Orthop Res* 27, 1612–8.
- Veasy, L. G. & Tani, L. Y. (2005). A new look at acute rheumatic mitral regurgitation. *Cardiol Young* 15, 568–77. Cambridge University Press.
- Vesely, I. (2003). The evolution of bioprosthetic heart valve design and its impact on durability. *Cardiovasc Pathol* 12, 277–86.
- Vorotnikova, E., McIntosh, D., Dewilde, A., Zhang, J., Reing, J. E., Zhang, L., Cordero, K., Bedelbaeva, K., Gourevitch, D. & other authors. (2010). Extracellular matrix-derived products modulate endothelial and progenitor cell migration and proliferation in vitro and stimulate regenerative healing in vivo. *Matrix Biol* 29, 690–700.
- Walker, C. A. & Spinale, F. G. (1999). The structure and function of the cardiac myocyte: A review of the fundamental concepts. *J Thorac Cardiovasc Surg* 118, 375–382.
- Walmsley, R. (1978). Anatomy of human mitral valve in adult cadaver and comparative anatomy of the valve. *Br Heart J* 40, 351–66.
- Watanabe, N., Ogasawara, Y., Yamaura, Y., Wada, N., Kawamoto, T., Toyota, E., Akasaka, T. & Yoshida, K. (2005). Mitral annulus flattens in ischemic mitral regurgitation: geometric differences between inferior and anterior myocardial infarction: a real-time 3-dimensional echocardiographic study. *Circulation* 112, 1458–62.
- Weissler, A. M., Peeler, R. G. & Roehll, W. H. (1961). Relationships between left ventricular ejection time, stroke volume, and heart rate in normal individuals and patients with cardiovascular disease. *Am Heart J* 62, 367–378.
- Wilcox, H. E., Korossis, S. A., Booth, C., Watterson, K. G., Kearney, J. N., Fisher, J. & Ingham, E. (2005). Biocompatibility and recellularization potential of an acellular porcine heart valve matrix. *J Heart Valve Dis* 14, 228–36; discussion 236–7.
- Wilson, G. J., Courtman, D. W., Klement, P., Lee, J. M. & Yeger, H. (1995). Acellular matrix: a biomaterials approach for coronary artery bypass and heart valve replacement. *Ann Thorac Surg* 60, S353–8.
- Wood, A. E., Healy, D. G., Nolke, L., Duff, D., Oslizlok, P. & Walsh, K. (2005). Mitral valve reconstruction in a pediatric population: late clinical results and predictors of long-term outcome. *J Thorac Cardiovasc Surg* 130, 66–73.

- Woods, T. & Gratzner, P. F. (2005). Effectiveness of three extraction techniques in the development of a decellularized bone-anterior cruciate ligament-bone graft. *Biomaterials* 26, 7339–49.
- Woon, C. Y. L., Pridgen, B. C., Kraus, A., Bari, S., Pham, H. & Chang, J. (2011). Optimization of human tendon tissue engineering: peracetic acid oxidation for enhanced reseeding of acellularized intrasynovial tendon. *Plast Reconstr Surg* 127, 1107–17.
- Xu, C. C., Chan, R. W., Weinberger, D. G., Efune, G. & Pawlowski, K. S. (2010). A bovine acellular scaffold for vocal fold reconstruction in a rat model. *J Biomed Mater Res A* 92, 18–32.
- Yamaura, Y., Yoshida, K., Hozumi, T., Akasaka, T., Okada, Y. & Yoshikawa, J. (1997). Three-dimensional echocardiographic evaluation of configuration and dynamics of the mitral annulus in patients fitted with an annuloplasty ring. *J Heart Valve Dis* 6, 43–7.
- Yang, S., Leong, K.-F., Du, Z. & Chua, C.-K. (2001). The Design of Scaffolds for Use in Tissue Engineering. Part I. Traditional Factors. *Tissue Eng* 7, 679–689. Mary Ann Liebert, Inc.
- Yiu, S. F., Enriquez-Sarano, M., Tribouilloy, C., Seward, J. B. & Tajik, A. J. (2000). Determinants of the degree of functional mitral regurgitation in patients with systolic left ventricular dysfunction: A quantitative clinical study. *Circulation* 102, 1400–6.
- Zdrahala, R. J. & Zdrahala, I. J. (1999). Journal of Biomaterials Applications. *J Biomater Appl*.
- Zehr, K. J., Yagubyan, M., Connolly, H. M., Nelson, S. M. & Schaff, H. V. (2005). Aortic root replacement with a novel decellularized cryopreserved aortic homograft: postoperative immunoreactivity and early results. *J Thorac Cardiovasc Surg* 130, 1010–5. Elsevier.
- Zhu, F., Otsuji, Y., Yotsumoto, G., Yuasa, T., Ueno, T., Yu, B., Koriyama, C., Hamasaki, S., Biro, S. & other authors. (2005). Mechanism of persistent ischemic mitral regurgitation after annuloplasty: importance of augmented posterior mitral leaflet tethering. *Circulation* 112, 1396–401.
- Zimmerman, J. (1966). The functional and surgical anatomy of the heart. *Ann R Coll Surg Engl* 39, 348–66.
- Zisch, A. H., Lutolf, M. P., Ehrbar, M., Raeber, G. P., Rizzi, S. C., Davies, N., Schmökel, H., Bezuidenhout, D., Djonov, V. & other authors. (2003). Cell-demand release of VEGF from synthetic, biointeractive cell ingrowth matrices for vascularized tissue growth. *FASEB J* 17, 2260–2.
- Zoghbi, W. (2003). American Society of Echocardiography: recommendations for evaluation of the severity of native valvular regurgitation with two-dimensional and Doppler echocardiography A

report from the American Society of Echocardiography's Nomenclature and Standards Com. *Eur J Echocardiogr* 4, 237–261.

Zund, G. (1997). The in vitro construction of a tissue engineered bioprosthetic heart valve. *Eur J Cardio-Thoracic Surg* 11, 493–497.